

UC Berkeley

UC Berkeley Electronic Theses and Dissertations

Title

Precision Higgs Physics, Effective Field Theory, and Dark Matter

Permalink

<https://escholarship.org/uc/item/0kq093s2>

Author

Henning, Brian Quinn

Publication Date

2015

Peer reviewed|Thesis/dissertation

Precision Higgs Physics, Effective Field Theory, and Dark Matter

by

Brian Quinn Henning

A dissertation submitted in partial satisfaction of the

requirements for the degree of

Doctor of Philosophy

in

Physics

in the

Graduate Division

of the

University of California, Berkeley

Committee in charge:

Professor Hitoshi Murayama, Chair

Professor Wick C. Haxton

Professor Phillip L. Geissler

Summer 2015

Precision Higgs Physics, Effective Field Theory, and Dark Matter

Copyright 2015
by
Brian Quinn Henning

Abstract

Precision Higgs Physics, Effective Field Theory, and Dark Matter

by

Brian Quinn Henning

Doctor of Philosophy in Physics

University of California, Berkeley

Professor Hitoshi Murayama, Chair

The recent discovery of the Higgs boson calls for detailed studies of its properties. As precision measurements are indirect probes of new physics, the appropriate theoretical framework is effective field theory. In the first part of this thesis, we present a practical three-step procedure of using the Standard Model effective field theory (SM EFT) to connect ultraviolet (UV) models of new physics with weak scale precision observables. With this procedure, one can interpret precision measurements as constraints on the UV model concerned. We give a detailed explanation for calculating the effective action up to one-loop order in a manifestly gauge covariant fashion. The covariant derivative expansion dramatically simplifies the process of matching a UV model with the SM EFT, and also makes available a universal formalism that is easy to use for a variety of UV models. A few general aspects of renormalization group running effects and choosing operator bases are discussed. Finally, we provide mapping results between the bosonic sector of the SM EFT and a complete set of precision electroweak and Higgs observables to which present and near future experiments are sensitive.

With a detailed understanding of how to use the SM EFT, we then turn to applications and study in detail two well-motivated test cases. The first is singlet scalar field that enables the first-order electroweak phase transition for baryogenesis; the second example is due to scalar tops in the MSSM. We find both Higgs and electroweak measurements are sensitive probes of these cases.

The second part of this thesis centers around dark matter, and consists of two studies. In the first, we examine the effects of relic dark matter annihilations on big bang nucleosynthesis (BBN). The magnitude of these effects scale simply with the dark matter mass and annihilation cross-section, which we derive. Estimates based on these scaling behaviors indicate that BBN severely constrains hadronic and radiative dark matter annihilation channels in the previously unconsidered dark matter mass region $\text{MeV} \lesssim m_\chi \lesssim 10 \text{ GeV}$. Interestingly, we find that BBN constraints on hadronic annihilation channels are competitive with similar bounds derived from the cosmic microwave background.

Our second study of dark matter concerns a possible connection with supersymmetry and the keV scale. Various theoretical and experimental considerations motivate models with high scale supersymmetry breaking. While such models may be difficult to test in colliders, we propose

looking for signatures at much lower energies. We show that a keV line in the X-ray spectrum of galaxy clusters (such as the recently disputed 3.5 keV observation) can have its origin in a universal string axion coupled to a hidden supersymmetry breaking sector. A linear combination of the string axion and an additional axion in the hidden sector remains light, obtaining a mass of order 10 keV through supersymmetry breaking dynamics. In order to explain the X-ray line, the scale of supersymmetry breaking must be about 10^{11-12} GeV. This motivates high scale supersymmetry as in pure gravity mediation or minimal split supersymmetry and is consistent with all current limits. Since the axion mass is controlled by a dynamical mass scale, this mass can be much higher during inflation, avoiding isocurvature (and domain wall) problems associated with high scale inflation. In appendix E we present a mechanism for dilaton stabilization that additionally leads to $\mathcal{O}(1)$ modifications of the gaugino mass from anomaly mediation.

For my parents, Mark and Mary

Contents

Contents	ii
1 Introduction	1
1.1 Precision Higgs physics and effective field theory	1
1.1.1 The Higgs, dimensional analysis, and the hierarchy problem	2
1.1.2 Natural solutions	5
1.1.3 Precision Higgs physics	7
1.1.4 The SM effective field theory	8
1.2 Dark matter	10
1.2.1 Cosmological evidence of dark matter	10
1.2.1.1 A diversion on the lower bound of allowed DM mass	12
1.2.2 Searching for DM	13
1.2.3 Dark matter and Big Bang nucleosynthesis	14
1.2.4 A keV string axion	16
2 How to Use the Standard Model Effective Field Theory	18
2.1 Covariant derivative expansion	23
2.1.1 Covariant evaluation of the tree-level and one-loop effective action	25
2.1.1.1 Covariant evaluation of the tree-level effective action	26
2.1.1.2 CDE of the one-loop effective action	28
2.1.2 CDE for fermions, gauge bosons, and summary formulas	31
2.1.3 Evaluating the CDE and universal results	35
2.1.3.1 Evaluating terms in CDE	35
2.1.3.2 Universal results	38
2.1.4 Example calculations	42
2.1.4.1 Electroweak triplet scalar	44
2.1.4.2 Extra EW scalar doublet	49
2.1.4.3 A $SU(2)_L$ quartet scalar	54
2.1.4.4 Kinetic mixing of gauge bosons	55
2.1.4.5 Heavy vector bosons in the triplet representation of $SU(2)_L$	56
2.2 Running of Wilson coefficients and choosing an operator set	58
2.2.1 When is RG running important?	59

2.2.2	Choosing an operator set in light of RG running analysis	60
2.2.3	Popular operator bases in the literature	61
2.3	Mapping Wilson coefficients onto observables	63
2.3.1	Electroweak precision observables	64
2.3.2	Triple gauge couplings	67
2.3.3	Deviations in Higgs decay widths	67
	2.3.3.1 Brief description of the results	68
	2.3.3.2 Detailed derivation	71
2.3.4	Deviations in Higgs production cross sections	73
2.4	Applications	74
2.4.1	Electroweak baryogenesis from a real singlet scalar	76
	2.4.1.1 Effects on precision observables	78
2.4.2	Supersymmetry and light scalar tops	81
2.5	Summary of results	83
3	Constraints on Light Dark Matter from Big Bang Nucleosynthesis	87
3.1	Energy injection into BBN	88
	3.1.1 Injection of hadronic energy	89
	3.1.2 Injection of electromagnetic energy	90
3.2	Constraints from BBN	91
	3.2.1 Hadronic constraints	93
	3.2.2 Electromagnetic constraints	93
	3.2.3 Other annihilation channels	94
3.3	Discussion	96
4	A keV String Axion from High Scale Supersymmetry	97
4.1	An explicit model	99
4.2	Cosmology	102
4.3	Discussion	103
A	Supplemental details for the CDE	106
A.1	CDE for fermions and gauge bosons	106
A.2	Useful identities	111
A.3	Evaluating terms in the CDE: results for the \mathcal{I}_n	114
B	Universality of Magnetic Dipole Term	116
B.1	Algebraic Proof	117
B.2	Physical Proof	120
C	Supplemental Details for Mapping Wilson Coefficients on to Physical Observables	122
C.1	Additional Feynman rules from dim-6 effective operators	122
	C.1.1 Feynman rules for vacuum polarization functions	122

C.1.2	Feynman rules for three-point vertices	125
C.2	Details on interference corrections to the Higgs decay widths	127
C.3	Details on interference corrections to Higgs production cross section	131
C.4	Calculation of residue modifications	134
C.5	Calculation of Lagrangian parameter modifications	134
D	Observational Abundances of Light Elements	137
E	Axion Potential and Dilaton Stabilization	138
E.1	Axion potential	138
E.1.1	$W_{\text{tree}} = 0$	138
E.1.2	$W_{\text{tree}} \neq 0$	141
E.2	Dilaton Stabilization	142
	Bibliography	145

Acknowledgments

This thesis, and my education in general, is the product of numerous educators, collaborators, friends, and family who shaped the path I wandered and supported me as I traveled it. In no reasonable manner can this acknowledgments page do justice to all these wonderful people, but I hope it can at least manage to capture my gratitude.

I thank Dr. T.J. Donahue for igniting my interest in scientific research. He opened the door to research and went above and beyond to create opportunities; moreover, he made science cool. The world benefits greatly from high school teachers like Dr. D. I was incredibly fortunate to have the opportunity of working in research labs at the University of Colorado Health Sciences Center while still in high school. For encouraging curiosity and taking the time to share a passion—all the while treating me like a colleague—I am so incredibly grateful to Doug, Holly, Jamie, Jim, Julie, Natalie, Petra, Tammy, and, especially, Adrie van Bokhoven. I may not have ended up studying cancer (certainly a nobler cause), but the time in those labs showed me the wonderful *community* formed by research scientists and cemented my desire to join it.

The physics department at Boston University grew my passion for physics. Ed Kearns took me on as an undergraduate researcher, letting me explore the workings of an experiment from coding, to electronics, to analysis. He provided genuine guidance and thoughtful opportunities solely aimed at bettering me as a physicist and person. I owe much to the Super Kamiokande group at BU, including Fanny Dufour, Dan Gastler, and Mike Litos. I cannot thank Jen Raaf enough, who really took me under her wing at BU and did so much more than show me how to make beautiful plots and deal with spiders. The Super-K group not only offered me insights into how experimental physics is done, but revealed just how collaborative and positive the experimental community is. This has shaped and will continue to shape my collaborations on the theoretical side. Besides the research group at BU, there are many faculty who influenced me including Steve Ahlen, Rob Carey, Ami Katz, So-Young Pi, Anatoli Polkovnikov, Martin Schmaltz, and, especially, my faculty mentor Andy Cohen, who I looked up to as an undergraduate and continue to now.

For the opportunity to study at Berkeley, all I can say is “wow”. Above all, I owe so much to my advisor Hitoshi Murayama. Hitoshi deserves many accolades, but let me bestow one that stands out from the perspective of a student. Hitoshi really listens. Any idea I brought up—from basic questions to day-dreaming on physics to good research ideas (even if often imprecise)—was met with genuine attention and thoughtfully responded to. There was never a pretense of needing to be right or have perfect understanding. Perhaps most importantly, Hitoshi never tried to steer an idea towards how he looked at it; he valued letting me explore things in my own way, adopting to my style and providing guidance as opposed to dictation. He is a genuine teacher, without ego. These qualities, so essential to my personal growth as a researcher, stand out to me perhaps because they do not come so naturally for myself. In this regard, I hope to emulate Hitoshi as I continue on in physics. Of course, I also hope to mimic in some small way his deep knowledge of many disparate subjects in theoretical and experimental physics as well as his ability to sway, politically and philosophically, the physics community and actually accomplish things. To reach his level is grand dreaming, but then again, he’d never discourage it himself. Who knows, maybe someday I’ll start an institute myself.

Besides my advisor, I'd like to thank my thesis committee members Phillip Geissler and Wick Haxton for asking many thoughtful questions and providing me with valuable feedback. I extend the same gratitude to Marjorie Shapiro, who served on my qualifying exam. I also want to thank Marjorie for being a valuable resource for personal support during my time at Berkeley.

I've been fortunate to have discussions with many great people during my time at Berkeley. Broadly, the members of the Berkeley Center of Theoretical Physics made this a unique and awesome place to be. There are too many to name, but let me acknowledge some of those responsible for the many insightful and delightful interactions I've had over the years: Alex Dahlen, Francesco D'Eramo, Marat Freytsis, Lawrence Hall, Yonit Hochberg, Grant Larsen, Zoltan Ligeti, Yasunori Nomura, Duccio Pappadopulo, Josh Ruderman, Kevin Schaeffer, Kohsaku Tobioka, Ziqi Yan, and Claire Zukowski.

I'm deeply grateful to my collaborators John Kehayias, David Pinner, and Tsutomu Yanagida. I'd especially like to thank Xiaochuan Lu, without whom, so much of this thesis would not have been practically possible. He is a pleasure to work with. Even though work with the following two people does not appear in this thesis, I'm heavily influenced by and owe much to Tom Melia and Yuji Tachikawa. Tom is a bundle of joy and a great friend. Yuji, perhaps unwittingly, gave me the confidence that I can make it as a physicist. He is one of those few people who I really hope to be like in my future career and life.

There are many to thank that made my graduate path practically possible. The administrative staff, here at Berkeley as well as at IPMU, solved so many of my issues and facilitated making opportunities possible. To name a few, I'd like to thank Yuuko Enomoto, LaVern Navarro, Midori Ozawa, Donna Sakima, and Anne Takizawa. It is also a great pleasure to thank Lynn Brantley and Doug Tuttle for a fellowship, as well as providing unbelievably awesome Tahoe retreats for the BCTP.

Berkeley is not only the place where I came into myself as a physicist, but also as a person. I feel expressive, loving, and whole here. It is not possible for me to name all who contributed to that, so instead let me acknowledge the dance parties, coffee shop chats, desert trips, openness, and all those who partook and made possible this culture. There are two people that I will single out. Johnny Pujol taught me the value of being positive. It amazes me that he always manages to find the good in things. Moreover, he somehow made me feel *cool* for doing physics, which makes me laugh as I write that down. Jillian Capdevielle has always encouraged me to love what I do and to follow curiosity. She has not only been a source of love and support, but also an inspiration for how much a human can do, even in the face of adversity. Her strength of character leaves me in awe and I love her very much.

Finally, I have benefited tremendously from my family, without whose care, support, and love I could not be where I am today. My two sisters, Alison and Lisa, keep me humbled and are simply awesome. My mom and dad are everything they should be and more. I think the only way to encompass just how much they have done for me and how much it means to me is by saying that, one day, I hope to do the same for my children.

Chapter 1

Introduction

This thesis, while falling under the general umbrella of physics beyond the Standard Model, has a natural divide into two topics; as such, I will split the introduction along this line. The first concerns the Standard Model effective field theory and its use for precision studies of the recently discovered Higgs boson.¹ The second topic centers around dark matter and examines indirect constraints that Big Bang nucleosynthesis can place on properties of dark matter and also the possible connection between keV scale dark matter with supersymmetry.²

In this introduction, I hope to explore more broadly the general motivating questions and ideas which underlie the topics of this thesis. While I roughly sketch the contents of this thesis in this introduction, more targeted outlines can be found at the beginning of each of the chapters. To emphasize concepts over contents, I have aimed to avoid equations and include many pictures in this introduction. This will also hopefully make up, in some small way, for the rather unfair equation to picture ratio of the following chapters. Many of the pictures and their captions stand alone; they are meant to provide complementary or supplemental information to the main text. Occasionally, these figures require more advanced information to fully understand them than is explained in body text; in these situations, I hope a non-expert reader can still glean some qualitative information.

Lastly, at this point I commit a grammatical faux pas and pass from the possessive pronoun to the royal “we” for the rest of this thesis.

1.1 Precision Higgs physics and effective field theory

On July 4th, 2012 the ATLAS and CMS experiments announced the discovery of a scalar-like resonance with a mass near 125 GeV [5, 6]. While the papers [5, 6] detailing the discovery show the appropriate scientific due diligence of only naming the properties for which there is clear evidence, those properties strongly suggested that the “scalar-like resonance” was the long anticipated Higgs

¹This part of the thesis is based on two published works [1, 2] completed with Xiaochuan Lu and Hitoshi Murayama.

²This part of the thesis is based on two published works [3, 4], the first completed with Hitoshi Murayama and the second with John Kehayias, Hitoshi Murayama, David Pinner, and Tsutomu Yanagida.

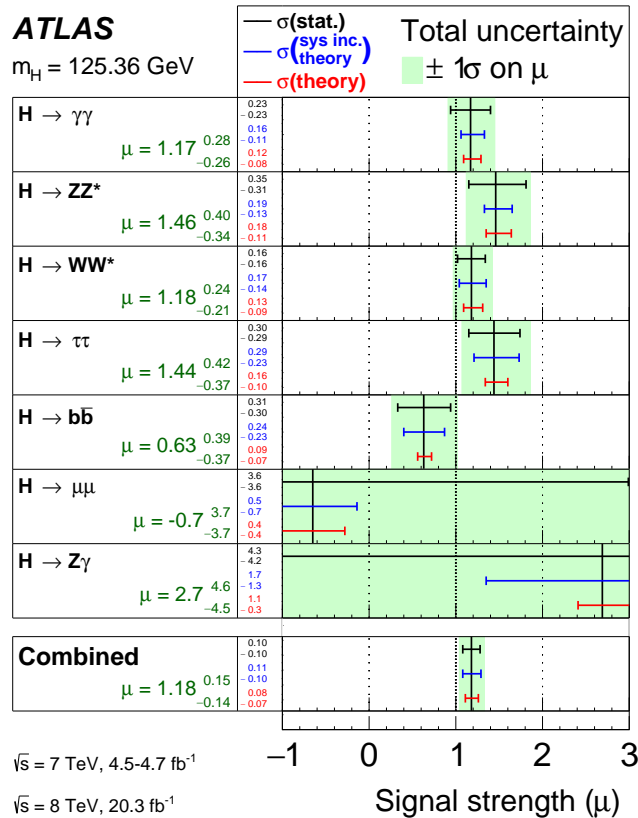


Figure 1.1: Observed signal strengths and uncertainties for decays of the Higgs boson, as measured by the ATLAS collaboration after the LHC run at $\sqrt{s} = 7$ and 8 TeV [7]. Signal strengths are normalized to Standard Model predictions, which occur at $\mu = 1$ in the figure. The figure and more information can be found in the ATLAS report [7].

boson. Subsequent data accumulated since that summer has conclusively shown that this resonance *is* the Higgs boson, *i.e.* that it is the particle excitation associated to the mechanism of electroweak symmetry breaking. The central question since the discovery of the Higgs is: do the properties of the Higgs hint at new physics beyond the Standard Model? Thus far, the measured properties of the Higgs are consistent with Standard Model predictions, see Fig. 1.1; further precise measurements in ongoing and future experiments are crucial to discern what new physics—if any—couples to the Higgs.

1.1.1 The Higgs, dimensional analysis, and the hierarchy problem

The Higgs boson is rather strange compared to the other known fundamental particles and there are good reasons to anticipate new physics to help explain its mysterious and unnatural properties. To understand why this is the case, we need to know what the Higgs achieves for the Standard

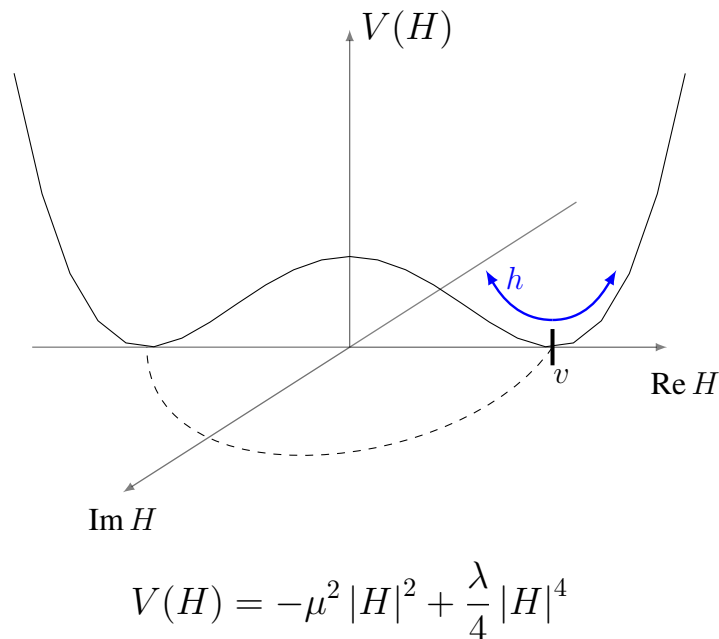


Figure 1.2: The Higgs potential. It is minimized at $\langle |H| \rangle = v$, where the Higgs takes a vacuum expectation value and spontaneously breaks electroweak symmetry. The physical Higgs boson, h , discovered at the LHC is the fluctuation around the minimum. Locally, the potential for h looks like $V(h) = \frac{1}{2}m_h^2 h^2 + \dots$ where $m_h^2 \approx (125 \text{ GeV})^2$ is the physical Higgs mass. A technical aside: In the diagram, two flat directions of the potential are suppressed (H is a doublet with two complex = four real degrees of freedom); therefore, the axes are more properly labeled as the real and imaginary parts one component of H . The flat direction along the bottom of the well together with the two suppressed flat directions correspond to the Nambu Goldstone modes which become the longitudinal components of the massive W^\pm and Z electroweak gauge bosons.

Model (SM). There is overwhelming evidence that the photon and the weak gauge bosons W^\pm and Z are unified under a common force, called the electroweak (EW) force or EW symmetry. Something must break this symmetry, as quite clearly the photon is massless while W^\pm and Z bosons are not. Perhaps most physically, some new physics is required to unitarize W^+W^- scattering. The simplest explanation is that there is an additional scalar (spin 0) particle. The dynamics of the underlying theory cause this scalar to condense in the vacuum—acquire a vacuum expectation value (vev)—thus spontaneously breaking EW symmetry. This is the Higgs boson.

The addition of the Higgs boson is the puzzle piece which neatly fits together electroweak symmetry and provides a mechanism for giving mass to fundamental particles, such as the weak gauge bosons and the electron. At first glance, this is very pleasing. Upon closer inspection, however, the whole thing begins to look a bit bizarre. The very same framework—local quantum field theory—that successfully predicted the unification of EW symmetry would also posit that the weak scale m_W lies *many* orders of magnitude beyond the observed value of $m_W \sim 100 \text{ GeV}$.

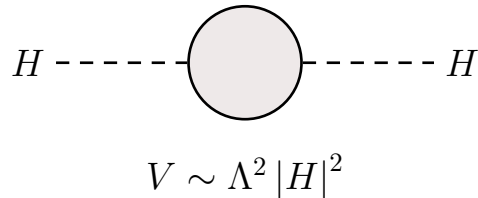
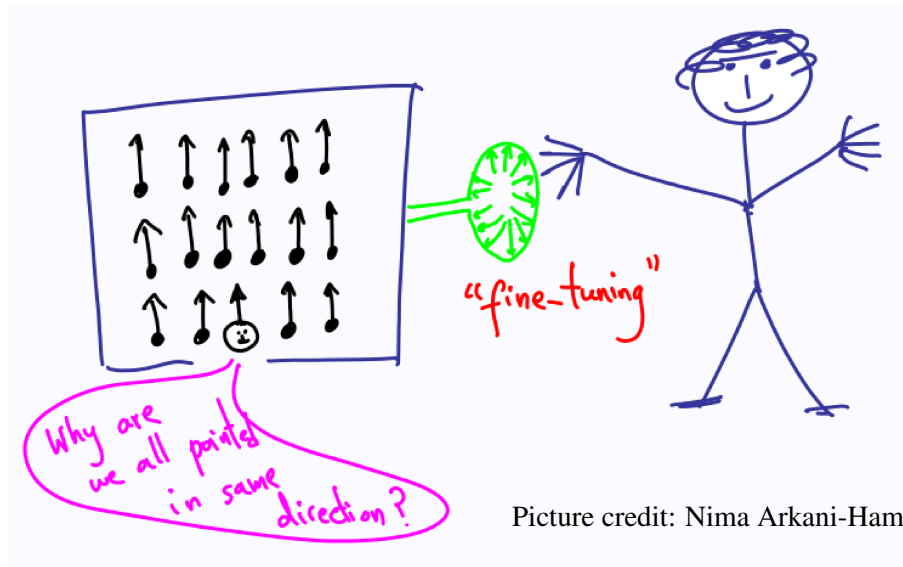


Figure 1.3: Absent some reason, quantum corrections to the Higgs mass-squared parameter (μ^2 in the previous figure) are quadratically sensitive to the scale of new physics, Λ . This follows from simple dimensional analysis. The two point function depicted corresponds to a term $|H|^2$ in the potential V . The potential has mass dimension four, while $|H|^2$ has mass dimension two; the extra two powers of mass dimension must come from some scale in the problem.

Based on the known particle content and interactions of the SM, to have the weak scale at the observed value requires an incredible fine tuning of parameters, on the order of one part in 10^{34} ! It is important to understand that such a fine tuning does not violate any physical principle per se (unlike, say the breakdown of unitarity if there was no Higgs), but it does stand affront to all of our experiences in physics and quantitative science.

A rather simple way to understand the unnaturalness of the weak scale is via dimensional analysis. The SM contains only a single dimensionful parameter, the Planck mass $M_{\text{pl}} \sim 10^{19}$ GeV, which sets the scale for when quantum effects of gravity must be taken into account. Dimensional analysis asserts that, unless there is some physical reason, any other dimensionful quantity that arises is proportional to an appropriate power of M_{pl} times some order one coefficient. In particular, dimensional analysis would predict the mass-squared parameter for the Higgs is $\mu^2 \sim c M_{\text{pl}}^2$ with c and $\mathcal{O}(1)$ coefficient. But the weak scale is at 100 GeV while $M_{\text{pl}} \sim 10^{19}$ GeV, so $c \sim 10^{-34}$! One either concludes that this is an incredible fine-tuning of parameters or there is some other physical reason which sets c to such a small value. This, in essence, is the so-called “fine-tuning problem” or “hierarchy problem”, referring to the large hierarchy between the weak scale and the Planck scale.

Even though dimensional analysis is the underlying reason why back-of-the-envelope estimates work in any field, it is important to see that this principle is already at work for the other parameters in the SM. We’ve stated that there is a mass parameter for scalar particles, like the Higgs, that is allowed in the theory. What about for fermions? In fact, chiral symmetry does not allow fundamental mass parameters for the fermions of the SM. The only way fermions of the SM can have a mass is if it arises dynamically, *e.g.* through a (chirally-symmetric) yukawa coupling to a scalar field, $\mathcal{L} \sim y \phi \psi \psi$, where the scalar ϕ obtains a vacuum expectation value. Here we see a specific reason, namely symmetry, that explains why fermion masses can be naturally small compared to M_{pl} . Besides fermion masses, there is another dimensionful parameter in the SM: $\Lambda_{\text{QCD}} \sim \text{GeV}$, the energy scale characterizing the masses of protons and neutrons. This scale is understood to emerge dynamically, as a result of QCD interactions being strongly coupled: $\Lambda_{\text{QCD}} \sim e^{-8\pi^2/g_s^2} M_{\text{pl}}$, where g_s is the QCD coupling constant at the UV scale (here taken to be M_{pl}). Dimensional analysis would suggest that the coupling constant, being a dimensionless parameter of the theory, is



Picture credit: Nima Arkani-Hamed

Figure 1.4: If no new physics enters between the weak scale and M_{pl} , then the mass-squared parameter μ^2 has to be incredibly fine-tuned to cancel the $\Lambda^2 \sim M_{\text{pl}}^2$ sized corrections. Models of new physics attempt to alleviate this fine-tuning by placing Λ much closer to the electroweak scale. Picture taken from a presentation by Nima Arkani-Hamed.

of order one. Because of the exponential suppression, however, $g_s \sim 1$ can easily give a large hierarchy between Λ_{QCD} and M_{pl} .

1.1.2 Natural solutions

Based on our experience with the other parameters in the Standard Model, as well as dimensional analysis in general, we search for a *reason* for the large hierarchy between the electroweak and Planck scales. It is important to note that such explanations generically invoke some form of new physics near the electroweak scale; if the new physics is much above the weak scale, the fine-tuning problem is reintroduced.

There are two explanations that have dominated the discussion on solutions to the hierarchy problem; in fact, we have encountered both already in the Standard Model in the discussion above. The first is supersymmetry, which is a symmetry that relates scalars to fermions. Because of this, the chiral symmetry which protects fermion masses is inherited by their scalar partners. Therefore, supersymmetry provides a symmetry to explain the small value of the Higgs mass (compared to the Planck scale). The second general explanation seeks to make the electroweak scale dynamically arise in the same way the QCD scale arises, *i.e.* to find some reason such that $m_{\text{weak}} \sim e^{-8\pi^2/g^2} \Lambda$ for some order one coupling g and some UV scale Λ (it could be $\Lambda = M_{\text{pl}}$). These models are known as composite models, as the Higgs and/or other SM particles typically are composite particles of

some other new, fundamental degrees of freedom (much like how hadrons—*e.g.* pions, protons, *etc.*—are composed of quarks).

From a theoretical perspective, the two general solutions to the hierarchy problem mentioned above are discriminated as weakly coupled versus strongly coupled. Supersymmetry is the only known, phenomenologically viable member of the weakly coupled camp. The theory space for strongly coupled solutions is larger—some promising and well known examples are technicolor, extra-dimensions, and little Higgs theories. And, of course, we can have strongly coupled models which are also supersymmetric.³

While both of the above general solutions provide reasons for a “natural” Higgs mass, it is worth pointing out that they generically predict different values of the Higgs mass. Because of this, the value of Higgs mass could be a pretty good indicator of one of the above scenarios. With a broad brush, weakly coupled scenarios predict a lighter Higgs mass, close to the EW gauge bosons in the ~ 90 - 115 GeV range, while strongly coupled scenarios predict heavier Higgs masses, typically > 150 GeV. Now that we have discovered the Higgs, we know its mass is 125 GeV, placing it (somewhat dishearteningly) in tepid waters for either scenario.

Before moving on, there is another explanation for the hierarchy problem worth mentioning which has become much more seriously considered over the past decade. The idea: maybe the Higgs mass simply is incredibly fine-tuned. In brief, it is plausible that our universe is one of many—part of a multiverse where the vacuum states of causally disconnected regions may differ, leading to different values of parameters and physical laws in these universes. Essentially, if the landscape of possible vacua is vast and there are ways to populate these vacua, our Universe may just happen to lie at an “unlikely” point where there are fine-tuned parameters. I put “unlikely” in quotes, since the way of determining these probabilities is currently not known (the so-called measure problem).

One of the reasons the multiverse has attracted such attention in recent years is that we know there is a naturalness problem worse than the electroweak hierarchy problem. In 1998, it was discovered that our vacuum energy (dark energy) is very very small, but non-zero; naturalness would predict Planck scale values—this appears to be a fine-tuning on the order of 10^{120} ! Besides anthropic reasoning with the multiverse, there is no known explanation for this fact. However, it is also reasonable to believe that the fine-tuning in the Higgs is qualitatively different than that of vacuum energy; the hierarchy problem with the Higgs comes from the experimentally verified framework of quantum field theory, while dark energy is intrinsically related to gravity where our understanding of quantum effects is limited and without experimental guidance.

³Besides providing natural explanations of the Higgs mass, many of the above models are attractive because they can explain other unknown physics. For example, they may provide candidate dark matter particles, unify the strong and electroweak forces into a grand unified theory, or play a pivotal role in understanding quantum gravity. While we will not discuss it in this thesis, supersymmetry hits all of these points and for this reason has long been the leading candidate for new physics scenarios (although, the fact that we have not seen supersymmetry at this stage makes it very difficult to satisfy all these points at once).

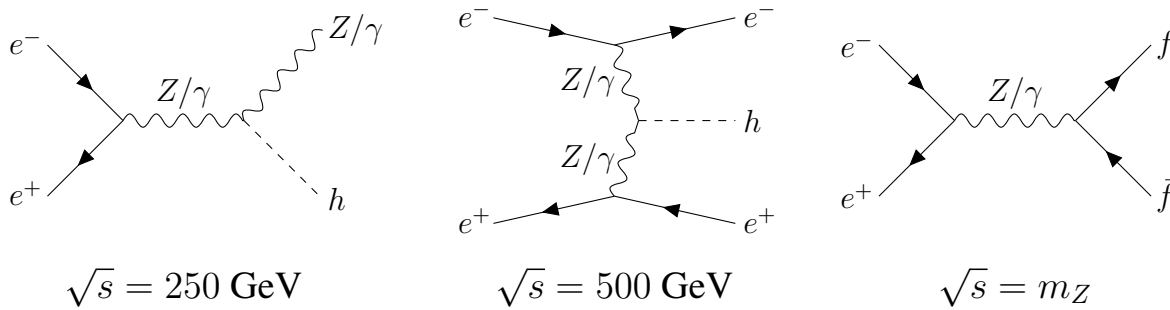


Figure 1.5: *Left and center:* Higgs boson production channels for an e^+e^- collider running at $\sqrt{s} = 250 \text{ GeV}$ and 500 GeV . *Right:* Possible future e^+e^- machines may do a run on the Z -pole to improve electroweak precision measurements, *i.e.* GigaZ at ILC and TeraZ at TLEP.

1.1.3 Precision Higgs physics

Having discovered the Higgs boson, its unnatural and mysterious features immediately become pressing questions. As sketched above, models of new physics address these questions by making the Higgs more natural if we can avoid a finely-tuned cancellation between the bare parameter and the quadratic divergence in its mass-squared and less mysterious if we can explain why there is only one scalar in the theory and what dynamics causes it to condense in the Universe. The new physics introduced in these models inevitably influences properties of the Higgs, such as decay rates, branching fractions, self-coupling, *etc.*

Obviously we need to study this new particle as precisely as we can, which calls for an e^+e^- collider such as the International Linear Collider (ILC) or a circular machine (TLEP/CEPC). An e^+e^- machine would be a Higgs factory, designed to operate in such a way to produce Higgs bosons in a controlled, repeatable fashion that is most amenable to teasing out the properties of the Higgs. The ILC has been through an intensive international study through six-year-long Global Design Effort that released the technical Design Report in 2013 [8]. Given the technical readiness, we hope to understand the fiscal readiness in the next few years. The studies on a very high intensity circular machine have just started [9].

In the past, precision measurements using electrons revealed the next important energy scale and justified the next big machine. The polarized electron-deuteron scattering at SLAC measured the weak neutral currents precisely [10], which led to the justification of Sp \bar{p} S and LEP colliders to study W/Z bosons. The precision measurements at SLC/LEP predicted the mass of the top quark [11] and the Higgs boson [12], which were verified at the Tevatron [13, 14] and LHC [5, 6], respectively. We hope that precision measurements of the Higgs boson will again point the way to a definite energy scale.

There is a caveat in the above narrative. In those past experiments, some form of new physics was all but guaranteed; the absence of new states would have conflicted with some deep physics principle, typically unitarity. Currently, there is no such bullet-proof argument for new physics at the LHC or future lepton colliders—as discussed earlier, fine-tuning remains a logical possibility.

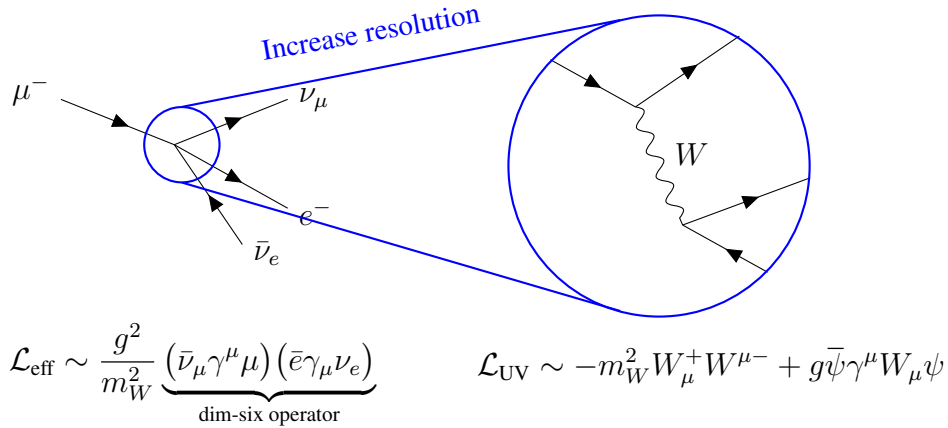


Figure 1.6: One of the first and most famous effective field theories is that describing the weak interactions. Here we have depicted how the muon decays via the weak interactions. This decay can be described by the effective dimension-six operator above. This operator is suppressed by the scale of where new physics enters, namely $\Lambda = m_W$. At short distances, we see that the effective theory is replaced by the UV theory which contains the W boson.

There is a growing camp, of which I am a member, that views this not as a problem, but an opportunity. In particular, I think it is important to *test* the hypothesis of fine-tuning if we do not find evidence of new physics.

A lepton collider is essential for ruling out new physics in regions of parameter space that can be very hard or impossible to access at the LHC. Together with the LHC, a lepton collider could test the hypothesis of fine-tuning down to the 1% level. A 1% fine-tuning is quite strange, but not without precedent in physics. A future 100 TeV proton collider could test fine-tuning to 10^{-4} levels, an unheard of level. In this regard, a future lepton and very high energy proton collider are complementary and essential if we wish to test the fine-tuning hypothesis.

1.1.4 The SM effective field theory

Precision physics programs offer *indirect* probes of new physics, thereby necessitating a model-independent framework to analyze potential patterns of deviation from known physics. This framework is most naturally formulated in the language of an effective field theory (EFT) which, for our interests, consists of the Standard Model (SM) supplemented with higher-dimension interactions,

$$\mathcal{L}_{\text{eff}} = \mathcal{L}_{\text{SM}} + \sum_i \frac{1}{\Lambda^{d_i-4}} c_i \mathcal{O}_i. \quad (1.1)$$

In the above, Λ is the cutoff scale of the EFT, \mathcal{O}_i are dimension d_i operators that respect the $SU(3)_c \times SU(2)_L \times U(1)_Y$ gauge invariance of \mathcal{L}_{SM} , and c_i are their Wilson coefficients. In the following, we loosely use the term Wilson coefficient to refer to either c_i or the operator coefficient, c_i/Λ^{d_i-4} . The meaning is clear from context.

In essence, effective field theory takes the relevant degrees of freedom and parameterizes all ways in which these degrees of freedom may interact. In the above, the SM fields are the relevant degrees of freedom, the operators \mathcal{O}_i describe possible interaction terms that are not present in the SM Lagrangian \mathcal{L}_{SM} , and the Wilson coefficients parameterize the strength of these interactions.

In practice, due to suppression by the high scale Λ , the irrelevant operators kept in the EFT are truncated at some dimension. The estimated per mille sensitivity of future precision Higgs programs, together with the present lack of evidence of BSM physics coupled to the SM, justifies keeping only the lowest dimension operators in the effective theory. In the SM effective theory this includes a single dimension-five operator that generates neutrino masses (that we henceforth ignore) and dimension-six operators.

The SM EFT described by Eq. 1.1 is the central topic of our analysis in Chap. 2. We will occupy ourselves with understanding how to *use* the SM EFT to probe and constrain new physics models. As with any effective field theory, there is a basic three step procedure to using it: matching, running, and mapping. In the first step, we take some model of new physics and match it onto the EFT, *i.e.* we integrate out heavy particles (that are not directly accessible in precision measurements) and obtain the interactions induced in the EFT. In essence, this amounts computing the Wilson coefficients in Eq. 1.1 in terms of the parameters describing the new physics. Next, renormalization group equations are used to evolve (run) the Wilson coefficients from the matching scale down to the energy scale at which observations are made. Finally, the Wilson coefficients at the observation scale are mapped onto physical observables, completing the connection between new physics and precision measurements.

In Chap. 2 we address each of these three steps in detail. Based on a technique introduced a few decades ago [15], we develop a method for computing the effective action through one-loop order in a manifestly gauge-covariant manner, termed the covariant derivative expansion (CDE). Compared to more traditional methods, *e.g.* Feynman diagrams, the CDE significantly eases computation of the Wilson coefficients since one never has to work with separate, gauge non-invariant pieces at intermediate steps of the calculation. We use the CDE to compute the Wilson coefficients in several non-trivial and phenomenologically interesting models of new physics.

In the past few years, there has been great progress in computing the anomalous dimension matrix in the SM EFT, which determines the renormalization group evolution of the Wilson coefficients. Our considerations of renormalization group running, therefore focus on determining when this step is of practical relevance and how to make use of existing calculations of the anomalous dimension matrix. This naturally leads us to a discussion of operator bases.

Of the dimension-six operators in the Standard Model EFT, purely bosonic operators (made from just Higgs and gauge bosons) especially lead to effects on present and future electroweak and Higgs precision observables. In our mapping analysis, we compute the effects of all CP conserving, purely bosonic dimension-six operators (16 in total) on precision Higgs and electroweak observables. Specifically, we compute their impacts to leading order (linear in the Wilson coefficients) on electroweak precision observables (S, T, U, V, W, X, Y), electroweak triple-gauge couplings, all Higgs partial decay rates, and all Higgs production cross-sections relevant for the LHC and a lepton collider.

Finally, after all the build up of understanding how to use the SM EFT, we put it to work to study

what precision Higgs measurements may tell us for two very different new physics scenarios. One is a singlet scalar coupled to the Higgs boson, where impacts arise at the tree level. It can achieve first-order electroweak phase transition which would allow electroweak baryogenesis. The other is the scalar top in the Minimal Supersymmetric Standard Model (MSSM), where impacts arise at the one-loop level. It will help minimize the fine-tuning in the Higgs mass-squared. In both cases, we find both precision Higgs and precision electroweak measurements to be sensitive probes.

1.2 Dark matter

1.2.1 Cosmological evidence of dark matter

How dark matter (DM) came to light is one of those stories that makes you love science. It has all of the ingredients: unexpected findings in experiments, quantitative arguments explainable to anyone who has taken an introductory physics course, upending privileged viewpoints about the nature of our Universe, evidence that essentially puts the nail in the coffin establishing its existence, and—perhaps most importantly—all the while remaining completely and utterly mysterious.

It begins in the 1930s when astronomer Fritz Zwicky observed that the velocities of galaxies further out in the Coma Cluster were much greater than could be explained by luminal matter. He suggested that there exists some other form of matter that is enclosed by the orbit to explain the large velocity of these objects.

Zwicky's observation was not fully appreciated until the 1970s when Vera Rubin and collaborators made detailed measurements of galactic rotational curves in spiral galaxies. Her group not only confirmed that rotational velocities do not decrease as the objects get further from luminal matter, but also observed that the rotational velocity curves flatten out to a somewhat constant value. If a form of matter existed in a halo about the galaxy, then this could explain the observed rotational curves. We call this matter dark matter.

It is a simple, informative, and fun exercise to determine the DM mass distribution in these of halos simply by requiring flat rotational curves. We only require Newton's force law. From $F = ma$ with $F = GmM/r^2$ Newton's gravitational force and $a = v^2/r$ since the orbit is essentially uniform circular motion, the velocity distribution is given by

$$v^2 = \frac{GM(r)}{r}. \quad (1.2)$$

For the velocity distribution to be constant as a function of radius, the amount of mass enclosed must grow linearly with the radius, $M(r) \propto r$. With $M(r) = \int d^3r \rho(r) \sim \int dr r^2 \rho(r)$, we easily see that the DM density falls with the inverse-square of the distance, $\rho(r) \propto 1/r^2$.

In addition to galactic rotation curves, we now have essentially irrefutable evidence for dark matter from detailed maps of the matter content in our Universe obtained by measurement of the cosmic microwave background and from gravitational lensing experiments that allow us to reconstruct detailed matter distributions in galaxies. We know that dark matter makes up about 80% of the matter in our Universe. We know that it had a profound impact on galaxy formation.

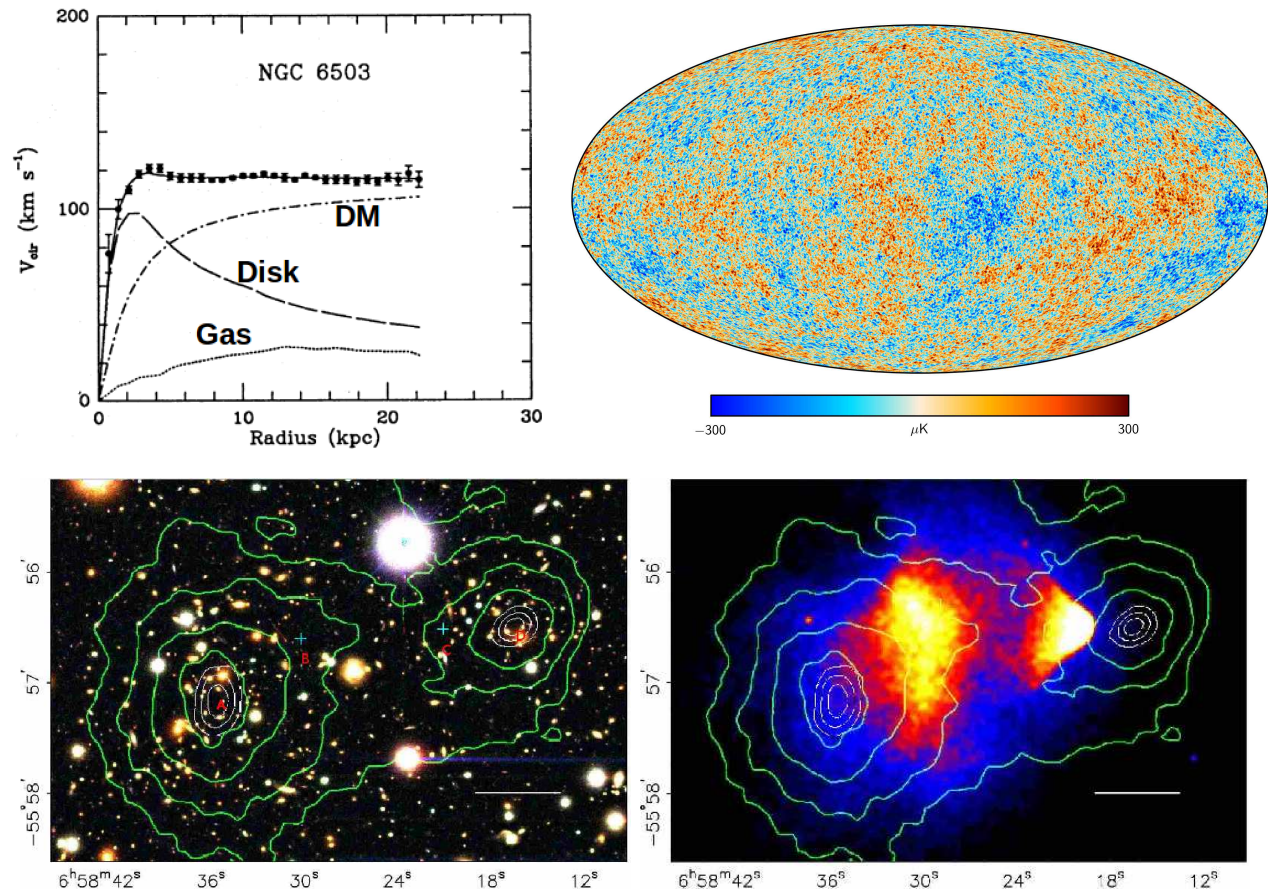


Figure 1.7: *Top left*: Observed galactic rotational curve together with predicted rotational curves from a DM halo, the galactic disc, and galactic gas [16].

Top right: As the Universe expanded and cooled, photons eventually were no longer energetic enough to prevent electrons and protons from binding together, and thus neutral hydrogen was formed and photons were left to wander freely. These photons make up the Cosmic Microwave Background (CMB) and reveal an incredible homogeneity of the Universe on large scales. Quite obviously, the Universe is not perfectly uniform at smaller distances. These inhomogeneities present as small ($\sim 10^{-5}$) differences in the temperature of the background radiation at different points in Universe. The picture shows a map of these anisotropies, as measured by the Planck satellite [17]. Variations in photon temperature arise from differing gravitational pull on the photons as a result of different amounts of dark matter in local regions. The anisotropies in the CMB, therefore, reveal a map of as well as the amount of DM in our Universe.

Bottom: The so-called bullet cluster, showing the matter distribution in the collision of two galaxy clusters [18]. In such a collision, the gas in the clusters (accounting for $\sim 90\%$ of the visible matter) is expected to collide and emit radiation, while stars, planets, and such will pass through (not a high enough density for collisions). Likewise, any dark matter present will pass through unaffected. The left shows the stars in the clusters, while the right shows the colliding gas. The contour lines mark lines of gravitational lensing, indicating where most of the mass is. The contours reveal that the vast majority of mass passed right through each other, and basically solidifies the existence of DM (see the title of the original paper [18]).

But all of this evidence is gravitational in nature and does not tell us much of anything about the particle nature of DM. One of the few properties we can say with any certainty is that DM has mass. This sounds like a pretty underwhelming statement—don’t all of those nice gravitational observations mentioned above provide some clue about the mass of dark matter? Sure they do, but if you felt the conclusion that DM has mass sounded less than profound, then your socks probably won’t be rocked by the next statement. The possibly allowed values of dark matter mass span more than 80 orders of magnitude! Specifically,

$$10^{-31} \text{ GeV} \lesssim m_{\text{DM}} \lesssim 10^{50} \text{ GeV}, \quad (1.3)$$

where we remind the reader that the proton has a mass of about one GeV and Earth’s mass is about 3×10^{51} GeV. The lower bound on the dark matter mass comes from the requirement that dark matter be localized on galactic scales [19]. The upper bound comes from micro-lensing searches for compact halo objects [20].

1.2.1.1 A diversion on the lower bound of allowed DM mass

By requiring that DM “fits” inside galaxies, we can obtain a lower bound on the dark matter mass [19]. I love this estimate, so let’s do it. The physics behind it is directly analogous to the hydrogen atom and Bohr radius. The smaller the mass of a particle, the longer its Compton wavelength, $\lambda \sim \hbar/mc$.⁴ We have observed features in dark matter density profiles down to about a kiloparsec ($\text{kpc} = 3 \times 10^{19}$ m). Therefore, to ensure that dark matter stays localized, we minimally need to require that the Compton wavelength of dark matter fits in this region, $\lambda_{\text{DM}} \lesssim r_0 \sim 1 \text{ kpc}$.

We can do better on this estimate, however. To bind a DM particle, we have the gravitational pull of other DM particles competing against the momentum of the DM particle (from the uncertainty principle, $p \sim \hbar/r_0$). The gravitational force is an inverse-square law, and recognize this to be the exact physics of the hydrogen atom and the Bohr radius. To understand our “gravitational atom”, let us review the hydrogen atom in a suggestive fashion. The Coulomb potential is given by

$$V_{\text{EM}}(r) = \frac{e^2}{r} = \frac{\hbar c e^2}{r \hbar c} = \alpha_{\text{EM}} \frac{\hbar c}{r},$$

where $\alpha_{\text{EM}} = e^2/\hbar c = 1/137$ is the fine-structure constant and characterizes the strength of the electromagnetic force. Note how we separated out a factor of $\hbar c$ in the above potential to arrive at the dimensionless coupling constant α_{EM} . If α_{EM} is very small, so that the electromagnetic force is very weak, then we expect a large binding radius for the electron with the proton. In other words, the Bohr radius is $r_B = \lambda_e/\alpha_{\text{EM}}$ where $\lambda_e = \hbar/m_e c$ is the Compton wavelength of the electron. Indeed, plugging in numbers we find the Bohr radius is half of an angstrom.

We follow the exact same steps for the “gravitational atom”. The gravitational potential is given by

$$V_G = \frac{G m_{\text{DM}} M}{r} = \alpha_G \frac{\hbar c}{r},$$

⁴We are using one other fact here: the kinetic energy of the particle is smaller than the mass. This is observationally true for DM; it has to be “cold” or “non-relativistic” in order for it to clump enough in the early Universe and start the process of galaxy formation.

where $\alpha_G \equiv Gm_{\text{DM}}M/\hbar c$ is a dimensionless coupling characterizing the strength of the gravitational force and $M(r)$ is the total mass of dark matter enclosed within r . As the equations are exactly the same as the hydrogen atom, we can immediately write down the Bohr radius,

$$r_B = \frac{\lambda_{\text{DM}}}{\alpha_G} = \frac{\hbar^2}{Gm_{\text{DM}}^2 M}.$$

Taking $r_B = r_0 \sim \text{kpc}$, we arrive at a lower bound on the DM mass. Concretely, taking as a very rough approximation a constant density⁵ $\rho_{\text{DM}} = 2 \times 10^{-22} \text{ kg/m}^3$ we have $M(r) = \int d^3r \rho_{\text{DM}} \sim \rho_{\text{DM}} r_0^3$ and we find

$$m_{\text{DM}} > \left(\frac{\hbar^2}{G\rho_{\text{DM}} r_0^4} \right)^{1/2} \sim 10^{-31} \text{ GeV}/c^2,$$

as quoted above.

1.2.2 Searching for DM

While we have a preponderance of gravitational evidence for dark matter, how do we go about trying to make up the dearth in knowledge of its physical properties? We will assume that DM couples to the Standard Model in some fashion besides via gravity. However, it remains a logical possibility that DM has no non-gravitational interactions with SM particles. But if this were the case, wouldn't it just be the pits? But seriously, there are good theoretical prejudices to believe that DM interacts weakly with our sector. Many models of new physics introduced to solve some other problem—the hierarchy problem, the strong CP problem, quantum gravity, *etc.*—often come with a DM candidate as an added bonus.

Ways to probe dark matter properties fall into two categories, direct and indirect detection. The basic idea of direct detection is to take a bunch of matter, stick it in a place (*e.g.* deep underground) where there is very little background of SM particles interacting with this matter, and search for events where a DM particle passes through the detector and scatters. Since DM is all around us (the local DM density is $0.3 \text{ GeV}/\text{cm}^3$), over a prolonged period a large number of DM particles pass through the detector. Therefore, despite the fact that DM interacts very weakly, there is a non-negligible chance of having a few scattering events. Another type of direct detection is if DM is produced in collisions at a high energy collider, such as the LHC.

On the other hand, indirect detection looks for remnants of dark matter interactions. One example is searching for DM annihilation or decay products of astrophysical origin, *e.g.* from our galactic center or from clusters of galaxies. Another example is to look for impacts that DM interactions may have on other systems, *e.g.* how they influence events in our cosmic history.

The work in this thesis centers around indirect detection. In Chap. 3 we will study how DM influences the formation of nuclei at the beginning of the Universe and in Chap. 4 we will provide a possible DM explanation for an unknown photon signal seen in stacks of galaxy clusters.

⁵The kiloparsec scale comes from observing that near the center of galaxies, the DM distribution is more cuspy, falling off faster than the $1/r^2$ discussed earlier. In this regime, the DM density is very much not constant. However, the change to the estimate is some order one number, which is unimportant for our purposes.

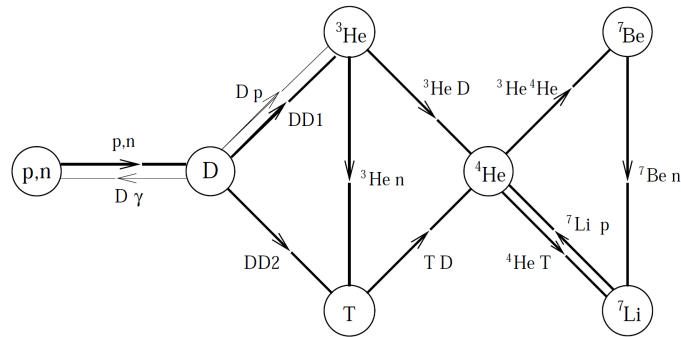


Figure 1.8: Network of nuclear reactions involved in nucleosynthesis [21].

1.2.3 Dark matter and Big Bang nucleosynthesis

Just after the Big Bang, the Universe was one extremely compact and extremely hot soup of matter. If we assume that dark matter has some interaction with SM, one obvious hypothesis to explore is what happens if DM is also a part of this hot soup. In other words, we postulate that DM is thermalized after the Big Bang through interactions with regular matter and ask how this impacts our cosmic evolution.

In slightly more detail, we assume dark matter is a weakly interacting massive particle that started its cosmic history in thermal equilibrium. This equilibrium is achieved by scattering off of hot SM particles in the thermal bath and annihilations from DM to SM particles and vice versa. As we have not “seen” dark matter directly, we know these interactions must be weak. As the Universe expands and cools, dark matter eventually falls out of thermal equilibrium because of the small dark matter coupling. As dark matter no longer efficiently annihilates, the dark matter density freezes-out.

The assumption of thermalization provides two powerful statements on DM: first, it restricts the allowed mass region to 11 orders of magnitude, $\text{keV} \lesssim m_\chi \lesssim 100 \text{ TeV}$, with the lower and upper bounds coming from the requirement that dark matter be cold [22] and its annihilation unitary [23], respectively. Second, if DM is a thermal relic, its annihilations must freeze-out to reach the observed current abundance, providing an estimate on the strength of DM interactions. In particular, assuming annihilation is s -wave dominated, in order to meet the observed abundance, freeze-out requires a weak scale cross-section that is nearly independent of mass, $\langle\sigma v\rangle_{\text{th}} \simeq 3 \times 10^{-26} \text{ cm}^3/\text{s}$.

Of course, some dark matter particles will occasionally meet and annihilate, but the number of such events is not sufficient to change the total amount of dark matter present in the Universe. Such relic annihilations can nevertheless leave imprints in our cosmic history or be detectable by searching for their annihilation products. In Chap. 3 we study how relic annihilations can impact the formation of light nuclei during Big Bang nucleosynthesis (BBN) through injection of hadronic and/or electromagnetic energy.

Big Bang theory posits that our Universe started as a very small, extraordinarily hot soup which has expanded and cooled to form the present day Universe. One of the first pieces of evidence for

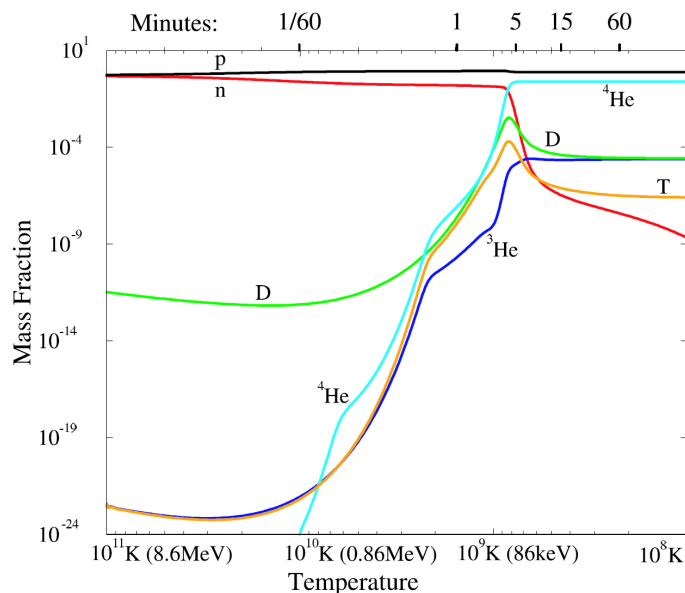


Figure 1.9: Predicted primordial abundances of light nuclei during BBN as the Universe expands and cools [21].

this theory was Big Bang nucleosynthesis, a process which quantitatively predicts the number of light nuclei that form as our Universe cooled. Here is a brief sketch of the events of BBN:

- About one second after the Big Bang, at temperatures of about 1 MeV, the Universe cooled to a point where neutrinos decoupled and set an initial relative abundance of neutrons relative to protons. The vast majority of neutrons end up in helium, so the relative abundance of hydrogen to helium in our Universe gives a test for the predicted relative abundance.⁶
- At $t \approx 100$ s ($T \approx 100$ keV) the the deuterium bottleneck opens up: the Universe has cooled to a point that it becomes energetically favorable for a neutron and proton to form deuterium. Although helium has a much larger binding energy, around 25 MeV, it was unlikely for two neutron and two protons to meet simultaneously to form ${}^4\text{He}$. Therefore, deuterium (binding energy of about 2 MeV) acts as a bottleneck since it must first be created before ${}^4\text{He}$ formation to proceed.
- With some deuterium present, higher mass nuclei can form. For example, a deuterium nucleus may capture a proton to form ${}^3\text{He}$ which may then collide with another deuterium

⁶This estimate is fairly easy to perform. Neutrons and protons are Boltzmann distributed. Therefore, at the time neutrinos decouple (no longer able to inter-convert neutrons and protons), their relative abundance is set by $n/p \approx e^{-(m_n - m_p)/T_{\text{dec}}} \approx 1/6$, where $T_{\text{dec}} \approx 0.7$ MeV. Free neutrons decay with a lifetime of 887 seconds, so by the time deuterium and helium begin to form, the neutron to proton ratio is slightly reduced, $n/p \approx \frac{1}{6} e^{-t_{\text{deuterium}}/\tau_n} \approx 1/7$. With $n/p = 1/7$, one easily sees that for approximately every ${}^4\text{He}$ nucleus we expect about 12 hydrogen nuclei. This leads to a predicted mass fraction of helium relative to hydrogen of $Y \approx 4/16 = 25\%$, which fits well with observations.

nucleus to produce ${}^4\text{He}$ plus a proton. Or a deuterium nucleus may capture a neutron to become ${}^3\text{H}$, which then collides with a ${}^4\text{He}$ nucleus to form ${}^7\text{Li}$.

- At about 3 minutes after the Big Bang, at $T \approx 50$ keV, BBN finishes and the relative abundances of nuclei are set. These nuclei eventually go on to become stars—we can observationally establish abundance of the nuclei, and therefore test BBN predictions, by studying the spectra of stars.

Computationally, the above picture emerges by solving a slew of coupled Boltzmann equations that describe the rates of nuclei formation as the Universe expands. Because of the many different nuclear reactions available, the coupled nature of these differential equations, and the fundamental role played by the expansion rate of the Universe, it is an extremely non-trivial result that the predicted abundances fit so well with the observed values. BBN was, and still is, one of the great triumphs of the Big Bang theory.

Because the physics of BBN is very well understood, it offers a particularly clean environment to probe non-standard effects, such as DM annihilation. As we will explain in Chap. 3, DM annihilations occurring during and after BBN can inject hadronic and/or electromagnetic energy which alters primordial abundances of the nuclei predicted by standard BBN. This allows us to place constraints on DM properties, such as its mass and annihilation rate. In our study, we provide a simple, physical explanation for understanding the scaling behavior of these constraints. Estimates based on these scaling behaviors indicate that BBN severely constrains hadronic and radiative dark matter annihilation channels in the previously unconsidered dark matter mass region $\text{MeV} \lesssim m_\chi \lesssim 10$ GeV. Interestingly, we find that BBN constraints on hadronic annihilation channels are competitive with similar bounds derived from the cosmic microwave background.

1.2.4 A keV string axion

In previous subsection, we considered dark matter to be stable—its presence potentially visible through relic annihilations with other DM particles. Another logical possibility is that DM is a long-lived particle that can eventually decay into SM particles. Based on the fact that the Universe currently holds much DM, clearly the lifetime must be on the order of the age of the Universe or greater.

Recently, an unidentified line at about 3.5 keV in the X-ray spectrum of galaxy clusters [24, 25] was observed. Although it has since been disputed by several other (non-) observations [26], it is interesting to consider that it (or a line observed in the future) could be a signal of dark matter decaying into photons. Two options immediately jump out. The first is the possibility that this is a sterile neutrino with a keV size mass. A sterile neutrino is a specific type of weakly interacting massive particle that would be thermalized in the early Universe, as discussed in the previous subsection. The other option is that the signal originates from an axion-like dark matter particle.

In Chap. 4, we will consider the second option, and propose a model to produce a keV size axion DM candidate that could explain the observed signal. Axions have a theoretical origin in the solution of the strong CP problem of QCD. We use the term axion more generally to refer to any

pseudo-Nambu Goldstone boson associated with the spontaneous breaking on an anomalous $U(1)$ global symmetry.

Specifically, we consider a supersymmetric setup and show how the keV scale can emerge generally and with an axion candidate near this scale. The present lack of evidence for supersymmetry (SUSY) and other long standing issues with phenomenological consequences of SUSY all seem to prefer a spectrum of supersymmetric scalar particles around $m_{\text{SUSY}} \approx 100\text{-}1000$ TeV. The minute we assume $m_{\text{SUSY}} \approx 1000$ TeV there is an immediately derived energy scale of $m_{\text{SUSY}}^2/M_{\text{pl}} \approx \text{keV}$.

One possibility is that m_{SUSY} may be the scale of supersymmetry breaking itself. Another possibility, which we pursue, is that $m_{\text{SUSY}} \approx 100\text{-}1000$ TeV may be the gravitino mass. In this case, the scale of SUSY breaking is large, $\Lambda_{\text{SUSY}} \approx (m_{\text{SUSY}}M_{\text{pl}})^{1/2} \approx 10^{12}$ GeV. The keV scale emerges parametrically as $\Lambda_{\text{SUSY}}^4/M_{\text{pl}}^3$. Moreover, we note that for an axion to reproduce the decay rate observed in [24, 25], the axion decay constant must be large, $f \approx 0.1M_{\text{pl}}$. Therefore, discussing only two scales, Λ_{SUSY} and M_{pl} seems well-warranted.

Note that the necessity of lifting flat directions to break SUSY means that dynamical supersymmetry breaking models generically contain spontaneously broken, anomalous $U(1)$ symmetries, thereby providing axion-like particles. However, these axions are generically heavy, on the order Λ_{SUSY} . However, if there is an additional axion-like particle which couples the dynamical SUSY breaking sector, a light linear-combination will survive.

Given the large axion decay constant and the coupling to electromagnetism, a well-motivated possibility is that axion arises from string theory. If we consider a universal string axion, which has couplings to all gauge sectors, then this string axion can mix with the axion from dynamical SUSY breaking to become an axion with a keV size mass that can decay to photons.

We provide an explicit model in Chap. 4 which produces the features outlined above. We address possible cosmological issues that arise from our explicit example, although some of our solutions to these issues can be applied more generally.

Chapter 2

How to Use the Standard Model Effective Field Theory

The discovery of a Standard Model (SM)-like Higgs boson [5, 6] is a milestone in particle physics. Direct study of this boson *will* shed light on the mysteries surrounding the origin of the Higgs boson and the electroweak (EW) scale. Additionally, it will potentially provide insight into some of the many long standing experimental observations that remain unexplained (see, *e.g.*, [27]) by the SM. In attempting to answer questions raised by the EW sector and these presently unexplained observations, a variety of new physics models have been proposed, with little clue which—if any—Nature actually picks.

It is exciting that ongoing and possible near future experiments can achieve an estimated per mille sensitivity on precision Higgs and EW observables [8, 9, 28–31]. This level of precision provides a window to indirectly explore the theory space of beyond the Standard Model (BSM) physics and place constraints on specific ultraviolet (UV) models. For this purpose, an efficient procedure of connecting new physics models with precision Higgs and EW observables is clearly desirable.

In this chapter, we make use of the Standard Model effective field theory (SM EFT) as a bridge to connect models of new physics with experimental observables. The SM EFT consists of the renormalizable SM Lagrangian supplemented with higher-dimension interactions:

$$\mathcal{L}_{\text{eff}} = \mathcal{L}_{\text{SM}} + \sum_i \frac{1}{\Lambda^{d_i-4}} c_i \mathcal{O}_i. \quad (2.1)$$

In the above, Λ is the cutoff scale of the EFT, \mathcal{O}_i are a set of dimension d_i operators that respect the $SU(3)_c \times SU(2)_L \times U(1)_Y$ gauge invariance of \mathcal{L}_{SM} , and c_i are their Wilson coefficients that run as functions $c_i(\mu)$ of the renormalization group (RG) scale μ . The estimated per-mille sensitivity of future precision Higgs measurements justifies truncating the above expansion at dimension-six operators.

It is worth noting that the SM EFT parameterized by the c_i of Eq. (2.1) is totally different from the widely used seven- κ parametrization (*e.g.*, [32]), which captures only a change in size of each of the SM-type Higgs couplings. In fact, the seven κ 's parameterize models that do not respect the

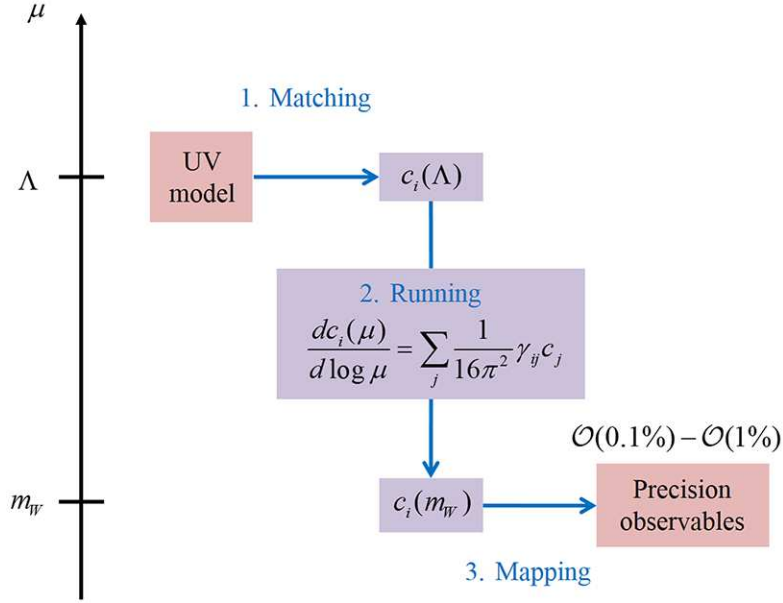


Figure 2.1: SM EFT as a bridge to connect UV models and weak scale precision observables.

electroweak gauge symmetry, and hence, violate unitarity. As a result, future precision programs can show spuriously high sensitivity to the κ . The SM EFT of Eq. (2.1), on the other hand, parameterizes new physics in directions that respect the SM gauge invariance and are therefore free from unitarity violations.¹

In an EFT framework, the connection of UV models² with low-energy observables is accomplished through a three-step procedure schematically described in Fig. 2.1.³ First, the UV model is matched onto the SM EFT at a high-energy scale Λ . This matching is performed order-by-order in a loop expansion. At each loop order, $c_i(\Lambda)$ is determined such that the S -matrix elements in the EFT and the UV model are the same at the RG scale $\mu = \Lambda$. Next, the $c_i(\Lambda)$ are run down to the weak scale $c_i(m_W)$ according to the RG equations of the SM EFT. The leading order solution to these RG equations is determined by the anomalous dimension matrix γ_{ij} . Finally, we use the effective Lagrangian at $\mu = m_W$ to compute weak scale observables in terms of the $c_i(m_W)$ and SM parameters of \mathcal{L}_{SM} . We refer to this third step as mapping the Wilson coefficients onto observables.

In the rest of this chapter we consider each of these three steps—matching, running, and mapping—in detail for the SM EFT. In the SM EFT, the main challenge presented at each step is complexity: truncating the expansion in (2.1) at dimension-six operators leaves us with $\mathcal{O}(10^2)$

¹Equation (2.1) is a linear-realization of EW gauge symmetry. An EFT constructed as a non-linear realization of EW gauge symmetry is, of course, perfectly acceptable.

²In this work we take “UV model” to generically mean the SM supplemented with new states that couple to the SM. In particular, the UV model does not need to be UV complete; it may itself be an effective theory of some other, unknown description.

³For an introduction to the basic techniques of effective field theories see, for example, [33].

independent deformations of the Standard Model.⁴ This large number of degrees of freedom can obscure the incredible simplicity and utility that the SM EFT has to offer. One of the main purposes of the present work is to provide tools and results to help a user employ the SM EFT and take advantage of the many benefits it can offer.

A typical scenario that we imagine is one where a person has some UV model containing massive BSM states and she wishes to understand how these states affect Higgs and EW observables. With a UV model in hand she can, of course, compute these effects using the UV model itself. This option sounds more direct and can, in principle, be more accurate since it does not require an expansion in powers of Λ^{-1} . However, performing a full computation with the UV model is typically quite involved, especially at loop-order and beyond, and needs to be done on a case-by-case basis for each UV model. Among the great advantages of using an EFT is that the computations related to running and mapping, being intrinsic to the EFT, only need to be done once; in other words, once the RG evolution and physical effects of the \mathcal{O}_i are known (to a given order), the results can be tabulated for general use.

Moreover, for many practical purposes, a full computation in the UV model does not offer considerable improvement in accuracy over the EFT approach when one considers future experimental resolution. The difference between an observable computed using the UV theory versus the (truncated) EFT will scale in powers of E_{obs}/Λ , typically beginning at $(E_{\text{obs}}/\Lambda)^2$, where $E_{\text{obs}} \sim m_W$ is the energy scale at which the observable is measured. The present lack of evidence for BSM physics coupled to the SM requires in many cases Λ to be at least a factor of a few above the weak scale. With an estimated per mille precision of future Higgs and EW observables, this means that the leading order calculation in the EFT will rapidly converge with the calculation from the UV model, providing essentially the same result for $\Lambda \gtrsim (\text{several} \times E_{\text{obs}})$.⁵ For the purpose of determining the physics reach of future experiments on specific UV models—*i.e.* estimating the largest values of Λ in a given model that experiments can probe—the EFT calculation is sufficiently accurate in almost all cases.

As mentioned above, the steps of RG running the \mathcal{O}_i and mapping these operators to observables are done within the EFT; once these results are known they can be applied to any set of $\{c_i(\Lambda)\}$ obtained from matching a given UV model onto the SM EFT. Therefore, an individual wishing to study the impact of some UV model on weak scale observables “only” needs to obtain the $c_i(\Lambda)$ at the matching scale Λ . We put “only” in quotes because this step, while straightforward, can also be computationally complex owing to the large number of operators in the SM EFT.

A large amount of literature pertaining to the SM EFT already exists, some of which dates back a few decades, and is rapidly growing and evolving. Owing to the complexity of the SM EFT, many results are scattered throughout the literature at varying levels of completeness. This body of research can be difficult to wade through for a newcomer (or expert) wishing to use the SM EFT to study the impact of BSM physics on Higgs and EW observables. We believe an explication from a UV perspective, oriented to consider how one uses the SM EFT as a bridge to connect UV models

⁴This counting excludes flavor. With flavor, this number jumps to $\mathcal{O}(10^3)$.

⁵For example, in considering the impact of scalar tops on the associated Zh production cross-section at an e^+e^- collider, Craig *et. al.* recently compared [34] the result of a full NLO calculation versus the SM EFT calculation. They found that the results were virtually indistinguishable for stop masses above 500 GeV.

with weak-scale precision observables, is warranted. We have strived to give such a perspective by providing new results and tools with the full picture of matching, running, and mapping in mind. Moreover, our results are aimed to be complete and systematic—especially in regards to the mapping onto observables—as well as usable and self-contained. These goals have obviously contributed to the considerable length of this chapter. In the rest of the present introduction, we summarize more explicitly our results in order to provide an overview for what is contained where in this chapter.

In section 2.1, we present a method to considerably ease the matching of a UV model onto the SM EFT. The SM EFT is obtained by taking a given UV model and integrating out the massive BSM states. The resultant effective action is given by (2.1), where the higher dimension operators are suppressed by powers of $\Lambda = m$, the mass of the heavy BSM states. Although every \mathcal{O}_i respects SM gauge invariance, traditional methods of evaluating the effective action, such as Feynman diagrams, require working with gauge non-invariant pieces at intermediate steps, so that the process of arranging an answer back into the gauge invariant \mathcal{O}_i can be quite tedious. Utilizing techniques introduced in [15, 35] and termed the covariant derivative expansion (CDE), we present a method of computing the effective action through one-loop order in a manifestly gauge-invariant manner. By working solely with gauge-covariant quantities, an expansion of the effective action is obtained that immediately produces the gauge-invariant operators \mathcal{O}_i of the EFT and their associated Wilson coefficients.

At one-loop order, the effective action that results when integrating out a heavy field Φ of mass m is generally of the form

$$\Delta S_{\text{eff},1\text{-loop}} \propto i\text{Tr} \log \left[D^2 + m^2 + U(x) \right], \quad (2.2)$$

where $D^2 = D_\mu D^\mu$ with D_μ a gauge covariant derivative and $U(x)$ depends on the light, SM fields. The typical method for evaluating the functional trace relies on splitting the covariant derivative into its component parts, $D_\mu = \partial_\mu - iA_\mu$ with A_μ a gauge field, and performing a derivative expansion in $\partial^2 - m^2$. This splitting clearly causes intermediate steps of the calculation to be gauge non-covariant. Many years ago, Gaillard found a transformation [15] that allows the functional trace to be evaluated while keeping gauge covariance manifest at every step of the calculation, which we derive and explain in detail in section 2.1. In essence, the argument of the logarithm in Eq. (2.2) is transformed such that the covariant derivative only appears in a series of commutators with itself and $U(x)$. The effective action is then evaluated in a series of “free propagators” of the form $(q^2 - m^2)^{-1}$ with q_μ a momentum parameter that is integrated over. The coefficients of this expansion are the commutators of D_μ with itself and $U(x)$ and correspond to the \mathcal{O}_i of the EFT. Thus, one immediately obtains the gauge-invariant \mathcal{O}_i of the effective action.

In our discussion, we clarify and streamline certain aspects of the derivation and use of the covariant derivative expansion of [15, 35]. Moreover, we generalize the results of [15, 35] and provide explicit formulas for scalars, fermions, and massless as well as massive vector bosons. As a sidenote, for massive gauge bosons it is known that the magnetic dipole coefficient is universal [36, 37]; in appendix B we present a new, completely algebraic proof of this fact. In addition to addressing the one-loop effective action, we present a method for obtaining the tree-level effective

action using a covariant derivative expansion. While this tree-level evaluation is very straightforward, to the best of our knowledge, it has not appeared elsewhere in the literature.

We believe the CDE to be quite useful in general, but especially so when used to match a UV model onto the SM EFT. It is perhaps not widely appreciated that an inverse mass expansion of the one-loop effective action is essentially universal; one of the benefits of the CDE is that this fact is transparent at all stages of the computation. Therefore, the results of the inverse mass expansion, Eq. (2.38), can be applied to a large number of UV models, allowing one to calculate one-loop matched Wilson coefficients with ease. To demonstrate this, we compute the Wilson coefficients of a handful of non-trivial examples that could be relevant for Higgs physics, including an electroweak triplet scalar, an electroweak scalar doublet (the two Higgs doublet model), additional massive gauge bosons, and several others.

In section 2.2 we consider the step of running Wilson coefficients from the matching scale Λ to the electroweak scale m_W where measurements are made. Over the past few years, the RG evolution of the SM EFT has been investigated quite intensively [38–48]. It is a great accomplishment that the entire one-loop anomalous dimension matrix within a complete operator basis has been obtained [40–43],⁶ as well as components of γ_{ij} in other operator bases [44, 45]. As the literature has been quite thorough on the subject, we have little to contribute in terms of new calculations; instead, our discussion on RG running primarily concerns determining when this step is important to use and how to use it. Since future precision observables have a sensitivity of $\mathcal{O}(0.1\%)$ - $\mathcal{O}(1\%)$, they will generically be able to probe new physics at one-loop order. RG evolution introduces a loop factor; therefore, as a rule of thumb, RG running of the $c_i(\Lambda)$ to $c_i(m_W)$ is usually only important if the $c_i(\Lambda)$ are tree-level generated. RG evolution includes a logarithm which may serve to counter its loop suppression; however, from $v^2/\Lambda^2 \sim 0.1\%$, we see that Λ can be probed at most to a few TeV, so that the logarithm is not large, $\log(\Lambda/m_W) \sim 3$. We note that this estimate also means that in a perturbative expansion a truncation by loop-order counting is reasonable.

A common theme in the literature on the SM EFT is the choice of an operator basis. We will discuss this in detail in section 2.2, but we would like to comment here on relevance of choosing an operator basis to the steps of matching and running. One does not need to choose an operator basis at the stage of matching a UV model onto the effective theory. The effective action obtained by integrating out some massive modes will simply produce a set of higher-dimension operators. One can then decide to continue to work with this UV generated operator set as it is, or to switch to a different set due to some other considerations. An operator basis needs to be picked once one RG evolves the Wilson coefficients using the anomalous dimension matrix γ_{ij} , as the anomalous dimension matrix is obviously basis dependent. When RG running is relevant, it is crucial that the operator basis be complete or overcomplete [40].

In section 2.3 we consider the mapping step, *i.e.* obtaining Higgs and EW precision observables as functions of the Wilson coefficients at the weak scale, $c_i(m_W)$. While there have been a variety of studies concerning the mapping of operators onto weak-scale observables in the literature [34, 42, 44, 45, 50–63], to the best of our knowledge, a complete and systematic list does not

⁶Not only is the computation of γ_{ij} practically useful, its structure may be hinting at something deep in regards to renormalization and effective actions [49].

exist yet. In this chapter, we study a complete set of the Higgs and EW precision observables that present and possible near future experiments can have a decent (1% or better) sensitivity on. These include the seven Electroweak precision observables (EWPO) S, T, U, W, Y, X, V up to p^4 order in the vacuum polarization functions, the three independent triple gauge couplings (TGC), the deviation in Higgs decay widths $\{\Gamma_{h \rightarrow f\bar{f}}, \Gamma_{h \rightarrow gg}, \Gamma_{h \rightarrow \gamma\gamma}, \Gamma_{h \rightarrow \gamma Z}, \Gamma_{h \rightarrow WW^*}, \Gamma_{h \rightarrow ZZ^*}\}$, and the deviation in Higgs production cross sections at both lepton and hadron colliders $\{\sigma_{ggF}, \sigma_{WWh}, \sigma_{Wh}, \sigma_{Zh}\}$. We write these precision observables up to linear power and tree-level order in the Wilson coefficients $c_i(m_W)$ of a complete set of dimension-six CP-conserving bosonic operators⁷ shown in Table 2.2. Quite a bit calculation steps are also listed in Appendix C. These include a list of two-point and three-point Feynman rules (appendix C.1) from operators in Table 2.2, interference corrections to Higgs decay widths (appendix C.2) and production cross sections (appendix C.3), and general analysis on residue modifications (appendix C.4) and Lagrangian parameter modifications (appendix C.5). With a primary interest in new physics that only couples with bosons in the SM, we have taken the Wilson coefficients of all the fermionic operators to be zero while calculating the mapping results. However, the general analysis we present for calculating the Higgs decay widths and production cross sections completely applies to fermionic operators.

With a detailed understanding of how to use the SM EFT, in section 2.4 we turn to applications and study in detail two models of new physics using the SM EFT. The first is a real, singlet scalar which can be used to achieve a strongly first-order electroweak phase transition. The second model addresses scalar tops in the MSSM. In each case, we integrate out the heavy states and obtain the Wilson coefficients at the matching scale using the covariant derivative expansion. We then consider RG evolution of these coefficients down to the weak scale; for the singlet, due to tree-level sized Wilson coefficients, RG running is important, while it is unnecessary for the scalar tops since all Wilson coefficients are of one-loop size. Finally, impacts of these models on electroweak and Higgs observables are studied using the results of our mapping Wilson coefficients onto physical observables. We find that future electroweak and Higgs observables will probe and constrain interesting parameter spaces in each of these two models.

2.1 Covariant derivative expansion

The point of this section is to present a method for computing the tree and one-loop effective action that leaves gauge invariance manifest *at every step of the calculation*. By this we mean that one only works with gauge covariant quantities, such as the covariant derivative. We find it somewhat surprising that this method—developed in the 80s by Gaillard [15] (see also her summer school lectures [64] and the work by Cheyette [35])—is not widely known considering the incredible simplifications it provides. Therefore, in order to spread the good word so to speak, we will explain the method of the covariant derivative expansion (CDE) as developed in [15, 35]. Along the way, we will present a more transparent expansion method to evaluate the CDE and provide generalized results for scalars, fermions, and massless as well as massive gauge bosons. We also

⁷In this chapter, we use the term “bosonic operators” to refer to the operators that contain only bosonic fields, *i.e.* Higgs and gauge bosons. Other operators will be referred to as “fermionic operators”.

show how to evaluate the tree-level effective action in manifestly gauge-covariant manner. In order to explicitly demonstrate the utility of the CDE, we take up a handful of non-trivial examples and compute their Wilson coefficients in the SM EFT.

Besides providing an easier computational framework, the CDE illuminates a certain universality in computing Wilson coefficients from different UV theories. This occurs because individual terms in the expansion split into a trace over internal indices (gauge, flavor, *etc.*) involving covariant derivatives times low energy fields—these are the operators in the EFT—times a simple momentum integral whose value corresponds to the Wilson coefficient of the operator. The UV physics is contained in the specific form of the covariant derivatives and low energy fields, but the momentum integral is independent of these details and therefore can be considered universal.

So far our discussion has been centered around the idea of integrating out some heavy mode to get an effective action, to which we claim the CDE is a useful tool. More precisely, the CDE is a technique for evaluating functional determinants of a generalized Laplacian operator, $\det[D^2 + U(x)]$, where D is some covariant derivative. Therefore the technique is not limited to gauge theories; in fact, the CDE was originally introduced in [15] primarily as a means for computing the one-loop effective action of non-linear sigma models. In these applications, the use of the CDE keeps the geometric structure of the target manifold and its invariance to field redefinitions manifest [15]. Moreover, functional determinants are prolific in the computation of the (1PI or Wilsonian) effective action to one-loop order. Therefore, the use of the CDE extends far beyond integrating out some heavy field and can be used as a tool to, for example, renormalize a (effective) field theory or compute thermal effects.

The 1980s saw considerable effort in developing methods to compute the effective action with arbitrary background fields. While we cannot expect to do justice to this literature, let us provide a brief outline of some relevant works. The CDE developed in [15, 35] built upon the derivative expansion technique of [65, 66]. A few techniques for covariant calculation of the one-loop effective action were developed somewhat earlier in [67]. While these techniques do afford considerable simplification over traditional methods, they are less systematic and more cumbersome than the CDE presented here [15]. In using a heat kernel to evaluate the effective action, a covariant derivative expansion has also been developed, see, *e.g.*, [68]. This method utilizes a position space representation and is significantly more involved than the approach presented here, where we work in Fourier space.

An outline for this section is as follows. In Sec. 2.1.1 we consider the tree and one-loop contributions to the effective action in turn and show how to evaluate each using a covariant derivative expansion. The tree-level result is very simple, as well as useful, and, to the best of our knowledge, has not been appeared in the literature before. The explicit extension to fermions and gauge bosons is provided in Sec. 2.1.2 together with summary formulas of the CDE for different spin particles. In Sec. 2.1.3 we demonstrate how to explicitly evaluate terms in the CDE. Following this, universal formulas for terms in the expansion are presented. As a first example using these results, we derive the β function for non-abelian gauge theory and present the Wilson coefficients for the purely gluonic dimension six operators for massive spin 0, 1/2, and 1 particles transforming under some representation of the gauge group. The universal formulas can also immediately be used to obtain the one-loop effective action for a wide variety of theories, as we show in Sec. 2.1.4 with a

variety of explicit examples. The examples considered are non-trivial demonstrations of the power of the CDE; moreover, they are models that may be relevant to Higgs and other BSM physics: they are related to supersymmetry, extended Higgs sectors, Higgs portal operators, little Higgs theories, extra-dimensional theories, and kinetic mixing of gauge bosons.

We have strived to make accessible the results of this section to a wide audience, primarily because we believe the CDE and its results to be so useful for practical and presently relevant computations. In doing so, however, this section is quite long and it may be helpful to provide a readers guide of sorts in addition to the above outline. Readers mainly interested in the basic idea of the CDE can consider reading the first section, Sec. 2.1.1, then looking over the universal results in Sec. 2.1.3 (and equation (2.38) in particular), and skimming a few of the examples in Sec. 2.1.4.

2.1.1 Covariant evaluation of the tree-level and one-loop effective action

Setting up the problem

Consider Φ to be a heavy, real scalar field of mass m that we wish to integrate out. Let $S[\phi, \Phi]$ denote the piece of the action in the full theory consisting of Φ and its interactions with Standard Model fields ϕ . The effective action resultant from integrating out Φ is given by

$$e^{iS_{\text{eff}}[\phi](\mu)} = \int \mathcal{D}\Phi e^{iS[\phi, \Phi](\mu)}. \quad (2.3)$$

The above defines the effective action at the scale $\mu \sim m$, where we have matched the UV theory onto the effective theory. In the following we do not write the explicit μ dependence and it is to be implicitly understood that the effective action is being computed at $\mu \sim m$.

Following standard techniques, S_{eff} can be computed to one-loop order by a saddle point approximation to the above integral. To do this, expand Φ around its minimum value, $\Phi = \Phi_c + \eta$, where Φ_c is determined by

$$\frac{\delta S[\phi, \Phi]}{\delta \Phi} = 0 \Rightarrow \Phi_c[\phi]. \quad (2.4)$$

Expanding the action around this minimum,

$$S[\phi, \Phi_c + \eta] = S[\Phi_c] + \frac{1}{2} \left. \frac{\delta^2 S}{\delta \Phi^2} \right|_{\Phi_c} \eta^2 + \mathcal{O}(\eta^3),$$

the integral is computed as⁸

$$\begin{aligned} e^{iS_{\text{eff}}[\phi]} &= \int \mathcal{D}\eta e^{iS[\phi, \Phi_c + \eta]} \\ &\approx e^{iS[\Phi_c]} \left[\det \left(- \left. \frac{\delta^2 S}{\delta \Phi^2} \right|_{\Phi_c} \right) \right]^{-1/2}, \end{aligned}$$

⁸The minus sign inside the logarithm comes from Wick rotating to Euclidean space, computing the path integral using the method of steepest descent, and then Wick rotating back to Minkowski space.

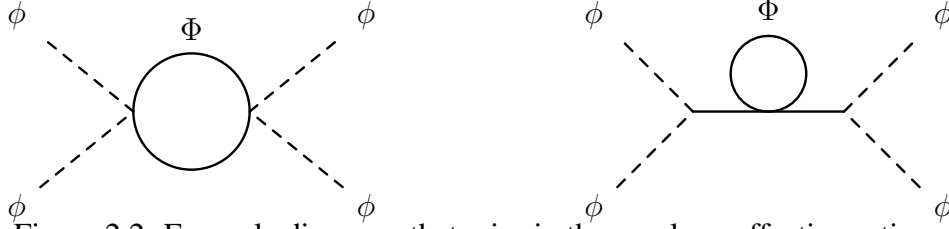


Figure 2.2: Example diagrams that arise in the one-loop effective action.

so that the effective action is given by

$$S_{\text{eff}} \approx S[\Phi_c] + \frac{i}{2} \text{Tr} \log \left(- \frac{\delta^2 S}{\delta \Phi^2} \Big|_{\Phi_c} \right). \quad (2.5)$$

The first term in the above is the tree-level piece when integrating out a field, *i.e.* solving for a field's equation of motion and plugging it back into the action, while the second term is the one-loop piece.

As is clear in the defining equation of the effective action, Eq. (2.3), the light fields ϕ are held fixed while the path integral over Φ is computed. The $\phi(x)$ fields are therefore referred to as background fields. The fact that the background fields are held fixed while only Φ varies in Eq. (2.3) leads to an obvious diagrammatic interpretation of the effective action: the effective action is the set of all Feynman diagrams with ϕ as external legs and only Φ fields as internal lines. The number of loops in these diagrams correspond to a loop expansion of the effective action.

The diagrams with external ϕ and internal Φ are sometimes referred to as one-light-particle irreducible (1LPI) in the sense that no lines of the light particle ϕ can be cut to obtain disjoint diagrams. Note, however, that some the diagrams may not be 1PI in the traditional sense. Figure 2.2 shows two example diagrams that could arise in the evaluation of the one-loop effective action; the diagram on the left is 1PI in the traditional sense, while the one on the right is not. The origin of non-1PI diagrams is $\Phi_c[\phi] \neq 0$. Moreover, these non-1PI diagrams are related to renormalization of the UV Lagrangian parameters, as is clear in the second diagram of Fig. 2.2. One can find more details on this in the explicit examples considered in Sec. 2.1.4.

2.1.1.1 Covariant evaluation of the tree-level effective action

First, we show how to evaluate the tree-level piece to the effective action in a covariant fashion. The most naïve guess of how to do this turns out to be correct: in the exact same way one would do a derivative expansion, one can do a covariant derivative expansion.

To have a tree-level contribution to the effective action there needs to be a term in the UV Lagrangian that is linear in the heavy field Φ . We take a Lagrangian,

$$\mathcal{L}[\Phi, \phi] \supset (\Phi^\dagger B(x) + \text{h.c.}) + \Phi^\dagger (-D^2 - m^2 - U(x))\Phi + \mathcal{O}(\Phi^3), \quad (2.6)$$

where $B(x)$ and $U(x)$ are generically functions of the light fields $\phi(x)$ and we have not specified the interaction terms that are cubic or higher in Φ . To get the tree-level effective action, one simply

solves the equation of motion for Φ , and plugs it back into the action. The equation of motion for Φ is

$$(P^2 - m^2 - U(x))\Phi = -B(x) + \mathcal{O}(\Phi^2),$$

where $P_\mu \equiv iD_\mu = i\partial_\mu + A_\mu(x)$ is the covariant derivative⁹ that acts on Φ . The solution of this gives $\Phi_c[\phi]$ denoted in Eq. (2.4). To leading approximation, we can linearize the above equation to solve for Φ_c ,

$$\Phi_c = -\frac{1}{P^2 - m^2 - U(x)}B(x). \quad (2.7)$$

If the covariant derivative were replaced with the partial derivative, $P^2 = -\partial^2$, one would evaluate the above in an inverse-mass expansion producing a series in ∂^2/m^2 . The exact same inverse-mass expansion can be used with the covariant derivative as well to obtain¹⁰

$$\begin{aligned} \Phi_c &= \left[1 - \frac{1}{m^2}(P^2 - U)\right]^{-1} \frac{1}{m^2}B \\ &= \frac{1}{m^2}B + \frac{1}{m^2}(P^2 - U)\frac{1}{m^2}B + \frac{1}{m^2}(P^2 - U)\frac{1}{m^2}(P^2 - U)\frac{1}{m^2}B + \dots \end{aligned} \quad (2.8)$$

In general, the mass-squared matrix need not be proportional to the identity, so that $1/m^2$ should be understood as the inverse of the matrix m^2 . In this case, $1/m^2$ would not necessarily commute with U and hence we used the matrix expansion from Eq. (2.21) in the above equation.

Plugging Φ_c back into the Lagrangian gives the tree-level effective action. Using the linearized solution to the equation of motion, Eq. (2.7), we have

$$\mathcal{L}_{\text{eff,tree}} = -B^\dagger \frac{1}{P^2 - m^2 - U(x)}B + \mathcal{O}(\Phi_c^3). \quad (2.9)$$

Although we have not specified the interactions in Eq. (2.6) that are cubic or higher in Φ , one needs to also substitute Φ_c for these pieces as well, as indicated in the above equation. The first few terms in the inverse mass expansion are

$$\mathcal{L}_{\text{eff,tree}} = B^\dagger \frac{1}{m^2}B + B^\dagger \frac{1}{m^2}(P^2 - U)\frac{1}{m^2}B + \dots + \mathcal{O}(\Phi_c^3). \quad (2.10)$$

⁹ $A_\mu = A_\mu^a T^a$ with T^a in the representation of Φ . We do not specify the coupling constant in the covariant derivative. Of course, the coupling constant can be absorbed into the gauge field; however, unless otherwise stated, for calculations in this chapter we implicitly assume the coupling constant to be in the covariant derivative. The primary reason we have not explicitly written the coupling constant is because Φ may carry multiple gauge quantum numbers. For example, if Φ is charged under $SU(2)_L \times U(1)_Y$ then we will take $D_\mu = \partial_\mu - igW_\mu - ig'YB_\mu$.

¹⁰This is trivially true. In the case of a partial derivative, $-\partial^2 - m^2 - U(x)$, the validity of the expansion relies not only on $\partial^2/m^2 \ll 1$ but also on $U(x)/m^2 \ll 1$, *i.e.* momenta in the EFT need to be less than m which also means the fields in the EFT need to be slowly varying on distance scales of order m^{-1} . Obviously, the same conditions can be imposed on the covariant derivative as a whole.

2.1.1.2 CDE of the one-loop effective action

Now let us discuss the one-loop piece of the effective action. Let Φ be field of mass m that we wish to integrate out to obtain a low-energy effective action in terms of light fields. Assume that Φ has quantum numbers under the low-energy gauge groups. The one-loop contribution to the effective action that results from integrating out Φ is

$$\Delta S_{\text{eff}} = ic_s \text{Tr} \log \left(-P^2 + m^2 + U(x) \right), \quad (2.11)$$

where $c_s = +1/2, +1,$ or $-1/2$ for Φ a real scalar, complex scalar, or fermion, respectively.¹¹

We evaluate the trace in the usual fashion by inserting a complete set of momentum and spatial states to arrive at

$$\Delta S_{\text{eff}} = ic_s \int d^4x \int \frac{d^4q}{(2\pi)^4} \text{tr} e^{iq \cdot x} \log \left(-P^2 + m^2 + U(x) \right) e^{-iq \cdot x}, \quad (2.12)$$

where the lower case “tr” denotes a trace on internal indices, *e.g.* gauge, spin, flavor, *etc.* For future shorthand we define $dx \equiv d^4x$ and $dq \equiv d^4q/(2\pi)^4$. Using the Baker-Campbell-Hausdorff (BCH) formula,

$$e^B A e^{-B} = \sum_{n=0}^{\infty} \frac{1}{n!} L_B^n A, \quad L_B A = [B, A], \quad (2.13)$$

together with the fact that we can bring the $e^{\pm iq \cdot x}$ into the logarithm, we see that the $P_\mu \rightarrow P_\mu + q_\mu$. Then, after changing variables $q \rightarrow -q$, the one-loop effective action is given by

$$\Delta S_{\text{eff}} = ic_s \int dx dq \text{tr} \log \left[- (P_\mu - q_\mu)^2 + m^2 + U(x) \right]. \quad (2.14)$$

Following [15, 35], we sandwich the above by $e^{\pm P^\mu \partial / \partial q^\mu}$

$$\Delta S_{\text{eff}} = ic_s \int dx dq \text{tr} e^{P \cdot \frac{\partial}{\partial q}} \log \left[- (P_\mu - q_\mu)^2 + m^2 + U(x) \right] e^{-P \cdot \frac{\partial}{\partial q}}. \quad (2.15)$$

In the above it is to be understood that the derivatives $\partial / \partial q$ and $\partial / \partial x \subset P$ act on unity to the right (for $e^{-P \cdot \partial / \partial q}$) and, by integration by parts, can be made to act on unity to the left (for $e^{P \cdot \partial / \partial q}$). Since the derivative of one is zero, the above insertion is allowed. We emphasize that the ability to insert $e^{\pm P \cdot \partial / \partial q}$ in Eq. (2.15) *does not* rely on cyclic property of the trace: the “tr” trace in Eq. (2.15) is over internal indices only and we therefore cannot cyclically permute the infinite dimensional matrices in Eq. (2.15).

One advantage of this choice of insertion is that it makes the linear term in P_μ vanish when transforming the combination $(P_\mu - q_\mu)$, and so the expansion starts from a commutator $[P_\mu, P_\nu]$,

¹¹The reason fermions have $c_s = -1/2$ instead of the usual -1 is because we have squared the usual argument of the logarithm, $\Delta S_{\text{eff}} = -\frac{i}{2} \text{Tr} \log(i\mathcal{D} + \dots)^2$, to bring it to the form in Eq. (2.11). See Appendix A.1 for details.

which is the field strength. Indeed, by making use of the BCH formula and the fact $(L_{P \cdot \partial / \partial q}) q_\mu = [P \cdot \partial / \partial q, q_\mu] = P_\mu$, we get

$$\begin{aligned}
 e^{P \cdot \frac{\partial}{\partial q}} (P_\mu - q_\mu) e^{-P \cdot \frac{\partial}{\partial q}} &= \sum_{n=0}^{\infty} \frac{1}{n!} (L_{P \cdot \partial / \partial q})^n P_\mu - \sum_{n=0}^{\infty} \frac{1}{n!} (L_{P \cdot \partial / \partial q})^n q_\mu \\
 &= -q_\mu + \sum_{n=1}^{\infty} \frac{n}{(n+1)!} (L_{P \cdot \partial / \partial q})^n P_\mu \\
 &= -q_\mu - \sum_{n=0}^{\infty} \frac{n+1}{(n+2)!} \left[P_{\alpha_1}, \left[\dots \left[P_{\alpha_n}, [D_\nu, D_\mu] \right] \right] \right] \frac{\partial^n}{\partial q_{\alpha_1} \dots \partial q_{\alpha_n}} \frac{\partial}{\partial q_\nu} \\
 &\equiv - \left(q_\mu + \tilde{G}_{\nu\mu} \frac{\partial}{\partial q_\nu} \right), \tag{2.16}
 \end{aligned}$$

and similarly,

$$e^{P \cdot \frac{\partial}{\partial q}} U e^{-P \cdot \frac{\partial}{\partial q}} = \sum_{n=0}^{\infty} \frac{1}{n!} \left[P_{\alpha_1}, \left[P_{\alpha_2}, \left[\dots \left[P_{\alpha_n}, U \right] \right] \right] \right] \frac{\partial^n}{\partial q_{\alpha_1} \dots \partial q_{\alpha_n}} \equiv \tilde{U}. \tag{2.17}$$

Bringing the $e^{\pm P \cdot \partial / \partial q}$ into the logarithm to compute the transformation of the integrand in Eq. (2.15), one gets the results obtained in [15, 35]

$$\Delta S_{\text{eff}} = \int dx \Delta \mathcal{L}_{\text{eff}} = i c_s \int dx \int dq \text{tr} \log \left[- \left(q_\mu + \tilde{G}_{\nu\mu} \frac{\partial}{\partial q_\nu} \right)^2 + m^2 + \tilde{U} \right], \tag{2.18}$$

where we have defined

$$\tilde{G}_{\nu\mu} = \sum_{n=0}^{\infty} \frac{n+1}{(n+2)!} \left[P_{\alpha_1}, \left[P_{\alpha_2}, \left[\dots \left[P_{\alpha_n}, [D_\nu, D_\mu] \right] \right] \right] \right] \frac{\partial^n}{\partial q_{\alpha_1} \partial q_{\alpha_2} \dots \partial q_{\alpha_n}}, \tag{2.19a}$$

$$\tilde{U} = \sum_{n=0}^{\infty} \frac{1}{n!} \left[P_{\alpha_1}, \left[P_{\alpha_2}, \left[\dots \left[P_{\alpha_n}, U \right] \right] \right] \right] \frac{\partial^n}{\partial q_{\alpha_1} \partial q_{\alpha_2} \dots \partial q_{\alpha_n}}. \tag{2.19b}$$

The commutators in the above correspond to manifestly gauge invariant higher dimension operators (HDOs): In Eq. (2.19a) the commutators of P 's with $[D_\nu, D_\mu] = -iG_{\nu\mu}$, where $G_{\nu\mu}$ is the gauge field strength, correspond to HDOs of the field strength and its derivatives. In Eq. (2.19b), the commutators will generate higher dimension derivative operators on the fields inside $U(x)$.

While it should be clear, it is worth emphasizing that x and $\partial / \partial x$ commute with q and $\partial / \partial q$, *i.e.* $P = i\partial / \partial x + A(x)$ and $U(x)$ commute with q and $\partial / \partial q$. This, together with the fact that the commutators in Eq. (2.19) correspond to HDOs, allows us to develop a simple expansion of Eq. (2.18) in terms of HDOs whose coefficients are determined from easy to compute momentum integrals, which we now describe.

Instead of working with the logarithm, we work with its derivative with respect to m^2 . Using ∂_μ to denote the derivative *with respect to* q , $\partial_\mu \equiv \partial/\partial q^\mu$, and defining $\Delta \equiv (q^2 - m^2)^{-1}$, the effective Lagrangian is

$$\Delta\mathcal{L}_{\text{eff}} = -ic_s \int dq \int dm^2 \text{tr} \frac{1}{\Delta^{-1} \left[1 + \Delta \left(\{q_\mu, \tilde{G}_{\nu\mu} \partial^\nu\} + \tilde{G}_{\sigma\mu} \tilde{G}_\nu^\sigma \partial^\mu \partial^\nu - \tilde{U} \right) \right]}. \quad (2.20)$$

In the above, Δ is a free propagator for a massive particle; we can develop an expansion of powers of Δ and its derivatives (from the q derivatives inside \tilde{G} and \tilde{U}) where the coefficients are the higher dimension operators. The derivatives and integrals in q are then simple, albeit tedious, to compute and correspond to the Wilson coefficient of the higher dimension operator. Explicitly, using

$$[A^{-1}(1 + AB)]^{-1} = A - ABA + ABABA - \dots, \quad (2.21)$$

we have (using obvious shorthand notation)

$$\begin{aligned} \Delta\mathcal{L}_{\text{eff}} = -ic_s \int dq dm^2 \text{tr} & \left[\Delta - \Delta \left(\{q, \tilde{G}\} + \tilde{G}^2 - \tilde{U} \right) \Delta \right. \\ & \left. + \Delta \left(\{q, \tilde{G}\} + \tilde{G}^2 - \tilde{U} \right) \Delta \left(\{q, \tilde{G}\} + \tilde{G}^2 - \tilde{U} \right) \Delta + \dots \right]. \end{aligned} \quad (2.22)$$

There are two points that we would like to draw attention to:

Power counting Power counting is very transparent in the expansion in Eq. (2.22). This makes it simple to identify the dimension of the operators in the resultant EFT and to truncate the expansion at the desired order. For example, the lowest dimension operator in $\tilde{G}_{\mu\nu}$ is the field strength $[D_\mu, D_\nu] = -iG_{\mu\nu}$; each successive term in \tilde{G} increases the EFT operator dimension by one through an additional P_α . The dimension increase from additional P 's is compensated by additional q derivatives which, by acting on Δ , increase the numbers of propagators.

Universality When the mass squared matrix m^2 is proportional to the identity then Δ commutes with the matrices in \tilde{G} and \tilde{U} . In this case, for any given term in the expansion in Eq. (2.22), the q integral trivially factorizes out of the trace and can be calculated separately. Because of this, there is a certain universality of the expansion in Eq. (2.22): specifics of a given UV theory are contained in P_μ and $U(x)$, but the coefficients of EFT operators are determined by the q integrals and can be calculated without any reference to the UV model.

Before we end this section, let us introduce a more tractable notation that we use in later calculations and results. As we already have used, $\partial_\mu \equiv \partial/\partial q^\mu$. The action of the covariant derivative on matrix is defined as a commutator and we use as shorthand $P_\mu A \equiv [P_\mu, A]$. We also

define $G'_{\mu\nu} \equiv [D_\mu, D_\nu]$.¹² To summarize and repeat ourselves:

$$\partial_\mu \equiv \frac{\partial}{\partial q^\mu}, \quad P_\mu A \equiv [P_\mu, A], \quad G'_{\mu\nu} \equiv [D_\mu, D_\nu]. \quad (2.23)$$

Finally, as everything is explicitly Lorentz invariant, we will typically not bother with raised and lowered indices. With this notation, \tilde{G} and \tilde{U} as defined in Eq. (2.19) are given by

$$\tilde{G}_{\nu\mu} = \sum_{n=0}^{\infty} \frac{n+1}{(n+2)!} (P_{\alpha_1} \dots P_{\alpha_n} G'_{\nu\mu}) \partial_{\alpha_1 \dots \alpha_n}^n, \quad (2.24a)$$

$$\tilde{U} = \sum_{n=0}^{\infty} \frac{1}{n!} (P_{\alpha_1} \dots P_{\alpha_n} U) \partial_{\alpha_1 \dots \alpha_n}^n. \quad (2.24b)$$

2.1.2 CDE for fermions, gauge bosons, and summary formulas

The CDE as presented in the previous subsection is for evaluating functional determinants of the form

$$\log \det (-P^2 + W(x)) = \text{Tr} \log (-P^2 + W(x)),$$

where $P_\mu = iD_\mu$ is a covariant derivative. As such, the results of the previous subsection apply for any generalized Laplacian operator of the form $-P^2 + W(x)$.¹³ The lightning summary is

$$\begin{aligned} \text{Tr} \log (-P^2 + W) &= \int dx dq \text{tr} e^{P \cdot \partial_q} e^{iq \cdot x} \log (-P^2 + W) e^{-iq \cdot x} e^{-P \cdot \partial_q} \\ &= \int dx dq \text{tr} \log \left[- \left(q_\mu + \tilde{G}_{\nu\mu} \partial_\nu \right)^2 + \tilde{W} \right], \end{aligned} \quad (2.25)$$

where we \tilde{G} and \tilde{W} are given in Eq. (2.24) with U replaced by W and we are using the notation defined in Eq. (2.23). In section 2.1.1.2 we took $W(x) = m^2 + U(x)$ for its obvious connection to massive scalar fields.

When we integrate out fermions and gauge bosons, at one-loop they also give functional determinants of generalized Laplacian operators of the form $-P^2 + W(x)$. It is straightforward to apply the steps of section 2.1.1.2 to these cases. Nevertheless, it is useful to tabulate these results for easy reference. Therefore, in this subsection we summarize the results for integrating out massive scalars, fermions, and gauge bosons. We also include the result of integrating out the high

¹²If $D_\mu = \partial/\partial x^\mu - igA_\mu$, then $G'_{\mu\nu}$ is related to the usual field strength as $G'_{\mu\nu} = [D_\mu, D_\nu] = -igG_{\mu\nu}$. In the case where we have integrated out multiple fields with possibly multiple and different gauge numbers, it is easier to just work with D_μ , hence the definition of $G'_{\mu\nu}$.

¹³This is loosely speaking, but applies to many of the cases physicists encounter. More correctly, the functional determinant should exist and so we actually work in Euclidean space and consider elliptic operators of the form $+P^2 + W(x)$ with W hermitian, positive-definite. The transformations leading to the CDE in section 2.1.1.2 then apply to these elliptic operators as well. In the cases we commonly encounter in physics, these properties are satisfied by the fact that operator is the second variation of the Euclidean action which is typically taken to be Hermitian and positive-definite.

energy modes of a massless gauge field. We relegate detailed derivations of the fermion and gauge boson results to appendix A.1. The results for fermions were first obtained in [15]¹⁴ and for gauge bosons in [35].

Let us state the general result and then specify how it specializes to the various cases under consideration. The one-loop effective action is given by

$$\Delta S_{\text{eff},1\text{-loop}} = ic_s \text{Tr} \log \left(-P^2 + m^2 + U(x) \right), \quad (2.26)$$

where the constant c_s and the form of U depend on the species we integrate out, as we explain below. After evaluating the trace and using the transformations introduced in [15] and explained in section 2.1.1.2, the one-loop effective Lagrangian is given by

$$\Delta \mathcal{L}_{\text{eff},1\text{-loop}} = ic_s \int dq \text{tr} \log \left[- \left(q_\mu + \tilde{G}_{\nu\mu} \partial_\nu \right)^2 + m^2 + \tilde{U} \right], \quad (2.27)$$

where the lower case trace, “tr”, is over internal indices and

$$\tilde{G}_{\nu\mu} = \sum_{n=0}^{\infty} \frac{n+1}{(n+2)!} (P_{\alpha_1} \dots P_{\alpha_n} G'_{\nu\mu}) \partial_{\alpha_1 \dots \alpha_n}^n, \quad (2.28a)$$

$$\tilde{U} = \sum_{n=0}^{\infty} \frac{1}{n!} (P_{\alpha_1} \dots P_{\alpha_n} U) \partial_{\alpha_1 \dots \alpha_n}^n, \quad (2.28b)$$

$$P_\mu = iD_\mu, \quad \partial_\mu \equiv \frac{\partial}{\partial q^\mu}, \quad G'_{\nu\mu} \equiv [D_\nu, D_\mu]. \quad (2.28c)$$

Real scalars The effective action originates from the Gaussian integral

$$\exp(i\Delta S_{\text{eff},1\text{-loop}}) = \int \mathcal{D}\Phi \exp \left[i \int dx \frac{1}{2} \Phi^T (P^2 - m^2 - M^2(x)) \Phi \right].$$

For this case, in Eqs. (2.26) and (2.27) we have

$$c_s = 1/2, \quad U(x) = M^2(x). \quad (2.29)$$

Complex scalars The effective action originates from the Gaussian integral

$$\exp(i\Delta S_{\text{eff},1\text{-loop}}) = \int \mathcal{D}\Phi \mathcal{D}\Phi^* \exp \left[i \int dx \Phi^\dagger (P^2 - m^2 - M^2(x)) \Phi \right].$$

For this case, in Eqs. (2.26) and (2.27) we have

$$c_s = 1, \quad U(x) = M^2(x) \quad (2.30)$$

¹⁴We note that there is an error in the results for fermions in [15] (see appendix A.1).

Massive fermions We work with Dirac fermions. The effective action originates from the Gaussian integral

$$\exp(i\Delta S_{\text{eff},1\text{-loop}}) = \int \mathcal{D}\psi \mathcal{D}\bar{\psi} \exp \left[i \int dx \bar{\psi} (\not{P} - m - M(x)) \psi \right],$$

where $\not{P} = \gamma^\mu P_\mu$ with γ^μ the usual gamma matrices. As shown in appendix A.1, in Eqs. (2.26) and (2.27) we have

$$c_s = -1/2, \quad U = U_{\text{ferm}} \equiv -\frac{i}{2} \sigma^{\mu\nu} G'_{\mu\nu} + 2mM + M^2 + \not{P}M, \quad (2.31)$$

where $\sigma^{\mu\nu} = i[\gamma^\mu, \gamma^\nu]/2$ and, by definition, $\not{P}M = [\not{P}, M]$. Note that the trace in (2.27) includes tracing over the spinor indices. The $2mM$ and M^2 terms in U_{ferm} and the $-P^2$ term are proportional to the identity matrix in the spinor indices which, since we use the 4×4 gamma matrices, is the 4×4 identity matrix $\mathbf{1}_4$.

Massless gauge fields We take pure Yang-Mills theory for non-abelian gauge group G ,

$$\mathcal{L}_{YM} = -\frac{1}{2g^2\mu(G)} \text{tr} F_{\mu\nu} F^{\mu\nu}, \quad F_{\mu\nu} = F_{\mu\nu}^a t_G^a,$$

where t_G^a are generators in the adjoint representation and $\mu(G)$ is the Dynkin index for the adjoint representation.¹⁵ We are considering the 1PI effective action, $\Gamma[A]$, of the gauge field A_μ .

We explain the essential details here and explicate them in full in appendix A.1. The 1PI effective action is evaluated using the background field method: the gauge field is expanded around a background piece and a fluctuating piece, $A_\mu(x) = A_{B,\mu}(x) + Q_\mu$, and we integrate out Q_μ . The field Q_μ is gauge-fixed in such a way as to preserve the background field gauge invariance. The gauge-fixed functional integral we evaluate is,

$$\begin{aligned} \exp(i\Gamma_{1\text{-loop}}[A_B]) &= \int \mathcal{D}Q_\mu^a \mathcal{D}c^a \mathcal{D}\bar{c}^a \\ &\times \exp \left[i \int dx -\frac{1}{2g^2} Q_\rho^a (P^2 + i\mathcal{J}^{\mu\nu} G'_{\mu\nu})_\sigma^{\rho,ab} Q^{\sigma,b} + \bar{c}^a (P^2)^{ab} c^b \right], \end{aligned}$$

where c^a are Fadeev-Popov ghosts. In the above, $G'_{\mu\nu} = [D_\mu, D_\nu]$ where $D_\mu = \partial_\mu - iA_{B,\mu}$ is the covariant derivative with respect to the background field, $\mathcal{J}^{\mu\nu}$ is the generator of Lorentz transformations on four-vectors,¹⁶ and we have taken Feynman gauge ($\xi = 1$).

¹⁵For representation R , the Dynkin index is given by $\text{tr} T_R^a T_R^b = \mu(R)\delta^{ab}$. For $SU(N)$, $\mu(G) = N$ while the fundamental representation has $\mu(\square) = 1/2$. In the adjoint representation $(t_G^b)_{ac} = if^{abc}$ where f^{abc} are the structure constants, $[T^a, T^b] = if^{abc}T^c$.

¹⁶Note the similarity with the fermion case, where $\sigma^{\mu\nu}/2$ is the generator of Lorentz transformations on spinors. Explicitly, the components of $\mathcal{J}^{\mu\nu}$ are given by $(\mathcal{J}^{\mu\nu})_{\rho\sigma} = i(\delta_\rho^\mu \delta_\sigma^\nu - \delta_\sigma^\mu \delta_\rho^\nu)$.

The effective Lagrangian is composed of two-pieces of the form in Eqs. (2.26) and (2.27) with $m^2 = 0$. The first is the ghost piece, for which $c_s = -1$ since the ghost fields are anti-commuting and $m^2 = U = 0$:

$$\text{Ghost piece: } c_s = -1, \quad m^2 = U = 0. \quad (2.32)$$

The second piece is from the gauge field Q_μ^a which gives Eqs. (2.26) and (2.27) with $m^2 = 0$, $c_s = 1/2$ since each component of Q_μ^a is a real boson, and $U = -i\mathcal{J} \cdot G'$

$$\text{Gauge piece: } c_s = 1/2, \quad U = U_{\text{gauge}} \equiv -i\mathcal{J}^{\mu\nu} G'_{\mu\nu}, \quad m^2 = 0. \quad (2.33)$$

With $m^2 = 0$, Eqs. (2.26) and (2.27) contain IR divergences. These IR divergences can be regulated by adding a mass term for Q_μ^a and c^a (essentially keeping m^2 in Eqs. (2.26) and (2.27)).

Massive vector bosons We consider a UV model with gauge group G that is spontaneously broken into H . A set of gauge bosons Q_μ^i , $i = 1, 2, \dots, \dim(G) - \dim(H)$ that correspond to the broken generators obtain mass m_Q by “eating” the Nambu-Goldstone bosons χ^i . Here, we restrict ourselves to the degenerate mass spectrum of all Q_μ^i for simplicity. These heavy gauge bosons form a representation of the unbroken gauge group. As we show in appendix B, the general gauge-kinetic piece of the Lagrangian up to quadratic term in Q_μ^i is

$$\mathcal{L}_{\text{g.k.}} \supset \frac{1}{2} Q_\mu^i \left\{ -P^2 g^{\mu\nu} + P^\nu P^\mu - [P^\mu, P^\nu] \right\}^{ij} Q_\nu^j, \quad (2.34)$$

where $P_\mu = iD_\mu$, with D_μ denotes the covariant derivative that contains only the unbroken gauge fields. One remarkable feature of this general gauge-kinetic term is that the coefficient of the “magnetic dipole term” $\frac{1}{2} Q_\mu^i \left\{ -[P^\mu, P^\nu] \right\}^{ij} Q_\nu^j$ is universal, namely that its coefficient is fixed to 1 relative to the “curl” terms $\frac{1}{2} Q_\mu^i \left\{ -P^2 g^{\mu\nu} + P^\nu P^\mu \right\}^{ij} Q_\nu^j$, regardless of the details of the symmetry breaking. In appendix B, we will give both an algebraic derivation and a physical argument to prove Eq. (2.34).

The piece shown in Eq. (2.34) is to be combined with a gauge boson mass term due to the symmetry breaking, a generalized R_ξ gauge fixing term which preserves the unbroken gauge symmetry, an appropriate ghost term, and a possible generic interaction term. More details about all these terms are in appendix A.1. The resultant one-loop effective action is given by computing

$$\begin{aligned} \exp(i\Delta S_{\text{eff},1\text{-loop}}) &= \int \mathcal{D}Q_\mu^i \mathcal{D}\chi^i \mathcal{D}c^i \mathcal{D}\bar{c}^i \\ &\times \exp \left\{ i \int dx \left[\frac{1}{2} Q_\mu^i \left(-P^2 g^{\mu\nu} + m_Q^2 g^{\mu\nu} - 2[P^\mu, P^\nu] + M^{\mu\nu} \right)^{ij} Q_\nu^j \right. \right. \\ &\left. \left. + \frac{1}{2} \chi^i (P^2 - m_Q^2)^{ij} \chi^j + \bar{c}^i (P^2 - m_Q^2)^{ij} c^j \right] \right\}, \quad (2.35) \end{aligned}$$

where c^i, \bar{c}^i denote the ghosts, $M^{\mu\nu}$ parameterizes the possible generic interaction term, and we have taken Feynman gauge $\xi = 1$. Clearly, the effective Lagrangian is composed of three-pieces of the form in Eqs. (2.26) and (2.27)

$$\text{Gauge piece: } c_s = 1/2, \quad U = -i\mathcal{J}^{\mu\nu} \left(G'_{\mu\nu} + \frac{1}{2}M_{\mu\nu} \right), \quad m^2 = m_Q^2 \quad (2.36a)$$

$$\text{Goldstone piece: } c_s = 1/2, \quad U = 0, \quad m^2 = m_Q^2. \quad (2.36b)$$

$$\text{Ghost piece: } c_s = -1, \quad U = 0, \quad m^2 = m_Q^2. \quad (2.36c)$$

2.1.3 Evaluating the CDE and universal results

In the present subsection we explicitly show how to evaluate terms in covariant derivative expansion of the one-loop effective action in Eqs. (2.20) and (2.22). Following this, we provide the results of the expansion through a given order in covariant derivatives. Specifically, for an effective action of the form $S_{\text{eff}} \propto \text{Tr} \log(-P^2 + m^2 + U)$, we provide the results of the CDE through dimension-six operators assuming U is at least linear in background fields. These results make no explicit reference to a specific UV model and therefore they are, in a sense, universal. This universal result is tabulated in Eq. (2.38) and can be immediately used to compute the effective action of a given UV model.

2.1.3.1 Evaluating terms in CDE

Let us consider how to evaluate expansion terms from the effective Lagrangian of Eq. (2.20), which we reproduce here for convenience

$$\Delta\mathcal{L}_{\text{eff},1\text{-loop}} = -ic_s \int dq \int dm^2 \text{tr} \frac{1}{\Delta^{-1} \left[1 - \Delta \left(-\{q_\mu, \tilde{G}_{\nu\mu}\} \partial_\nu - \tilde{G}_{\mu\sigma} \tilde{G}_{\nu\sigma} \partial_\mu \partial_\nu + \tilde{U} \right) \right]}.$$

In the above, \tilde{G} and \tilde{U} are as defined in Eq. (2.24), $dq \equiv d^4q/(2\pi)^4$, $\Delta \equiv 1/(q^2 - m^2)$, and we employ the shorthand notation defined in (2.23). We also used the fact that $\{q_\mu, \tilde{G}_{\nu\mu}\} \partial_\nu = \{q_\mu, \tilde{G}_{\nu\mu}\} \partial_\nu$ which follows from $\{A, BC\} = \{A, B\}C + B\{C, A\}$ and the antisymmetry of $\tilde{G}_{\nu\mu}$, $\tilde{G}_{\nu\mu} = -\tilde{G}_{\mu\nu}$. Using the matrix expansion

$$\frac{1}{A^{-1}(1 - AB)} = \sum_{n=0}^{\infty} (AB)^n A,$$

we define the integrals

$$\mathcal{I}_n \equiv \text{tr} \int dq dm^2 \left[\Delta \left(-\{q, \tilde{G}\} \partial - \tilde{G}^2 \partial^2 + \tilde{U} \right) \right]^n \Delta.$$

The effective action from a given \mathcal{I}_n integral is given by $\Delta\mathcal{L}_{\mathcal{I}_n} = -ic_s \mathcal{I}_n$.

$\tilde{G}_{\nu\mu}$ and \tilde{U} are infinite expansions in covariant derivatives of $G'_{\nu\mu}$ and U , and thus contain higher-dimension operators. Therefore, each \mathcal{I}_n is an infinite expansion containing these HDOs. For this work, motivated by present and future precision measurements, we are interested in corrections up to dimension-six operators. This dictates how many \mathcal{I}_n we have to calculate as well as what order in $\tilde{G}_{\nu\mu}$ and \tilde{U} we need to expand within a given \mathcal{I}_n .

As a typical example to demonstrate how to evaluate the \mathcal{I}_n , we consider \mathcal{I}_1 ,

$$\mathcal{I}_1 = \text{tr} \int dq dm^2 \Delta \left(- \{q, \tilde{G}\} \partial - \tilde{G}^2 \partial^2 + \tilde{U} \right) \Delta. \quad (2.37)$$

This term is fairly easy to compute and captures the basic steps to evaluate any of the \mathcal{I}_n while also highlighting a few features that are unique to low order terms in the expansion. We remind the reader that q_μ and ∂_μ commute with P_μ and U , which is what makes the \mathcal{I}_n very simple to compute. We also assume that the mass-squared matrix m^2 commutes with $G'_{\mu\nu}$ and \tilde{U} .¹⁷ In this case, Δ commutes with the HDOs in \tilde{G} and \tilde{U} , *i.e.* $[\Delta, P_{\alpha_1} \dots P_{\alpha_n} G'_{\mu\nu}] = 0$ and similarly for the HDOs in \tilde{U} . This allows us to separate the q -integral from the trace over the HDOs.

Let us now evaluate \mathcal{I}_1 in (2.37). We consider the \tilde{U} term first,

$$\mathcal{I}_1 \supset \text{tr} \int dq dm^2 \Delta \tilde{U} \Delta = \sum_{n=0}^{\infty} \frac{1}{n!} \text{tr}(P_{\alpha_1} \dots P_{\alpha_n} U) \times \int dq \Delta \partial_{\alpha_1 \dots \alpha_n}^n \Delta.$$

Recall that the covariant derivative action on a matrix is defined as the commutator, *e.g.* $P_\alpha U = [P_\alpha, U]$. Since the trace of a commutator vanishes, all the $n \geq 1$ terms become total derivatives after the evaluation of the trace, and therefore do not contribute to the effective action. Thus,

$$\text{tr} \int dq dm^2 \Delta \tilde{U} \Delta = \text{tr} U \times \int dq dm^2 \Delta^2.$$

The above term is divergent. It may be the case—as in the above integral—that the order of integration does not commute and changes the divergent structure of the integral. In these cases, to properly capture the divergent structure (and therefore define counter-terms) the integral on m^2 should be performed first since we are truly evaluating $\int dq \int dm^2 \frac{\partial}{\partial m^2} \text{tr} \log(\dots)$.¹⁸ In this chapter, we use dimensional regularization with $\overline{\text{MS}}$ for our renormalization scheme, in which case

$$\text{tr} U \int dq dm^2 \Delta^2 = \text{tr} U \int dq \Delta = -\frac{i}{(4\pi)^2} m^2 \left(\log \frac{m^2}{\mu^2} - 1 \right) \text{tr} U,$$

¹⁷ This is always the case if m^2 is proportional to identity, *i.e.* if every particle integrated out has the same mass. If we integrate out multiple particles with different masses, typically m^2 commutes with $G'_{\mu\nu}$ but, in general, will not commute with U . For m^2 to commute with $G'_{\mu\nu}$, in the operator $P^2 - m^2 - U(x)$, it amounts to assuming P_μ and m^2 are block diagonal of the form $P_\mu = \text{diag}(P_\mu^{(1)}, \dots, P_\mu^{(n)})$ and $m^2 = \text{diag}(m_1^2, \dots, m_n^2)$. Physically, this means we are integrating out n particles, where the i th particle has mass-squared m_i^2 and a covariant derivative $P_\mu^{(i)}$ associated to its gauge interactions. The block-diagonal mass matrix means we diagonalized the mass matrix before integrating out the particles. If U happens to have the same block-diagonal structure, then of course m^2 commutes with U as well.

¹⁸ Simple power counting easily shows that divergences in \mathcal{I}_n can only occur for $n = 0, 1$, and 2. In the expansions of \tilde{G} and \tilde{U} within $\mathcal{I}_{0,1,2}$, it is not difficult to see that there are only four non-vanishing divergent terms: \mathcal{I}_0 , in \mathcal{I}_1 they are the $\text{tr} U$ and $\text{tr} G'_{\mu\nu} G'_{\rho\sigma}$ terms, and in \mathcal{I}_2 it is the $\text{tr} U^2$ term.

where μ is the renormalization scale.

We now turn our attention to the pieces in \mathcal{I}_1 involving $\tilde{G}_{\mu\nu}$. The term linear in \tilde{G} in \mathcal{I}_1 vanishes since it is the trace of a commutator, as was the case for the higher derivative terms in \tilde{U} discussed above. Thus, only the \tilde{G}^2 term is non-zero and we seek to evaluate

$$\mathcal{I}_1 \supset -\text{tr} \int dq dm^2 \Delta \tilde{G}_{\mu\sigma} \tilde{G}_{\nu\sigma} \partial_{\mu\nu}^2 \Delta.$$

We evaluate the above up to dimension-six operators. Since $G'_{\mu\nu} = -[P_\mu, P_\nu]$ is $\mathcal{O}(P^2)$, we need the expansion of $\tilde{G}\tilde{G}$ to $\mathcal{O}(P^6)$:

$$\begin{aligned} \tilde{G}_{\mu\sigma} \tilde{G}_{\nu\sigma} \partial_{\mu\nu}^2 &= \frac{1}{4} G'_{\mu\sigma} G'_{\nu\sigma} \partial_{\mu\nu}^2 + \frac{1}{9} (P_\alpha G'_{\mu\sigma}) (P_\beta G'_{\nu\sigma}) \partial_{\alpha\beta\mu\nu}^4 \\ &+ \frac{1}{16} \left[G'_{\mu\sigma} (P_{\beta_1} P_{\beta_2} G'_{\nu\sigma}) \partial_{\beta_1\beta_2\mu\nu}^4 + (P_{\alpha_1} P_{\alpha_2} G'_{\mu\sigma}) G'_{\nu\sigma} \partial_{\alpha_1\alpha_2\mu\nu}^4 \right], \end{aligned}$$

where we dropped the $\mathcal{O}(P^5)$ terms since they vanish as required by Lorentz invariance. It is straightforward to plug the above back into \mathcal{I}_1 and compute the q -derivatives and integrals. For example, the $G'^2 \partial^2$ requires computing

$$\begin{aligned} \int dq dm^2 \Delta \partial_{\mu\nu}^2 \Delta &= \int dq dm^2 \Delta (-2g_{\mu\nu} \Delta^2 + 8q_\mu q_\nu \Delta^3) \\ &= 2g_{\mu\nu} \int dq dm^2 (-\Delta^3 + q^2 \Delta^4) \\ &= 2g_{\mu\nu} \int dq \left(-\frac{1}{2} \Delta^2 + \frac{1}{3} q^2 \Delta^4 \right) \\ &= 2g_{\mu\nu} \cdot \frac{i}{(4\pi)^2} \cdot \frac{1}{6} \cdot \left(\log \frac{m^2}{\mu^2} - 1 \right), \end{aligned}$$

where we computed the m^2 integral first and used dimensional regularization with $\overline{\text{MS}}$. Thus, we see that

$$\mathcal{I}_1 \supset -\frac{1}{4} \text{tr}(G'_{\mu\sigma} G'_{\nu\sigma}) \int dq dm^2 \Delta \partial_{\mu\nu}^2 \Delta = -\frac{i}{(4\pi)^2} \cdot \left(\log \frac{m^2}{\mu^2} - 1 \right) \cdot \frac{1}{12} \cdot \text{tr}(G'_{\mu\nu} G'_{\mu\nu}),$$

which we clearly recognize as a contribution to the β function of the gauge coupling constant.

The other $\mathcal{O}(P^6)$ terms in the expansion of \tilde{G}^2 are computed similarly. In appendix A.2 we tabulate several useful identities that frequently occur, such as $\partial_{\alpha_1 \dots \alpha_n}^n \Delta$ and what this becomes under the q -integral. For example, in the above computation we used

$$\partial_{\mu\nu}^2 \Delta = -2g_{\mu\nu} \Delta^2 + 8q_\mu q_\nu \Delta^3 \Rightarrow \text{under } q\text{-integral: } \partial_{\mu\nu}^2 \Delta = 2g_{\mu\nu} (-\Delta^2 + q^2 \Delta^3).$$

The end result of computing the q -integrals for the $\mathcal{O}(P^6)$ terms in \mathcal{I}_1 gives

$$-\text{tr} \int dq dm^2 \Delta \tilde{G}_{\mu\sigma} \tilde{G}_{\nu\sigma} \partial_{\mu\nu}^2 \Delta \supset -\frac{i}{(4\pi)^2} \frac{1}{30} \frac{1}{m^2} \text{tr} \left\{ \begin{aligned} &\frac{4}{9} \left[(P_\mu G'_{\mu\nu})^2 + (P_\mu G'_{\nu\sigma})(P_\mu G'_{\nu\sigma}) + (P_\mu G'_{\nu\sigma})(P_\nu G'_{\mu\sigma}) \right] \\ &+ \frac{1}{2} \left[G'_{\mu\nu} (P^2 G_{\mu\nu} + P_\mu P_\sigma G'_{\sigma\nu} + P_\sigma P_\mu G'_{\sigma\nu}) \right] \end{aligned} \right\}.$$

There are only two possible dimension-six operators involving just P_μ and $G'_{\mu\nu}$, namely $\text{tr} (P_\mu G'_{\mu\nu})^2$ and $\text{tr} (G'_{\mu\nu} G'_{\nu\sigma} G'_{\sigma\mu})$. Using the Bianchi identity and integration by parts, $\text{tr} [A(P_\mu B)] = -\text{tr} [(P_\mu A)B] + \text{total deriv.}$, the above can be arranged into just these two dimension-six operators:

$$-\frac{i}{(4\pi)^2} \frac{1}{m^2} \left[\frac{1}{135} \text{tr} (P_\mu G'_{\mu\nu})^2 + \frac{1}{90} \text{tr} (G'_{\mu\nu} G'_{\nu\sigma} G'_{\sigma\mu}) \right].$$

Combining all these terms together, we find the contribution to the effective Lagrangian from \mathcal{I}_1 is

$$\begin{aligned} \Delta \mathcal{L}_{\mathcal{I}_1} = -ic_s \mathcal{I}_1 = &-\frac{c_s}{(4\pi)^2} \left[\left(\log \frac{m^2}{\mu^2} - 1 \right) \frac{1}{12} \text{tr} (G'_{\mu\nu} G'_{\mu\nu}) + \frac{1}{m^2} \frac{1}{135} \text{tr} (P_\mu G'_{\mu\nu})^2 \right. \\ &\left. + \frac{1}{m^2} \frac{1}{90} \text{tr} (G'_{\mu\nu} G'_{\nu\sigma} G'_{\sigma\mu}) \right] + \text{dim-8 operators.} \end{aligned}$$

For the reader following closely, we note that the only contribution to $\text{tr} (G'_{\mu\nu})^2$ is the above term from \mathcal{I}_1 , while $\text{tr} (P_\mu G'_{\mu\nu})^2$ and $\text{tr} G'^3$ also receive contributions from \mathcal{I}_2 .

In a similar fashion, one can compute the other \mathcal{I}_n . In the next subsection we tabulate the result of all possible contributions to dimension-six operators from the \mathcal{I}_n ; in appendix A.3 the results for each individual \mathcal{I}_n are listed.

2.1.3.2 Universal results

We just showed how to evaluate terms in the CDE to a given order. Here we tabulate the results that allow one to compute the one-loop effective action through dimension-six operators. In the next subsection we use these results to obtain the dimension-six Wilson coefficients of the SM EFT for several non-trivial BSM models.

The one-loop effective action is given by

$$\Delta S_{\text{eff},1\text{-loop}} = ic_s \text{Tr} \log \left(-P^2 + m^2 + U(x) \right),$$

where, as discussed these in section 2.1.2, c_s and $U(x)$ depend on the species we integrate out. We assume that the mass-squared matrix m^2 commutes with U and $G'_{\mu\nu}$. Under this assumption, we tabulate results of the CDE through dimension-six operators. In general, U may have terms which

are linear in the background fields.¹⁹ In this case, although the scaling dimension of U is two, its operator dimension may be one. Simple power counting tells us that we will have to evaluate terms in the \mathcal{I}_n integrals of Eq. (2.1.3.1) through \mathcal{I}_6 .²⁰ In appendix A.3, we give the result of this calculation for each of the relevant terms in \mathcal{I}_1 - \mathcal{I}_6 . Gathering all of the terms together, the one-loop effective action is:

$$\begin{aligned}
 \Delta\mathcal{L}_{\text{eff,1-loop}} = & \frac{c_s}{(4\pi)^2} \text{tr} \left\{ \right. \\
 & + m^4 \left[-\frac{1}{2} \left(\log \frac{m^2}{\mu^2} - \frac{3}{2} \right) \right] \\
 & + m^2 \left[- \left(\log \frac{m^2}{\mu^2} - 1 \right) U \right] \\
 & + m^0 \left[-\frac{1}{12} \left(\log \frac{m^2}{\mu^2} - 1 \right) G_{\mu\nu}^{\prime 2} - \frac{1}{2} \log \frac{m^2}{\mu^2} U^2 \right] \\
 & + \frac{1}{m^2} \left[-\frac{1}{60} (P_\mu G'_{\mu\nu})^2 - \frac{1}{90} G'_{\mu\nu} G'_{\nu\sigma} G'_{\sigma\mu} - \frac{1}{12} (P_\mu U)^2 - \frac{1}{6} U^3 - \frac{1}{12} U G'_{\mu\nu} G'_{\mu\nu} \right] \\
 & + \frac{1}{m^4} \left[\frac{1}{24} U^4 + \frac{1}{12} U (P_\mu U)^2 + \frac{1}{120} (P^2 U)^2 + \frac{1}{24} (U^2 G'_{\mu\nu} G'_{\mu\nu}) \right. \\
 & \quad \left. - \frac{1}{120} [(P_\mu U), (P_\nu U)] G'_{\mu\nu} - \frac{1}{120} [U[U, G'_{\mu\nu}]] G'_{\mu\nu} \right] \\
 & + \frac{1}{m^6} \left[-\frac{1}{60} U^5 - \frac{1}{20} U^2 (P_\mu U)^2 - \frac{1}{30} (U P_\mu U)^2 \right] \\
 & \left. + \frac{1}{m^8} \left[\frac{1}{120} U^6 \right] \right\}. \tag{2.38}
 \end{aligned}$$

Equation (2.38) is one of the central results that we present, so let us make a few comments about it:

¹⁹For example, a Yukawa interaction $y\phi\bar{\psi}\psi$ for massive fermions leads to a term linear in the light field ϕ : from Eq. (2.31), $U_{\text{ferm}} \supset 2mM(x) = ym\phi$.

²⁰While this is tedious, it isn't too hard. Moreover, there are many terms within each \mathcal{I}_n that we don't need to compute since they lead to too large of an operator dimension. For example, the only term in \mathcal{I}_6 that we need to compute is

$$\mathcal{I}_6 = \text{tr} \int dq dm^2 \left[\Delta(-\{q, \tilde{G}\})\partial - \tilde{G}^2\partial^2 + \tilde{U} \right]^6 \Delta \supset \text{tr} U^6 \int dq dm^2 \Delta^7 = \text{tr} U^6 \cdot \frac{i}{(4\pi)^2} \cdot \frac{1}{120} \cdot \frac{1}{m^8}.$$

All other terms in \mathcal{I}_6 have too large of operator dimension and can be dropped.

- This formula is the expansion of a functional trace of the form $ic_s \text{Tr} \log [-P^2 + m^2 + U(x)]$ where $P_\mu = iD_\mu$ is a covariant derivative and $U(x)$ is an arbitrary function of spacetime. We have worked in Minkowski space and defined the one-loop action and Lagrangian from $ic_s \text{Tr} \log [-P^2 + m^2 + U] = \Delta S_{\text{eff},1\text{-loop}} = \int d^4x \Delta \mathcal{L}_{\text{eff},1\text{-loop}}$.
- The results of Eq. (2.38) are valid when the mass-squared matrix m^2 commutes with $U(x)$ and $G'_{\mu\nu} = [D_\mu, D_\nu]$.
- The lower case “tr” in (2.38) is over internal indices. These indices may include gauge indices, Lorentz indices (spinor, vector, *etc.*), flavor indices, *etc.*.
- c_s is a constant which relates the functional trace to the effective action, á la the first bullet point above. For example, for real scalars, complex scalars, Dirac fermions, gauge bosons, and Fadeev-Popov ghosts $c_s = 1/2, 1, -1/2, 1/2,$ and -1 , respectively. $U(x)$ is a function of the background fields. In section 2.1.2 we discussed the form of $U(x)$ for various particle species, namely scalars, fermions, and gauge bosons.
- Given the above statements, it is clear that (2.38) is universal in the sense that it applies to any effective action of the form $\text{Tr} \log (-P^2 + m^2 + U)$.²¹ For any specific theory, one only needs to determine the form of the covariant derivative P_μ and the matrix $U(x)$ and then (2.38) may be used. We provide several examples in the next subsection.
- Equation (2.38) is an expansion of the effective Lagrangian through dimension-six operators. U has scaling dimension two, but its operator dimension may be one or greater. In the case U contains a term with unit operator dimension, one needs all the terms in (2.38) to capture all dimension-six operators.
- The lines proportional to $m^4, m^2,$ and m^0 in (2.38) come from UV divergences in the evaluation of the trace; μ is a renormalization scale and we used dimensional regularization and $\overline{\text{MS}}$ scheme.
- The lines proportional to m^2 and m^0 can always be absorbed by renormalization. They can also be used to find the contribution of the particles we integrate out to the β -functions of operators.

Evaluation of the pure glue pieces

The operators involving only gauge bosons, G'^2 at dimension four and $(PG')^2$ and G'^3 at dimension six, are determined solely by stating the field content and their representations under the gauge groups. As such, we can evaluate these terms more generally. For the dimension four term G'^2 we will immediately produce the β function of Yang-Mills coupling constant.

We take a simple gauge group and evaluate the contribution of different particle species to these pure glue operators. For a semi-simple group, the following results apply to each individual gauge

²¹Under the assumption m^2 commutes with U and $G'_{\mu\nu}$; see the second bullet point.

group. The covariant derivative is given by $D_\mu = \partial_\mu - igA_\mu$ so that $G'_{\mu\nu} = [D_\mu, D_\nu] = -igG_{\mu\nu}$ where $G_{\mu\nu}$ is the Yang-Mills field strength.

All particle species contribute to renormalization of the Yang-Mills kinetic term, $-(G_{\mu\nu}^a)^2/4$, through the $\text{tr} G_{\mu\nu}^{\prime 2}$ term in (2.38). In addition, the magnetic moment coupling for fermions and gauge bosons is contained within U , $U \supset -iS^{\mu\nu}G'_{\mu\nu}$ where $S^{\mu\nu}$ is the Lorentz generator in a given representation—see Eqs. (2.31) and (2.33). This term then contributes to the Yang-Mills kinetic term through $\text{tr} U^2$. Evaluating these terms for a particle with spin j particle and representation R under the gauge group we have

$$-c_s \frac{1}{12} \text{tr} G_{\mu\nu}^{\prime 2} = \frac{g^2}{3} \cdot c_s \cdot d(j) \cdot \mu(R) \times \left(\frac{1}{4} G_{\mu\nu}^a G^{a\mu\nu} \right),$$

where $d(j)$ is the number of components of the spin j particle²² and $\mu(R)$ is the Dynkin index of the R^{th} representation, $\text{tr} T_R^a T_R^b = \mu(R) \delta^{ab}$. For the $\text{tr} U^2$ term we have

$$-c_s \frac{1}{2} \text{tr} U^2 \supset -c_s \frac{g^2}{2} \text{tr} \left(S^{\mu\nu} G_{\mu\nu} S^{\rho\sigma} G_{\rho\sigma} \right) = -4g^2 \cdot c_s \cdot k(j) \cdot \mu(R) \times \left(\frac{1}{4} G_{\mu\nu}^a G^{a\mu\nu} \right),$$

where $k = 1$ ($k = 2$) for Dirac spinors (vectors).²³ Combining these terms together, we see that a given species that we integrate out produces

$$\Delta S_{\text{eff},1\text{-loop}} \supset \frac{g^2}{(4\pi)^2} \left[c_s \mu(R) \left(\frac{1}{3} d(j) - 4k(j) \right) \right] \log \frac{\mu^2}{m^2} \times \left(-\frac{1}{4} G_{\mu\nu}^a G^{a\mu\nu} \right). \quad (2.39)$$

We recognize the term in square brackets as the contribution to the one-loop β function coefficient.²⁴ In particular, for scalars, fermions, and vector bosons (including the ghost contribution, Eq. (2.32)), we have

$$c_s \mu(R) \left(\frac{1}{3} d(j) - 4k(j) \right) = \mu(R) \begin{cases} \frac{1}{3} & \text{complex scalars} \\ -\frac{2}{3} + 2 = \frac{4}{3} & \text{Dirac fermions} \\ \frac{1}{2} \left(\frac{4}{3} - 8 \right) - \frac{1}{3} = -\frac{11}{3} & \text{vector bosons} \end{cases} .$$

In a similar fashion, we can compute the dimension-six pure glue operators. In Eq. (2.38), these come from $\text{tr}(P_\mu G'_{\mu\nu})^2$ and $\text{tr}(G'_{\mu\nu} G'_{\nu\sigma} G'_{\sigma\mu})$ as well as $\text{tr} U^3$ and $\text{tr}(P_\mu U)^2$ when U contains the

²² $d = 1, 4,$ and 4 for scalars, Dirac fermions, and vectors, respectively.

²³In the spinor representation and vector representations $S^{\mu\nu} = \sigma^{\mu\nu}/2$ and $S^{\mu\nu} = \mathcal{J}^{\mu\nu}$, respectively. With this, $\text{tr} S^{\mu\nu} S^{\rho\sigma} = k(j)(g^{\mu\rho} g^{\nu\sigma} - g^{\mu\sigma} g^{\nu\rho})$ with $k(j = 1/2) = 1$ for spinors, $k(j = 1) = 2$ for vectors, and, obviously, $k(j = 0) = 0$ for scalars.

²⁴For massless particles, the m^2 inside the logarithm should be interpreted as an IR regulator. Note that interpreting this result as the contribution to the running of the coupling constant means we are regarding this as the 1PI effective action or an EFT where the particle of mass m remains in the spectrum, its mass small compared to the cutoff of the EFT. In the case where we are integrating out a heavy particle of mass m , as is well known, we are still picking up the massive particle's contribution to the β function since dimensional regularization is a mass-independent renormalization scheme. Of course, since we have integrated out the massive species we should not include its contribution to the running of the coupling constant in the low-energy EFT.

$$\mathcal{L}_{\text{eff,1-loop}} \supset \frac{1}{(4\pi)^2} \frac{1}{m^2} \frac{g^2}{60} \mu(R) \left(a_{2s} \mathcal{O}_{2G} + a_{3s} \mathcal{O}_{3G} \right)$$

a_{2s}	a_{3s}	
2	2	complex scalar
16	-4	Dirac fermion
-37	3	massive vector

Table 2.1: Contribution of different massive species to the purely gluonic dimension-six operators, computed from (2.41). The operators \mathcal{O}_{2G} and \mathcal{O}_{3G} are defined in Eq. (2.40). The particle has mass m and transforms in the R^{th} representation of the group, with $\mu(R)$ its index. Real scalars are half the value of complex scalars. For $U(1)$ gauge groups, $\mu(R)$ is replaced by Q^2 and a_{2s} by the number of degrees of freedom transforming under the $U(1)$, where Q the charge of the massive particle under the $U(1)$. Note that, by anti-symmetry of the Lorentz indices, \mathcal{O}_{3G} vanishes for abelian groups.

magnetic moment coupling. These traces are straightforward to compute. Defining the dimension-six operators

$$\mathcal{O}_{2G} \equiv -\frac{1}{2} (D_\mu G_{\mu\nu}^a)^2, \quad \mathcal{O}_{3G} \equiv \frac{g}{3!} f^{abc} G_{\mu\nu}^a G_{\nu\sigma}^b G_{\sigma\mu}^c, \quad (2.40)$$

we find

$$\begin{aligned} -\frac{c_s}{60} \text{tr} (P_\mu G'_{\mu\nu})^2 &= \frac{g^2}{30} \cdot c_s \cdot d(j) \cdot \mu(R) \times \mathcal{O}_{2G}, \\ -\frac{c_s}{90} \text{tr} (G'_{\mu\nu} G'_{\nu\sigma} G'_{\sigma\mu}) &= \frac{g^2}{30} \cdot c_s \cdot d(j) \cdot \mu(R) \times \mathcal{O}_{3G}, \\ -\frac{c_s}{6} \text{tr} U^3 &= 2g^2 \cdot c_s \cdot k(j) \cdot \mu(R) \times \mathcal{O}_{3G}, \\ -\frac{c_s}{12} \text{tr} (P_\mu U)^2 &= 2g^2 \cdot c_s \cdot k(j) \cdot \mu(R) \times \left(-\mathcal{O}_{3G} - \frac{1}{3} \mathcal{O}_{2G} \right). \end{aligned}$$

Adding these terms up we have

$$\Delta \mathcal{L}_{\text{eff,1-loop}} \supset \frac{1}{(4\pi)^2} \frac{1}{m^2} \frac{g^2}{30} c_s \mu(R) \left[d(j) \times \mathcal{O}_{3G} + \left(d(j) - 20k(j) \right) \times \mathcal{O}_{2G} \right]. \quad (2.41)$$

In Table 2.1 we tabulate these coefficients for different species, where in the massive gauge boson case, proper contributions from Goldstone and ghosts are already included.

2.1.4 Example calculations

In this subsection, we give several example models where we calculate the effective action using the covariant derivative expansion. As we will explicitly see, computing the Wilson coefficients for a given model proceeds in an essentially algorithmic fashion. If there is a tree-level contribution to the effective action, we use Eq. (2.10). For the one-loop contribution, we use Eq. (2.38). Given a model, the brunt of the work is to identify the appropriate U to plug into Eqs. (2.10) and (2.38)

and then to evaluate the traces in these equations. In the following matching calculations, it should be understood that all the Wilson coefficients obtained are at the matching scale Λ , namely that all our results are actually about $c_i(\Lambda)$. That said, throughout this subsection we drop the specification of RG scale.

A note on terminology. We frequently, and somewhat inappropriately, refer to the use of Eqs. (2.10) and (2.38) as “using the CDE”. If we are just using the results in these equations, then such a statement is technically incorrect. The expansion of the effective action in these two equations can be obtained from *any* consistent method to compute the effective action. The CDE is a *particular* method which considerably eases obtaining these results, but, nevertheless, is still just a means to the end. With this clarification, we hope the reader can forgive our sloppy language in this section.

In demonstrating how to use the CDE to compute the effective action, we would also like to pick models that are of phenomenological interest. As such, we focus on models that couple to the bosonic sector of the SM, with particular attention towards those models which generate tree-level Wilson coefficients. UV models that generate tree-level Wilson coefficients of the bosonic operators in Table 2.2 may substantially contribute to precision observables. As a result, these models are typically either already tightly constrained or will be probed in future. Note that RG running may be of practical relevance when the Wilson coefficient is generated at tree-level (see the discussion in section 2.2).

With the above motivations, we would like to make a list of possible UV models that have tree-level contributions to the effective action. Let us limit this list to heavy scalars which can couple at tree-level to the Higgs sector via renormalizable interactions. There are only four such theories:

1. A real singlet scalar Φ

$$\Delta\mathcal{L} \supset \Phi |H|^2. \quad (2.42)$$

2. A real (complex) $SU(2)_L$ triplet scalar $\Phi_0 = \Phi_0^a \tau^a$ ($\Phi_1 = \Phi_1^a \tau^a$) with hypercharge $Y_\Phi = 0$ ($Y_\Phi = 1$)

$$\Delta\mathcal{L} \supset H^\dagger \Phi_0 H, \quad (2.43)$$

$$\Delta\mathcal{L} \supset H^\dagger \Phi_1 \tilde{H} + c.c., \quad (2.44)$$

where $\tilde{H} = i\sigma^2 H^*$.

3. A complex $SU(2)_L$ doublet scalar Φ with $U(1)_Y$ hypercharge $Y_\Phi = \frac{1}{2}$

$$\Delta\mathcal{L} \supset |H|^2 (\Phi^\dagger H + c.c.). \quad (2.45)$$

4. A complex $SU(2)_L$ quartet scalar $\Phi_{3/2}$ ($\Phi_{1/2}$) with hypercharge $Y_\Phi = \frac{3}{2}$ ($Y_\Phi = \frac{1}{2}$)

$$\Delta\mathcal{L} \supset \Phi^\dagger H^3 + c.c., \quad (2.46)$$

We now show that the above list exhausts the possibilities of heavy scalars that couple via renormalizable interactions to the Higgs and produce tree-level Wilson coefficients. In order to have tree-level generated Wilson coefficients, the UV Lagrangian must contain a term that is linear in the heavy field. Therefore, we need to count all possible Lagrangian terms formed by Φ and H that are linear in Φ . After appropriate diagonalization of Φ and H , we do not need to consider the quadratic terms. Then there are only two types of renormalizable interactions $H^a H^b \Phi^{ab}$ and $H^a H^b H^c \Phi^{abc}$, where we have written the SM Higgs field H in terms of its four real components H^a with $a = 1, 2, 3, 4$. Because only symmetric combinations are non-vanishing, it is clear that there are in total 10 real components Φ^{ab} that are enumerated by No.1 and No.2 in the above list, and 20 real components Φ^{abc} that are enumerated by No.3 and No.4.

In the rest of this subsection, except for the real singlet scalar, we will discuss in detail the examples above and compute their effective actions through one-loop order. Additionally, we will compute the one-loop effective action of two other examples: (1) a heavy $U(1)$ gauge boson that kinetically mixes with hypercharge, and (2) massive vector bosons that transform in the triplet of (unbroken) $SU(2)_L$ and couple universally to fermions. The latter model can arise in extra-dimension and little Higgs theories.

We mention that later in this chapter (Sec. 2.4) we will return to the real singlet scalar as well as the example of degenerate scalar tops in the MSSM. We will turn to these examples after studying the steps of RG running (Sec. 2.2) and mapping Wilson coefficients onto physical observables (Sec. 2.3). Through the examples of the singlet scalar and scalar tops in the MSSM, we will show in explicit detail how the steps of matching, running, and mapping work for a given UV model. Therefore, we postpone the calculation of the Wilson coefficients at the matching scale for these models until Sec. 2.4.

When there is a non-zero tree-level contribution, $\Phi_c \neq 0$, the dependence of the one-loop functional determinant on the classical configuration can introduce divergences into the Wilson coefficients of operators with dimension greater than four. These terms generically are associated with renormalization of parameters in the UV Lagrangian (see the discussion at the beginning of Sec. 2.1.1, around Fig. 2.2). Therefore, the effects of the contributions can be absorbed into a redefinition (renormalization scheme dependence) of the UV Lagrangian parameters, and hence dropped from the matching analysis. Another natural scheme choice is to use $\overline{\text{MS}}$. In $\overline{\text{MS}}$ scheme, from Eq. (2.38), there is a finite contribution to higher dimension operators from the $\text{tr } U$ piece. To show where this difference arises in doing calculations, in our examples of the triplet scalar and doublet scalar we will use the $\overline{\text{MS}}$ renormalization scheme, while for all the other examples we will absorb the divergences of HDOs into the UV Lagrangian parameters. For the latter case, this essentially amounts to dropping Φ_c from the one-loop calculation.

2.1.4.1 Electroweak triplet scalar

Let us consider an electroweak triplet scalar Φ with neutral hypercharge. The Lagrangian contains the trilinear interaction $H^\dagger \Phi H$, where H is the electroweak Higgs doublet. This interaction, being linear in Φ , leads to a tree-level contribution to the effective action when we integrate out Φ .

$\mathcal{O}_{GG} = g_s^2 H ^2 G_{\mu\nu}^a G^{a,\mu\nu}$	$\mathcal{O}_H = \frac{1}{2}(\partial_\mu H ^2)^2$
$\mathcal{O}_{WW} = g^2 H ^2 W_{\mu\nu}^a W^{a,\mu\nu}$	$\mathcal{O}_T = \frac{1}{2}(H^\dagger \overleftrightarrow{D}_\mu H)^2$
$\mathcal{O}_{BB} = g'^2 H ^2 B_{\mu\nu} B^{\mu\nu}$	$\mathcal{O}_R = H ^2 D_\mu H ^2$
$\mathcal{O}_{WB} = 2gg' H^\dagger \tau^a H W_{\mu\nu}^a B^{\mu\nu}$	$\mathcal{O}_D = D^2 H ^2$
$\mathcal{O}_W = ig(H^\dagger \tau^a \overleftrightarrow{D}^\mu H) D^\nu W_{\mu\nu}^a$	$\mathcal{O}_6 = H ^6$
$\mathcal{O}_B = ig' Y_H (H^\dagger \overleftrightarrow{D}^\mu H) \partial^\nu B_{\mu\nu}$	$\mathcal{O}_{2G} = -\frac{1}{2}(D^\mu G_{\mu\nu}^a)^2$
$\mathcal{O}_{3G} = \frac{1}{3!} g_s f^{abc} G_\rho^{a\mu} G_\mu^{b\nu} G_\nu^{c\rho}$	$\mathcal{O}_{2W} = -\frac{1}{2}(D^\mu W_{\mu\nu}^a)^2$
$\mathcal{O}_{3W} = \frac{1}{3!} g \epsilon^{abc} W_\rho^{a\mu} W_\mu^{b\nu} W_\nu^{c\rho}$	$\mathcal{O}_{2B} = -\frac{1}{2}(\partial^\mu B_{\mu\nu})^2$

Table 2.2: CP conserving dimension-six bosonic operators.

While our main purpose here is to demonstrate how to use the CDE, we note that EW triplet scalars are phenomenologically interesting [69] and well studied (for a recent study of triplet collider phenomenology and constraints see, *e.g.*, [70]). As shown below, the electroweak T parameter is generated at tree-level due to the custodial violating interaction $H^\dagger \Phi H$. The strong constraints on the T parameter require the triplet scalar to have a large mass, $m \gg v$. In this regime, the leading terms of the EFT are quite accurate.

For readers interested in comparing the CDE with traditional Feynman diagram techniques, we note that triplet scalars were studied within the EFT framework in [71] where the Wilson coefficients were calculated using Feynman diagrams (see the appendices of [71]). Tree-level Feynman diagrams involving scalar propagators are straightforward to deal with; yet, we believe that even in this simple case the CDE offers a significantly easier method of calculation. In particular, at no point do we (1) have to break the Lagrangian into gauge non-covariant pieces to obtain Feynman rules, (2) look up a table of higher dimension operators to know how to rearrange the answer back into a gauge-invariant form, or (3) consider various momenta configurations of external particles in order to extract which particular higher dimension operator is generated.

Tree-level matching

Let $\Phi = \Phi^a T^a$ be an electroweak, real scalar triplet with hypercharge $Y_\Phi = 0$.²⁵ We take the $SU(2)_L$ generators in the fundamental representation, $T^a = \tau^a = \sigma^a/2$ with σ^a the Pauli matrices. The Lagrangian involving Φ and its interactions with the Standard Model Higgs doublet is given by²⁶

$$\mathcal{L}[\Phi, H] = \frac{1}{2}(D_\mu \Phi^a)^2 - \frac{1}{2}m^2 \Phi^a \Phi^a + 2\kappa H^\dagger \tau^a H \Phi^a - \eta |H|^2 \Phi^a \Phi^a - \frac{1}{4}\lambda_\Phi (\Phi^a \Phi^a)^2, \quad (2.47)$$

where $D_\mu \Phi = [D_\mu, \Phi] = (\partial_\mu \Phi^a + g\epsilon^{abc} W_\mu^b \Phi^c) T^a = (D_\mu \Phi^a) T^a$. The interaction $H^\dagger \Phi H$, being linear in Φ , leads to a tree-level contribution to the effective action. To calculate this contribution,

²⁵For $Y_\Phi \neq 0$, Φ^a must be complex. Only for $Y_\Phi = 0$ or 1 can Φ have a trilinear interaction with H .

²⁶The coupling names and normalization are chosen to coincide with those in [71].

we follow the steps outlined in section 2.1.1.1. Introducing an obvious vector notation and writing the Lagrangian as in Eq. (2.6),

$$\mathcal{L} = \frac{1}{2} \vec{\Phi}^T (P^2 - m^2 - U) \vec{\Phi} + \vec{\Phi} \cdot \vec{B} + \mathcal{O}(\Phi^3), \quad U = 2\eta |H|^2 \quad \text{and} \quad \vec{B} = 2\kappa H^\dagger \vec{\tau} H, \quad (2.48)$$

we solve the equation of motion for Φ and plug it back into the action. Linearizing the equation of motion, we have

$$\vec{\Phi}_c = -\frac{1}{P^2 - m^2 - U} \vec{B}. \quad (2.49)$$

The tree-level effective action is given by $\mathcal{L}_{\text{eff,tree}}[H] = \mathcal{L}[\Phi_c, H]$. Performing an inverse mass expansion on Φ_c , the effective action through dimension-six operators is,

$$\mathcal{L}_{\text{eff,tree}} = \frac{1}{2m^2} \vec{B} \cdot \vec{B} + \frac{1}{2m^4} \vec{B}^T (P^2 - U) \vec{B} + \text{dim 8 operators},$$

where the factor of two difference from Eq. (2.10) occurs because $\vec{\Phi}$ is real.

Now we need to evaluate the terms in the above. For the $\vec{B} \cdot \vec{B}$ term we have²⁷

$$B^a B^a = 4\kappa^2 (H^\dagger \tau^a H)(H^\dagger \tau^a H) = \kappa^2 |H|^4,$$

from which it follows

$$B^a U B^a = 2\eta \kappa^2 |H|^6.$$

Integrating by parts, the term involving the covariant derivative is $\vec{B}^T (-D^2) \vec{B} = (D_\mu \vec{B})^2$ where

$$D_\mu B^a \propto D_\mu (H^\dagger \tau^a H) = (D_\mu H)^\dagger \tau^a H + H^\dagger \tau^a (D_\mu H).$$

Squaring this, using the identity in the previous footnote and the one in Eq. (A.34) we have

$$\begin{aligned} (D_\mu B^a)^2 &= \kappa^2 (H^\dagger \overleftrightarrow{D}^\mu H)^2 + 4\kappa^2 |H|^2 |D_\mu H|^2 \\ &= 2\kappa^2 (\mathcal{O}_T + 2\mathcal{O}_R), \end{aligned}$$

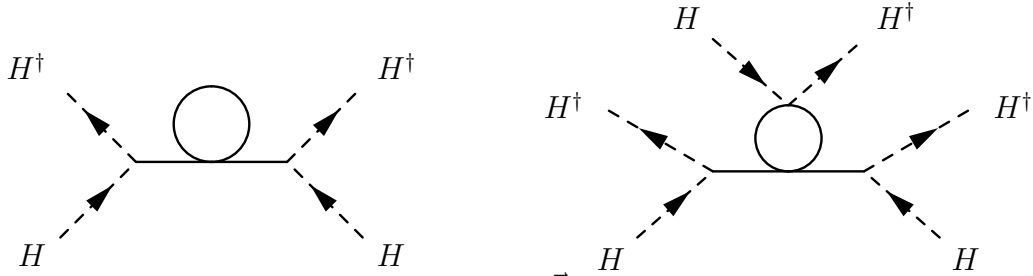
where $H^\dagger \overleftrightarrow{D}^\mu H = H^\dagger (D_\mu H) - (D_\mu H)^\dagger H$ and the operators $\mathcal{O}_{T,R}$ are as defined in Table 2.2.

Putting it all together, we find

$$\mathcal{L}_{\text{eff,tree}} = \frac{\kappa^2}{2m^2} |H|^4 + \frac{\kappa^2}{m^4} (\mathcal{O}_T + 2\mathcal{O}_R) - \frac{\eta \kappa^2}{m^4} \mathcal{O}_6, \quad (2.50)$$

where $\mathcal{O}_6 = |H|^6$. As mentioned previously, these results were also obtained in [71] using Feynman diagrams.²⁸ The first term in the above can be absorbed into the renormalization of the Higgs quartic coupling. As we will discuss in section 2.3, \mathcal{O}_T contributes to the electroweak T parameter. Thus, we see in the effective theory that the T parameter is generated at tree-level.

One-loop level matching


 Figure 2.3: Feynman diagrams for $\vec{\Phi}_c \neq 0$ effects at one-loop.

Let us also calculate the one-loop effective action from integrating out the scalar triplet. It is given by

$$\Delta S_{\text{eff},1\text{-loop}} = \frac{i}{2} \text{Tr} \log \left[- \frac{\delta^2 S}{\delta \Phi^2} \Big|_{\Phi=\Phi_c} \right] = \frac{i}{2} \text{Tr} \log [- P^2 + m^2 + U'],$$

with

$$U' = 2\eta |H|^2 \cdot \mathbf{1}_3 + \lambda_\Phi \left[(\vec{\Phi}_c^T \cdot \vec{\Phi}_c) \cdot \mathbf{1}_3 + 2\vec{\Phi}_c \vec{\Phi}_c^T \right],$$

where $\mathbf{1}_3$ is the 3×3 identity matrix and we explicitly wrote it above to remind the reader that each piece in U' is a matrix. The term in square brackets above is due to the fact that there is a non-zero tree-level piece, *i.e.* that $\vec{\Phi}_c \neq 0$. Diagrammatically, this term leads to connected, but not 1PI, diagrams of the sort shown in Fig. 2.3. Such diagrams are clearly associated with renormalization of parameters in the UV Lagrangian, *e.g.* Φ 's mass m or the cross-quartic coupling η in the left and right panels of Fig. 2.3, respectively. We recall that Φ_c is given by Eq. (2.49),

$$\vec{\Phi}_c = \frac{1}{m^2} \vec{B} + \frac{1}{m^4} (P^2 - U) \vec{B} + \dots$$

To evaluate the one-loop effective action, we take the universal results from Eq. (2.38) with $c_s = 1/2$ since Φ^a is a real scalar. As U' contains no term that is linear in fields, for dimension-six and less operators we take the m^2 , m^0 , and m^{-2} terms from Eq. (2.38)

$$\begin{aligned} 32\pi^2 \Delta \mathcal{L}_{\text{eff},1\text{-loop}} = & -m^2 \left(\log \frac{m^2}{\mu^2} - 1 \right) \text{tr} U' - \frac{1}{12} \left(\log \frac{m^2}{\mu^2} - 1 \right) \text{tr} G_{\mu\nu}^{\prime 2} - \frac{1}{2} \log \frac{m^2}{\mu^2} \text{tr} U'^2 \\ & + \frac{1}{m^2} \left[-\frac{1}{60} \text{tr} (P_\mu G'_{\mu\nu})^2 - \frac{1}{90} \text{tr} G'_{\mu\nu} G'_{\nu\sigma} G'_{\sigma\mu} - \frac{1}{12} \text{tr} (P_\mu U')^2 - \frac{1}{6} \text{tr} U'^3 - \frac{1}{12} \text{tr} U' G'_{\mu\nu} G'_{\mu\nu} \right]. \end{aligned} \quad (2.51)$$

²⁷Here and below we use the following relation for generators T^a in the fundamental representation of $SU(N)$: $(T^a)_{ij} (T^a)_{kl} = \frac{1}{2} (\delta_{il} \delta_{jk} - \frac{1}{N} \delta_{ij} \delta_{kl})$.

²⁸The notation in the first reference of [71] uses the three operators \mathcal{O}_1 , \mathcal{O}_2 , and \mathcal{O}'_T where we added the prime since it is not the same as our \mathcal{O}_T . What they call \mathcal{O}'_T is now more commonly called \mathcal{O}_{HD} . In our notation, $\mathcal{O}'_T = |H^\dagger D_\mu H|^2 \equiv \mathcal{O}_{HD} = (\mathcal{O}_H - \mathcal{O}_T)/2$, $\mathcal{O}_1 = -(\mathcal{O}_R + \mathcal{O}_H)$, and $\mathcal{O}_2 = \mathcal{O}_R$.

We are interested in the dimension-six operators generated by integrating out Φ ; since the $\mathcal{O}(\Phi_c^2)$ term in U' is minimally quartic in SM fields, $\mathcal{O}(\Phi_c^2) \sim \mathcal{O}(H^4) + \dots$, we can set $U' \approx U = 2\eta |H|^2$ in the second line of the above equation. In the first line of (2.51), higher dimension operators arise because $\Phi_c \neq 0$; by simple power counting, to capture the dim-6 operators we need to take $\Phi_c \approx \vec{B}/m^2 + (P^2 - U)\vec{B}/m^4$ in the $\text{tr } U'$ term and $\Phi_c \approx \vec{B}/m^2$ in the $\text{tr } U'^2$ term.²⁹

To evaluate the traces in (2.51), recall that $G'_{\mu\nu} = [D_\mu, D_\nu]$. Since Φ is in the adjoint of $SU(2)_L$, $G'_{\mu\nu} = [D_\mu, D_\nu] = -igW_{\mu\nu}^a t_G^a$ where the generators t_G^a are in the adjoint representation, so $\text{tr}(t_G^a t_G^b) = 2\delta^{ab}$. Keeping only up to dimension-six operators and using the operator definitions given in table 2.2, the traces evaluate to³⁰

$$\begin{aligned}
 \text{tr } U' &\supset 5\lambda_\Phi \vec{\Phi}_c^2 && \supset 20 \frac{\lambda_\Phi \kappa^2}{m^6} (-\eta \mathcal{O}_6 + \mathcal{O}_T + 2\mathcal{O}_R) \\
 \text{tr } U'^2 &\supset 20 \frac{\lambda_\Phi \kappa^2 \eta}{m^4} |H|^6 && = 20 \frac{\kappa^2 \eta \lambda_\Phi}{m^4} \mathcal{O}_6 \\
 \text{tr } U^3 &= 3(2\eta |H|)^3 && = +24\eta^3 \mathcal{O}_6 \\
 \text{tr}(P_\mu U)^2 &= -3(2\eta \partial_\mu |H|^2)^2 && = -24\eta^2 \mathcal{O}_H \\
 \text{tr } U G'_{\mu\nu} G'_{\mu\nu} &= -4\eta g^2 |H|^2 (W_{\mu\nu}^a)^2 && = -4\eta \mathcal{O}_{WW} \\
 \text{tr } G'^3 &= -g^3 \epsilon_{abc} W_{\mu\nu}^a W_{\nu\sigma}^b W_{\sigma\mu}^c && = -6g^2 \mathcal{O}_{3W} \\
 \text{tr}(P_\mu G'_{\mu\nu})^2 &= 2g^2 (D_\mu W_{\mu\nu}^a)^2 && = -4g^2 \mathcal{O}_{2W}
 \end{aligned}$$

²⁹As a side comment, we note that the terms in the first line of Eq. (2.51) can be used to find the contribution of Φ to the beta functions of SM couplings. In particular, the triplet contributes to the running of the Higgs' mass and quartic coupling and also to the $SU(2)_L$ gauge coupling g . This is easy to see since

$$\begin{aligned}
 \text{tr } U' &= 3U + 5 \frac{\lambda_\Phi}{m^4} \vec{B}^T \vec{B} + \text{dim-six ops} = 6\eta |H|^2 + 5 \frac{\lambda_\Phi \kappa^2}{m^4} |H|^4 \\
 \text{tr } U'^2 &= 3U^2 + \text{dim-six ops} = 12\eta^2 |H|^4 + \dots \\
 \text{tr } G'^2_{\mu\nu} &= -2g^2 (W_{\mu\nu}^a)^2.
 \end{aligned}$$

³⁰For example,

$$\begin{aligned}
 \text{tr } U'^2 &= \text{tr} \left[U \cdot \mathbf{1}_3 + \frac{\lambda_\Phi}{m^4} (\vec{B}^T \vec{B} \cdot \mathbf{1}_{3 \times 3} + 2\vec{B} \vec{B}^T) \right]^2 \\
 &\supset 2 \frac{\lambda_\Phi}{m^4} U \cdot \text{tr} (\vec{B}^T \vec{B} \cdot \mathbf{1}_{3 \times 3} + 2\vec{B} \vec{B}^T) \\
 &= 2 \frac{\lambda_\Phi}{m^4} U \cdot (5\vec{B}^T \vec{B}) \Rightarrow U = 2\eta |H|^2, \vec{B}^T \vec{B} = \kappa^2 |H|^4 \Rightarrow \\
 &= 20 \frac{\kappa^2 \eta \lambda_\Phi}{m^4} |H|^6
 \end{aligned}$$

Plugging these back into (2.51), the dimension-six operators in the one-loop effective action are

$$\begin{aligned} \Delta\mathcal{L}_{\text{eff,1-loop,dim 6}} = \frac{1}{32\pi^2} \frac{1}{m^2} \left[\frac{g^2}{15} (\mathcal{O}_{2W} + \mathcal{O}_{3W}) + 2\eta^2 \mathcal{O}_H + \frac{\eta}{3} \mathcal{O}_{WW} - 4\eta^3 \mathcal{O}_6 \right. \\ \left. + 20 \frac{\lambda_\Phi \kappa^2}{m^2} \left(-\eta \mathcal{O}_6 + \mathcal{O}_T + 2\mathcal{O}_R \right) \right]. \end{aligned} \quad (2.52)$$

Note that for the present example we use $\overline{\text{MS}}$ renormalization scheme, whose scheme-dependent finite pieces manifest as the terms proportional to λ_Φ in the above. These terms are associated to the renormalization of the Φ mass and the cross-quartic coupling η , see Fig. 2.3; one can in principle choose a different scheme so that these contributions vanish. Finally, we reiterate that the above effective Lagrangian is at the matching scale $\mu = m$, hence why the logarithm pieces from Eq. (2.51) vanish (this is scheme-independent).

2.1.4.2 Extra EW scalar doublet

Here we integrate out an additional electroweak scalar doublet Φ with hypercharge $Y_\Phi = -1/2$ and mass $m^2 \gg v^2$. This is essentially the two Higgs doublet model (2HDM) where the mass term for the extra scalar is taken large compared to the EW symmetry breaking scale.

The general Lagrangian for a 2HDM model can be rather complex; often, if the UV model doesn't already impose some restriction on the 2HDM model (as it does in, *e.g.*, supersymmetry), then some other simplifying approximation is made to make more tractable the study of the second doublet. Below, we will consider the most general scalar sector for the second EW doublet; this is rather easy to handle within our EFT framework and requires little additional effort.³¹

The most general Lagrangian consisting of an extra EW scalar doublet Φ with $Y_\Phi = -1/2$ interacting with the Higgs sector is given by

$$\begin{aligned} \mathcal{L} \supset & |D_\mu \Phi|^2 - m^2 |\Phi|^2 - \frac{\lambda_\Phi}{4} |\Phi|^4 \\ & + (\eta_H |\tilde{H}|^2 + \eta_\Phi |\Phi|^2) (\tilde{H}^\dagger \Phi + \Phi^\dagger \tilde{H}) \\ & - \lambda_1 |\tilde{H}|^2 |\Phi|^2 - \lambda_2 |\tilde{H}^\dagger \Phi|^2 - \lambda_3 [(\tilde{H}^\dagger \Phi)^2 + (\Phi^\dagger \tilde{H})^2]. \end{aligned} \quad (2.53)$$

where $D_\mu \Phi = (\partial_\mu - igW_\mu^a \tau^a - ig'Y_\Phi B_\mu) \Phi$, $\tau^a = \sigma^a/2$ are the $SU(2)_L$ generators in the fundamental representation, and $\tilde{H} \equiv i\sigma_2 H^*$ so that $\epsilon^{\alpha\beta} \Phi_\alpha H_\beta = \tilde{H}^\dagger \Phi$. The first line of the above is the potential of Φ alone, the second line contains a linear term in Φ which leads to a tree-level contribution to the effective action, while the last line contains interactions with the Higgs doublet H that appear in the effective action at one-loop order.

The main purpose of this section is to show how to use the covariant derivative expansion; in this regard, we remain agnostic to restrictions specific 2HDM models might impose on the Lagrangian in (2.53). However, let us make a few, brief comments. Here we focus on the Higgs

³¹Of course, a large reason why this is much easier in the EFT framework is because we have made the simplifying assumption that the second doublet is heavy.

sector and have not included a Yukawa sector with couplings to Φ ; these would lead to tree-level generated dimension-six operators involving only fermions. If a parity $\Phi \rightarrow -\Phi, H \rightarrow H$ is imposed, then the terms in the second line of (2.53) and extra Yukawa terms are forbidden. This parity prevents Φ from developing a vacuum expectation value³² and Φ in this case is sometimes known as an “inert Higgs” [72]. Finally, imposing an exact or approximate global $U(1)$ on Φ eliminates the second line in (2.53), the term proportional to λ_3 in (2.53), and any potential Yukawa terms involving Φ .

Tree-level matching

When we integrate out the massive doublet the term linear in Φ in (2.53), $\eta_H |H|^2 (\tilde{H}^\dagger \Phi + \text{h.c.})$, leads to a tree-level contribution to the effective action. As this interaction is cubic in the Higgs field, it is simple to see that the only dimension-six operator will be $\mathcal{O}_6 = |H|^6$. Concretely, B from the general tree-level formula Eq. (2.10) is given by $B = \eta_H |H|^2 \tilde{H}$. The solution to the linearized equation of motion is

$$\Phi_c = -\frac{1}{P^2 - m^2 - \lambda_1 |H|^2 - \lambda_2 \tilde{H} \tilde{H}^\dagger} B \approx \frac{1}{m^2} B = \frac{\eta_H}{m^2} |H|^2 \tilde{H}, \quad (2.54)$$

and the tree-level effective action through dimension-six operators is

$$\Delta \mathcal{L}_{\text{eff,tree,dim-6}} = \frac{1}{m^2} B^\dagger B = \frac{\eta_H^2}{m^2} |H|^6 = \frac{\eta_H^2}{m^2} \mathcal{O}_6. \quad (2.55)$$

One-loop-level matching

Let us now find the one-loop effective action from integrating out the massive scalar doublet Φ in Eq. (2.53). One of the main reasons we provide these examples is to show how to use the covariant derivative expansion. All the couplings in Eq. (2.53) make the effective action calculation complicated, but not very difficult. For the moment, however, let us make several simplifying assumptions on the couplings simply so that the basic setup and use of the CDE is not obscured. After we show the CDE for the simpler Lagrangian, we will return to the full Lagrangian in Eq. (2.53) and use the CDE to compute the one-loop effective action.

Simplifying case

For the simplifying assumptions, let us impose a global $U(1)$ on Φ so that $\eta_H = \eta_\Phi = \lambda_3 = 0$ in the Lagrangian. Again, we will come back and let these terms be non-zero shortly. In this case, there is no tree-level effective action. We integrate Φ out of the Lagrangian

$$\mathcal{L} \supset \Phi^\dagger (-D^2 - m^2 - \lambda_1 |H|^2 - \lambda_2 \tilde{H} \tilde{H}^\dagger) \Phi.$$

³²Since we assume $m^2 > 0$, Φ can only get a vacuum expectation value via the term linear in Φ in (2.53), i.e. the $\eta_\Phi |H|^2 (\tilde{H}^\dagger \Phi + \text{h.c.})$ term.

After performing the gaussian integral we are left with the effective action

$$\Delta S_{\text{eff,1-loop}} = i\text{Tr} \log [-P^2 + m^2 + A],$$

where we defined

$$A \equiv \lambda_1 |H|^2 + \lambda_2 \tilde{H} \tilde{H}^\dagger. \quad (2.56)$$

From here, we can use the universal formula in Eq. (2.38) with $c_s = 1$ since Φ is a complex boson and A substituted for U in (2.38). At this point, we are essentially done; all that is left is to compute the traces.

Let us give a few examples of trace computations by considering $\text{tr}(G'_{\mu\nu} G'_{\nu\sigma} G'_{\sigma\mu})$ and $\text{tr}(AG'_{\mu\nu} G'_{\mu\nu})$. The covariant derivative acting on Φ is $D_\mu = \partial_\mu - igW_\mu - ig'Y_\Phi B_\mu \cdot \mathbf{1}_2$ where we have explicitly denoted the 2×2 identity matrix by $\mathbf{1}_2$. Therefore,

$$G'_{\mu\nu} = [D_\mu, D_\nu] = -igW_{\mu\nu}^a \tau^a - ig'Y_\Phi B_{\mu\nu} \cdot \mathbf{1}_2.$$

In $\text{tr}G'^3$ the anti-symmetry on the Lorentz indices only leaves $\text{tr}W^3$ non-vanishing. Thus,³³

$$\text{tr} G'_{\mu\nu} G'_{\nu\sigma} G'_{\sigma\mu} = ig^3 \text{tr} W_{\mu\nu} W_{\nu\sigma} W_{\sigma\mu} = -\frac{g^3}{2} \mu(R) \epsilon_{abc} W_{\mu\nu}^a W_{\nu\sigma}^b W_{\sigma\mu}^c = -3g^2 \mu(R) \mathcal{O}_{3W},$$

where $\mu(R)$ is the Dynkin index for representation R and is equal to $1/2$ for the fundamental representation and \mathcal{O}_{3W} is as defined in table 2.2.

For $\text{tr}(AG'_{\mu\nu} G'_{\mu\nu})$ we have

$$\begin{aligned} \text{tr}(AG'_{\mu\nu} G'_{\mu\nu}) &= -\text{tr} \left[A \times (gW_{\mu\nu}^a \tau^a + g'Y_\Phi B_{\mu\nu} \cdot \mathbf{1}_2)^2 \right] \\ &= -g^2 \text{tr}(AW_{\mu\nu} W_{\mu\nu}) - g'^2 Y_\Phi^2 B_{\mu\nu} B_{\mu\nu} \text{tr} A - 2gg' Y_\Phi B_{\mu\nu} \text{tr}(AW_{\mu\nu}), \end{aligned}$$

using $\text{tr}A\tau^a = \lambda_2 \tilde{H}^\dagger \tau^a \tilde{H} = -\lambda_2 H^\dagger \tau^a H$ and a few other manipulations, it is straightforward to see that

$$\begin{aligned} \text{tr}(AG'_{\mu\nu} G'_{\mu\nu}) &= -(2\lambda_1 + \lambda_2) \left(\frac{g^2}{4} |H|^2 W_{\mu\nu}^a W_{\mu\nu}^a + g'^2 Y_\Phi^2 |H|^2 B_{\mu\nu} B_{\mu\nu} \right) + 2gg' \lambda_2 Y_\Phi (H^\dagger \tau^a H) W_{\mu\nu}^a B_{\mu\nu} \\ &= -(2\lambda_1 + \lambda_2) \left(\frac{1}{4} \mathcal{O}_{WW} + Y_\Phi^2 \mathcal{O}_{BB} \right) + \lambda_2 Y_\Phi \mathcal{O}_{WB}. \end{aligned}$$

Returning to the full Lagrangian

Now we return to the full Lagrangian in (2.53) and leave all couplings non-zero. This makes the calculation more complicated; however, it will not be too difficult—we will simply need to

³³We used

$$\text{tr}(T^a T^b T^c) = \frac{1}{2} \text{tr} \left([T^a, T^b] T^c + \underbrace{\{T^a, T^b\}}_{\text{vanishes by } W^a W^b W^c \text{ anti-symm}} T^c \right) = \frac{i}{2} f^{abd} \text{tr} T^d T^c = \frac{i}{2} \mu(R) f^{abc}$$

evaluate some traces which, while tedious, is very straightforward. In many regards, most of the work goes into setting up the matrix that we are tracing over.

To evaluate the one-loop effective action, we expand the action around the solution to the equation of motion, $\Phi = \Phi_c + \sigma$. Because the interaction $(\tilde{H}^\dagger \Phi)^2$ is holomorphic in Φ , it is easiest to treat Φ and Φ^* as separate variables. This is equivalent to splitting Φ into its real and imaginary pieces, although more convenient to work with. Then, upon expanding $\Phi = \Phi_c + \sigma$ and doing a little algebra, the terms quadratic in σ are

$$\mathcal{L}[\Phi_c + \sigma] \supset \frac{1}{2}(\sigma^\dagger \quad \sigma^T) \begin{pmatrix} P^2 - m^2 - A' & -2V \\ -2V^\dagger & (P^T)^2 - m^2 - A'^T \end{pmatrix} \begin{pmatrix} \sigma \\ \sigma^* \end{pmatrix}, \quad (2.57)$$

where

$$\begin{aligned} A' &= A - \eta_\Phi (\tilde{H}^\dagger \Phi_c + \Phi_c \tilde{H}^\dagger + \text{h.c.}) + \frac{\lambda_\Phi}{2} (|\Phi_c|^2 + \Phi_c \Phi_c^\dagger), \\ V &= \lambda_3 \tilde{H} \tilde{H}^T - \eta_\Phi \Phi_c \tilde{H}^T + \frac{\lambda_\Phi}{4} \Phi_c \Phi_c^T. \end{aligned} \quad (2.58)$$

A few comments:

- We are treating σ and σ^* as separate variables, which is the same procedure as working with the real and imaginary parts of σ .
- The one-loop effective action is given by

$$\Delta S_{\text{eff},1\text{-loop}} = \frac{i}{2} \text{Tr} \log (\dots),$$

with the matrix in (2.57) inserted into the trace. Note the factor of 1/2; we take $c_s = 1/2$ since we are treating σ and σ^* as separate, real variables.

- The classical configuration is given by

$$\Phi_c = \left[\frac{1}{m^2} + \frac{1}{m^4} (P^2 - A) + \dots \right] B.$$

Recall that $B \sim \mathcal{O}(H^3)$ and $A \sim \mathcal{O}(H^2)$. Keeping up to dimension-six operators, for the traces below we need to keep the above two terms in Φ_c for $\text{tr} U$, only the leading term for $\text{tr} U^2$, and we can drop Φ_c from the other traces.

We now use the CDE to compute $\Delta S_{\text{eff},1\text{-loop}}$. In the CDE formulas, we take

$$P_\mu = \begin{pmatrix} P_\mu & 0 \\ 0 & P_\mu^T \end{pmatrix}, \quad m^2 = \begin{pmatrix} m^2 \mathbf{1}_2 & 0 \\ 0 & m^2 \mathbf{1}_2 \end{pmatrix}, \quad U = \begin{pmatrix} A' & 2V \\ 2V^\dagger & A'^T \end{pmatrix}, \quad (2.59)$$

where $\mathbf{1}_2$ is the 2×2 identity matrix. The effective action is of the form $\text{Tr} \log (-P^2 + m^2 + U)$, so that the transformation $e^{\pm P^\mu \partial / \partial q^\mu}$ in Eq. (2.15) is still allowed and the CDE proceeds as discussed.

Thus, we can immediately use the universal results in Eq. (2.38) with matrices P_μ and U defined as above in (2.59), and all that is left to do is evaluate some traces. Tabulating only dim-6 operators, using the operator definitions in Table 2.2, and including a factor of $1/2$ for convenience, we find

$$\begin{aligned}
 \frac{1}{2}\text{tr} U &= \text{tr} A' && \supset \left[\frac{3}{2}\lambda_\Phi\eta_H^2 + 6\eta_\Phi(\lambda_1 + \lambda_2) \right] \mathcal{O}_6/m^4 \\
 &&& -6\eta_\Phi\eta_H(\mathcal{O}_R + \mathcal{O}_H)/m^4 \\
 \frac{1}{2}\text{tr} U^2 &= \text{tr} A'^2 + 4\text{tr} VV^\dagger && \supset -4(3\lambda_1 + 3\lambda_2 + \lambda_3)\eta_H\eta_\Phi \mathcal{O}_6/m^2 \\
 \frac{1}{2}\text{tr} U^3 &= \text{tr} A'^3 + 6\text{tr} (AVV^\dagger + A^TV^\dagger V) && = (2\lambda_1^3 + 3\lambda_1^2\lambda_2 + 3\lambda_1\lambda_2^2 + \lambda_2^3 + 12(\lambda_1 + \lambda_2)\lambda_3^2)\mathcal{O}_6 \\
 \frac{1}{2}\text{tr}(P_\mu U)^2 &= \text{tr}(P_\mu A)^2 + 4\text{tr}(P_\mu V P_\mu^T V^\dagger) && = -(4\lambda_1^2 + 4\lambda_1\lambda_2 + \lambda_2^2 + 4\lambda_3^2)\mathcal{O}_H - 2(\lambda_2^2 + 4\lambda_3^2)\mathcal{O}_R \\
 &&& -(\lambda_2^2 - 4\lambda_3^2)\mathcal{O}_T \\
 \frac{1}{2}\text{tr} U G'_{\mu\nu} G'_{\mu\nu} &= \text{tr} A G'_{\mu\nu} G'_{\mu\nu} && = -(2\lambda_1 + \lambda_2) \left(\frac{1}{4}\mathcal{O}_{WW} + Y_\Phi^2 \mathcal{O}_{BB} \right) + \lambda_2 Y_\Phi \mathcal{O}_{WB} \\
 \frac{1}{2}\text{tr} G'^3 &= ig^3 \text{tr} W_{\mu\nu} W_{\nu\sigma} W_{\sigma\mu} && = -\frac{3}{2}g^2 \mathcal{O}_{3W} \\
 \frac{1}{2}\text{tr}(P_\mu G'_{\mu\nu})^2 &= \frac{g^2}{2} (D_\mu W_{\mu\nu}^a)^2 + 2g'^2 Y_\Phi^2 (\partial_\mu B_{\mu\nu})^2 && = -g^2 \mathcal{O}_{2W} - 4g'^2 Y_\Phi^2 \mathcal{O}_{2B}
 \end{aligned} \tag{2.60}$$

Plugging these traces into Eq. (2.38) we obtain the one-loop effective Lagrangian. We summarize the results below.

Electroweak scalar doublet summary

We took an electroweak scalar doublet Φ with hypercharge $Y_\Phi = -1/2$ and Lagrangian

$$\begin{aligned}
 \mathcal{L} \supset & |D_\mu \Phi|^2 - m^2 |\Phi|^2 - \frac{\lambda_\Phi}{4} |\Phi|^4 + (\eta_H |H|^2 + \eta_\Phi |\Phi|^2) (\Phi \cdot H + \text{h.c.}) \\
 & - \lambda_1 |H|^2 |\Phi|^2 - \lambda_2 |\Phi \cdot H|^2 - \lambda_3 [(\Phi \cdot H)^2 + \text{h.c.}],
 \end{aligned} \tag{2.61}$$

and integrated out Φ to find the dimension-six operators of the effective action matched at one-loop order.

The tree-level effective action, given in Eq. (2.55), only contains $\mathcal{O}_6 = |H|^6$. The one-loop effective action is obtained from plugging the traces in Eq. (2.60) into (2.38). This piece contains a host of dimension-six operators that affect electroweak and Higgs physics. In summary, the effective Lagrangian at the matching scale is given by

$$\begin{aligned}
 \mathcal{L}_{\text{eff}} = \mathcal{L}_{\text{SM}} + \frac{1}{m^2} & \left(c_6 \mathcal{O}_6 + c_H \mathcal{O}_H + c_T \mathcal{O}_T + c_R \mathcal{O}_R + c_{BB} \mathcal{O}_{BB} + c_{WW} \mathcal{O}_{WW} \right. \\
 & \left. + c_{WB} \mathcal{O}_{WB} + c_{3W} \mathcal{O}_{3W} + c_{2W} \mathcal{O}_{2W} + c_{2B} \mathcal{O}_{2B} \right),
 \end{aligned} \tag{2.62}$$

where the Wilson coefficients are given in Table 2.3. As in the previous example with the triplet scalar, we have used $\overline{\text{MS}}$ renormalization scheme. In this scheme, the non-zero finite pieces at the matching scale $\mu = m$ are given by the terms in Table 2.3 involving the parameters η_Φ , η_H , and λ_Φ .

$c_H = \frac{1}{(4\pi)^2} [6\eta_\Phi \eta_H + \frac{1}{12} (4\lambda_1^2 + 4\lambda_1 \lambda_2 + \lambda_2^2 + 4\lambda_3^2)]$	$c_{BB} = \frac{1}{(4\pi)^2} \frac{1}{12} Y_\Phi^2 (2\lambda_1 + \lambda_2)$	$c_{3W} = \frac{1}{(4\pi)^2} \frac{1}{60} g^2$
$c_T = \frac{1}{(4\pi)^2} \frac{1}{12} (\lambda_2^2 - 4\lambda_3^2)$	$c_{WW} = \frac{1}{(4\pi)^2} \frac{1}{48} (2\lambda_1 + \lambda_2)$	$c_{2W} = \frac{1}{(4\pi)^2} \frac{1}{60} g^2$
$c_R = \frac{1}{(4\pi)^2} [6\eta_\Phi \eta_H + \frac{1}{6} (\lambda_2^2 + 4\lambda_3^2)]$	$c_{WB} = -\frac{1}{(4\pi)^2} \frac{1}{12} \lambda_2 Y_\Phi$	$c_{2B} = \frac{1}{(4\pi)^2} \frac{1}{60} 4g'^2 Y_\Phi^2$

$c_6 = \eta_H^2 + \frac{1}{(4\pi)^2} \left[\frac{3}{2} \lambda_\Phi \eta_H^2 + 6\eta_\Phi (\lambda_1 + \lambda_2) - \frac{1}{6} (2\lambda_1^3 + 3\lambda_1^2 \lambda_2 + 3\lambda_1 \lambda_2^2 + \lambda_2^3) - 2(\lambda_1 + \lambda_2) \lambda_3^2 \right]$

Table 2.3: Wilson coefficients c_i for the operators \mathcal{O}_i in Table 2.2 generated from integrating out a massive electroweak scalar doublet Φ with hypercharge $Y_\Phi = -1/2$. g and g' denote the gauge couplings of $SU(2)_L$ and $U(1)_Y$, respectively. The couplings $\lambda_{1,2,3}$ and $\eta_{\Phi,H}$ are defined by the Lagrangian in Eq. (2.61); they are associated with various interactions between Φ and the SM Higgs doublet H .

2.1.4.3 A $SU(2)_L$ quartet scalar

In this example, we consider a heavy complex $SU(2)_L$ quartet scalar Φ with mass m and SM hypercharge $Y_\Phi = \frac{3}{2}$. An allowed ΦH^3 coupling to the Higgs leads to tree-level contributions in the effective action. For brevity, we will ignore other interaction terms with the Higgs, *e.g.* $|\Phi|^2 |H|^2$, as well as the quartet's self-couplings—they can be easily included as in previous examples. This amounts to taking $U = 0$ in Eq. 2.38. Thus, we consider the following Lagrangian

$$\Delta\mathcal{L} = \Phi^\dagger (-D^2 - m^2) \Phi - (\Phi^\dagger B + c.c.), \quad (2.63)$$

where $\Phi = (\Phi_1, \Phi_2, \Phi_3, \Phi_4)^T$, with each component being eigenstate of the third $SU(2)_L$ generator $t_\Phi^3 = \text{diag}(\frac{3}{2}, \frac{1}{2}, -\frac{1}{2}, -\frac{3}{2})$, and $B \sim H^3$. Specifically,

$$B = \begin{pmatrix} H_1^3 \\ \sqrt{3} H_1^2 H_2 \\ \sqrt{3} H_1 H_2^2 \\ H_2^3 \end{pmatrix}, \quad (2.64)$$

where H_1 and H_2 are components of the SM Higgs field $H = (H_1, H_2)^T$.³⁴

Again, we follow the procedure described in Section 2.1.1.1 to compute the tree-level effective Lagrangian. We first get the equation of motion

$$(-D^2 - m^2) \Phi_c = B,$$

³⁴For quartet scalar Φ with $Y_\Phi = 1/2$, B would be given by $(\tilde{H} \equiv i\sigma_2 H)$

$$B_{Y=1/2} = \begin{pmatrix} H_1^2 \tilde{H}_1 \\ \frac{1}{\sqrt{3}} H_1^2 \tilde{H}_2 + \frac{2}{\sqrt{3}} H_1 H_2 \tilde{H}_1 \\ \frac{1}{\sqrt{3}} H_2^2 \tilde{H}_1 + \frac{2}{\sqrt{3}} H_1 H_2 \tilde{H}_2 \\ H_2^2 H_2 \end{pmatrix}. \quad (2.65)$$

which gives the solution

$$\Phi_c = -\frac{1}{D^2 + m^2} B \approx -\frac{1}{m^2} B.$$

Plugging this solution back to Eq. (2.63), we get

$$\Delta\mathcal{L}_{\text{eff,tree}} = -B^\dagger \Phi_c \approx \frac{1}{m^2} B^\dagger B = \frac{1}{m^2} |H|^6 = \frac{1}{m^2} \mathcal{O}_6. \quad (2.66)$$

Because we are ignoring other interactions that Φ may have, at one-loop we only get dimension-six operators solely involving gauge fields. The general contribution of particles to the pure glue Wilson coefficients was given in Table 2.1. The quartet is the spin 3/2 representation of $SU(2)$ and has Dynkin index $\mu(R) = 5$. Therefore, for \mathcal{O}_{2W} and \mathcal{O}_{3W} , we find

$$\Delta\mathcal{L}_{\text{eff,1-loop}} \supset \frac{1}{(4\pi)^2} \frac{1}{m^2} \frac{g^2}{6} (\mathcal{O}_{2W} + \mathcal{O}_{3W}). \quad (2.67)$$

For $U(1)$ gauge groups we can also use the results of Table 2.1: replace $a_{2s}\mu(R)$ with $n_\Phi Q^2$, where Q is the charge of Φ under the $U(1)$ and n_Φ is the number of real-degrees of freedom in Φ . (Note that, by anti-symmetry on the Lorentz indices, \mathcal{O}_{3G} vanishes if the group is abelian.) For the case at hand, the quartet has hypercharge 3/2 and four complex (eight real) degrees of freedom. Therefore,

$$\Delta\mathcal{L}_{\text{eff,1-loop}} \supset \frac{1}{(4\pi)^2} \frac{1}{m^2} \frac{3}{10} g'^2 \mathcal{O}_{2B}. \quad (2.68)$$

2.1.4.4 Kinetic mixing of gauge bosons

In this example, we consider a heavy $U(1)$ gauge boson K_μ with mass m_K that has a kinetic mixing with the SM $U(1)_Y$ gauge boson B_μ ,

$$\Delta\mathcal{L} = -\frac{1}{4} K_{\mu\nu} K^{\mu\nu} + \frac{1}{2} m_K^2 K_\mu K^\mu - \frac{k}{2} B^{\mu\nu} K_{\mu\nu}, \quad (2.69)$$

where $K_{\mu\nu}$ denotes the field strength $K_{\mu\nu} = \partial_\mu K_\nu - \partial_\nu K_\mu$. Again, the tree-level effective Lagrangian can be obtained by following the procedure described in Section 2.1.1.1. We first find the equation of motion of this heavy gauge boson K_μ ,

$$\partial_\nu K^{\mu\nu} + k(\partial_\nu B^{\mu\nu}) = m_K^2 K^\mu,$$

which, as usual for vector bosons, can be decomposed into two equations,

$$\begin{aligned} \partial_\mu K^\mu &= 0, \\ (-\partial^2 - m_K^2) K^\mu &= -k(\partial_\nu B^{\mu\nu}). \end{aligned}$$

Solving these, we get the classical solution

$$K_{c\mu} = \frac{k}{\partial^2 + m_K^2} (\partial^\nu B_{\mu\nu}) \approx \frac{k}{m_K^2} (\partial^\nu B_{\mu\nu}). \quad (2.70)$$

Next we plug this solution back into the UV model Lagrangian (Eq. (2.69)) to get the tree-level effective Lagrangian. With $B^{\mu\nu}K_{\mu\nu} = 2(\partial_\nu B^{\mu\nu})K_\mu$, we obtain

$$\begin{aligned}
 \Delta\mathcal{L}_{\text{eff,tree}} &= -\frac{1}{2}K_{c\mu} [(-\partial^2 - m_K^2)g^{\mu\nu} + \partial^\mu\partial^\nu] K_{c\nu} - \frac{k}{2}B^{\mu\nu}K_{c\mu\nu} \\
 &= \frac{k}{2}(\partial_\nu B^{\mu\nu})K_{c\mu} - k(\partial_\nu B^{\mu\nu})K_{c\mu} \\
 &= -\frac{k}{2}(\partial_\nu B^{\mu\nu})K_{c\mu} \\
 &= \frac{k^2}{m_K^2}\mathcal{O}_{2B}.
 \end{aligned} \tag{2.71}$$

Note that this example has a trivial one-loop contribution to the effective action.

2.1.4.5 Heavy vector bosons in the triplet representation of $SU(2)_L$

Here we consider an example involving heavy vector bosons transforming under a low-energy (unbroken) non-abelian gauge symmetry. Massive vector bosons generically arise in, for example, extra-dimensional compactifications [73] and little Higgs theories [74]. We wish to draw attention to the comparative simplicity with the present covariant method versus traditional loop methods involving massive vector bosons. For example, this method could be readily employed to study massive vector bosons whose tree-level contributions are absent due to, *e.g.*, KK-parity [75] in extra-dimensional models or T-parity [76] in little Higgs models.

We consider an $SU(2)_1 \times SU(2)_2$ gauge symmetry with a scalar Φ transforming as a bifundamental. We take the Standard Model fermions and Higgs field to be localized to the $SU(2)_1$ gauge group. (We suppress color and hypercharge; the full gauge symmetry is $SU(2)_1 \times SU(2)_2 \times U(1)_Y \times SU(3)_c$.) The scalar Φ takes a vev, breaking the $SU(2)$ groups down to their diagonal subgroup, which we identify with the weak interactions of the SM, $SU(2)_1 \times SU(2)_2 \rightarrow SU(2)_L$. This is simply a deconstructed [77] version of an extra-dimensional model (*e.g.* [78]), where the weak gauge bosons, being a diagonal combination of the $SU(2)_1 \times SU(2)_2$ gauge bosons, “propagate in the bulk”, while the SM fermions and Higgs only transform under one gauge group and are therefore “localized”.

The relevant kinetic terms of the Lagrangian are

$$\Delta\mathcal{L}_K = -\frac{1}{2}\text{tr}(F_1^{\mu\nu})^2 - \frac{1}{2}\text{tr}(F_2^{\mu\nu})^2 + \frac{1}{2}\text{tr}(\mathcal{D}_\mu\Phi)^\dagger(\mathcal{D}^\mu\Phi), \tag{2.72}$$

where the scalar Φ transforms as a bifundamental, $\Phi \rightarrow U_1\Phi U_2^\dagger$. The covariant derivative of the UV theory is given by³⁵

$$\mathcal{D}_\mu = \partial_\mu - ig_1 A_{1\mu} - ig_2 A_{2\mu},$$

³⁵Note that the action of \mathcal{D}_μ on Φ is $\mathcal{D}_\mu\Phi = \partial_\mu\Phi - ig_1 A_{1\mu}\Phi + ig_2\Phi A_{2\mu}$

where g_i and $A_{i\mu} = A_{i\mu}^a \tau_i^a$ are the gauge coupling and gauge bosons of the $SU(2)_i$ with the generators τ_i^a taken in the fundamental representation. A vacuum expectation value for Φ ,

$$\langle \Phi \rangle = \frac{1}{\sqrt{2}} \begin{pmatrix} v & 0 \\ 0 & v \end{pmatrix},$$

breaks $SU(2)_1 \times SU(2)_2 \rightarrow SU(2)_L$. The mass eigenstates are

$$Q^a \equiv \frac{1}{\sqrt{g_1^2 + g_2^2}} (g_1 A_1^a - g_2 A_2^a), \quad (2.73a)$$

$$W^a \equiv \frac{1}{\sqrt{g_1^2 + g_2^2}} (g_2 A_1^a + g_1 A_2^a), \quad (2.73b)$$

where W^a are the SM gauge bosons corresponding to the unbroken symmetry $SU(2)_L$, and Q^a obtain a mass $m_Q^2 = (g_1^2 + g_2^2)v^2/4$ from the Higgs mechanism. Q_μ transforms in the adjoint of the unbroken $SU(2)_L$.

In terms of the mass eigenstates, the covariant derivative becomes

$$\mathcal{D}_\mu = \partial_\mu - igW_\mu^a \tau_L^a - iQ_\mu^a \left(\frac{g_1^2}{\sqrt{g_1^2 + g_2^2}} \tau_1^a - \frac{g_2^2}{\sqrt{g_1^2 + g_2^2}} \tau_2^a \right), \quad (2.74)$$

where $\tau_L^a = \tau_1^a + \tau_2^a$ are the unbroken generators and we identify $g \equiv g_1 g_2 / \sqrt{g_1^2 + g_2^2}$ as the weak coupling constant of the SM. We expand Φ around $\langle \Phi \rangle$,

$$\Phi = \frac{1}{\sqrt{2}} (v + h) \begin{pmatrix} 1 & 0 \\ 0 & 1 \end{pmatrix} + i\sqrt{2}\chi^a \tau^a. \quad (2.75)$$

where the χ^a are the Nambu-Goldstone bosons transforming in the adjoint (triplet) representation of the unbroken $SU(2)_L$ and h is the massive Higgs field.

Now we integrate out the massive Q_μ . At tree-level, Q_μ couples to the $SU(2)_L$ source current. At loop-level, we need to gauge fix—as summarized in section 2.1.2, we take a generalized R_ξ gauge which preserves the unbroken $SU(2)_L$ gauge symmetry (simply promote ∂_μ in the usual R_ξ gauge to D_μ). Expanding out \mathcal{L}_K in terms of W_μ , Q_μ , χ , and adding the gauge fixing piece $\mathcal{L}_{\text{g.f.}}$, the ghost term $\mathcal{L}_{\text{ghost}}$, and the interaction \mathcal{L}_I between Q_μ and the SM fields,

$$\Delta \mathcal{L}_K \supset -\frac{1}{2} \text{tr}(D^\mu Q^\nu - D^\nu Q^\mu)^2 + ig \text{tr}([Q^\mu, Q^\nu] W_{\mu\nu}) + \text{tr}(D_\mu \chi - m_Q Q_\mu)^2, \quad (2.76a)$$

$$\mathcal{L}_{\text{g.f.}} = -\frac{1}{\xi} \text{tr}(\xi m_Q \chi + D^\mu Q_\mu)^2, \quad (2.76b)$$

$$\mathcal{L}_{\text{ghost}} \supset \bar{c}^a (-D^2 - \xi m_Q^2)^{ab} c^b, \quad (2.76c)$$

$$\mathcal{L}_I = \frac{g_1^4}{4(g_1^2 + g_2^2)} |H|^2 Q_\mu^a Q^{a\mu} + \frac{g_1^2}{\sqrt{g_1^2 + g_2^2}} Q_\mu^a J_W^{a\mu}, \quad (2.76d)$$

we find the Lagrangian up to quadratic terms in Q_μ^a to be,

$$\begin{aligned} \Delta\mathcal{L} = & \frac{1}{2}Q_\mu^a \left\{ D^2 g^{\mu\nu} - D^\nu D^\mu + m_Q^2 g^{\mu\nu} + [D^\mu, D^\nu] + \frac{1}{\xi} D^\mu D^\nu + \frac{g_1^4}{2(g_1^2 + g_2^2)} |H|^2 g^{\mu\nu} \right\}^{ab} Q_\nu^b \\ & + \frac{g_1^2}{\sqrt{g_1^2 + g_2^2}} Q_\mu^a J_W^{a\mu} + \frac{1}{2} \chi^a (-D^2 - \xi m_Q^2)^{ab} \chi^b + \bar{c}^a (-D^2 - \xi m_Q^2)^{ab} c^b, \end{aligned} \quad (2.77)$$

where H denotes the SM Higgs field and $J_W^{a\mu}$ is the source current of the SM W_μ^a . Working with Feynman gauge $\xi = 1$, we get

$$\begin{aligned} \Delta\mathcal{L} = & \frac{1}{2}Q_\mu^a \left\{ D^2 g^{\mu\nu} + m_Q^2 g^{\mu\nu} + 2[D^\mu, D^\nu] + \frac{g_1^4}{2(g_1^2 + g_2^2)} |H|^2 g^{\mu\nu} \right\}^{ab} Q_\nu^b \\ & + \frac{g_1^2}{\sqrt{g_1^2 + g_2^2}} Q_\mu^a J_W^{a\mu} + \frac{1}{2} \chi^a (-D^2 - m_Q^2)^{ab} \chi^b + \bar{c}^a (-D^2 - m_Q^2)^{ab} c^b. \end{aligned} \quad (2.78)$$

This Lagrangian is clearly in the form of Eq. (2.35), supplemented by a linear interaction term.

Although the heavy fields Q_μ^a couple directly to the fermions in SM, upon using the equation of motion $D_\mu W^{a\mu\nu} = J_W^{a\nu}$, the tree-level effective Lagrangian can be written in a way such that it only contains bosonic operators. To see this, we first solve the equation of motion for Q_μ at leading order,

$$Q_c^{a\mu} = -\frac{g_1^2}{\sqrt{g_1^2 + g_2^2}} \frac{1}{m_Q^2} J_W^{a\mu}. \quad (2.79)$$

Then we plug this back into Eq. (2.78) and obtain the tree-level effective Lagrangian:

$$\Delta\mathcal{L}_{\text{eff,tree}} = \frac{1}{2} \frac{g_1^2}{\sqrt{g_1^2 + g_2^2}} Q_{c\mu}^a J_W^{a\mu} = -\frac{1}{2m_Q^2} \frac{g_1^4}{g_1^2 + g_2^2} J_W^a J_W^{a\mu} = \frac{g_1^4}{g_1^2 + g_2^2} \frac{1}{m_Q^2} \mathcal{O}_{2W}. \quad (2.80)$$

The one-loop effective Lagrangian can be read off from Table 2.1 and Eq. (2.38) using U as in Eq. (2.36a) with $M^{\mu\nu} = \frac{g_1^4}{2(g_1^2 + g_2^2)} |H|^2 g^{\mu\nu}$:

$$\begin{aligned} \Delta\mathcal{L}_{\text{eff,1-loop}} = & \frac{1}{(4\pi)^2} \frac{1}{m_Q^2} \left[\frac{g^2}{20} (3\mathcal{O}_{3W} - 37\mathcal{O}_{2W}) + \frac{1}{4} \left(\frac{g_1^4}{g_1^2 + g_2^2} \right)^2 \mathcal{O}_H \right. \\ & \left. - \frac{1}{24} \left(\frac{g_1^4}{g_1^2 + g_2^2} \right)^3 \mathcal{O}_6 \right]. \end{aligned} \quad (2.81)$$

2.2 Running of Wilson coefficients and choosing an operator set

To connect with measurements, the Wilson coefficients $c_i(\Lambda)$ determined at the matching scale Λ need to be evolved down to the weak scale m_W according to their renormalization group (RG)

equations. From the perspective of *using* the SM EFT, the most important question surrounding RG running is whether or not it is relevant. In other words, when is it sufficient to simply take the zeroth order solution $c_i(m_W) = c_i(\Lambda)$ versus higher order corrections? This, of course, depends on the sensitivity of present and future precision measurements. We discuss details below, but a short rule of thumb is that RG running is relevant only if $c_i(\Lambda)$ is generated at tree-level.

If one needs to include RG running, it follows from the above rule of thumb that it is sufficient to take just the leading order correction. At leading order, the RG equations are governed by the anomalous dimension matrix γ_{ij} ,

$$\frac{dc_i(\mu)}{d \log \mu} = \sum_j \frac{1}{16\pi^2} \gamma_{ij} c_j, \quad (2.82)$$

whose leading order solution is

$$c_i(m_W) = c_i(\Lambda) - \sum_j \frac{1}{16\pi^2} \gamma_{ij} c_j(\Lambda) \log \frac{\Lambda}{m_W}. \quad (2.83)$$

Computing γ_{ij} in the SM EFT is no small endeavor; fortunately, results for the one-loop anomalous dimension matrix are known [40–45]. To consistently make use of these results, the main issue concerns operator bases—as with any matrix, the components γ_{ij} depend on the basis in which the matrix is expressed! We will discuss how the choice of operator sets affects the expression and use of γ_{ij} . Following this, we will give a short summary of common basis choices in the literature and how to go between them.

2.2.1 When is RG running important?

Although the running of Wilson coefficients is a conceptually important step, there turn out to be strong requirements on the class of UV models for it to be of practical relevance. Near future measurements have an estimated sensitivity at the per mille level: from $v^2/\Lambda^2 \sim 0.1\%$, we see that Λ can be probed at most up to a few TeV. So the logarithm is not large, $\log(\Lambda/m_W) \sim 3$, and therefore loop order counting in perturbative expansions is reasonable.

Counting by loop order, per mille level precision means that we can truncate perturbative calculations at one-loop. Since RG evolution contributes a loop factor, the running of $c_j(\Lambda)$ into $c_i(m_W)$, $i \neq j$, will be of practical relevance if $c_j(\Lambda)$ is of tree-level size. In particular, if $c_j(\Lambda)$ is generated at one-loop level, then its contribution to $c_i(m_W)$ from RG running is of two loop size and hence negligible. Additionally, even in the case that $c_j(\Lambda)$ is generated at tree level, its contribution to $c_i(m_W)$ is subdominant if $c_i(\Lambda)$ is also generated at tree level. Therefore, as a rule of thumb, one needs to take account for RG evolution of c_j into c_i only when both of the following conditions are satisfied:

1. $c_j(\Lambda)$ is generated at tree level from the UV model.
2. $c_i(\Lambda)$ is not generated at tree level from the UV model.

The fact that $c_j(\Lambda)$ need to be generated at tree-level for RG running to be important is a strong requirement—many motivated models of new physics only generate Wilson coefficients at one-loop level. Familiar examples of such cases are SUSY with R-parity, extra dimensions with KK parity, and little Higgs models with T parity. The parity in all these examples is a discrete symmetry which forces the new particles to always come in pairs, hence leading only to loop-level contributions of Wilson coefficients.

Let us discuss this rule of thumb in the context of the examples in Sec. 2.1.4 where a heavy scalar couples at tree-level to the Higgs sector. There are only four such models! Among these, the $SU(2)$ scalar doublet and quartet only generate $\mathcal{O}_6 = |H|^6$ at tree-level. Since \mathcal{O}_6 does not run into other dimension-six operators, the RG running is trivial. Therefore, RG analysis is only relevant for the two other examples in the list. An explicit example of this RG analysis can be found in [1], where we found the RG-induced constraints on the singlet example of Sec. 2.1.4 to be quite constraining.

2.2.2 Choosing an operator set in light of RG running analysis

As mentioned before, the anomalous dimension matrix γ_{ij} has been computed in the literature [40–45]. When RG running analysis is relevant, one just needs to make use of the known γ_{ij} appropriately.

There are many dimension-six operators that respect the SM gauge invariance. However, some of these operators are redundant in the sense that they lead to the same physical effects. The relations among these operators stem from group identities, integration by parts, and use of the equations of motion; the first two of these are obvious, the latter is a result of the fact that physical quantities are on-shell, and therefore respect the equations of motion. An operator set is said to be *complete* if it can capture all possible physical effects stemming from the higher dimension operators. A complete operator set with a minimal number of operators is called an “operator basis”. We will discuss specific operator basis for the SM EFT in the next subsection.

Note that when performing calculations (matching, RG running, *etc.*), the theory does not select for a particular operator set or basis—choosing an operator set is something imposed by hand. *A priori*, there is no clear criteria to tell which operator set is “best”, or if using a non-redundant versus redundant set of operators is “better”. In general, there are three types of operator sets: (1) an operator basis, (2) an overcomplete set that has some redundant operators, and (3) an incomplete set that lacks of some components compared to a complete operator basis. For a consistent RG analysis, one generically should choose a complete operator set such that the RG running (Eq. (2.82)) is closed [40].

Before discussing the above three choices of operator sets, we would like to include a relevant technical remark that regard how the anomalous dimension matrix is computed. One first chooses an operator set and then computes the anomalous dimension matrix for this operator set. For a chosen operator set, there are generically two types of contributions to γ_{ij} : the *direct contribution* where \mathcal{O}_j generates \mathcal{O}_i directly through a loop Feynman diagram, and the *indirect contribution* where \mathcal{O}_j generates some \mathcal{O}_k outside the operator set chosen, whose elimination (through the equations of motion or an operator identity) in turn gives \mathcal{O}_i .

- Working with a Complete Operator Basis

This case is fairly straightforward. The full anomalous dimension matrix γ_{ij} in the “standard basis” (see the next subsection for definition) has been computed [40–42]. One can simply carry out a basis transformation to obtain the γ_{ij} in the new basis.

- Working with an Overcomplete Operator Set

Sometimes it is helpful to use a redundant operator set because it can make the physics more transparent. For example, the matching from a UV model may generate an overcomplete set of effective operators. An obvious drawback of working with an overcomplete set of operators is that the size of γ_{ij} would be larger than necessary, and that the value of γ_{ij} would not be unique [40]. However, this does not necessarily mean that γ_{ij} is harder to calculate. For example, consider the extreme case of using all the dim-6 operators, before using equations of motion to remove any redundant combination. This is a super overcomplete set, and as a result the size of γ_{ij} would be way larger than that in the standard basis. But with this choice of operator set, all the contributions to γ_{ij} are direct contributions by definition. Some of these direct contributions would become indirect in a smaller operator set, and one has to accommodate them by using equations of motion or operator identities, which is a further step of calculation. Therefore, in some cases, it is the reduction from an over complete set to an exact complete set that requires more work. Note that the ambiguity in the explicit form of γ_{ij} from using an over-complete basis does not cause any problem when computing physical effects.

- Working with an Incomplete Operator Set

An operator basis contains 59 operators, which has 76 (2499) real valued Wilson coefficients for the number of generation being one (three) [42]. Practically, that is a very large basis to work with. In some cases, only a small number of operators are relevant to the physics considered and it is tempting to just focus on this small, incomplete set for the purpose of simplification. However, while a complete or overcomplete operator basis is obviously guaranteed to be RG closed, an incomplete operator set is typically not. When the incomplete operator set is not RG closed, Eq. (2.82) no longer holds. To fix this problem, one can view the incomplete operator set $\{\mathcal{O}_i\}$ as a subset of a certain complete operator basis $\{\mathcal{O}_i, \mathcal{O}_a\}$. Once this full operator basis is specified, one has a clear definition of the sub matrix γ_{ij} to compute the RG induced effects. Obviously, the off-diagonal block γ_{ai} is generically nonzero, which means some operator \mathcal{O}_a outside the chosen operator set $\{\mathcal{O}_i\}$ can also be RG induced. In this case, the generation of \mathcal{O}_a could bring additional constraints on the UV model under consideration. Ignoring these effects makes the constraints over conservative (see also the discussion in section 2 of [45]).

2.2.3 Popular operator bases in the literature

Here we summarize a few popular choices of dimension-six operator bases that are commonly used in the literature (see [57] for a recent review). These sets have been developed with two

different types of motivations: (1) completeness, and (2) phenomenological relevance. In spite of that, however, they are actually not very different from each other. In this subsection, we will briefly describe each basis and then discuss the relation among them.

With a motivation of completeness, one starts with enumerating all the possible dim-6 operators that respect the Standard Model gauge symmetry. Some combinations of these operators are zero due to simple operator identities.³⁶ One can use these redundancies to remove operators and shrink the operator set. In addition, many other combinations are zero upon using equation of motions, and hence would not contribute to physical observables which are on-shell quantities. These combinations can also be removed because they are redundant in respect of describing physics.³⁷ After all of these reductions, one arrives at an operator set that is non-redundant but still complete, in a sense that it has the full capability of describing the physical effects of any dim-6 operators. Clearly, the non-redundant, complete set of operators forms an “operator basis”. There are, of course, multiple choices of operator bases, all related by usual basis transformations.

The first attempt of this completeness motivated construction dates back to [79], where 80 dim-6 operators were claimed to be independent. However, it was later discovered that there were still some redundant combinations within the set of 80. The non-redundant basis was eventually found to contain only 59 dim-6 operators [80]. (There are also 5 baryon violating operators, bringing the total to 64, which are typically dropped from the analysis). To respect this first success, we will call the 59 dim-6 operators listed in [80] the “standard basis”. During the past year, the full anomalous dimension matrix γ_{ij} has been calculated in the standard basis [40–43].

The second type of motivation in choosing an operator set is the relevance to phenomenology. With this kind of motivation, one usually starts with a quite small set of operators that are immediately relevant to the physics concerned. However, if RG running effects are important, a complete operator set is required for the analysis. As discussed in the previous subsection, one can then extend the initial operator set into a complete operator basis by adding enough non-redundant operators to it. Popular operator bases constructed along this line include the “EGGM basis” [45], the “HISZ basis” [81], and the “SILH basis” [44, 55, 82]. These three bases are all motivated by studying physics relevant to the Higgs boson and the electroweak bosons. As a result, they all maximize the use of bosonic operators. In fact, these bases are very closely related to each other. Consider the following seven operators $\{\mathcal{O}_W, \mathcal{O}_B, \mathcal{O}_{WW}, \mathcal{O}_{WB}, \mathcal{O}_{BB}, \mathcal{O}_{HW}, \mathcal{O}_{HB}\}$, where \mathcal{O}_{HW} and \mathcal{O}_{HB} are defined as

$$\mathcal{O}_{HW} \equiv 2ig(D^\mu H)^\dagger \tau^a (D^\nu H) W_{\mu\nu}^a, \quad (2.84)$$

$$\mathcal{O}_{HB} \equiv ig'(D^\mu H)^\dagger (D^\nu H) B_{\mu\nu}, \quad (2.85)$$

³⁶For example, $0 = 2|H^\dagger D_\mu H|^2 - \frac{1}{2}(\partial_\mu |H|^2)^2 + \frac{1}{2}(H^\dagger \overleftrightarrow{D}^\mu H)^2$ is an operator identity that makes use of integration by parts.

³⁷An example identity which makes use of the equations of motion is $0 = (\partial_\mu B^{\mu\nu})^2 - j_{\mu,Y}^2$, where $B^{\mu\nu}$ is the hypercharge field strength and $j_{\mu,Y}$ is its associated current.

and the other five are defined in Table 2.2. There are two identities among them as following

$$O_W = O_{HW} + \frac{1}{4}(O_{WW} + O_{WB}), \quad (2.86)$$

$$O_B = O_{HB} + \frac{1}{4}(O_{BB} + O_{WB}). \quad (2.87)$$

So only five out of the seven are non-redundant. The difference among ‘‘EGGM basis’’, ‘‘HISZ basis’’, and ‘‘SILH basis’’ just lies in different ways of choosing five operators out of these seven: ‘‘EGGM basis’’ drops $\{O_{HW}, O_{HB}\}$, ‘‘HISZ basis’’ drops $\{O_W, O_B\}$, and ‘‘SILH basis’’ drops $\{O_{WW}, O_{WB}\}$.

The three phenomenologically motivated bases are not that different from the standard basis either. As mentioned before, due to motivation difference, the second type maximizes the use of bosonic operators. It turns out that to obtain the ‘‘EGGM basis’’ from the standard basis, one only needs to do the following basis transformation (trading five fermionic operators into five bosonic operators using equation of motion):

$$(H^\dagger \tau^a \overleftrightarrow{D}^\mu H)(\bar{L}_1 \gamma_\mu \tau^a L_1) \rightarrow O_W = ig(H^\dagger \tau^a \overleftrightarrow{D}^\mu H)(D^\nu W_{\mu\nu}^a), \quad (2.88)$$

$$(H^\dagger \overleftrightarrow{D}^\mu H)(\bar{e} \gamma_\mu e) \rightarrow O_B = ig' Y_H (H^\dagger \overleftrightarrow{D}^\mu H)(\partial^\nu B_{\mu\nu}), \quad (2.89)$$

$$(\bar{u} \gamma^\mu t_s^A u)(\bar{d} \gamma_\mu t_s^A d) \rightarrow O_{2G} = -\frac{1}{2}(D^\mu G_{\mu\nu}^a)^2, \quad (2.90)$$

$$(\bar{L}_1 \gamma^\mu \tau^a L_1)(\bar{L}_1 \gamma_\mu \tau^a L_1) \rightarrow O_{2W} = -\frac{1}{2}(D^\mu W_{\mu\nu}^a)^2, \quad (2.91)$$

$$(\bar{e} \gamma^\mu e)(\bar{e} \gamma_\mu e) \rightarrow O_{2B} = -\frac{1}{2}(\partial^\mu B_{\mu\nu})^2. \quad (2.92)$$

2.3 Mapping Wilson coefficients onto observables

So far we have described how to compute the Wilson coefficients $c_i(\Lambda)$ from a given UV model and how to run them down to the weak scale $c_i(m_W)$ with the appropriate anomalous dimension matrix γ_{ij} . This section then is devoted to the last step in Fig. 2.1 — mapping c_i ³⁸ onto the weak scale precision observables. The Wilson coefficients c_i will bring various corrections to the precision observables at the weak scale. The goal of this section is to study the deviation of each weak scale precision observable as a function of c_i .

It is worth noting that our SM EFT parameterized by Eq. (2.1) and c_i is totally different from the widely used seven- κ parametrization (for example see [32]), which parameterizes only a size change in each of the SM type Higgs couplings. The seven- κ actually parameterize models that do not respect the electroweak gauge symmetry and hence violates unitarity. As a result, future precision programs show spuriously high sensitivity on them. Our SM EFT on the other hand,

³⁸Throughout this section, all the Wilson coefficients mentioned will be at the weak scale $\mu = m_W$. In order to reduce the clutter, we hence suppress this specification of the RG scale and use c_i as a shorthand for $c_i(m_W)$.

$\mathcal{O}_{GG} = g_s^2 H ^2 G_{\mu\nu}^a G^{a,\mu\nu}$	$\mathcal{O}_H = \frac{1}{2}(\partial_\mu H ^2)^2$
$\mathcal{O}_{WW} = g^2 H ^2 W_{\mu\nu}^a W^{a,\mu\nu}$	$\mathcal{O}_T = \frac{1}{2}(H^\dagger \overleftrightarrow{D}_\mu H)^2$
$\mathcal{O}_{BB} = g'^2 H ^2 B_{\mu\nu} B^{\mu\nu}$	$\mathcal{O}_R = H ^2 D_\mu H ^2$
$\mathcal{O}_{WB} = 2gg' H^\dagger \tau^a H W_{\mu\nu}^a B^{\mu\nu}$	$\mathcal{O}_D = D^2 H ^2$
$\mathcal{O}_W = ig(H^\dagger \tau^a \overleftrightarrow{D}^\mu H) D^\nu W_{\mu\nu}^a$	$\mathcal{O}_6 = H ^6$
$\mathcal{O}_B = ig' Y_H (H^\dagger \overleftrightarrow{D}^\mu H) \partial^\nu B_{\mu\nu}$	$\mathcal{O}_{2G} = -\frac{1}{2}(D^\mu G_{\mu\nu}^a)^2$
$\mathcal{O}_{3G} = \frac{1}{3!} g_s f^{abc} G_\rho^{a\mu} G_\mu^{b\nu} G_\nu^{c\rho}$	$\mathcal{O}_{2W} = -\frac{1}{2}(D^\mu W_{\mu\nu}^a)^2$
$\mathcal{O}_{3W} = \frac{1}{3!} g \epsilon^{abc} W_\rho^{a\mu} W_\mu^{b\nu} W_\nu^{c\rho}$	$\mathcal{O}_{2B} = -\frac{1}{2}(\partial^\mu B_{\mu\nu})^2$

Table 2.4: Dimension-six bosonic operators for our mapping analysis.

parameterize new physics in the direction that respects the SM gauge invariance and is therefore free from unitarity violations.

In order to provide a concrete mapping result, we need to specify a set of operators to work with. Keeping in mind a special interest in UV models in which new physics is CP preserving and couples with the SM only through the Higgs and gauge bosons, we choose the set of dim-6 operators that are purely bosonic and CP conserving. All the dim-6 operators satisfying these conditions are listed in Table 2.2. This set of effective operators coincides with the set chosen in [45], supplemented by the operators \mathcal{O}_D and \mathcal{O}_R . Wilson coefficients of all the fermionic operators are assumed to be zero.

There are four categories of precision observables on which present and near future precision programs will be able to reach a per mille level sensitivity: (1) Electroweak Precision Observables (EWPO), (2) Triple Gauge Couplings (TGC), (3) Higgs decay widths, and (4) Higgs production cross sections. In the mapping calculation, we can keep only up to linear order of Wilson coefficients and we only include tree-level diagrams of the Wilson coefficients. This is because the near future precision experiments will only be sensitive to one-loop physics, and we practically consider each power of $\frac{1}{\Lambda^2} c_i$ as one-loop size, since it is already known that the SM is a very good theoretical description and the deviations should be small. Although in some UV models Wilson coefficients can arise at tree-level, the corresponding $\frac{1}{\Lambda^2}$ must be small enough to be consistent with the current constraints. So considering $\frac{1}{\Lambda^2} c_i$ as one-loop size is practically appropriate.

Our convention when expanding the Higgs doublet around the EW breaking vacuum is to take $H = (0 \quad v + h/\sqrt{2})^T$ where $v \approx 174$ GeV.

2.3.1 Electroweak precision observables

Electroweak precision observables represent the oblique corrections to the propagators of electroweak gauge bosons. Specifically, there are four transverse vacuum polarization functions:

$S = -\frac{4c_Z s_Z}{\alpha} \Pi'_{3B}(0)$ $X = -\frac{1}{2} m_W^2 \Pi''_{3B}(0)$
$T = \frac{1}{\alpha} \frac{1}{m_W^2} [\Pi_{WW}(0) - \Pi_{33}(0)]$ $U = \frac{4s_Z^2}{\alpha} [\Pi'_{WW}(0) - \Pi'_{33}(0)]$ $V = \frac{1}{2} m_W^2 [\Pi''_{WW}(0) - \Pi''_{33}(0)]$
$W = -\frac{1}{2} m_W^2 \Pi''_{33}(0)$
$Y = -\frac{1}{2} m_W^2 \Pi''_{BB}(0)$

Table 2.5: Definitions of the EWPO parameters, where the single/double prime denotes the first/second derivative of the transverse vacuum polarization functions.

$\Pi_{WW}(p^2)$, $\Pi_{ZZ}(p^2)$, $\Pi_{\gamma\gamma}(p^2)$, and $\Pi_{\gamma Z}(p^2)$,³⁹ each of which can be expanded in p^2

$$\Pi(p^2) = a_0 + a_2 p^2 + a_4 p^4 + \mathcal{O}(p^6). \quad (2.93)$$

Two out of these expansion coefficients are fixed to zero by the masslessness of the photon: $\Pi_{\gamma\gamma}(0) = \Pi_{\gamma Z}(0) = 0$. Another three combinations are fixed (absorbed) by the definition of the three free parameters g , g' , and v in electroweak theory. So up to p^2 order, there are three left-over parameters that can be used to test the predictions of the model. These are the Peskin-Takeuchi parameters S , T , and U [83, 85], which capture all possible non-decoupling electroweak oblique corrections. As higher energy scales were probed at LEP II, it was proposed to also include the coefficients of p^4 terms, which brings us four additional parameters W , Y , X , V [84, 86, 87].

So in total, we have seven EWPO parameters in consideration, S, T, U, W, Y, X, V . In this work, we take the definitions of them as listed in Table 2.5,⁴⁰ where for the purpose of conciseness,

³⁹Throughout this thesis, we use $\Pi(p^2)$ to denote the additional part of the transverse vacuum polarization function due to the Wilson coefficients. In a more precise notation, one should use $\Pi^{\text{new}}(p^2)$ as in [83] or $\delta\Pi(p^2)$ as in [84] for it, but we simply use $\Pi(p^2)$ to reduce the clutter. That said, our $\Pi(p^2)$ at leading order is linear in c_i .

⁴⁰Our definitions in Table 2.5 agree with [85] and [87]. Many other popular definitions are in common use as well (e.g. see [29, 83, 84]). The main differences lie in the choice of using derivatives of $\Pi(p^2)$ evaluated at $p^2 = 0$, such as $\Pi'_{WW}(0)$, etc., versus using some form of finite distance subtraction, such as $\frac{\Pi_{WW}(m_W^2) - \Pi_{WW}(0)}{m_W^2}$, etc. Up to p^4 order in $\Pi(p^2)$, this discrepancy would only cause a disagreement in the result of U . For example, the definition in [83] would result in nonzero U parameter from the custodial preserving operator \mathcal{O}_{2W} : $U = \frac{s_Z^4}{\alpha} \frac{4m_Z^2}{\Lambda^2} c_{2W} \neq 0$. In this work, we stick to the definition in [85] to make U a purely custodial violating parameter. Under our definition, $U = 0$ at dim-6 level.

$S = \frac{c_Z^2 s_Z^2}{\alpha} \frac{4m_Z^2}{\Lambda^2} (4c_{WB} + c_W + c_B)$	$W = \frac{m_W^2}{\Lambda^2} c_{2W}$
$T = \frac{1}{\alpha} \frac{2v^2}{\Lambda^2} c_T$	$Y = \frac{m_W^2}{\Lambda^2} c_{2B}$
$U = 0$	$X = V = 0$

Table 2.6: EWPO parameters in terms of Wilson coefficients.

we use the alternative set $\{\Pi_{33}, \Pi_{BB}, \Pi_{3B}\}$ instead of $\{\Pi_{ZZ}, \Pi_{\gamma\gamma}, \Pi_{\gamma Z}\}$.⁴¹ And due to the relation $W^3 = c_Z Z + s_Z A$ and $B = -s_Z Z + c_Z A$,⁴² the two set are simply related by the transformations

$$\Pi_{33} = c_Z^2 \Pi_{ZZ} + s_Z^2 \Pi_{\gamma\gamma} + 2c_Z s_Z \Pi_{\gamma Z}, \quad (2.94)$$

$$\Pi_{BB} = s_Z^2 \Pi_{ZZ} + c_Z^2 \Pi_{\gamma\gamma} - 2c_Z s_Z \Pi_{\gamma Z}, \quad (2.95)$$

$$\Pi_{3B} = -c_Z s_Z \Pi_{ZZ} + c_Z s_Z \Pi_{\gamma\gamma} + (c_Z^2 - s_Z^2) \Pi_{\gamma Z}. \quad (2.96)$$

Table 2.6 summarizes the mapping results of the seven EWPO parameters, *i.e.* each of them as a linear function (to leading order) of the Wilson coefficients c_i . These results are straightforward to calculate. First, we calculate $\Pi_{WW}(p^2)$, $\Pi_{ZZ}(p^2)$, $\Pi_{\gamma\gamma}(p^2)$, and $\Pi_{\gamma Z}(p^2)$ in terms of c_i . This can be done by expanding out the dim-6 operators in Table 2.4, identifying the relevant Lagrangian terms, and reading off the two-point Feynman rules. The details of these steps together with the results of $\Pi_{WW}(p^2)$, $\Pi_{ZZ}(p^2)$, $\Pi_{\gamma\gamma}(p^2)$, and $\Pi_{\gamma Z}(p^2)$ (Table C.1) are shown in Appendix C.1. Next, we compute the alternative combinations $\Pi_{WW}(p^2) - \Pi_{33}(p^2)$, $\Pi_{33}(p^2)$, $\Pi_{BB}(p^2)$, $\Pi_{3B}(p^2)$ using the transformation relations Eq. (2.94)-Eq. (2.96), the results of which are also summarized in Appendix C.1 (Table C.2). Finally, we combine Table C.2 with the definitions of EWPO parameters (Table 2.5) to obtain the results in Table 2.6.

We would like to emphasize the importance of W and Y parameters. It should be clear from the definitions Table 2.5 that the seven EWPO parameters fall into four different classes: $\{S, X\}$, $\{T, U, V\}$, $\{W\}$, and $\{Y\}$. Therefore W and Y out of the four p^4 order EWPO parameters supplement the classes formed by S, T, U (see also the discussions in [87]). Our mapping results in Table 2.6 also show that W and Y are practically more important compared to X and V , for W and Y are nonzero while X and V vanish at dim-6 level.

⁴¹One may also be concerned that these definitions through the transverse polarization functions $\Pi(p^2)$ are not generically gauge invariant. In principle, these $\Pi(p^2)$ functions can be promoted to gauge invariant ones $\bar{\Pi}(p^2)$ by a ‘‘pinch technique’’ prescription. (For examples, see discussions in [56, 88, 89].)

⁴²Throughout this work, we adopt the notation $c_Z \equiv \cos \theta_Z$ *etc.*, with θ_Z denoting the weak mixing angle. We do not use θ_W in order to avoid clash with the Wilson coefficient for the operator \mathcal{O}_W .

$$\begin{aligned} \delta g_1^Z &= -\frac{m_Z^2}{\Lambda^2} c_W \\ \delta \kappa_\gamma &= \frac{4m_W^2}{\Lambda^2} c_{WB} \\ \lambda_\gamma &= -\frac{m_W^2}{\Lambda^2} c_{3W} \end{aligned}$$

Table 2.7: TGC parameters in terms of Wilson coefficients.

2.3.2 Triple gauge couplings

The TGC parameters can be described by the a phenomenological Lagrangian [90–92]

$$\begin{aligned} \mathcal{L}_{\text{TGC}} &= igc_Z Z^\mu \cdot g_1^Z (\hat{W}_{\mu\nu}^- W^{+\nu} - \hat{W}_{\mu\nu}^+ W^{-\nu}) + igW_\mu^+ W_\nu^- (\kappa_Z \cdot c_Z \hat{Z}^{\mu\nu} + \kappa_\gamma \cdot s_Z \hat{A}^{\mu\nu}) \\ &\quad + \frac{ig}{m_W^2} \hat{W}_\mu^{-\rho} \hat{W}_{\rho\nu}^+ (\lambda_Z \cdot c_Z \hat{Z}^{\mu\nu} + \lambda_\gamma \cdot s_Z \hat{A}^{\mu\nu}), \end{aligned} \quad (2.97)$$

where $\hat{V}_{\mu\nu} \equiv \partial_\mu V_\nu - \partial_\nu V_\mu$. Among the five parameters above, there are two relations due to an accidental custodial symmetry. We take g_1^Z , κ_γ , and λ_γ as the three independent parameters. The other two can be expressed as [92]

$$\kappa_Z = g_1^Z - \frac{s_Z^2}{c_Z^2} (\kappa_\gamma - 1), \quad (2.98)$$

$$\lambda_Z = \lambda_\gamma. \quad (2.99)$$

The SM values of TGC parameters are $g_{1,\text{SM}}^Z = \kappa_{\gamma,\text{SM}} = 1$, $\lambda_{\gamma,\text{SM}} = 0$. Their deviations from SM are currently constrained at percent level [93], and will be improved to 10^{-4} level at ILC500 (see the second reference in [8]). Their mapping results are summarized in Table 2.7.⁴³

2.3.3 Deviations in Higgs decay widths

The dim-6 operators bring deviations in the Higgs decay widths from the Standard Model. In this chapter, we study all the SM Higgs decay modes that near future linear colliders can have sub-percent sensitivity on, *i.e.* $\Gamma \in \{\Gamma_{h \rightarrow f\bar{f}}, \Gamma_{h \rightarrow gg}, \Gamma_{h \rightarrow \gamma\gamma}, \Gamma_{h \rightarrow \gamma Z}, \Gamma_{h \rightarrow WW^*}, \Gamma_{h \rightarrow ZZ^*}\}$. Our analysis for the decay modes through off-shell vector gauge bosons $h \rightarrow WW^*$ and $h \rightarrow ZZ^*$ apply to all their fermionic modes, namely that $h \rightarrow WW^* \rightarrow Wl\bar{\nu}/Wd\bar{u}$ and $h \rightarrow ZZ^* \rightarrow Zf\bar{f}$.

For each decay width Γ above, we define its deviation from the SM

$$\epsilon \equiv \frac{\Gamma}{\Gamma_{\text{SM}}} - 1. \quad (2.100)$$

It turns out that at leading order (linear power) in c_i , this deviation is generically a sum of three parts, (1) the “interference correction” ϵ_I , (2) the “residue correction” ϵ_R , and (3) the “parametric

⁴³These results are also obtained in [45].

$$\begin{aligned}
 \epsilon_{h\bar{f}f,I} &= 0 \\
 \epsilon_{hgg,I} &= \frac{(4\pi)^2}{\text{Re}A_{hgg}^{\text{SM}}} \frac{16v^2}{\Lambda^2} c_{GG} \\
 \epsilon_{h\gamma\gamma,I} &= \frac{(4\pi)^2}{\text{Re}A_{h\gamma\gamma}^{\text{SM}}} \frac{8v^2}{\Lambda^2} (c_{WW} + c_{BB} - c_{WB}) \\
 \epsilon_{h\gamma Z,I} &= \frac{(4\pi)^2}{\text{Re}A_{h\gamma Z}^{\text{SM}}} \frac{4v^2}{\Lambda^2} \frac{1}{c_Z} \left[2(c_Z^2 c_{WW} - s_Z^2 c_{BB}) - (c_Z^2 - s_Z^2) c_{WB} \right] \\
 \epsilon_{hWW^*,I} &= \left[2I_a(\beta_W) - I_b(\beta_W) \right] \frac{m_W^2}{\Lambda^2} c_{2W} - \left[2I_b(\beta_W) - I_c(\beta_W) \right] \frac{4m_W^2}{\Lambda^2} c_{WW} \\
 &\quad - I_a(\beta_W) \frac{2m_W^2}{\Lambda^2} c_W - I_b(\beta_W) \frac{v^2}{\Lambda^2} c_R + \frac{2m_h^2}{\Lambda^2} c_D \\
 \epsilon_{hZZ^*,I} &= + \left[2I_a(\beta_Z) - I_b(\beta_Z) \right] \frac{m_Z^2}{\Lambda^2} (c_Z^2 c_{2W} + s_Z^2 c_{2B}) \\
 &\quad - \left[2I_b(\beta_Z) - I_c(\beta_Z) \right] \frac{4m_Z^2}{\Lambda^2} (c_Z^4 c_{WW} + s_Z^4 c_{BB} + c_Z^2 s_Z^2 c_{WB}) \\
 &\quad - I_a(\beta_Z) \frac{2m_Z^2}{\Lambda^2} (c_Z^2 c_W + s_Z^2 c_B) + I_b(\beta_Z) \frac{v^2}{\Lambda^2} (2c_T - c_R) + \frac{2m_h^2}{\Lambda^2} c_D \\
 &\quad + \frac{eQ_f 2c_Z^2 s_Z}{g(T_f^3 - s_Z^2 Q_f)} \left\{ \begin{aligned} &\left[I_a(\beta_Z) - I_b(\beta_Z) - 1 \right] \frac{m_Z^2}{\Lambda^2} (c_{2W} - c_{2B} - c_W + c_B) \\ &+ I_d(\beta_Z) \frac{m_Z^2}{\Lambda^2} \left[2c_Z^2 c_{WW} - 2s_Z^2 c_{BB} - (c_Z^2 - s_Z^2) c_{WB} \right] \end{aligned} \right\}
 \end{aligned}$$

Table 2.8: Interference corrections ϵ_I to Higgs decay widths, with $\beta_W \equiv \frac{m_W}{m_h}$, $\beta_Z \equiv \frac{m_Z}{m_h}$, and the auxiliary integrals $I_a(\beta)$, $I_b(\beta)$, $I_c(\beta)$, $I_d(\beta)$ listed in Eq. (C.29)-(C.32) of the appendix. The A_{hgg}^{SM} , $A_{h\gamma\gamma}^{\text{SM}}$, and $A_{h\gamma Z}^{\text{SM}}$ are the standard form factors, whose expressions are listed in Eq. (C.33)-(C.35) of Appendix C.2.

correction” ϵ_P :

$$\epsilon = \epsilon_I + \epsilon_R + \epsilon_P. \quad (2.101)$$

In the following, we will first give a brief description of the meaning and the mapping results of each part, and then explain in detail how to derive these results.

2.3.3.1 Brief description of the results

- “Interference Correction” ϵ_I

ϵ_I captures the effects of new, amputated Feynman diagrams $iM_{\text{AD,new}}(c_i)$ introduced by the dim-6 effective operators. This modifies the value of the total amputated diagram

$$iM_{\text{AD}} = iM_{\text{AD,SM}} + iM_{\text{AD,new}}(c_i). \quad (2.102)$$

	ϵ_R	ϵ_P
$\Gamma_{hf\bar{f}}$	Δr_h	$\Delta w_{y_f^2}$
Γ_{hgg}	0	0
$\Gamma_{h\gamma\gamma}$	0	0
$\Gamma_{h\gamma Z}$	0	0
Γ_{hWW^*}	$\Delta r_h + \Delta r_W$	$3\Delta w_{g^2} + \Delta w_{v^2}$
Γ_{hZZ^*}	$\Delta r_h + \Delta r_Z$	$3\Delta w_{g^2} + \Delta w_{v^2} + \left(3\frac{s_Z^2}{c_Z^2} - \frac{2s_Z^2 Q_f}{T_f^3 - s_Z^2 Q_f}\right) \Delta w_{s_Z^2}$

Table 2.9: Residue corrections ϵ_R and parametric corrections ϵ_P to Higgs decay widths. The explicit results in terms of the dim-6 Wilson coefficients of the residue modifications $\Delta r_h, \Delta r_W, \Delta r_Z$ and parameter modifications $\Delta w_{g^2}, \Delta w_{v^2}, \Delta w_{s_Z^2}, \Delta w_{y_f^2}$ are listed, respectively, in Tables C.3 and C.4 of Appendix C.

Upon modulus square, the cross term, namely the interference between the new amplitude and the SM amplitude, gives the leading order contribution to the deviation:

$$\epsilon_I = \frac{\int d\Pi_f \overline{M_{\text{AD,SM}}^* M_{\text{AD,new}}(c_i)} + c.c.}{\int d\Pi_f |M_{\text{AD,SM}}|^2}, \quad (2.103)$$

where $\int d\Pi_f$ denotes the phase space integral, and the overscore denotes any step needed for getting the unpolarized result, namely a sum of final spins and/or an average over the initial spins, if any. The results of ϵ_I are summarized in Table 2.8. Details of the calculation are relegated to an appendix. Specifically, in Appendix C.1 we list out the new set of Feynman rules generated by the dim-6 operators; in Appendix C.2 we list out all the relevant new amputated diagrams involved in each ϵ_I . Due to the phase space integral, there are some complicated auxiliary integrals involved in the results. The definitions and values of these auxiliary integrals are given in Eq. (C.29)-(C.32). The $A_{hgg}^{\text{SM}}, A_{h\gamma\gamma}^{\text{SM}}$, and $A_{h\gamma Z}^{\text{SM}}$ in Table 2.8 are the standard form factors, detailed expressions of which are shown in Eq. (C.33)-(C.35) of the appendix.

- “Residue Correction” ϵ_R

ϵ_R captures the effects of residue modifications at the pole mass, *i.e.* wavefunction corrections, by the dim-6 effective operators. We know from the LSZ reduction formula that the invariant amplitude iM equals the value of amputated diagram iM_{AD} multiplied by the

square root of the mass pole residue r_k of each external leg particle k

$$iM = \left(\prod_{k \in \{\text{external legs}\}} r_k^{1/2} \right) \cdot iM_{\text{AD}}. \quad (2.104)$$

Besides the corrections to iM_{AD} discussed before, a mass pole residue modification Δr_k of an external leg particle k also feeds into the decay width deviation. Upon modulus square, this part of deviation is

$$\epsilon_R = \sum_{k \in \{\text{external legs}\}} \Delta r_k. \quad (2.105)$$

The results of ϵ_R for each decay width are summarized in the second column of Table 2.9. The values of the relevant residue modifications Δr_k are listed in Appendix C.4 (Table C.3). Note that, unlike the interference correction ϵ_I , the residue correction ϵ_R corresponds to a contribution with the size of $\Gamma_{\text{SM}} \times c_i$. But for Γ_{hgg} , $\Gamma_{h\gamma\gamma}$, and $\Gamma_{h\gamma Z}$, the SM value Γ_{SM} is already of one-loop size. So $\epsilon_{hgg,R}$, $\epsilon_{h\gamma\gamma,R}$, and $\epsilon_{h\gamma Z,R}$ should be one-loop size in Wilson coefficients, namely that $\frac{1}{16\pi^2} \times c_i$. Therefore, to our order of approximation, this size should be neglected for consistency, hence why $\epsilon_R = 0$ for Γ_{hgg} , $\Gamma_{h\gamma\gamma}$, and $\Gamma_{h\gamma Z}$ in Table 2.9.

- “Parametric Correction” ϵ_P

ϵ_P captures how the dim-6 effective operators modify the parameters of the SM Lagrangian. When computing the decay width Γ , one usually writes it in terms of a set of Lagrangian parameters $\{\rho\}$, which in our case are $\{\rho\} = \{g^2, v^2, s_Z^2, y_f^2\}$. So $\Gamma = \Gamma(\rho, c_i)$ is what one usually calculates. However, the deviation ϵ is supposed to be a physical observable that describes the change of the relation between Γ and other physical observables $\{obs\}$, which in our case can be taken as $\{obs\} = \{\hat{\alpha}, \hat{G}_F, \hat{m}_Z^2, \hat{m}_f^2\}$. So one should eliminate $\{\rho\}$ in terms of $\{obs\}$. This elimination brings additional dependence on $\{c_i\}$, because the Wilson coefficients also modify the relation between $\{\rho\}$ and $\{obs\}$ through $\rho = \rho(obs, c_i)$. Therefore, to include the full dependence on c_i , one should write the decay width as

$$\Gamma = \Gamma(\rho(obs, c_i), c_i). \quad (2.106)$$

The ϵ_I and ϵ_R discussed previously only take into account of the explicit dependence on c_i , with $\{\rho\}$ held fixed. The implicit dependence on c_i through modifying the Lagrangian parameter ρ is what we call “parametric correction”:

$$\epsilon_P = \sum_{\rho \in \{g^2, v^2, s_Z^2, y_f^2\}} \frac{\partial \ln \Gamma(\rho, c_i)}{\partial \ln \rho} \Delta \ln \rho = \sum_{\rho \in \{g^2, v^2, s_Z^2, y_f^2\}} \frac{\partial \ln \Gamma(\rho, c_i)}{\partial \ln \rho} \Delta w_\rho, \quad (2.107)$$

where Δw_ρ denotes the Lagrangian parameter modification

$$\Delta w_\rho = \Delta \ln \rho = \frac{\Delta \rho}{\rho}. \quad (2.108)$$

The parametric correction ϵ_P in terms of Δw_ρ are summarized in the third column of Table 2.9. And a detailed calculation of Δw_ρ is in Appendix C.5, with the results summarized in Table C.4. As with the residue correction case, $\epsilon_{hgg,P}$, $\epsilon_{h\gamma\gamma,P}$, and $\epsilon_{h\gamma Z,P}$ are one-loop size in Wilson coefficients and hence neglected for consistency.

2.3.3.2 Detailed derivation

Clearly from Eq. (2.1), the SM EFT goes back to the SM when all $c_i = 0$. Thus, up to linear power of c_i , the deviation defined in Eq. (2.100) is

$$\epsilon \equiv \frac{\Gamma}{\Gamma_{\text{SM}}} - 1 = \frac{\Gamma(c_i)}{\Gamma(c_i = 0)} - 1 = \left. \frac{d \ln \Gamma}{dc_i} \right|_{c_i=0} c_i. \quad (2.109)$$

As explained before, this function $\Gamma(c_i)$ in Eq. (2.109) should be understood as the dependence of Γ on $\{c_i\}$ with the values of $\{obs\}$ held fixed. Practically, it is most convenient to first compute both Γ and $\{obs\}$ in terms of the Lagrangian parameters $\{\rho\}$:

$$\Gamma = \Gamma(\rho, c_i), \quad (2.110)$$

$$obs = obs(\rho, c_i), \quad (2.111)$$

One can then plug the inverse of the second function $\rho = \rho(obs, c_i)$ into the first to get

$$\Gamma(c_i) = \Gamma(\rho(obs, c_i), c_i). \quad (2.112)$$

This makes it clear that in addition to the explicit dependence on c_i , Γ also has an implicit dependence on c_i through the Lagrangian parameters $\rho(obs, c_i)$:

$$\frac{d \ln \Gamma}{dc_i} = \frac{\partial \ln \Gamma(\rho, c_i)}{\partial c_i} + \sum_{\rho} \frac{\partial \ln \Gamma(\rho, c_i)}{\partial \ln \rho} \frac{\partial \ln \rho(obs, c_i)}{\partial c_i}. \quad (2.113)$$

Putting it another way, the first term in the above shows the deviation when ρ are fixed numbers. But ρ are not fixed numbers. They are a set of Lagrangian parameters determined by a set of experimental measurements obs through relations that get modified by c_i as well. So the truly fixed numbers are the experimental inputs obs . By adding the second piece in Eq. (2.113), we get the full amount of deviation with obs as fixed input numbers. By putting obs in the place of $\ln \Gamma$, one can also explicitly check that Eq. (2.113) keeps obs fixed. Making use of the fact

$$\frac{\partial \ln \rho(obs, c_i)}{\partial c_i} = \left. \frac{d \ln \rho}{dc_i} \right|_{obs=\text{const}} = - \frac{\left. \frac{\partial(obs)}{\partial c_i} \right|_{\rho}}{\left. \frac{\partial(obs)}{\partial \ln \rho} \right|_{c_i}}, \quad (2.114)$$

we clearly see that

$$\frac{d(obs)}{dc_i} = \frac{\partial(obs)}{\partial c_i} + \sum_{\rho} \frac{\partial(obs)}{\partial \ln \rho} \Big|_{c_i} \frac{\partial \ln \rho(obs, c_i)}{\partial c_i} = 0. \quad (2.115)$$

Because of Eq. (2.113), the deviation Eq. (2.109) is split into two parts

$$\begin{aligned}\epsilon &= \left. \frac{\partial \ln \Gamma(\rho, c_i)}{\partial c_i} \right|_{c_i=0} c_i + \sum_{\rho} \left[\left. \frac{\partial \ln \Gamma(\rho, c_i)}{\partial \ln \rho} \right|_{c_i=0} \left(\left. \frac{\partial \ln \rho(\text{obs}, c_i)}{\partial c_i} \right|_{c_i=0} c_i \right) \right] \\ &= \left. \frac{\partial \ln \Gamma(\rho, c_i)}{\partial c_i} \right|_{c_i=0} c_i + \epsilon_P,\end{aligned}\quad (2.116)$$

where the implicit dependence part is defined as the parametric correction ϵ_P

$$\epsilon_P \equiv \sum_{\rho} \left. \frac{\partial \ln \Gamma(\rho, c_i)}{\partial \ln \rho} \right|_{c_i=0} \Delta w_{\rho}, \quad (2.117)$$

with the parameter modifications Δw_{ρ} defined as

$$\Delta w_{\rho} \equiv \left. \frac{\partial \ln \rho(\text{obs}, c_i)}{\partial c_i} \right|_{c_i=0} c_i = \Delta \ln \rho = \frac{\Delta \rho}{\rho}. \quad (2.118)$$

The explicit dependence part can be further split by noting that

$$iM_{\text{AD}} = iM_{\text{AD,SM}} + iM_{\text{AD,new}}(c_i), \quad (2.119)$$

$$iM = \left(\prod_{k \in \{\text{external legs}\}} r_k^{1/2} \right) \cdot iM_{\text{AD}}, \quad (2.120)$$

$$\Gamma(\rho, c_i) = \frac{1}{2m_h} \int d\Pi_f \overline{|M|^2} = \frac{1}{2m_h} \left(\prod_{k \in \{\text{external legs}\}} r_k \right) \cdot \int d\Pi_f \overline{|M_{\text{AD}}|^2}. \quad (2.121)$$

Therefore we have

$$\begin{aligned}\left. \frac{\partial \ln \Gamma(\rho, c_i)}{\partial c_i} \right|_{c_i=0} c_i &= \left. \frac{\partial \ln \left[\int d\Pi_f \overline{|M_{\text{AD}}|^2} \right]}{\partial c_i} \right|_{c_i=0} c_i + \sum_{k \in \{\text{external legs}\}} \left. \frac{\partial \ln r_k}{\partial c_i} \right|_{c_i=0} c_i \\ &= \left. \frac{\Delta \left(\int d\Pi_f \overline{|M_{\text{AD}}|^2} \right)}{\int d\Pi_f \overline{|M_{\text{AD}}|^2}} \right|_{c_i=0} + \sum_{k \in \{\text{external legs}\}} \left. \frac{\Delta r_k}{r_k} \right|_{c_i=0} \\ &= \frac{\int d\Pi_f \overline{M_{\text{AD,SM}}^* M_{\text{AD,new}}(c_i) + c.c.}}{\int d\Pi_f \overline{|M_{\text{AD,SM}}|^2}} + \sum_{k \in \{\text{external legs}\}} \Delta r_k \\ &= \epsilon_I + \epsilon_R,\end{aligned}\quad (2.122)$$

with ϵ_I and ϵ_R defined as

$$\epsilon_I \equiv \frac{\int d\Pi_f \overline{M_{\text{AD,SM}}^* M_{\text{AD,new}}(c_i) + c.c.}}{\int d\Pi_f \overline{|M_{\text{AD,SM}}|^2}}, \quad (2.123)$$

$$\epsilon_R \equiv \sum_{i \in \{\text{external legs}\}} \Delta r_i. \quad (2.124)$$

So in summary, the total deviation in decay width has three parts $\epsilon = \epsilon_I + \epsilon_R + \epsilon_P$, with

$$\epsilon_I = \frac{\int d\Pi_f \overline{M_{\text{AD,SM}}^* M_{\text{AD,new}}(c_i) + c.c.}}{\int d\Pi_f |M_{\text{AD,SM}}|^2}, \quad (2.125)$$

$$\epsilon_R = \sum_{i \in \{\text{external legs}\}} \Delta r_i, \quad (2.126)$$

$$\epsilon_P = \sum_{\rho \in \{g^2, v^2, s_Z^2, y_f^2\}} \left. \frac{\partial \ln \Gamma(\rho, c_i)}{\partial \ln \rho} \right|_{c_i=0} \Delta w_\rho, \quad (2.127)$$

where

$$\Delta w_\rho \equiv \left. \frac{\partial \ln \rho(\text{obs}, c_i)}{\partial c_i} \right|_{c_i=0} c_i = \Delta \ln \rho = \frac{\Delta \rho}{\rho}. \quad (2.128)$$

For each decay width in consideration, we computed these three parts of deviation. The results are summarized in Table 2.8 and Table 2.9. It is worth noting that this splitting is a convenient intermediate treatment of the calculation, but each of ϵ_I , ϵ_R , ϵ_P alone would not be physical, because it depends on the renormalization scheme as well as the choice of operator basis. It is the total sum of the three that reflects the physical deviation in the decay widths.

2.3.4 Deviations in Higgs production cross sections

The dim-6 operators also induce deviations in the Higgs production cross sections. In this chapter, we focus on the production modes $\sigma \in \{\sigma_{ggF}, \sigma_{WWH}, \sigma_{Wh}, \sigma_{Zh}\}$, which are the most important ones for both hadron colliders such as the LHC and possible future lepton colliders such as the ILC. As with the decay width case, we define the cross section deviation

$$\epsilon \equiv \frac{\sigma}{\sigma_{\text{SM}}} - 1. \quad (2.129)$$

Again, there are three types of corrections

$$\epsilon = \epsilon_I + \epsilon_R + \epsilon_P. \quad (2.130)$$

The mapping results are summarized in Table 2.10 and Table 2.11. Relevant new amputated Feynman diagrams for ϵ_I are listed in Appendix C.3. The calculation of the interference correction to σ_{WWH} turns out to be very involved. Its lengthy analytical expression $\epsilon_{WWH,I}(s)$ does not help much, so we instead show its numerical results in Table 2.10. The auxiliary functions $f_a(s)$, $f_b(s)$, $f_c(s)$ in $\epsilon_{WWH,I}(s)$ are defined in Appendix C.3 (Eq. (C.52)-(C.54)), where more details of the phase space integral are also shown. The numerical values of $f_a(s)$, $f_b(s)$, $f_c(s)$ are plotted in Fig. 2.4. We also provide [Mathematica code](#) so that one can make use of these auxiliary functions.⁴⁴

⁴⁴This code can be found at <http://hitoshi.berkeley.edu/HiggsEFT/auxiliary.html>

$$\begin{aligned}
 \epsilon_{ggF,I} &= \frac{(4\pi)^2}{\text{Re}(A_{hgg}^{\text{SM}})} \frac{16v^2}{\Lambda^2} c_{GG} \\
 \epsilon_{WWh,I}(s) &= \left[-f_b(s) - f_c(s) \right] \frac{2m_W^2}{\Lambda^2} c_{2W} + \left[-f_a(s) + 2f_c(s) \right] \frac{8m_W^2}{\Lambda^2} c_{WW} \\
 &\quad + \left[f_b(s) + 2f_c(s) \right] \frac{2m_W^2}{\Lambda^2} c_W + f_c(s) \frac{2v^2}{\Lambda^2} c_R + \frac{2m_h^2}{\Lambda^2} c_D \\
 \epsilon_{Wh,I} &= \frac{1}{1 - \eta_W^2} \left[\begin{aligned} &-\frac{2s}{\Lambda^2} c_{2W} + I_{VH}(\eta_h, \eta_W) \frac{16m_W^2}{\Lambda^2} c_{WW} \\ &+ (1 + 2\eta_W^2 - \eta_W^4) \frac{2s}{\Lambda^2} c_W + (2 - \eta_W^2) \frac{2v^2}{\Lambda^2} c_R \end{aligned} \right] + \frac{2m_h^2}{\Lambda^2} c_D \\
 \epsilon_{Zh,I} &= \frac{1}{1 - \eta_Z^2} \left[\begin{aligned} &-\frac{2s}{\Lambda^2} (c_Z^2 c_{2W} + s_Z^2 c_{2B}) \\ &+ I_{VH}(\eta_h, \eta_Z) \frac{16m_Z^2}{\Lambda^2} (c_Z^4 c_{WW} + s_Z^4 c_{BB} + c_Z^2 s_Z^2 c_{WB}) \\ &+ (1 + 2\eta_Z^2 - \eta_Z^4) \frac{2s}{\Lambda^2} (c_Z^2 c_W + s_Z^2 c_B) \\ &+ (2 - \eta_Z^2) \frac{2v^2}{\Lambda^2} (-2c_T + c_R) \end{aligned} \right] + \frac{2m_h^2}{\Lambda^2} c_D \\
 &\quad + \frac{2eQ_f c_Z^2 s_Z}{g(T_f^3 - s_Z^2 Q_f)} \left\{ \begin{aligned} &-\frac{s}{\Lambda^2} (c_{2W} - c_{2B} - c_W + c_B) \\ &+ I_{VH}(\eta_h, \eta_Z) \frac{4m_Z^2}{\Lambda^2} \left[2c_Z^2 c_{WW} - 2s_Z^2 c_{BB} - (c_Z^2 - s_Z^2) c_{WB} \right] \end{aligned} \right\}
 \end{aligned}$$

Table 2.10: Interference corrections ϵ_I to Higgs production cross sections, with $\eta_h \equiv \frac{m_h}{\sqrt{s}}$, $\eta_Z \equiv \frac{m_Z}{\sqrt{s}}$, and the auxiliary function defined as $I_{VH}(\eta_h, \eta_V) \equiv 1 + \frac{6(1-\eta_h^2+\eta_V^2)(1-\eta_V^2)}{(1-\eta_h^2+\eta_V^2)^2+8\eta_V^2}$. The numerical results of the auxiliary functions $f_a(s)$, $f_b(s)$, and $f_c(s)$ in $\epsilon_{WWh,I}(s)$ are shown in Fig. 2.4.

2.4 Applications

With the results of the previous sections at our disposal, let us turn to applying the SM EFT to study what precision Higgs measurements may tell us for two physically motivated, yet very different, new physics scenario. In each case, we will go through the three-step procedure of matching the UV model onto the SM EFT (Sec. 2.1), RG running the Wilson coefficients down to the weak scale (Sec. 2.2), and mapping onto physical observables (Sec. 2.3).

The first model we study is a real singlet scalar coupled to the Higgs boson, where impacts arise at tree-level. This single degree of freedom is sufficient to achieve a first-order electroweak phase transition which would allow for electroweak baryogenesis. Because Wilson coefficients are generated at tree-level, we may wonder if RG running effects are important, a lá our discussion in section 2.2. Indeed, this turns out to be the case; electroweak precision observables—specifically the S and T parameters—are generated in the RG flow of the tree-level-generated Wilson coefficient associated to $\mathcal{O}_H = (\partial_\mu |H|^2)^2/2$. Besides generating EW precision observables in its RG

	ϵ_R	ϵ_P
σ_{ggF}	0	0
σ_{WWh}	Δr_h	$4\Delta w_{g^2} + \Delta w_{v^2}$
σ_{Wh}	$\Delta r_h + \Delta r_W$	$3\Delta w_{g^2} + \Delta w_{v^2}$
σ_{Zh}	$\Delta r_h + \Delta r_Z$	$3\Delta w_{g^2} + \Delta w_{v^2} + \left(3\frac{s_Z^2}{c_Z^2} - \frac{2s_Z^2 Q_f}{T_f^3 - s_Z^2 Q_f}\right) \Delta w_{s_Z^2}$

Table 2.11: Residue corrections ϵ_R and parametric corrections ϵ_P to Higgs production cross sections. The results of residue modifications and parameter modifications are listed in Tables C.3 and C.4 of Appendix C.

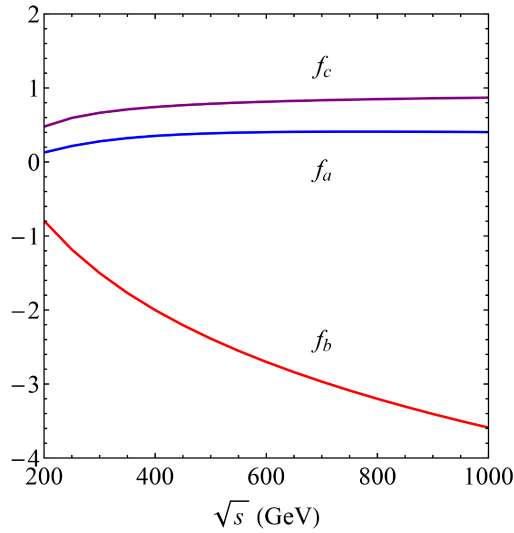


Figure 2.4: Numerical results of auxiliary functions $f_a(s)$, $f_b(s)$, and $f_c(s)$ in $\epsilon_{WW_{h,l}}(s)$. Mathematica code for these auxiliary functions can be found at <http://hitoshi.berkeley.edu/HiggsEFT/auxiliary.html>.

running, \mathcal{O}_H also leads to the physical effect of modifying the Higgs wave function upon EW symmetry breaking—the so-called Higgs “oblique” correction. This oblique correction is nothing but the residue correction—discussed in section 2.3—for the Higgs, Δr_h . Associated Zh production at a future e^+e^- machine is quite sensitive to this oblique correction. We find that the sensitivity to this oblique correction at proposed future e^+e^- machines would completely explore the viable parameter space for the singlet to allow a first-order EW phase transition. We also find strong, complementary constraints from future increased precision measurements of S and T parameters

at a GigaZ or TeraZ program.

The second model study is the Minimal Supersymmetric Standard Model (MSSM) with light scalar tops. Among the supersymmetric particles, scalar tops (stops) play an especially important role in radiative corrections—lighter stops help minimize the fine-tuning in the Higgs mass-squared. Wilson coefficients are generated at one-loop level. Therefore, RG running is parametrically of two-loop order and hence negligible. Because stops are charged under all the SM gauge symmetries, they generate many dimension-six operators when we integrate them out (in fact, every operator in table 2.2 is generated). The use of our results from the covariant derivative expansion dramatically eases the process of obtaining the Wilson coefficients of these operators. Stops can impact many physical processes related to the Higgs and EW bosons; we find that future precision higgs and EW measurements can play a useful role in exploring the parameter space that minimizes fine-tuning in the Higgs sector.

Before proceeding, we have a technical comment. There is a caveat in interpreting Wilson coefficients as the inverse of heavy particle masses if BSM states couple directly to the Higgs. The Wilson coefficients in Eq. 2.1, $\mathcal{L}_{\text{eff}} = \mathcal{L}_{SM} + \sum_i c_i \mathcal{O}_i / \Lambda^{d_i-4}$, are computed with mass parameters in the Lagrangian, while the actual mass eigenvalues receive additional contribution from the Higgs vev and mixings. This difference is accounted for by higher-dimension operators which are dropped in our analysis. Therefore, the experimental sensitivities on Wilson coefficients do not translate directly into those on heavy particle masses. We will quantify this difference in each of the examples below.

2.4.1 Electroweak baryogenesis from a real singlet scalar

We consider a gauge singlet, real scalar field S that couples to the SM via a Higgs portal,

$$\mathcal{L} = \mathcal{L}_{SM} + \frac{1}{2} (\partial_\mu S)^2 - \frac{1}{2} m_S^2 S^2 - A |H|^2 S - \frac{1}{2} k |H|^2 S^2 - \frac{1}{3!} \mu S^3 - \frac{1}{4!} \lambda_S S^4. \quad (2.131)$$

There are several motivations for studying this singlet model. This single additional degree of freedom can successfully achieve a strongly first-order electroweak phase transition (EWPT) [94]. Additionally, singlet sectors of the above form—with particular relations among the couplings—arise in the NMSSM [95] and its variants, *e.g.* [96, 97]. Finally, the effects of Higgs portal operators are captured through the trilinear and quartic interactions $S |H|^2$ and $S^2 |H|^2$, respectively.

Obtaining the Wilson coefficients

For $m_S \gg m_H$ the singlet can be integrated out and matched onto the SM EFT. Because of the interaction linear in the singlet, $\mathcal{L} \supset -A |H|^2 S$, there is a tree-level contribution to the effective action. To compute this tree-level piece, we follow the procedure described in section 2.1.1.1 taking $P_\mu = i\partial_\mu$ and $B = -A |H|^2$. The solution to the linearized equation of motion is,

$$S_c \approx -\frac{1}{\partial^2 + m_S^2 + k |H|^2} A |H|^2 \approx -\frac{1}{m_S^2} A |H|^2 + \frac{1}{m^4} (\partial^2 + k |H|^2) A |H|^2.$$

Plugging this solution back to Eq. (2.131), we get the tree-level effective Lagrangian

$$\begin{aligned}\Delta\mathcal{L}_{\text{eff,tree}} &= -A|H|^2 S_c + \frac{1}{2}S_c(-\partial^2 - m_S^2 - k|H|^2)S_c - \frac{1}{3!}\mu S_c^3 - \frac{1}{4!}\lambda_S S_c^4 \\ &\approx \frac{1}{2m_S^2}A^2|H|^4 + \frac{A^2}{m_S^4}\mathcal{O}_H + \left(-\frac{kA^2}{2m_S^4} + \frac{1}{3!}\frac{\mu A^3}{m_S^6}\right)\mathcal{O}_6.\end{aligned}\quad (2.132)$$

We recall the definitions of the dimension-six operators from table 2.2, $\mathcal{O}_H = (\partial_\mu |H|^2)^2/2$ and $\mathcal{O}_6 = |H|^6$.

Next let us compute the 1-loop piece of the effective Lagrangian, which according to Eq. (2.5), is

$$\begin{aligned}\Delta S_{\text{eff,1-loop}} &= \frac{i}{2}\text{Tr} \log \left(-\frac{\delta^2 S}{\delta S_c^2} \Big|_{S_c} \right) = \frac{i}{2}\text{Tr} \log \left(\partial^2 + m_S^2 + k|H|^2 + \mu S_c + \frac{1}{2}\lambda_S S_c^2 \right) \\ &= \frac{i}{2}\text{Tr} \log \left(\partial^2 + m_S^2 + k|H|^2 \right).\end{aligned}\quad (2.133)$$

In going to the second line we have dropped the classical solution S_c .⁴⁵ The above is clearly in the form of Eq. (2.11), with $P_\mu = i\partial_\mu$, $U = k|H|^2$, and $G'_{\mu\nu} = [D_\mu, D_\nu] = [\partial_\mu, \partial_\nu] = 0$. Plugging these specific values of U and $G'_{\mu\nu}$ into Eq. (2.38), we obtain

$$\begin{aligned}\Delta\mathcal{L}_{\text{eff,1-loop}} &= \frac{1}{2(4\pi)^2} \frac{1}{m_S^2} \left[-\frac{1}{12}(P_\mu U)^2 - \frac{1}{6}U^3 \right] \\ &= \frac{1}{2(4\pi)^2} \frac{1}{m_S^2} \left[\frac{k^2}{12}(\partial_\mu |H|^2)^2 - \frac{k^3}{6}|H|^6 \right] \\ &= \frac{1}{(4\pi)^2} \frac{1}{m_S^2} \left(\frac{k^2}{12}\mathcal{O}_H - \frac{k^3}{12}\mathcal{O}_6 \right).\end{aligned}\quad (2.134)$$

Thus we see that the only \mathcal{O}_H and \mathcal{O}_6 are generated when we integrate out the singlet, and that both of these operators receive contributions at tree and one-loop level. Practically, because c_H and c_6 have a tree-level contribution, we can ignore the one-loop correction as it is relatively negligible. In summary, we find the Wilson coefficients at the matching scale $\Lambda = m_S$ to be

$$c_H(m_S) = \frac{A^2}{m_S^2} + \frac{1}{(4\pi)^2} \frac{k^2}{12} \approx \frac{A^2}{m_S^2}, \quad (2.135a)$$

$$c_6(m_S) = -\frac{kA^2}{2m_S^2} + \frac{1}{6} \frac{\mu A^3}{m_S^4} - \frac{1}{(4\pi)^2} \frac{k^3}{12} \approx -\frac{kA^2}{2m_S^2} + \frac{1}{6} \frac{\mu A^3}{m_S^4}. \quad (2.135b)$$

In the following physics analysis, we will only keep the tree-level piece.

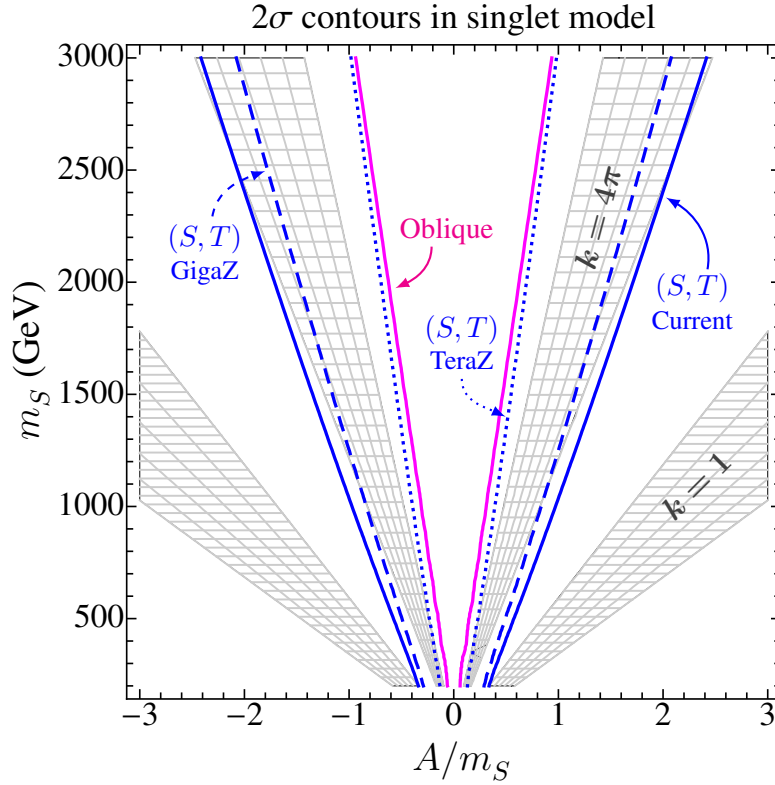


Figure 2.5: 2σ contours of future precision measurements on the singlet model in Eq. (2.131). Regions below the contours will be probed. The magenta contour is the 2σ sensitivity to the universal Higgs oblique correction in Eq. (2.137) at ILC 500up. Blue contours show the 2σ RG-induced constraints from the S and T parameters in Eqs. (2.141)-(2.142) from current measurements (solid) [29] and future sensitivities at ILC GigaZ (dashed) [30] and TLEP TeraZ (dotted) [98]. Regions of a viable first order EW phase transition, from Eq. (2.144), are shown in the gray, hatched regions for $k = 1$ and 4π .

2.4.1.1 Effects on precision observables

After integrating out the scalar, the resultant low-energy theory contains a finite correction to the Higgs potential as well as the operators \mathcal{O}_H and \mathcal{O}_6 :

$$\mathcal{L}_{\text{eff}}(\mu = \mu_S) = \mathcal{L}_{\text{SM}} + \frac{A^2}{2m_S^2} |H|^4 + \frac{A^2}{m_S^4} \mathcal{O}_H - \left(\frac{A^2 k}{m_S^4} - \frac{1}{6} \frac{A^3 \mu}{m_S^6} \right) \mathcal{O}_6, \quad (2.136)$$

where, per our discussion around Eq. 2.135, we have only retained the tree-level contribution to the effective action at the matching scale $\mu = m_S$.

⁴⁵In the renormalization scheme of the CDE results in Eq. (2.38), S_c contributes a finite term to \mathcal{O}_6 from the $\text{tr}U$ term in Eq. (2.38). Compared to the tree-level contribution, this finite piece one-loop suppressed and hence negligible for the present analysis.

Upon electroweak symmetry breaking, \mathcal{O}_H modifies the wavefunction of the physical Higgs h and therefore universally modifies all the Higgs couplings through the residue correction Δr_h (Table C.3 in Appendix C),

$$\Delta r_h = -\frac{2v^2}{\Lambda^2} c_H = -\frac{2v^2}{m_S^2} c_H, \quad (2.137)$$

where $c_H = A^2/m_S^2$. This universal *Higgs oblique correction*⁴⁶ Δr_h can be quite sensitive to new physics [99–101] since future lepton colliders, such as the ILC, can probe it at the per mille level [28]. In Fig. 2.5, we show the 2σ contour of this oblique correction. The contour is obtained by combining the future expected sensitivities of Higgs couplings across all 7 channels in Table 1-20 of [28] for an ILC 500up program, except for the $h\gamma\gamma$ channel where we used the updated value provided by the second column in Table 6 of [102]. As shown, the ILC is quite sensitive to this oblique correction, exploring masses up to several TeV and much of the parameter space of the singlet’s couplings to the SM.

In addition to the oblique correction, \mathcal{O}_H will generate measurable contributions to electroweak precision observables (EWPO) under renormalization group evolution. This is an explicit example where the RG running effects discussed in section 2.2 are important. In particular, \mathcal{O}_H renormalizes into \mathcal{O}_W , \mathcal{O}_B , and \mathcal{O}_T , which contribute to the S and T parameters; because \mathcal{O}_H is generated at tree-level at $\Lambda = m_S$, this leads to a one-loop size contribution to the EWPOs at the weak scale. Let us take the results for the anomalous dimension matrix calculated in [45],⁴⁷

$$\gamma_{c_H \rightarrow c_W} = \gamma_{c_H \rightarrow c_B} = -\frac{1}{3}, \quad \gamma_{c_H \rightarrow c_T} = \frac{3}{2}g'^2. \quad (2.138)$$

Combining this with our mapping result (table 2.6 of section 2.3),

$$S = \frac{c_Z^2 s_Z^2}{\alpha} \frac{4m_Z^2}{\Lambda^2} [4c_{WB}(m_W) + c_W(m_W) + c_B(m_W)] \quad (2.139)$$

$$T = \frac{1}{\alpha} \frac{2v^2}{\Lambda^2} c_T(m_W), \quad (2.140)$$

we find for the singlet model at hand,

$$S = \frac{1}{6\pi} \left[\frac{2v^2}{m_S^2} c_H(m_S) \right] \log \frac{m_S}{m_W}, \quad (2.141)$$

$$T = -\frac{3}{8\pi \cos^2 \theta_W} \left[\frac{2v^2}{m_S^2} c_H(m_S) \right] \log \frac{m_S}{m_W}. \quad (2.142)$$

It is worth noting that S and T are highly correlated—current fits find a correlation coefficient of +0.91 [29]—while the RG evolution of c_H generates S and T in the orthogonal direction of this

⁴⁶In the literature, this Higgs oblique correction is sometimes denoted by δZ_h . In our notation, $\delta Z_h = -\Delta r_h$.

⁴⁷We note that the work [45] calculates γ_{ij} within a complete operator basis even though they provide only a subset of the full anomalous dimension matrix. Further, upon changing bases, the results of [45] agree with another recent computation of the full anomalous dimension matrix [40–42].

correlation, as depicted in Fig. 2.7. This orthogonality feature enhances the sensitivity of EWPO to oblique Higgs corrections, even when the new physics does not directly couple to the EW sector.

The current best fit of the S and T parameters are [29]

$$S = 0.05 \pm 0.09, \quad T = 0.08 \pm 0.07. \quad (2.143)$$

This precision is already sensitive to potential next-to-leading order physics which typically comes with a loop suppression, as in our singlet model. Future lepton colliders will significantly increase the precision measurements of S and T ; a GigaZ program at the ILC would increase precision to $\Delta S = \Delta T = 0.02$ [8, 30] while a TeraZ program at TLEP estimates precision of $\Delta S = 0.007$, $\Delta T = 0.004$ [9, 98]. Constraints on our singlet model from current and prospective future lepton collider measurements of S and T are shown in Fig. 2.5. As seen in the figure, the combination of increased precision measurements together with the fact that the singlet generates S and T in the anti-correlated direction, makes these EWPO a particularly sensitive probe of the singlet. Note that the apparent lack of improvement by GigaZ is an artifact of current non-zero central values in S and T .

As previously mentioned, this simple singlet model can achieve a strongly first-order EW phase transition. Essentially, this occurs by having a negative quartic Higgs coupling while stabilizing the potential with \mathcal{O}_6 ,

$$V_H \sim a_2 |H|^2 - a_4 |H|^4 + a_6 |H|^6,$$

for positive coefficients $a_{4,6}$. Within a thermal mass approximation,⁴⁸ a first-order EWPT occurs when [94]

$$\frac{4v^4}{m_H^2} < \frac{2m_s^4}{kA^2} < \frac{12v^4}{m_H^2}, \quad (2.144)$$

where we have set $\mu = 0$ for simplicity. The lower bound comes from requiring EW symmetry breaking at zero temperature, while the upper bound comes from requiring $a_4 > 0$, which guarantees the phase transition is first order.

The region of viability for a strongly first-order EWPT within the singlet model is shown in Fig. 2.5, for nominal values of the coupling k (note that k has an upper limit of $k \lesssim 4\pi$ from perturbativity and lower limit $k > 0$ from stability). Current EWPO already constrain a substantial fraction of the viable parameter space, while future lepton colliders will probe the entire parameter space.

Finally, we comment on the accuracy of the present calculation. Upon EW symmetry breaking, $H \rightarrow v + h/\sqrt{2}$, the singlet gains an additional contribution to its mass-squared of order kv^2 and mixes with h . The light eigenstate of this mixing is the physical Higgs with mass 125 GeV. As discussed earlier, these effects make the mass eigenvalue of the heavy scalar differ from the inverse of the Wilson coefficient in the effective Lagrangian Eq. (2.136). The difference is of the order of

$$\frac{kv^2}{m_S^2} \times \max\left[1, \frac{A^2}{m_S^2}\right].$$

⁴⁸ A full one-loop calculation at finite temperature does not drastically alter the bounds in Eq. (2.144); the lower bound remains the same, while the upper bound is numerically raised by about 25% [103]. This region is still well probed by future lepton colliders.

We note that this difference is very small over most of the region shown in Fig. 2.5.

2.4.2 Supersymmetry and light scalar tops

As a second benchmark scenario, we consider the MSSM with light scalar tops (stops) and examine the low energy EFT resultant from integrating out these states. Stops hold a privileged position in alleviating the naturalness problem, *e.g.* [104]. This motivates us to consider a spectrum with light stops while other supersymmetric partners are decoupled. Since the stops carry all SM gauge quantum numbers, all of the dimension-six operators in Table 2.2 are generated at leading order (1-loop). Therefore, they also serve as an excellent computational example to estimate the parametric size of Wilson coefficients of the operators in Table 2.2 resultant from heavy scalar particles with SM quantum numbers. Since the Wilson coefficients are generated at 1-loop leading order, we discard, as an approximation, the relatively smaller RG running effects (2-loop) of the Wilson coefficients.

Obtaining the Wilson coefficients

We integrate out the multiplet $\Phi = (\tilde{Q}_3, \tilde{t}_R)^T$, the Lagrangian of which up to quadratic order is given by

$$\mathcal{L} = \Phi^\dagger (-D^2 - m^2 - U) \Phi, \quad (2.145)$$

where

$$m^2 = \begin{pmatrix} m_{\tilde{Q}_3}^2 & 0 \\ 0 & m_{\tilde{t}_R}^2 \end{pmatrix}, \quad (2.146)$$

and the matrix U is

$$\begin{aligned} U &= \begin{pmatrix} (y_t^2 s_\beta^2 + \frac{1}{2} g^2 c_\beta^2) \tilde{H} \tilde{H}^\dagger + \frac{1}{2} g^2 s_\beta^2 H H^\dagger - \frac{1}{2} (g'^2 Y_Q c_{2\beta} + \frac{1}{2} g^2) |H|^2 & y_t s_\beta X_t \tilde{H} \\ y_t s_\beta X_t \tilde{H}^\dagger & (y_t^2 s_\beta^2 - \frac{1}{2} g'^2 Y_{t_r} c_{2\beta}) |H|^2 \end{pmatrix} \\ &\equiv \begin{pmatrix} \tilde{k} \tilde{H} \tilde{H}^\dagger + k H H^\dagger + \lambda_L |H|^2 & X_t \tilde{H} \\ X_t \tilde{H}^\dagger & \lambda_R |H|^2 \end{pmatrix} \\ &\equiv \begin{pmatrix} A_L & X_t \tilde{H} \\ X_t \tilde{H}^\dagger & A_R \end{pmatrix} \end{aligned}$$

where we have defined

$$\begin{aligned} A_L &\equiv \tilde{k} \tilde{H} \tilde{H}^\dagger + k H H^\dagger + \lambda_L |H|^2 & A_R &\equiv \lambda_R |H|^2 & y_t s_\beta X_t &\rightarrow X_t \\ \tilde{k} &\equiv y_t^2 s_\beta^2 + \frac{1}{2} g^2 c_\beta^2 & k &\equiv \frac{1}{2} g^2 s_\beta^2 & \lambda_L &\equiv -\frac{1}{2} (g'^2 Y_Q c_{2\beta} + \frac{1}{2} g^2) \\ \lambda_R &\equiv y_t^2 s_\beta^2 - \frac{1}{2} g'^2 Y_{t_r} c_{2\beta} \end{aligned}$$

Now with both the representation and the interaction matrix U at hand, we are ready to make use of Eq. (2.38) to compute the Wilson coefficients. However, in order for Eq. (2.38) to be valid,

we need U to commute with the mass square matrix m^2 , which limits us to the degenerate mass scenario $m_{\tilde{Q}_3}^2 = m_{\tilde{t}_R}^2 \equiv m_{\tilde{t}}^2$. It is also worth noting that due to the appearance of X_t , U is no longer quadratic in H , but also contains a linear term in H . This means that one has to keep up to $\mathcal{O}(U^6)$ in computing the Wilson coefficients of dimension-six operators. Another thing to keep in mind while evaluating the terms in Eq. (2.38) is that \tilde{Q}_3 and \tilde{t}_R have different charges under the SM gauge group, and the covariant derivative D_μ or $P_\mu = iD_\mu$ should take on the appropriate form for each,

$$P_\mu = \begin{pmatrix} P_{L\mu} & 0 \\ 0 & P_{R\mu} \end{pmatrix}.$$

For example, the commutator $[P_\mu, U]$ is,

$$[P_\mu, U] = \begin{pmatrix} [P_{L\mu}, A_L] & X_t(P_\mu \tilde{H}) \\ X_t(P_\mu \tilde{H})^\dagger & [P_{R\mu}, A_R] \end{pmatrix}.$$

Through a straightforward, albeit tedious use of Eq. (2.38), we obtain the final result of Wilson coefficients listed in Table 2.12.

Effects on precision observables

As in the previously considered singlet model, these Wilson coefficients will correct Higgs widths universally through Eq. (2.137), as well as contribute to S and T parameters through Eq. (2.139)-(2.140). In contrast to the singlet case, the stops contribute to both the oblique correction (via \mathcal{O}_H) and EWPOs (via \mathcal{O}_{WB} , \mathcal{O}_W , \mathcal{O}_B and \mathcal{O}_T) at leading order (1-loop). Additionally, vertex corrections to $h \rightarrow gg$ and $h \rightarrow \gamma\gamma$ decay widths—arising from \mathcal{O}_{GG} , \mathcal{O}_{WW} , \mathcal{O}_{BB} , and \mathcal{O}_{WB} —are sensitive probes since these are loop-level processes within the SM. The deviations from the SM decay rates are given by

$$\epsilon_{hgg} \equiv \frac{\Gamma_{hgg}}{\Gamma_{hgg}^{\text{SM}}} - 1 = \frac{(4\pi)^2}{\text{Re}A_{hgg}^{\text{SM}}} \frac{16v^2}{m_{\tilde{t}}^2} c_{GG}, \quad (2.147)$$

$$\epsilon_{h\gamma\gamma} \equiv \frac{\Gamma_{h\gamma\gamma}}{\Gamma_{h\gamma\gamma}^{\text{SM}}} - 1 = \frac{(4\pi)^2}{\text{Re}A_{h\gamma\gamma}^{\text{SM}}} \frac{8v^2}{m_{\tilde{t}}^2} (c_{WW} + c_{BB} - c_{WB}), \quad (2.148)$$

where A_{hgg}^{SM} and $A_{h\gamma\gamma}^{\text{SM}}$ are the standard form factors in their respective SM decay rates (see, *e.g.*, [105]).

2σ sensitivity contours are shown in Fig. 2.6. We stress that here we are focused on the experimental sensitivities on the scalar top mass, while assuming improvements on relevant theoretical uncertainties will catch up in time. Analogous to the case of the singlet model, $m_{\tilde{t}}$ in the plot differs from the mass eigenvalue by about $\frac{1}{2} \frac{m_{\tilde{t}}^2}{m_{\tilde{t}}^2} \times \max\left(1, \frac{X_t^2}{m_{\tilde{t}}^2}\right)$. As seen in Fig. 2.6, future precision Higgs and EW measurements from the ILC offer comparable sensitivities while a TeraZ program significantly increases sensitivity. Moreover, the most natural region of the MSSM—where $X_t \sim \sqrt{6}m_{\tilde{t}}$ and $m_{\tilde{t}} \sim 1$ TeV (*e.g.* [107])—can be well probed by future precision measurements.

$c_{GG} = \frac{h_t^2}{(4\pi)^2} \frac{1}{12} \left[\left(1 + \frac{1}{12} \frac{g'^2 c_{2\beta}}{h_t^2} \right) - \frac{1}{2} \frac{X_t^2}{m_{\tilde{t}}^2} \right]$ $c_{WW} = \frac{h_t^2}{(4\pi)^2} \frac{1}{16} \left[\left(1 - \frac{1}{6} \frac{g'^2 c_{2\beta}}{h_t^2} \right) - \frac{2}{5} \frac{X_t^2}{m_{\tilde{t}}^2} \right]$ $c_{BB} = \frac{h_t^2}{(4\pi)^2} \frac{17}{144} \left[\left(1 + \frac{31}{102} \frac{g'^2 c_{2\beta}}{h_t^2} \right) - \frac{38}{85} \frac{X_t^2}{m_{\tilde{t}}^2} \right]$	$c_{WB} = -\frac{h_t^2}{(4\pi)^2} \frac{1}{24} \left[\left(1 + \frac{1}{2} \frac{g^2 c_{2\beta}}{h_t^2} \right) - \frac{4}{5} \frac{X_t^2}{m_{\tilde{t}}^2} \right]$ $c_W = \frac{h_t^2}{(4\pi)^2} \frac{1}{40} \frac{X_t^2}{m_{\tilde{t}}^2}$ $c_B = \frac{h_t^2}{(4\pi)^2} \frac{1}{40} \frac{X_t^2}{m_{\tilde{t}}^2}$
--	--

$c_{3G} = \frac{g_s^2}{(4\pi)^2} \frac{1}{20}$ $c_{3W} = \frac{g^2}{(4\pi)^2} \frac{1}{20}$ $c_{2G} = \frac{g_s^2}{(4\pi)^2} \frac{1}{20}$ $c_{2W} = \frac{g^2}{(4\pi)^2} \frac{1}{20}$ $c_{2B} = \frac{g'^2}{(4\pi)^2} \frac{1}{20}$	$c_H = \frac{h_t^4}{(4\pi)^2} \frac{3}{4} \left[\left(1 + \frac{1}{3} \frac{g'^2 c_{2\beta}}{h_t^2} + \frac{1}{12} \frac{g'^4 c_{2\beta}^2}{h_t^4} \right) - \frac{7}{6} \frac{X_t^2}{m_{\tilde{t}}^2} \left(1 + \frac{1}{14} \frac{(g^2 + 2g'^2) c_{2\beta}}{h_t^2} \right) + \frac{7}{30} \frac{X_t^4}{m_{\tilde{t}}^4} \right]$ $c_T = \frac{h_t^4}{(4\pi)^2} \frac{1}{4} \left[\left(1 + \frac{1}{2} \frac{g^2 c_{2\beta}}{h_t^2} \right)^2 - \frac{1}{2} \frac{X_t^2}{m_{\tilde{t}}^2} \left(1 + \frac{1}{2} \frac{g^2 c_{2\beta}}{h_t^2} \right) + \frac{1}{10} \frac{X_t^4}{m_{\tilde{t}}^4} \right]$ $c_R = \frac{h_t^4}{(4\pi)^2} \frac{1}{2} \left[\left(1 + \frac{1}{2} \frac{g^2 c_{2\beta}}{h_t^2} \right)^2 - \frac{3}{2} \frac{X_t^2}{m_{\tilde{t}}^2} \left(1 + \frac{1}{12} \frac{(3g^2 + g'^2) c_{2\beta}}{h_t^2} \right) + \frac{3}{10} \frac{X_t^4}{m_{\tilde{t}}^4} \right]$ $c_D = \frac{h_t^2}{(4\pi)^2} \frac{1}{20} \frac{X_t^2}{m_{\tilde{t}}^2}$
---	--

$c_6 = -\frac{h_t^6}{(4\pi)^2} \frac{1}{2}$	$\left\{ \begin{aligned} & \left[1 + \frac{1}{12} \frac{(3g^2 - g'^2) c_{2\beta}}{h_t^2} \right]^3 + \left[-\frac{1}{12} \frac{(3g^2 + g'^2) c_{2\beta}}{h_t^2} \right]^3 + \left(1 + \frac{1}{3} \frac{g'^2 c_{2\beta}}{h_t^2} \right)^3 \\ & - \frac{X_t^2}{m_{\tilde{t}}^2} \left[2 \left(1 + \frac{1}{12} \frac{(3g^2 - g'^2) c_{2\beta}}{h_t^2} \right) \left(1 + \frac{1}{8} \frac{(g^2 + g'^2) c_{2\beta}}{h_t^2} \right) + \left(1 + \frac{1}{3} \frac{g'^2 c_{2\beta}}{h_t^2} \right)^2 \right] \\ & + \frac{X_t^4}{m_{\tilde{t}}^4} \left[1 + \frac{1}{8} \frac{(g^2 + g'^2) c_{2\beta}}{h_t^2} \right] - \frac{X_t^6}{m_{\tilde{t}}^6} \frac{1}{10} \end{aligned} \right\}$
---	--

Table 2.12: Wilson coefficients c_i for the operators \mathcal{O}_i in Table 2.2 generated from integrating out MSSM stops with degenerate soft mass $m_{\tilde{t}}$. g_s, g , and g' denote the gauge couplings of $SU(3)$, $SU(2)_L$, and $U(1)_Y$, respectively, $h_t = m_t/v$ with $v = 174\text{GeV}$, and $\tan\beta = \langle H_u \rangle / \langle H_d \rangle$ in the MSSM.

2.5 Summary of results

With the discovery of the Higgs boson, we now have an exciting opportunity to experimentally delve into some of the most pressing questions in particle physics of the last half century. Precise measurements of the Higgs' properties and other electroweak observables is crucial to unraveling what new physics—if any—may or may not lie near the weak scale. As precision measurements offer an indirect probe of new physics, the natural framework to study possible deviations from the Standard Model is effective field theory.

In the vein of studying how specific new models of physics affect precision observables, we have aimed in this work to provide tools to easily make use of the Standard Model effective field theory. As with any EFT, there is a practical three-step procedure that one makes use of: matching the UV theory onto the EFT at the scale where heavy states are integrated out, RG evolving the EFT down to the scale where measurements are made, and mapping the EFT onto observables at the measurement scale. While each of these steps is straightforward in the abstract, in practice they can be complicated for the SM EFT primarily due to the large number of higher dimension

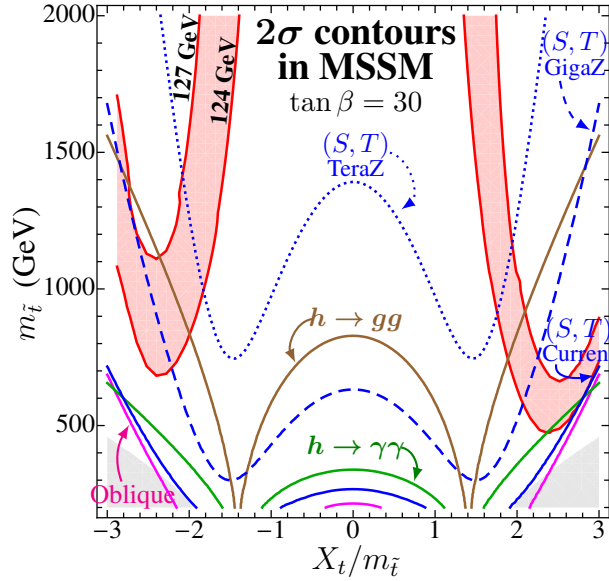


Figure 2.6: 2σ contours of precision Higgs and EW observables as a function of $m_{\tilde{t}}$ and X_t in the MSSM. The contours show 2σ sensitivity of ILC 500up to the universal Higgs oblique correction (magenta) and modifications of $h \rightarrow gg$ (brown) and $h \rightarrow \gamma\gamma$ (green). Constraints from S and T parameters are shown in blue for current measurements (solid), ILC GigaZ (dashed), and TLEP TeraZ (dotted). The shaded red region shows contours of Higgs mass between 124-127 GeV in the MSSM [106]. The shaded gray regions are unphysical because one of the stop mass eigenvalues becomes negative.

operators in the SM EFT. Here we provide a summary of some of the central results in this chapter.

In section 2.1 we developed the covariant derivative expansion, which allows one to compute the tree and one-loop effective action at the matching scale in a manifestly gauge covariant fashion. This calculation at tree-level is particularly obvious, and was explained in Sec. 2.1.1.1. At one-loop, the effective action can be brought to the form (Eq. (2.18))

$$\Delta S_{\text{eff},1\text{-loop}} = ic_s \text{Tr} \log [-P^2 + m^2 + U(x)] = ic_s \int d^4x \frac{d^4q}{(2\pi)^4} \text{tr} \log \left[- \left(q_\mu + \tilde{G}_{\nu\mu} \frac{\partial}{\partial q_\nu} \right)^2 + m^2 + \tilde{U} \right]$$

where $\tilde{G}_{\nu\mu}$ and \tilde{U} , Eq. (2.19), are expansions containing HDOs through commutators of the covariant derivative P_μ with itself and the low-energy (SM) fields in $U(x)$, together with derivatives of the auxiliary momentum q_μ . The general form of $U(x)$ for scalars, fermions, and vector bosons is summarized in Sec. 2.1.2.

The above effective action is then evaluated in an inverse mass expansion, leading to universal formulas for the one-loop effective action. In the case that m^2 commutes with $U(x)$, we explicitly performed this covariant derivative expansion and the general results up through dimension-six operators is given in Eq. (2.38). With these results, in Sec. 2.1.4 we computed the Wilson coefficients of dimension-six operators for numerous physically interesting and non-trivial models of

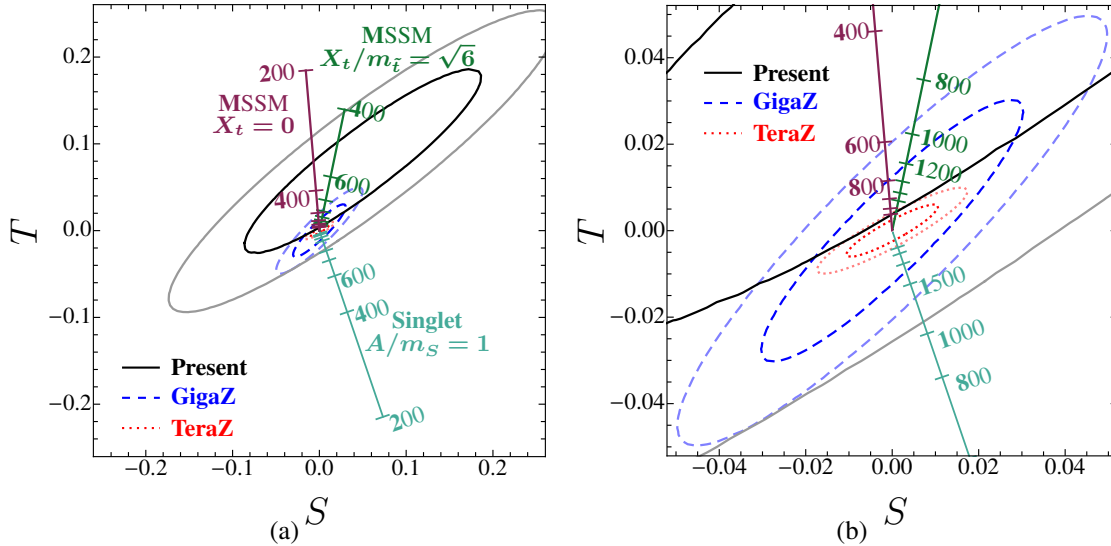


Figure 2.7: The 1σ (darker) and 2σ (lighter) ellipses of precision EW parameters S and T . We show current fits (solid, black) together with projected sensitivities at ILC GigaZ (dashed, blue) and TLEP TeraZ (dotted, red). The lines show the size of S and T parameters in our singlet model with $A = m_S$ (teal) and in the MSSM with $\tan\beta = 30$ for $X_t = \sqrt{6}m_{\tilde{t}}$ (green) and $X_t = 0$ (purple). The tick marks show specific mass values in each model; $m_{\tilde{t}}$ values in 200 GeV increments starting from $m_{\tilde{t}} = 200$ GeV for $X_t = 0$ and $m_{\tilde{t}} = 400$ GeV for $X_t = \sqrt{6}m_{\tilde{t}}$ in the MSSM; m_S values in 200 GeV increments between 200-1000 GeV and 500 GeV increments between 1000-3000 GeV in the singlet model.

new physics. Besides the inherent physical interest of the UV models considered, these examples hopefully offer a pedagogical explanation of how the CDE can be used to easily obtain the effective action at the matching scale.

In section 2.2 we considered the step of RG running Wilson coefficients at the matching scale down to the observation scale. At leading order, this involves making use of the anomalous dimension matrix γ_{ij} . In the past few years, there has been great progress on computing γ_{ij} . Instead of examining the technical details of this calculation, we explored the questions of when are these results needed and how to make use of them. Due to the per-mille sensitivity of present and future precision measurements, as a general rule of thumb RG running needs to be considered only when Wilson coefficients are generated at tree-level when new states are integrated out. If one does need to make use of RG evolution, the most practical ingredient one needs to understand to make use of existing computations of γ_{ij} concerns RG closure and choice of an operator basis. We provided a brief explanation of the choice of operator sets as well as common operator bases in the literature and how one can go between these bases.

Finally, in section 2.3 we studied how higher dimension operators impact precision observables. In particular, we computed the impact of all purely bosonic dimension-six operators (Ta-

ble 2.4) on electroweak precision observables, Higgs' decay widths, and Higgs production cross sections. This calculation was done to leading (linear) order in the Wilson coefficients. While various parts of these results have been computed in the literature previously, we believe our results offer the first complete and systematic results for the bosonic operators we considered.

The effect of the bosonic HDOs on the electroweak precision observables and triple gauge couplings can be found in Tables 2.6 and 2.7, respectively. For the Higgs decay widths and production cross sections, we considered the deviations that the HDOs lead to relative to the SM prediction,

$$\epsilon = \frac{\Gamma}{\Gamma_{\text{SM}}} - 1 \text{ and } \epsilon = \frac{\sigma}{\sigma_{\text{SM}}} - 1.$$

These deviations can be further refined into the impact of the HDOs in diagrammatic interference, residue (wavefunction) corrections, and changes to Lagrangian parameters (Sec 2.3.3.1). In other words,

$$\epsilon = \epsilon_I + \epsilon_R + \epsilon_P,$$

where $\epsilon_{I,R,P}$ stand for interference, residue, and parametric corrections, respectively. The values of $\epsilon_{I,R,P}$ in terms of the dimension-six Wilson coefficients can be found in tables 2.8 and 2.9 for Higgs decay widths and tables 2.10 and 2.11 for Higgs production cross sections.

Besides being the appropriate, model-independent framework to study precision observables, effective field theory provides great simplification to studying how specific new models of physics impact precision observables. We have outlined in detail the algorithmic procedure for doing this with the SM EFT. Given a UV model, one can easily match it onto the SM EFT using the covariant derivative expansion. One then decides if RG running down to the weak scale is of practical relevance; if it is, existing computations of the anomalous dimension matrix can be employed to do this step. At the weak scale, one then simply takes the Wilson coefficients of the bosonic operators and plugs them into tables 2.6-2.11 to study the deviations the UV model induces on electroweak and Higgs observables. We hope that the tools and results developed in this chapter not only highlight the utility of the SM EFT, but also demonstrate how one can use the SM EFT with relative ease.

Chapter 3

Constraints on Light Dark Matter from Big Bang Nucleosynthesis

Dark matter populates our universe, representing more than 80% of the total matter content. While astrophysical and cosmological measurements have elucidated the amount of dark matter (DM) in our universe as well as its role in galactic formation and distributions, we know very little about the nature of DM. For example, one of the few properties of DM that we can say anything with certainty is that dark matter has mass. But even the allowed mass values can span over 80 orders of magnitude, $10^{-22} \text{ eV} \lesssim m_\chi \lesssim 10^{59} \text{ eV}$, with the lower bound coming from requirement of localization on galactic scales [19] and the upper bound from micro-lensing searches for compact halo objects [20].

Despite our ignorance, we remain hopeful that theoretical models can provide a framework for experimentally probing dark matter directly and indirectly. For example, in this work we consider dark matter to be a weakly interacting massive particle that started its cosmic history in thermal equilibrium and froze-out as the universe cooled. The assumption of thermalization provides two powerful statements on DM: first, it restricts the allowed mass region to 11 orders of magnitude, $\text{keV} \lesssim m_\chi \lesssim 100 \text{ TeV}$, with the lower and upper bounds coming from the requirement that dark matter be cold [22] and its annihilation unitary [23], respectively. Second, if DM is a thermal relic, its annihilations must freeze-out to reach the observed current abundance, providing an estimate on the strength of DM interactions. In particular, assuming annihilation is s -wave dominated, in order to meet the observed abundance, freeze-out requires a weak scale cross-section that is nearly independent of mass, $\langle\sigma v\rangle_{\text{th}} \simeq 3 \times 10^{-26} \text{ cm}^3/\text{s}$.

After freeze-out, relic annihilations that occur may have observational consequences in two different scenarios. First, present day annihilations may be indirectly observed by searching the sky for their annihilation products (for a review, see [108]). In the second scenario, relic annihilations can inject hadronic and/or electromagnetic energy that may alter events in our cosmic history, namely big bang nucleosynthesis (BBN) and recombination (CMB). Because the physics of nucleosynthesis and recombination are well understood, they offer particularly clean environments in which to probe non-standard effects, such as DM annihilation. In addition, changes to BBN and CMB by non-standard processes depend only on the type and rate of energy injection into the bath,

and therefore leave BBN and CMB essentially decoupled from the high-energy details allowing relatively model-independent statements to be made.

In this chapter, we focus specifically on how relic annihilations from thermal dark matter affect nucleosynthesis. However, it is useful to describe in general how injected hadronic and electromagnetic energy alter nucleosynthesis and recombination. During nucleosynthesis, injection of hadronic and/or electromagnetic energy alters the abundances of nuclei via (i) energetic nucleons and photons dissociating nuclei and (ii) pions inter-converting background nucleons, thus raising the n/p ratio and therefore the primordial ${}^4\text{He}$ mass fraction. As for recombination, injected electromagnetic energy ionizes hydrogen atoms and therefore broadens the surface of last scattering. This results in scale dependent changes to the temperature and polarization power spectra, especially in the low l modes.

Now that we live in an era of precision CMB and BBN measurements, quantifying the effect of energy injection has led to powerful constraints on non-standard effects such as decay of long-lived particles [109–117] and dark matter annihilation [109, 113, 118–128]. In the case of dark matter annihilation, the primary result obtained from analysis of the injected energy on nucleosynthesis and recombination is an upper bound on the DM annihilation cross-section, $\langle\sigma v\rangle$, as a function of the DM mass. In particular, detailed analysis of the CMB has constrained s -wave annihilation to hadronic or electromagnetic channels to be less than the thermal cross-section required for freeze-out, $\langle\sigma v\rangle < \langle\sigma v\rangle_{\text{th}}$, for $m_\chi \lesssim 10$ GeV [123, 126–128]. Studies of s -wave annihilation on BBN have been performed by Hisano *et. al.* for $m_\chi \gtrsim 100$ GeV [119, 120] and separately by Jedamzik and Pospelov for $m_\chi \gtrsim$ several GeV [121], while lower mass regions have remained unconsidered.

From previous works [119–121] that consider the effect of DM annihilation on BBN, the constraint on the annihilation cross-section appears to have a simple power law dependence on the DM mass, $\langle\sigma v\rangle \propto m_\chi^\delta$, where the power for hadronic (electromagnetic) energy injection is $\delta \approx 3/2$ ($= 1$). In this chapter, we explain these scaling behaviors and the range of DM masses for which they hold. Then we extrapolate the bounds to previously unconsidered DM masses and find that BBN constrains $\langle\sigma v\rangle < \langle\sigma v\rangle_{\text{th}}$ for few GeV $\lesssim m_\chi \lesssim 10$ GeV (30 MeV $\lesssim m_\chi \lesssim 75$ MeV) for the case of hadronic (electromagnetic) energy injection.

The structure of this chapter is as follows: in section 3.1 we discuss how injection of hadronic and electromagnetic energy alters BBN, and in particular, how these effects scale with the dark matter mass and annihilation cross-section. In section 3.2, we use these scaling laws along with results from precise numerical treatment [119] to estimate constraints on DM annihilation in a previously unconsidered low mass region. Our estimates indicate that BBN places a constraint on hadronic annihilation channels that is competitive and independent of the CMB constraint. We also discuss how these bounds change for annihilation to other Standard Model particles. Finally, we summarize our results in section 3.3.

3.1 Energy injection into BBN

Injected energy from dark matter annihilations occurring after $T \sim 1$ MeV can alter the primordial abundances of the light elements. Details of the evolution of injected energy and its ef-

fects on nucleosynthesis are thoroughly discussed in [112]. Quantifying the change on primordial abundances boils down to calculating the spectrum of a given produced hadron/nucleus H_i . This spectrum, $f_{H_i} = dn_{H_i}/dE_{H_i}$, is a complicated function that depends on the dynamics of the injected energy, the nuclear network leading to the production/destruction of H_i , and the rate of DM annihilation. In this work, we focus on the dependence of this spectrum on the DM's mass and annihilation cross-section. Since production/destruction of H_i begins with an annihilation event, df_{H_i}/dt is proportional to the DM annihilation rate,

$$\frac{df_{H_i}}{dt} \propto \frac{dn_\chi}{dt} = -n_\chi^2 \langle \sigma v \rangle. \quad (3.1)$$

Here, $\langle \sigma v \rangle$ is the thermally-averaged annihilation cross-section which we take to be s -wave dominated and time independent and n_χ is the number density of DM. For the range of DM masses considered, BBN occurs after freeze-out and therefore the number density of DM is fixed by observational abundance

$$n_\chi(t) = \frac{\Omega_\chi \rho_{\text{crit}}}{m_\chi} \frac{1}{a(t)^3} \propto \frac{1}{m_\chi}. \quad (3.2)$$

Hence, the DM injection rate scales as

$$\frac{dn_\chi}{dt} \propto -\frac{\langle \sigma v \rangle}{m_\chi^2}. \quad (3.3)$$

This has a simple physical interpretation: as dark matter mass decreases, in order to fit the observed abundance there needs to be more DM particles, which in turn leads to more annihilation events. In addition to the DM annihilation rate, the spectrum of produced/destroyed H_i will depend on the DM mass through the dynamics of the type of energy injected, which we now consider.

3.1.1 Injection of hadronic energy

Hadrons (p, n, π^\pm , etc.) resultant from DM annihilation can primarily alter BBN through proton-neutron interconversion (π^\pm) and hadro-dissociation (p, n) [109, 112]. Interconversion of p and n by energetic pions before the formation of D and ${}^4\text{He}$ ($T \sim 100$ keV) can increase the n/p ratio set by ν decoupling at $T \sim \text{MeV}$. Since almost all neutrons end up in ${}^4\text{He}$ (see, *e.g.* [129]), the increase of n/p leads to a larger ${}^4\text{He}$ primordial mass fraction, Y_p .

Energetic nucleons produced by DM annihilation alter primordial abundances through collisions with nuclei. The dominant effect of energetic neutrons and protons is to hadro-disassociate ${}^4\text{He}$ which in turn leads to an increased production of D, ${}^3\text{H}$, ${}^3\text{He}$, and ${}^6\text{Li}$. Electromagnetic interactions with background photons and electrons tend to thermalize the nucleons, so hadro-dissociation only becomes efficient when the universe dilutes enough so that the electromagnetic interactions lose their stopping power. This occurs below $T \sim 100$ keV for neutrons and $T \sim 10$ keV for protons [112]. Because the primordial abundance of ${}^4\text{He}$ is much larger than other nuclides (for example, $n_{\text{D}}/n_{{}^4\text{He}} \sim \mathcal{O}(10^{-3})$), BBN is more sensitive to enhanced production of other nuclides than to processes which alter the primordial ${}^4\text{He}$ abundance. Therefore, hadro-dissociation of ${}^4\text{He}$

leading to increased production of other nuclides—namely D, ^3H , ^3He , and ^6Li —provides the most stringent constraints from BBN.

Since we wish to understand the change in a given nuclide’s primordial abundance as a function of $\langle\sigma v\rangle$ and m_χ , we consider how the amount of hadro-dissociation depends on these parameters. As in equation (3.1), the amount of hadro-dissociation is proportional to the dark matter annihilation rate, $dn_\chi/dt \propto \langle\sigma v\rangle/m_\chi^2$. Since hadro-dissociation proceeds through energetic nucleons, further dependence on m_χ essentially comes from the number of energetic nucleons produced in an annihilation event, *i.e.* the nucleon multiplicity [109, 110].¹ Assuming annihilation into quarks, $\chi\chi \rightarrow q\bar{q}$, the nucleon multiplicity can be approximated by the multiplicity in e^+e^- collisions at $\sqrt{s} = 2m_\chi$. To leading order in QCD, the average charged particle multiplicity has the following dependence on \sqrt{s} [130–132]:

$$\langle n_{\text{ch}} \rangle = a \exp \left(\sqrt{\frac{24}{\beta_0}} \sqrt{\log \left(\frac{s}{\Lambda^2} \right)} \right) + c \quad (3.4)$$

where $\beta_0 = 11 - 2n_f/3$, Λ is the renormalization scale, and a and c are constants. Apart from overall normalization, for $\sqrt{s} = 2m_\chi$ above several GeV, the above is well approximated by $(\sqrt{s})^{0.5 \pm \epsilon} \sim m_\chi^{0.5 \pm \epsilon}$ with $\epsilon \sim 0.05$.

The dependence of the amount of hadro-dissociation on the rate of DM annihilation and the nucleon multiplicity implies that the Boltzmann term for production/destruction of nuclei H_i approximately scales with DM as:

$$\left[\frac{dn_{H_i}}{dt} \right]_{\text{hadronic}} \propto m_\chi^{1/2} \frac{\langle\sigma v\rangle}{m_\chi^2} = \frac{\langle\sigma v\rangle}{m_\chi^{3/2}} \quad (3.5)$$

This scaling is expected to hold down to $m_\chi \sim \text{few GeV}$, below which hadro-dissociation quickly goes to zero since an annihilation event can no longer produce nucleons. This behavior implies that constraints on $\langle\sigma v\rangle$ from BBN approximately scale as $m_\chi^{3/2}$, which is confirmed by precise numerical calculations for $m_\chi \gtrsim 10 \text{ GeV}$ [119–121] and shown in figure 3.1.

3.1.2 Injection of electromagnetic energy

Electromagnetic showering of energetic photons and leptons in the early universe produces many photons [133] which can photo-dissociate nuclei and alter primordial abundances [111, 112].

Photo-dissociation is a significant effect only when the energetic photons do not thermalize. Precise calculations of the evolution of electromagnetic cascades in the early universe can be found in the literature [133], but the dominant effects are easily understood. Because of the small baryon-to-photon ratio, $\eta \sim \mathcal{O}(10^{-10})$, photons will pair produce off background photons ($\gamma + \gamma_{\text{bkg}} \rightarrow e^+ +$

¹Technically, it is the spectrum of nucleons per annihilation event, dN_N/dE_N , that is of interest. The dependence of this spectrum on $\sqrt{s} = 2m_\chi$ comes from the low $x = E_N/\sqrt{s}$ behavior of the parton fragmentation functions $D_i^N(x, \sqrt{s})$. The dependence of the multiplicity on \sqrt{s} shown in the text is inherited from dN_N/dE_N ’s dependence on \sqrt{s} [130, 131].

e^-) if their energy is above the threshold energy, $E_{\text{th}} \approx m_e^2/22T$. Therefore, photo-dissociation only becomes efficient when the binding energy drops below the threshold for pair production.

Of the possible photo-dissociation channels, destruction of ${}^4\text{He}$ dominates since ${}^4\text{He}$ is the most abundant of the light nuclei by a few orders of magnitude. Since $E_{b,{}^4\text{He}} \sim 20$ MeV, photo-dissociation of ${}^4\text{He}$ does not become relevant until $T \lesssim 0.5$ keV. The dominant photo-dissociation channels of ${}^4\text{He}$ are to ${}^3\text{H}$ or ${}^3\text{He}$ plus a nucleon [111]. Therefore, photo-dissociation of ${}^4\text{He}$ most noticeably leads to overproduction of ${}^3\text{He}$ (${}^3\text{H}$ decays to ${}^3\text{He}$ with a half-life of about 14 years). Overproduction of D and ${}^6\text{Li}$ may also result from ${}^4\text{He}$ photo-destruction. In the case of deuterium, it can be directly produced in photo-spallation of ${}^4\text{He}$ [111] or in capture of the neutron from $\gamma + \alpha_{\text{bkg}} \rightarrow {}^3\text{He} + n$ on a background proton. Non-thermal production of ${}^6\text{Li}$ may occur if the spallation product ${}^3\text{H}$ or ${}^3\text{He}$ is captured on a background ${}^4\text{He}$, ${}^3\text{H} + \alpha_{\text{bkg}} \rightarrow {}^6\text{Li} + n$ or ${}^3\text{He} + \alpha_{\text{bkg}} \rightarrow {}^6\text{Li} + p$. Because the observed abundance of ${}^6\text{Li}$ is very small, non-thermal production of ${}^6\text{Li}$ via photo-dissociation of ${}^4\text{He}$ can have a noticeable impact [134, 135].

Assuming annihilation into radiative channels ($\chi\chi \rightarrow \gamma\gamma$ or $\chi\chi \rightarrow l^+l^-$), we wish to extract how production/destruction of nuclei H_i due to photo-dissociation depends on DM mass. As in the case of hadro-dissociation, the amount of photo-dissociation is proportional to the amount of DM annihilation, dn_χ/dt . The amount of photo-dissociation also depends on the number of photons produced in an annihilation event and the subsequent electromagnetic cascade. Because there is no mass gap for the photon, the number of photons produced is proportional to the visible energy (e^\pm and γ) from the annihilation event, E_{vis} . For example, annihilation to electrons or muons have $E_{\text{vis}} = 2m_\chi$ and $E_{\text{vis}} \sim 2m_\chi/3$, respectively.

The amount of photo-dissociation implies that the Boltzmann term for production/destruction of nuclei H_i due to photo-dissociation is inversely proportional to the DM mass,

$$\left[\frac{dn_{H_i}}{dt} \right]_{\text{P.D.}} \propto \frac{\langle \sigma v \rangle}{m_\chi} \left(\frac{E_{\text{vis}}}{m_\chi} \right). \quad (3.6)$$

Therefore, if DM annihilates into radiative channels, constraints on $\langle \sigma v \rangle$ from BBN scale as m_χ , which is confirmed by precise numerical calculations for $m_\chi \gtrsim 10$ GeV [119, 121, 122] and shown in figure 3.1. This scaling can be expected to hold down close to the binding energy of ${}^4\text{He}$, $E_{b,{}^4\text{He}} \sim 20$ MeV. In the case of non-thermal production of ${}^6\text{Li}$ this scaling holds down to ~ 60 MeV. This is because the daughter ${}^3\text{H}$ or ${}^3\text{He}$ from photo-dissociation of ${}^4\text{He}$ needs about 10 MeV kinetic energy to efficiently capture on background ${}^4\text{He}$ [111], thus requiring $E_\gamma \gtrsim 60$ MeV. Note that constraints from the CMB also exhibit the scaling behavior $\langle \sigma v \rangle \propto m_\chi$ [123–128] since the amount of visible energy from the annihilation is what dictates how many photons will be produced.

3.2 Constraints from BBN

Relic dark matter annihilations alter the primordial abundances of nuclei from standard BBN predictions. In the case of s -wave annihilation, as discussed in the previous section, the scaling of

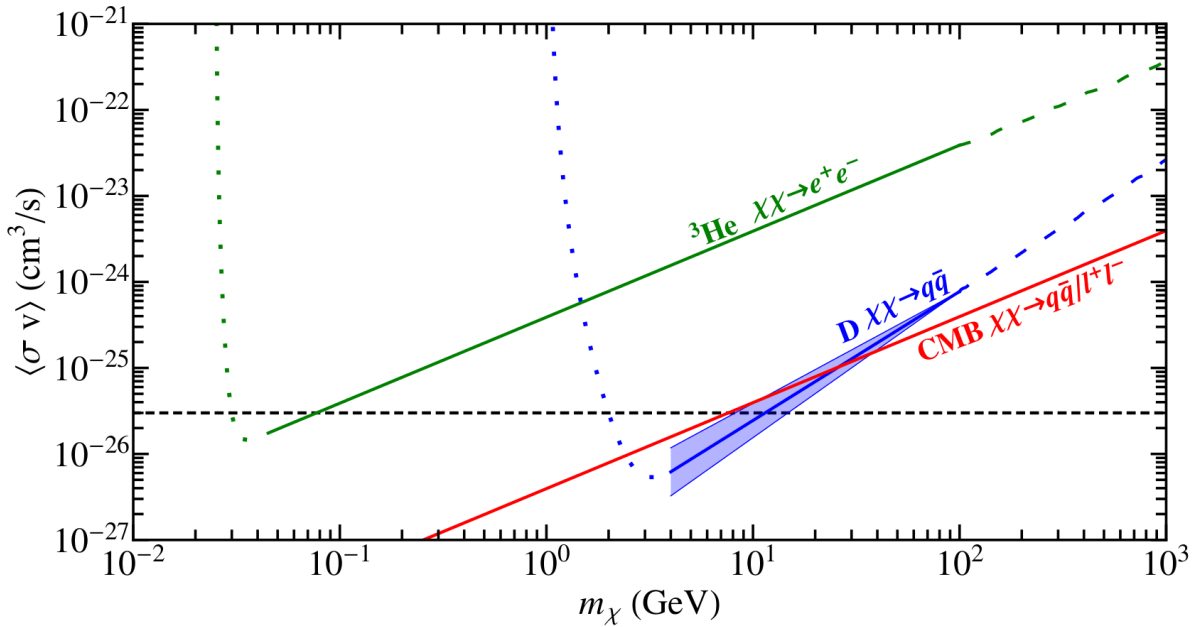


Figure 3.1: BBN constraints on hadronic (blue) and radiative (green) annihilation channels from D and ${}^3\text{He}$ overproduction, respectively. The solid blue (green) line is our estimate based on the scaling behavior $\langle\sigma v\rangle \propto m_\chi^{1.5\pm 0.2}$ ($\langle\sigma v\rangle \propto m_\chi$) for hadronic (radiative) annihilation. The long dashed lines indicate bounds on $\chi\chi \rightarrow b\bar{b}$ (blue) and $\chi\chi \rightarrow e^+e^-$ (green) from Hisano *et al.* [119]. The dotted blue and green lines is a rendering of where we expect these scaling laws to break down, but their exact shape and placement requires precise numerical treatment. The red line is the bound from the CMB, whose normalization is set by constraints on $\chi\chi \rightarrow b\bar{b}$ at 95% C.L. from Natarajan [128] and extended using the scaling $\langle\sigma v\rangle \propto m_\chi$ [123–128]. For CMB, the important quantity is visible energy injection, and therefore annihilation to quarks or charged leptons give roughly the same constraint.

these effects on DM mass and annihilation cross-section is given in equations (3.5) and (3.6) for hadronic and radiative annihilation channels, respectively.

In this chapter, we use BBN to place an upper bound on $\langle\sigma v\rangle$ for the previously unconsidered low DM mass region of $\text{MeV} \lesssim m_\chi \lesssim 10 \text{ GeV}$. To do this we adopt the bound on $\langle\sigma v\rangle$ at $m_\chi = 100 \text{ GeV}$ from Hisano *et al.* [119] and extrapolate the bounds to the low mass region using (3.5) and (3.6).

While a precise treatment requires numerical simulation, results from other works [119–122] indicate that the scaling behavior in (3.5) and (3.6) is robust. We will discuss where this scaling behavior breaks down and how precise our estimates are.

Since we adopt the constraints of Hisano *et al.* [119] as a starting point, the observational abundances used to place bounds are the same as in that work. These observational abundances are discussed in appendix D.

3.2.1 Hadronic constraints

As discussed in equation (3.5), constraints on $\langle\sigma v\rangle$ from hadronic energy injection are approximately proportional to $m_\chi^{2-\alpha}$ where $\alpha \approx 0.5$ comes from the dependence of the nucleon multiplicity on $\sqrt{s} = 2m_\chi$, i.e. $\langle n_N \rangle$ is approximately proportional to m_χ^α . As m_χ approaches a GeV, this scaling is expected to break down and constraints on $\langle\sigma v\rangle$ to rapidly weaken since annihilations no longer produce energetic nucleons that dissociate background ${}^4\text{He}$.

The scaling $\langle\sigma v\rangle \propto m_\chi^{1.5}$ assumes the dominant effect on primordial abundances is hadro-dissociation of background ${}^4\text{He}$. While hadro-dissociation does dominate, there may be other processes which contribute a small but non-negligible amount. For example, DM annihilations may further enhance primordial D, ${}^3\text{He}$, and ${}^6\text{Li}$ abundances through (1) photo-dissociation of background ${}^4\text{He}$ by energetic photons produced in the hadronic jet and from electromagnetic energy loss and (2) more background ${}^4\text{He}$ to dissociate from $p - n$ interconversion by pions at $T \gtrsim 100$ keV. While these contributions are sub-dominant to hadro-dissociation of background ${}^4\text{He}$, precise numerical treatment is needed to evaluate the relative size and scaling with m_χ of all possible effects. The scaling behavior with m_χ might also be modified by the number of secondary energetic nucleons produced from hadro-dissociation processes, although this effect is subdominate [112].

Our goal in this work is to derive conservative estimates. Therefore, to parameterize our ignorance on the interplay of all effects in calculating constraints on $\langle\sigma v\rangle$ for a given mass, we include an uncertainty in the scaling

$$\langle\sigma v\rangle \propto m_\chi^{1.5 \pm \delta} \quad (3.7)$$

where we take the uncertainty to be $\delta = 0.2$ [119].

In Ref [119] the authors consider annihilation into b quarks, $\chi\chi \rightarrow b\bar{b}$. From the primordial deuterium abundance they derive an upper bound $\langle\sigma v\rangle \leq 7.7 \times 10^{-25} \text{ cm}^3/\text{s}$ for $m_\chi = 100 \text{ GeV}$. As shown in figure 3.1, the scaling (3.7) implies $\langle\sigma v\rangle < \langle\sigma v\rangle_{\text{th}} = 3 \times 10^{-26} \text{ cm}^3/\text{s}$ for

$$m_b \lesssim m_\chi \leq 11.4_{-3.2}^{+3.3} \text{ GeV}. \quad (3.8)$$

For annihilation to bottom quarks, the constraint is cutoff at $m_b \sim 5 \text{ GeV}$. While the above constraint is for $\chi\chi \rightarrow b\bar{b}$, similar results are anticipated for annihilation to other quark species. However, in the case of annihilation to lighter quarks, we expect the constraint on $\langle\sigma v\rangle$ falls off as $m_\chi \rightarrow m_N \sim \text{GeV}$, but where and how rapidly this occurs can only be obtained from numerical analysis.

3.2.2 Electromagnetic constraints

Constraints on $\langle\sigma v\rangle$ from electromagnetic energy injection are proportional to m_χ . Electromagnetic energy primarily alters primordial abundance through photo-dissociation of ${}^4\text{He}$, leading to enhanced production of other nuclides. Therefore, the scaling $\langle\sigma v\rangle \propto m_\chi$ holds as long as the DM annihilation and subsequent shower produce photons energetic enough to dissociate ${}^4\text{He}$.

As discussed earlier, the observable consequences of overproduction as a result of ${}^4\text{He}$ photo-dissociation are largest for ${}^3\text{He}$. In [119], Hisano *et. al.* study the annihilation channel $\chi\chi \rightarrow$

e^+e^- and derive an upper bound of $\langle\sigma v\rangle \leq 3.9 \times 10^{-23} \text{ cm}^3/\text{s}$ for $m_\chi = 100 \text{ GeV}$ from ${}^3\text{He}$ overproduction. As shown in figure 3.1, the scaling $\langle\sigma v\rangle \propto m_\chi$ implies $\langle\sigma v\rangle < \langle\sigma v\rangle_{\text{th}} = 3 \times 10^{-26} \text{ cm}^3/\text{s}$ for

$$30 \text{ MeV} \lesssim m_\chi \leq 77 \text{ MeV} \quad (3.9)$$

The constraints fall off when the electrons from the DM annihilation can no longer produce photons energetic enough to dissociate ${}^4\text{He}$. The photo-dissociation cross-section for ${}^4\text{He}$, $\sigma_{{}^4\text{He}\gamma \rightarrow \dots}$, proceeds through the giant dipole resonance and only becomes efficient when $E_\gamma \gtrsim 25 \text{ MeV}$ [111, 136]. An electron from the DM annihilation event with $E_{e^\pm} = m_\chi$ near this threshold produces energetic photons via inverse-Compton scattering off background photons. Inverse-Compton scattering is a relatively hard event, with $\sim 80\%$ of the momentum transferred to the scattered photon. Therefore we expect the constraints on $\chi\chi \rightarrow e^+e^-$ from ${}^3\text{He}$ overproduction to fall off around 30 MeV.

3.2.3 Other annihilation channels

The constraints (3.8) and (3.9) for hadronic and electromagnetic energy injection are obtained from DM annihilation to $b\bar{b}$ and e^+e^- , respectively. It is useful to consider how these constraints would change for different annihilation channels. Nucleosynthesis is sensitive to the amount of hadronic and electromagnetic energy injected into the bath and is therefore essentially decoupled from the high energy details of the dark matter annihilation. Therefore, in order to understand how different DM annihilation channels alter BBN, it is sufficient to specify the annihilation products and ask what particles are produced in the resulting hadronic and/or electromagnetic cascade.

In the case of annihilation into hadronic channels, we do not anticipate the constraints from different quark species (u, d, s, c) to change much from the case of annihilation to bottom quarks. Injected hadronic energy primarily alters BBN through dissociation of nuclei by energetic nucleons resultant from the hadronization of the initial state quarks. At energies much larger than the nucleon mass, the spectrum of nucleons does not significantly depend on the initial state quark. As the DM mass gets near the nucleon mass, $E \gtrsim m_N$, the nucleon spectrum from hadronization will differ between initial state quark species. For lighter quark species, the main change from the constraint for $\chi\chi \rightarrow b\bar{b}$ (3.8) is that the bounds will fall off at a DM mass lower than $m_b \sim 5 \text{ GeV}$. Therefore, for annihilation to quarks, we generically expect $\langle\sigma v\rangle_{\chi\chi \rightarrow q\bar{q}} < \langle\sigma v\rangle_{\text{th}}$ for few GeV $\lesssim m_\chi \lesssim 11 \pm \text{few GeV}$ where the lower limit comes from the inability to produce energetic nucleons in the annihilation event and will have a slight dependence on initial quark species, beyond the precision of these estimates.

Annihilation to photons, electrons, or muons will alter BBN through the injection of electromagnetic energy. From equation (3.6), constraints on the DM annihilation cross-section are inversely proportional to the amount of injected visible energy (electrons and photons),

$$\langle\sigma v\rangle \propto m_\chi \left(\frac{m_\chi}{E_{\text{vis}}} \right). \quad (3.10)$$

In the case of annihilation to photons or electrons $E_{\text{vis}} = 2m_\chi$. For annihilation to muons, $E_{\text{vis}} \sim 2m_\chi/3$ and therefore the constraints on $\langle\sigma v\rangle$ for $\chi\chi \rightarrow \mu^+\mu^-$ are weakened by a factor of ~ 3 from

the case of $\chi\chi \rightarrow e^+e^-$. Therefore, we estimate that ${}^3\text{He}$ overproduction bounds $\langle\sigma v\rangle_{\chi\chi\rightarrow\mu^+\mu^-} \lesssim 1 \times 10^{-25} (m_\chi/m_\mu) \text{ cm}^3/\text{s}$ and is valid for $m_\chi \geq m_\mu$.

BBN constraints on annihilation to taus, $\chi\chi \rightarrow \tau^+\tau^-$, come from the injection of electromagnetic energy from the τ decay products. Despite the large hadronic branching fraction in the τ decay, since $m_\tau < 2m_N$, annihilation to τ 's cannot produce nucleons which would alter nucleosynthesis through hadro-dissociation of ${}^4\text{He}$. While the hadronic products of τ decay (pions and kaons) will slightly affect the primordial ${}^4\text{He}$ mass fraction through interconversion of background n and p at $100 \text{ keV} \lesssim T \lesssim \text{MeV}$, they predominantly alter standard BBN through the electromagnetic energy in their decay products. Taking the average fraction of visible energy in a τ decay to be 0.31 [119], overproduction of ${}^3\text{He}$ from photo-dissociation of ${}^4\text{He}$ bounds $\langle\sigma v\rangle_{\chi\chi\rightarrow\tau^+\tau^-} \lesssim 1 \times 10^{-24} (m_\chi/10 \text{ GeV}) \text{ cm}^3/\text{s}$.

Finally, we comment on annihilation to neutrinos. Injection of energetic neutrinos during nucleosynthesis has been considered in the context of a long-lived particle decay [137–139]. While neutrinos have impact nucleosynthesis much less than colored or charged particles, here we estimate the magnitude of effects on nucleosynthesis from annihilation to neutrinos and show that the effects are, at most, as large as $\mathcal{O}(10^{-4})$ the effect of radiative annihilation channels. High energy neutrinos may pair produce charged leptons off of background neutrinos, $\nu + \bar{\nu}_{\text{bkg}} \rightarrow l^+ + l^-$. If this reaction happens after $T \sim 0.5 \text{ keV}$, the photons in the electromagnetic shower of the charged leptons can photo-dissociate nuclei and alter their primordial abundances [137–139]. Charged leptons are also generically produced in the annihilation through radiation of a (real or virtual) weak boson by one of the final state neutrinos, *e.g.* $\chi\chi \rightarrow \nu_i \bar{l}_i W^{(*)} \rightarrow \nu_i \bar{l}_i \bar{\nu}_j l_j$.²

Both processes—high energy neutrinos pair producing off the neutrino background and annihilation to a multi-body final state—are important for charged lepton production, and therefore for BBN constraints. For charged lepton pair production off a background neutrino the rate of interaction is approximately $\Gamma_{\nu\bar{\nu}_{\text{bkg}}\rightarrow l^+l^-} \sim G_F^2 m_\chi T_\nu n_{\nu,\text{bkg}}$. This reaction can occur as long as the initial neutrino is above the threshold for pair production, $E_\nu E_{\nu_{\text{bkg}}} = m_\chi T_\nu \geq m_l^2$, which for production of e^+e^- occurring after $T \sim 0.5 \text{ keV}$ requires $m_\chi \gtrsim \text{GeV}$. The fraction of neutrinos that pair produce after $T \sim 0.5 \text{ keV}$ is then approximately³

$$\int_{t(T\sim 0.5 \text{ keV})}^{t_f} dt \Gamma_{\nu\bar{\nu}_{\text{bkg}}\rightarrow l^+l^-} \sim 2 \times 10^{-4} \left(\frac{m_\chi}{100 \text{ GeV}} \right) \left(\frac{T}{0.5 \text{ keV}} \right)^2. \quad (3.11)$$

Note that if the initial neutrino is energetic enough, high energy secondary neutrinos from neutrino-neutrino scattering can play a role [138, 139]. As for the multi-body final state, the relative amount of charged lepton production via neutrino radiation of a weak boson is approximately $G_F^2 m_\chi^4 / 16\pi^2$ for $m_\chi \ll M_W$ and can be as large as $\alpha_w / 4\pi \sim 3 \times 10^{-3}$ when the weak boson is radiated on shell. Thus, depending on the energy of the initial neutrino, both the high energy neutrinos

²Of course, if the primary annihilation channel is through neutrinos, annihilation to l^+l^- is generated at loop order and is model-dependent. Given a model, this annihilation can be calculated and the bounds for $\chi\chi \rightarrow l^+l^-$ used. We focus on radiation of a weak boson giving a three- or four-body final state since it is model-independent.

³Cosmological redshift for the energetic neutrino can actually occur since $\Gamma_{\nu\bar{\nu}_{\text{bkg}}\rightarrow l^+l^-} < H$. However, to not complicate our point, we do not include it in the estimate. Cosmological redshift lowers the fraction of neutrinos that pair produce charged leptons, but does not change our conclusions.

themselves and branching to multi-body final states can have the same order-of-magnitude effect on nucleosynthesis, which is what was found in [139]. Based on these considerations, we estimate that bounds on annihilation to neutrinos are weaker than bounds on radiative annihilation channels by $\mathcal{O}(10^{-4} - 10^{-6})$ for $m_\chi \gtrsim \text{GeV}$ and by $\sim G_F^2 m_\chi^4 / 16\pi^2$ for $m_\chi \lesssim \text{GeV}$. For this reason, annihilation to neutrinos is essentially negligible for BBN.

3.3 Discussion

In this chapter we have examined the effects of dark matter annihilations during the epoch of big bang nucleosynthesis. We emphasize that, in terms of the annihilation itself, the magnitude of these effects depend only on the rate of energy injection (*i.e.* the DM annihilation rate) and the type of energy injected (hadrons, charged leptons, *etc.*). With this procedure, we have explained how changes to primordial abundances of nuclei scale with the dark matter mass and annihilation cross-section. These scaling behaviors are robust and have been observed in precise numerical treatments of DM annihilation during BBN [119–122].

The dependence of changes to nucleosynthesis on the dark matter mass and annihilation cross-section, along with results from precise numerical calculation [119], have allowed us to estimate constraints on $\langle\sigma v\rangle$ for the previously unconsidered low DM mass region $\text{MeV} \lesssim m_\chi \lesssim 10 \text{ GeV}$. Interestingly, our estimates indicate that BBN rules out generic *s*-wave annihilation to quarks (radiative $e^+e^-, \gamma\gamma$) for few $\text{GeV} \lesssim m_\chi \lesssim 10 \text{ GeV}$ ($30 \text{ MeV} \lesssim m_\chi \lesssim 500 \text{ MeV}$).

Our results have focused on the case that the thermally averaged annihilation cross-section is independent of time (*s*-wave annihilation). For scenarios in which $\langle\sigma v\rangle$ depends on time, changes to the time-independent case can be understood from a modification of the rate of annihilation, $\Gamma_{\text{ann}} = n_\chi(t)\langle\sigma v\rangle(t)$. For example, if the annihilation is *s*-wave suppressed, $\langle\sigma v\rangle$ will decrease in time [129] and therefore have less impact on BBN. On the other side, as studied in [122], Sommerfeld [140] or Breit-Wigner [141] type enhancements lead to $\langle\sigma v\rangle$ increasing in time and having a stronger impact on nucleosynthesis.

Besides making our estimates precise, our results warrant a full numerical treatment for a few reasons. Our estimates indicate that *s*-wave annihilation to quarks is ruled out starting around $m_\chi \sim 10 \text{ GeV}$, which is competitive with the current bound from CMB [127, 128]. In estimating constraints for light DM, we extrapolated the results of Hisano *et. al.* [119], whose philosophy was to provide conservative constraints. Given that BBN provides an independent, and possibly more stringent, constraint than CMB, it is worthwhile to perform a full numerical calculation that also quantifies the confidence limit on the constraints placed.

Chapter 4

A keV String Axion from High Scale Supersymmetry

The hierarchy problem has dominated much of the discussion on physics beyond the Standard Model (SM) in the past three decades, and supersymmetry emerged as the leading contender to solve this problem. In order to solve the problem fully, there was much anticipation that supersymmetry should be discovered very soon after the LHC began operating. Unfortunately, the LHC Run-I at 7–8 TeV placed a very strong lower limit, typically above a TeV, on superparticle masses [142], even though the quantitative limits are quite sensitive to the assumptions on the mass spectrum as well as the decay modes.

In addition, the discovered mass of the Higgs boson at 125 GeV [143] is higher than what was expected in the Minimal Supersymmetric Standard Model (MSSM). If we rely on the radiative corrections [144] from superparticles to raise the mass of the Higgs boson, we need to place scalar top quarks above a TeV. Finally, there have been long standing issues with supersymmetry, such as the absence of effects from large flavor-changing neutral currents, cosmological problems with the gravitino, and string moduli, which all prefer a supersymmetry spectrum with scalars around $m_{\text{SUSY}} \approx 100\text{--}1000$ TeV. If we take these hints seriously, direct searches for supersymmetry at collider experiments will be very difficult in the foreseeable future.

It is important to ask the question of whether there are alternative ways to find an experimental hint for supersymmetry. We argue in this chapter that the energy scale $m_{\text{SUSY}}^2/M_{\text{pl}} \approx \text{keV}$ may provide us with an indirect window to supersymmetry beyond the reach of accelerator experiments. Here M_{pl} is the reduced Planck scale, $M_{\text{pl}} \simeq 2.4 \times 10^{18}$ GeV.

The recent observation of an unidentified line at about 3.5 keV in the X-ray spectrum of galaxy clusters [24, 25] hints at new particles at the keV energy scale. Although it has since been disputed by several other (non-) observations [26], it is interesting to consider that it (or a line observed in the future) could be a signal of dark matter decaying into photons. Even if we attribute this particular line to astrophysical processes, looking for new lines in X-rays is a continuing prospect. The possibility of linking such a low energy signal to physics at very high scales is an intriguing new avenue that we will explore in this work, using the 3.5 keV line as our guiding example. However, the types of models we will consider are rather generic and are not tied only to this

specific experimental result.

Inspired by this observation, we investigate how supersymmetry may be relevant to the observed excess in X-rays from clusters of galaxies. Given the monochromatic line feature, it is tempting to consider a dark matter particle decaying into two photons. Note the Landau–Yang theorem that a vector cannot decay into two photons. Thus we consider a scalar particle decaying into two photons.¹ Then we need to understand the radiative stability of the keV energy scale, in addition to the origin of the keV scale itself.

The minute we assume that m_{SUSY} may be around 1000 TeV, there is a possible derived energy scale of $m_{\text{SUSY}}^2/M_{\text{pl}} \approx \text{keV}$. One immediate possibility that comes to mind is that m_{SUSY} may be the scale of supersymmetry breaking itself, such as in low-energy gauge mediation [146], and keV is the mass scale of the gravitino or moduli. This possibility was examined already in the literature. For example, the gravitino [147] or moduli [148–150] may be dark matter. The decay of the moduli in this context may produce an X-ray signal from the clusters of galaxies [151, 152]. However, there are several non-trivial problems in gauge mediation, such as the μ -problem, the overproduction of gravitinos, and producing the correct Higgs boson mass (there are consistent models evading such difficulties, though, as in [146]).

We point out in this chapter that there is an alternative possibility. $m_{\text{SUSY}} \approx 100\text{--}1000$ TeV may be the gravitino mass. This possibility has attracted quite a bit of interest in the literature recently, starting from anomaly mediation [153] and leading up to pure gravity mediation [154] or minimal split supersymmetry [155]. In this case the scale of supersymmetry breaking is $\Lambda_{\text{SUSY}} \approx (m_{\text{SUSY}}M_{\text{pl}})^{1/2} \approx 10^{12}$ GeV. The keV scale emerges parametrically as $\Lambda_{\text{SUSY}}^4/M_{\text{pl}}^3$.

If the new particle is a scalar, the keV mass scale must be protected against radiative corrections. The most effective mechanism is if the particle is a pseudo-Nambu–Goldstone-boson (pNGB). We call it generically an *axion* even though it may not have anything to do with the solution to the strong CP problem of QCD. The possibility that a pNGB may explain the origin of the 3.5 keV photon line has been also been considered elsewhere [156]. In this chapter, we point out how such a pNGB can have a natural origin in the context of high scale supersymmetry.

The scalar decay proceeds through a dimension-five operator suppressed by scale M with a rate $\Gamma \approx m^3/8\pi M^2$. For a 7 keV particle, the observed decay rate² is well-described by the energy scale $M \approx 0.1M_{\text{pl}}$. If interpreted as the axion decay constant $M = 32\pi^2 f$, $f \approx 10^{15}$ GeV. Therefore, discussing only two important scales, Λ_{SUSY} and M_{pl} , seems well-warranted.

Given the large scale M and the coupling to electromagnetism, a well motivated possibility is to consider the scalar to be a modulus or axion field from string theory, where such properties can occur naturally, e.g. [157]. We will consider the “universal” or model-independent string axion, the defining properties of which we take to be the high scale decay constant and a universal coupling to all $F\tilde{F}$. Thus the string axion couples to the hidden sector responsible for dynamical SUSY breaking and it may have a mass $m \sim \Lambda_{\text{SUSY}}^2/f$. However, *this is not the case if the hidden sector contains an anomalous, global $U(1)$ symmetry that is spontaneously broken*. In this case,

¹However, there may be an alternative possibility that a fermion, such as a sterile neutrino, decays into a light active neutrino and a photon, through a suppressed mixing between the sterile and active neutrinos (see e.g. the review [145]).

²Of course, by changing slightly the scale M the rate can be below current experimental bounds.

a second axion emerges which mixes with the string axion and leaves a massless eigenstate. Note that a spontaneously broken, anomalous $U(1)$ is a common feature of dynamical SUSY breaking models; the necessity of lifting flat directions in order to break supersymmetry typically induces non-zero vacuum expectation values, thus breaking global symmetries.

In the above scenario, where the SUSY breaking sector contains both a string axion and a hidden sector axion, instead of an exactly massless axion *we actually expect a non-zero, suppressed mass for the axion*. Gravity is believed to not respect global symmetries (see, e.g., [158]) and these violations may show up in a low-energy effective theory as higher dimension operators that explicitly break a global symmetry. Such explicit violations of the hidden sector $U(1)$ give a small, non-zero mass to the light axion. An axion with a keV scale mass and $f \approx 10^{15}$ GeV together with a high supersymmetry breaking scale suggest an explicit $U(1)$ violating mass-squared operator suppressed by $1/M_{\text{pl}}^2 f$ leading to an axion mass $m \approx \Lambda^4/M_{\text{pl}}^2 f$.

The rest of this chapter explores an explicit example of the general scenario outlined above. We consider a string axion coupled to the IYIT model of dynamical supersymmetry breaking [159]. When the scale of supersymmetry breaking is large, $\Lambda_{\text{SUSY}} \approx 10^{11-12}$ GeV, this model contains an axion that can produce the 3.5 keV X-ray line seen in [24, 25]. As discussed above, we believe the phenomena seen in our explicit example to be common. For example, we note that it occurs in other models of dynamical SUSY breaking such as the 4-1 model [160].

Following the demonstration of the 7 keV axion dark matter candidate, we address potential cosmological issues that arise in our explicit example. Some of these issues, such as isocurvature fluctuations, are common to setups based on our general mechanism. However, we believe the mechanisms employed to overcome certain cosmological issues in our explicit example can be applied in more general scenarios.

We also include two supplementary sections in Appendix E. In the first, we give in detail the calculation of the axion spectrum for our explicit example. While the techniques there can be found throughout the literature, we include the derivation to keep our results self-contained. The second section of Appendix E presents a new mechanism for dilaton stabilization. As a result of this mechanism the axion develops an F -term; interestingly, this effects the gaugino masses at the $\mathcal{O}(1)$ level compared to their values from anomaly mediation.

4.1 An explicit model

As an explicit realization of our setup, we consider the minimal IYIT model [159]. The model consists of four quark superfields Q^i , $i = 1, \dots, 4$, charged under a $Sp(1) \simeq SU(2)$ gauge symmetry together with gauge singlets Z_{ij} in the $\mathbf{6}$ of the $SU(4)$ flavor symmetry. Supersymmetric $SU(2)$ gauge dynamics lead to a quantum modified moduli space with $\text{Pf}(QQ) = \Lambda^4$, where Λ is the dynamical scale of the theory. The gauge singlets couple to the quarks via a tree-level superpotential $W = \lambda Z_{ij} Q^i Q^j$. Supersymmetry is broken by the F -term for Z , which cannot be simultaneously satisfied with the quantum constraint.

The model contains a non-anomalous R-symmetry and an anomalous $U(1)_h$ symmetry under which Q and Z have charges $(0, 1)$ and $(2, -2)$, respectively. The $U(1)_h$ symmetry, which has a

non-anomalous \mathbb{Z}_4 subgroup, is spontaneously broken by the quantum constraint. Therefore the phase of Q is the hidden sector axion a_h with decay constant $f_h \sim \Lambda$.

In addition to the fields Q and Z , we consider a string axion coupled to the gauge dynamics with strength $1/(32\pi^2 f_s)$. The $SU(2)$ dynamical scale then contains the string axion a_s ,

$$\Lambda = \mu e^{-\frac{8\pi^2}{b_0 g^2}} e^{\frac{ia_s}{b_0 f_s}} = |\Lambda| e^{\frac{ia_s}{b_0 f_s}}, \quad (4.1)$$

where g is the gauge coupling and b_0 is the coefficient of the one-loop beta function. For $Sp(N_c)$ gauge theories $b_0 = 2(N_c + 1)$, so for the scenario at hand $b_0 = 4$. Presently, we consider the dilaton and fermion partners of the string axion to be stabilized and therefore non-dynamical. Otherwise, we would replace ia_s by the chiral multiplet A_s in Eq. (4.1). In Appendix E.2 we present a possible mechanism of stabilization.

The superpotential (with all indices suppressed) is

$$W = \lambda Z Q Q + \frac{\mathcal{A}}{\Lambda^2} (\text{Pf}(Q Q) - \Lambda^4), \quad (4.2)$$

where the quantum constraint is enforced by the Lagrange multiplier \mathcal{A} . In Appendix E.1 we work out the effective theory and axion spectrum in detail while keeping track of factors of 4π using naïve dimensional analysis (NDA) [161, 162]. However, it is simple to see the basic results. Schematically, taking $Q Q \sim \Lambda^2 e^{2ia_h/f_h}$ and replacing $\Lambda^4 \rightarrow \Lambda^4 e^{ia_s/f_s}$ in the quantum constraint, it is easy to see that the F -term for \mathcal{A} produces a potential for the axions a_h and a_s ,

$$V(a_h, a_s) \sim \Lambda^4 \left[1 - \cos \left(\frac{4a_h}{f_h} - \frac{a_s}{f_s} \right) \right]. \quad (4.3)$$

The above potential makes it clear that one linear combination of axions gains a mass of order Λ^2/f_h (for $f_s \gg f_h$) while the orthogonal combination is massless.³

As discussed previously, we generically expect quantum gravity to violate the $U(1)_h$ symmetry. Such explicit violations give the massless axion from above a small, non-zero mass. To this end, we consider the leading operator that violates the $U(1)_h$ symmetry while respecting the R -symmetry and the non-anomalous discrete $\mathbb{Z}_4 \subset U(1)_h$. With this criteria, the leading operator is a deformation of the superpotential of the form⁴

$$W \supset \lambda' \frac{1}{M_{\text{pl}}^4} Z (Q Q)^3. \quad (4.4)$$

We note that since the vacuum is located at $\langle Z \rangle = 0$ [163] (see also Appendix E.1), the above is the leading order term to the superpotential containing Z .

³Once a constant is added to the superpotential to cancel the cosmological constant, the field Z has a small expectation value $\langle Z \rangle \sim m_{3/2}$. Therefore, the massless axion is, in fact, a linear combination of a_h, a_s , and the R axion (the phase of Z).

⁴A Kähler operator of the form $Z^* Z (Q Q)^2 / M_{\text{pl}}^4$ also respects the same symmetries and leads to the same order mass term as the operator in Eq. (4.4).

There are lower dimension operators that explicitly violate $U(1)_h$, e.g. $\delta W = c \text{Pf}(QQ)/M_{\text{pl}}$, and therefore lead to different parametrics for the axion mass. These operators violate the R -symmetry and it is conceivable that this leads to their suppression, e.g. $c \sim m_{3/2}/M_{\text{pl}} \sim \Lambda^2/M_{\text{pl}}^2$ which gives a parametrically similar axion mass as the operator in Eq. (4.4). Thus we will consider only the operator of Eq. (4.4) in the following analysis.

The explicit violation of the $U(1)_h$ symmetry in Eq. (4.4) gives a mass to the light axion through the F -term for Z and is worked out in detail in Appendix E.1. To leading order, the mass of the light axion is

$$m_a^2 \approx \frac{2\lambda\lambda'}{(4\pi)^4} \frac{\Lambda^8}{M_{\text{pl}}^4 f_s^2} = 2 \frac{\lambda\lambda'}{(\lambda/4\pi)^4} \frac{F^4}{M_{\text{pl}}^4 f_s^2}. \quad (4.5)$$

where $F = \lambda\Lambda^2/(4\pi)^2$ is the scale of SUSY breaking [161] (see also Appendix E.1, Eq. (E.12)). As emphasized previously in a more general context, here we explicitly see that the spectrum contains an axion with a suppressed mass $m_a \approx \Lambda^4/M_{\text{pl}}^2 f_s$.

Through its string axion component, the light axion couples directly to Standard Model photon operator $F\tilde{F}$ with strength $1/f_s$. We can express the dynamical scale Λ in terms of the decay rate,

$$\Gamma = \frac{\alpha_{\text{EM}}^2 m_a^3}{64\pi^3 f_s^2}, \quad (4.6)$$

as

$$\Lambda = \left(\frac{2\pi\alpha_{\text{EM}}^2 m_a^5 M_{\text{pl}}^4}{\lambda\lambda' \Gamma} \right)^{1/8}. \quad (4.7)$$

Experimental results [24, 25] determine $m_a \approx 7$ keV and $\Gamma \approx 5.7 \times 10^{-53}$ GeV. In the strongly-coupled vacuum the coupling λ becomes non-perturbative and $\mathcal{O}(4\pi)$. Taking $\lambda' \sim 1$, the supersymmetry breaking scale is

$$\sqrt{F} \sim 10^{11.5} \text{ GeV}, \quad (4.8)$$

with a gravitino mass

$$m_{3/2} = \frac{F}{M_{\text{pl}}} \sim \mathcal{O}(10)\text{-}\mathcal{O}(100) \text{ TeV}. \quad (4.9)$$

We see that we have constructed an explicit model for the string axion coupled to a hidden supersymmetry breaking sector where the scale of supersymmetry breaking must be high to match the experimental X-ray line.

We also know more about the spectrum of this model. The field Z has charge 2 under the \mathbb{Z}_4 symmetry; it cannot couple to $W^\alpha W_\alpha$ to give the gauginos mass. Thus we are lead to anomaly mediation (although see Appendix E.2 for modifications to the gaugino mass), which also fits nicely with the gravitino mass above and the known Higgs mass. We can easily incorporate this model in pure gravity mediation [154] or minimal split supersymmetry [155] models, to complete the extension of the SM.

4.2 Cosmology

Although the recent observation of B-modes in the CMB by the BICEP2 collaboration [164] has been shown to be consistent with expectations from dust [165, 166], it has nevertheless renewed interest in models with a high inflationary scale, $H_{\text{inf}} \sim 10^{14}$ GeV, at the upper end of the currently-allowed range [167]. Large values of H_{inf} present several cosmological challenges to any realistic model; for instance, isocurvature fluctuations of the nearly-massless axions must be suppressed. Furthermore, given a SUSY breaking scale of $\Lambda \sim 10^{11-12}$ GeV $< H_{\text{inf}}$, domain walls are a potential problem due to the spontaneous breaking of the \mathbb{Z}_4 symmetry after inflation.

It should be noted that the domain wall issue is a model-specific one, which may be avoided by altering the dynamical SUSY breaking sector. For example, the \mathbb{Z}_4 symmetry may be gauged, or a model without a residual discrete symmetry may be chosen. Of course, it may be that $H_{\text{inf}} < \Lambda$, although in this case isocurvature fluctuations may still pose a problem. For the purposes of this section, we will focus on the model presented in the previous section and present a consistent cosmological history that addresses the aforementioned issues in the presence of a high inflationary scale.

For $\Lambda \sim 10^{12}$ GeV, as required by the analysis in the previous section, the dynamical sector is weakly coupled during inflation. Thus domain walls would be formed after reheating, once the temperature fell below Λ . However, since Λ is a dynamical scale, we will show that it may be temporarily increased during inflation. Taking $H_{\text{inf}} \lesssim \Lambda \lesssim \rho_{\text{inf}}^{1/4}$ will ensure that the \mathbb{Z}_4 symmetry is broken during inflation without the IYIT vacuum energy dominating that of the inflaton.

Consider the gauge coupling of $SU(2)$ set by a gauge kinetic function $f = \{(1/g_0^2) + c(\phi^2/M_{\text{pl}}^2)\} W^\alpha W_\alpha$ with W^α the hidden sector gauge field strength, ϕ a singlet, and g_0 a coupling set by string theory and compactification. A superpotential of the form $\kappa Y(\phi^2 - M_{\text{pl}}^2)$, for a coupling κ and a superfield Y , gives the singlet a large vev. Generically, ϕ has a Hubble induced soft mass during inflation; if κ is sufficiently small, $\kappa \lesssim H_{\text{inf}}/M_{\text{pl}}$, then $\langle \phi \rangle \sim 0$ and the effective coupling $1/g^2 \approx 1/g_0^2$ is strong. The dynamical scale, Λ , is easily of order 10^{15} GeV during inflation. Domain walls are thus avoided as the \mathbb{Z}_4 symmetry is broken during inflation by the IYIT meson condensate, so long as the reheating temperature is sufficiently low, $T_R \lesssim \Lambda$.

Even with $\Lambda \sim 10^{15}$ GeV, the light axion is still essentially massless compared to H_{inf} , leading to a potential isocurvature problem. This may be avoided by further increasing the light axion mass during inflation, so that $m_a \sim H_{\text{inf}}$.⁵ This may be accomplished by including a $U(1)_h$ -violating coupling of the IYIT quarks to the inflaton sector, giving an inflaton-field-dependent mass to the light axion. For concreteness, we assume a chaotic inflation scenario as described in [168]. Here the Kähler potential respects a shift symmetry on the inflaton chiral multiplet, H , which is broken by a mass term in the super potential, $W \supset mHX$. We couple the IYIT quarks to the X chiral multiplet in the Kähler potential, $K \supset X^\dagger X \text{Pf}(QQ)/M^4 + \text{h.c.}$ Once the dynamical

⁵Note that the heavy axion mass, $m_{a'} \sim \Lambda$, is already heavy relative to H_{inf} due to the impact of the ϕ singlet on the dynamical scale.

SUSY breaking sector becomes strongly coupled, this gives a mass term for a_h :

$$V \supset m^2 h^\dagger h \left[1 - \frac{\Lambda^4}{M^4} \cos \left(\frac{4a_h}{f_h} \right) \right]. \quad (4.10)$$

Here, h , the psuedo-scalar component of H , is the inflaton. Taking $m^2 \langle h^\dagger h \rangle \sim H_{\text{inf}}^2 M_{\text{pl}}^2$ and $f_h \sim \Lambda$, we have $m_a \sim 4H_{\text{inf}} (\Lambda M_P / M^2)$. Thus, there will be no isocurvature problem for $M \lesssim 10^{17}$ GeV.

Having given the light axion a large mass during inflation, it remains to show that the appropriate misalignment can still be generated. If the coupling, c , of the singlet to the gauge kinetic term is complex, then the imaginary part may be removed by a shift in the string axion, $a_s \rightarrow a_s + \text{Im}(c) \langle \phi \rangle / M_{\text{pl}}$. When $\langle \phi \rangle = 0$, the axions will find their minimum at the origin. After inflation, however, we have $\langle \phi \rangle \sim M_{\text{pl}}$, and the heavy axion will relax to its new minimum at $(4a_h/f_h - a_s/f_s) \sim \text{Im}(c)$. The effective potential for the light axion is then approximately

$$V \sim \frac{2\lambda\lambda'}{(4\pi)^4} \frac{\Lambda^8}{M_{\text{pl}}^4} \cos \left(2 \text{Im}(c) + \frac{2a_s}{f_s} \right). \quad (4.11)$$

Since both axions were pinned to the origin during inflation, this generates a misalignment of $a \sim \text{Im}(c) f_s$. In order that this misalignment is sufficient to reproduce the observed abundance of dark matter, we must have $\text{Im}(c) \sim 10^{-4}$.

Since ϕ was trapped at the origin during inflation, one may worry that coherent oscillations of ϕ about its new minimum would come to dominate the energy density of the Universe. Subsequent ϕ decays could lead to overproduction of winos. However, if the Hubble induced mass remains significant as ϕ relaxes, then ϕ will adiabatically roll to its minimum and such oscillations do not occur. It is straightforward to check that, at the time the inflaton decays, ϕ is displaced from its minimum at M_{pl} by an amount $\Delta\phi \sim H^2 / (\kappa^2 M_{\text{pl}})$, where the Hubble constant H is evaluated at the inflaton decay time. For a reheating temperature $T_R \sim 10^9$ GeV and $\kappa \sim 10^{-5}$, $\Delta\phi \sim 10^{-7}$ GeV. This very small misalignment does not produce any appreciable amount of ϕ oscillations.

One may further worry that domain walls are formed from the spontaneous breaking of the \mathbb{Z}_2 symmetry on ϕ by $\langle \phi \rangle \neq 0$. These domain walls are an artifact of our choice of the function of ϕ in front of the gauge kinetic term and in the superpotential. Other functions of ϕ will do just as well. In particular, we can add an explicit \mathbb{Z}_2 breaking term $\epsilon\phi$ into the superpotential to collapse the domain walls without changing our main results.

The dilaton superpartner to the string axion may similarly become misaligned after inflation, depending on the exact form of its Kähler potential. A mechanism such as that proposed in [169] allows for the dilaton to adiabatically roll to its minimum, and therefore its misalignment is not dangerous.

4.3 Discussion

The 3.5 keV X-ray line observed in [24, 25] allows the exciting possibility that it may originate from dark matter. Tests of this dark matter hypothesis are predominately limited to indirect detection. Since the initial observation, followup studies [26] have called into doubt this X-ray line. As

there are now several conflicting observations and the possible implications are far reaching, it behooves us to continue to observe with future X-ray experiments. As briefly studied in [24], future X-ray observations of galaxy clusters by the Astro-H Observatory can distinguish the dark matter hypothesis from other astrophysical sources that may be masquerading as a dark matter signal. We also note that a promising place to look for a clean signal is from dwarf spheroidal galaxies. These smaller galaxies can be dominated by non-baryonic matter and yield a signal with smaller backgrounds. Even if this 3.5 keV line is a red herring, the types of models we have presented give an exciting link from a future X-ray signal to physics at very high scales. This motivates further dedicated time to observe these dwarf galaxies and galaxy clusters.

We briefly comment on other phenomenological consequences. For example, the wino is stable and will generically be a sub-dominant component of the dark matter in the Universe. It is in principle possible to indirectly detect the wino dark matter utilizing gamma ray observations of dwarf spheroidal galaxies or the galactic center [170]. However, it may be very challenging since the wino indirect cross-section scales as the density squared. As for the direct detection of the wino at the LHC, see [171].

Embedding our mechanism into pure gravity mediation gives generic predictions about the gluino mass. For example, for $m_{3/2} \approx 50\text{-}100$ TeV then the gluino mass is in a detectable range at the LHC. For a slightly larger gravitino mass, $m_{3/2} \approx 200$ TeV, we would expect $m_{\tilde{g}} \approx 4\text{-}5$ TeV, and the gluino would be hard to detect at the LHC. However, if the $\mathcal{O}(1)$ mass cancellation from the dilaton stabilization mechanism in Appendix E.2 takes place, then the gluino mass can be $m_{\tilde{g}} \approx 2\text{-}3$ TeV even for $m_{3/2} \approx 200$ TeV, and is therefore detectable.

Motivated by recent experimental results in the X-ray spectrum of galaxy clusters and the current situation in particle physics beyond the SM, we have explored the possibility of linking a keV signal to supersymmetry breaking at a much higher scale, around $10^{11\text{-}12}$ GeV. This exciting experimental link between such different energy scales is possible through a light axion, a mixture of a string theory and a hidden (supersymmetry-breaking) sector axion, which gains only a small mass from the supersymmetry breaking sector.

As an example demonstrating this possibility, we constructed a model with dynamical supersymmetry breaking from the IYIT model coupled to a string axion. One sees explicitly that there is a linear combination of axions which does not gain a large mass, but only a small mass once the superpotential includes higher dimensional operators. This mass is directly related to the scale of the hidden sector, and thus supersymmetry breaking. Using the X-ray results as input, we find the scale of supersymmetry breaking to be $\mathcal{O}(10^{11.5})$ GeV. This scale fits nicely with models like pure gravity mediation or minimal split supersymmetry.

Rather than producing a light axion to explain an X-ray signal, one can instead construct similar models for the QCD axion. In this case one needs to suppress operators to even higher dimension to produce a lighter axion. Instead of using an $Sp(1)$ gauge group, a larger group such as $Sp(5)$ should be used. Then we have a model for high-scale supersymmetry breaking with a light QCD axion solving the strong CP problem.

Given the lack of experimental evidence for supersymmetry thus far, together with theoretical arguments for considering models which may be difficult to see at colliders in the immediate future, it can be fruitful to pursue new avenues for signals of supersymmetry. In this chapter we

have shown a model which is well-motivated theoretically and experimentally, and suggests a hint for supersymmetry in the keV sky.

Appendix A

Supplemental details for the CDE

This appendix shows some details in using the CDE method. First, in appendix [A.1](#), we present some details of the derivation of CDE for fermions and gauge bosons. Appendix [A.2](#) then list out quite a bit useful identities that one frequently encounters while using CDE. Finally, appendix [A.3](#) shows intermediate steps in deriving the universal formula of the CDE.

A.1 CDE for fermions and gauge bosons

Fermions

We now consider the functional determinant for massive fermion fields and provide the formulas for the covariant derivative expansion for them. We work in the notation of Dirac fermions, denoting the gamma matrices by γ^μ and employing slashed notation, *e.g.* $\not{D} = \gamma^\mu D_\mu$. This discussion is easily modified if one wants to consider Weyl fermions and use two-component notation.

Consider the Lagrangian containing the fermions to be

$$\mathcal{L}[\psi, \phi] = \bar{\psi}(i\not{D} - m - M(x))\psi, \quad (\text{A.1})$$

where m is the fermion mass and $M(x)$ is in general dependent on the light fields $\phi(x)$. Upon integrating over the Grassman valued fields in the path integral, the one-loop contribution to the effective action is given by

$$S_{\text{eff},1\text{-loop}} \equiv \Delta S_{\text{eff}} = -i\text{Tr} \log (\not{P} - m - M), \quad (\text{A.2})$$

where, as before, $P_\mu \equiv iD_\mu$. Using $\text{Tr} \log AB = \text{Tr} \log A + \text{Tr} \log B$ and the fact that the trace is invariant under changing signs of gamma matrices we have

$$\begin{aligned} \Delta S_{\text{eff}} &= -\frac{i}{2} \left[\text{Tr} \log (-\not{P} - m - M) + \text{Tr} \log (\not{P} - m - M) \right] \\ &= -\frac{i}{2} \text{Tr} \log \left(-\not{P}^2 + m^2 + 2mM + M^2 + \not{P}M \right). \end{aligned} \quad (\text{A.3})$$

where $\not{P}M \equiv [\not{P}, M]$, as defined in Eq. (2.23). With $\gamma^\mu\gamma^\nu = (\{\gamma^\mu, \gamma^\nu\} + [\gamma^\mu, \gamma^\nu])/2 = g^{\mu\nu} - i\sigma^{\mu\nu}$,

$$\not{P}^2 = P^2 + \frac{i}{2}\sigma^{\mu\nu}[D_\mu, D_\nu] = P^2 + \frac{i}{2}\sigma \cdot G', \quad (\text{A.4})$$

where $G'_{\mu\nu} \equiv [D_\mu, D_\nu]$, as defined in Eq. (2.23).

We thus see that the trace for fermions,

$$\text{Tr} \log \left(-P^2 + m^2 - \frac{i}{2}\sigma^{\mu\nu}G'_{\mu\nu} + 2mM + M^2 + \not{P}M \right), \quad (\text{A.5})$$

is of the form $\text{Tr} \log(-P^2 + m^2 + U)$. Therefore, all the steps in evaluating the trace and shifting by the covariant derivative using $e^{\pm P \cdot \partial / \partial q}$ are the same as previously considered and we can immediately write down the answer from Eq. (2.18). Defining

$$U_{\text{ferm}} \equiv -\frac{i}{2}\sigma^{\mu\nu}G'_{\mu\nu} + 2mM + M^2 + \not{P}M, \quad (\text{A.6})$$

the one-loop effective Lagrangian for fermions is then given by

$$\Delta\mathcal{L}_{\text{eff,ferm}} = -\frac{i}{2} \int dq \text{tr} \log \left[- \left(q_\mu + \tilde{G}_{\nu\mu}\partial_\nu \right)^2 + \tilde{U}_{\text{ferm}} \right], \quad (\text{A.7})$$

where \tilde{G} and \tilde{U}_{ferm} are defined as in Eq. (2.24) with $U \rightarrow U_{\text{ferm}}$.

We note that the result originally obtained in [15] contains an error (see Eq. (4.21) therein compared to our result Eq. (A.7)). This mistake originates from an error in Eq. (4.17) of [15] where a term proportional to $[\tilde{G}_{\mu\nu}\partial_\nu, \tilde{G}_{\rho\sigma}\partial_\sigma] \neq 0$ was missing.

Massless gauge bosons

Here we consider the one-loop contribution to the 1PI effective action from massless gauge fields. The spirit here is slightly different from our previous discussions involving massive scalars and fermions; we are not integrating the gauge bosons out of the theory but instead are evaluating the 1PI effective action. Nevertheless, the manipulations are exactly the same since the one-loop contribution to the 1PI effective action is still a functional trace of the form $\text{Tr} \log(D^2 + U)$.

In evaluating the 1PI effective action, we split the gauge boson into a background piece plus fluctuations around this background, $A_\mu = A_{B,\mu} + Q_\mu$, and perform the path integral over the fluctuations Q_μ while holding the background $A_{B,\mu}$ fixed. In order to do the path integral, one must gauge fix the Q_μ fields. At first glance, one might think that gauge fixing destroys the possibility of keeping gauge invariance manifest while evaluating the one-loop effective action. However, this turns out not to be the case. It is well known that there is a convenient gauge fixing condition that leaves the gauge symmetry of the background $A_{B,\mu}$ field manifest, *i.e.* it only gauge fixes Q_μ and not $A_{B,\mu}$. This technique is known as the background field method (for example, see [172] and references therein).¹ Because the gauge symmetry of the background $A_{B,\mu}$ field is not fixed,

¹All techniques of evaluating effective actions are, by the definition of holding fields fixed while doing a path integral, background field methods. Nevertheless, the term ‘‘background field method’’ is usually taken to refer to employing this special gauge fixing condition while evaluating the 1PI effective action.

we will still be able to employ the techniques of the covariant derivative expansion, allowing a manifestly gauge invariant computation of the one-loop effective action.

The issues around gauge symmetry are actually quite distinct for the background field method versus the CDE. However, because similar words are used in both discussions, it is worth clarifying what aspects of gauge symmetry are handled in each case. The background field method makes it manifestly clear that the effective action of $A_{B,\mu}$ possesses a gauge symmetry by only gauge fixing the fluctuating field Q_μ . This is an all orders statement. However, when evaluating the effective action order-by-order, one still works with the non-covariant quantities $A_{B,\mu}$, Q_μ , and $\partial/\partial x^\mu$ at intermediate steps.² The covariant derivative expansion, on the other hand, is a technique for evaluating the *one-loop* effective action that keeps gauge invariance manifest at all stages of the computation by working with gauge covariant quantities such as D_μ . To understand this point more explicitly, one can compare the method of the CDE presented in this paper and in [35] with the evaluation of the functional determinant using the component fields as presented in detail in Peskin and Schroeder [173].

Now onto the calculation, we take pure $SU(N)$ gauge theory,

$$\mathcal{L}[A_\mu] = -\frac{1}{2Ng^2} \text{tr} F_{\mu\nu}^2 = -\frac{1}{4g^2} (F_{\mu\nu}^a)^2, \quad (\text{A.8})$$

where $F_{\mu\nu} = F_{\mu\nu}^a t^a$ and we take the t^a in the adjoint representation, $\text{tr} t^a t^b = N\delta^{ab}$, $(t^b)_{ac} = if^{abc}$. We denote the covariant derivative as $\mathcal{D}_\mu = \partial_\mu - iA_\mu$ with the field strength defined as usual, $F_{\mu\nu} = i[\mathcal{D}_\mu, \mathcal{D}_\nu]$. Note that we have normalized the gauge field such that the coupling constant does not appear in the covariant derivative.

Let $\Gamma[A_B]$ be the 1PI effective action. To find $\Gamma[A_B]$, we split the gauge field into a background piece and a fluctuating piece, $A_\mu = A_{B,\mu} + Q_\mu$, and integrate out the Q_μ fields.³ The one-loop contribution to Γ comes from the quadratic terms in Q_μ . We have

$$\mathcal{D}_\mu = \partial_\mu - i(A_{B,\mu} + Q_\mu) \equiv D_\mu - iQ_\mu, \quad (\text{A.9a})$$

$$F_{\mu\nu} = i[D_\mu, D_\nu] + D_\mu Q_\nu - D_\nu Q_\mu - i[Q_\mu, Q_\nu] \equiv G_{\mu\nu} + Q_{\mu\nu} - i[Q_\mu, Q_\nu], \quad (\text{A.9b})$$

$$\mathcal{L} = -\frac{1}{2Ng^2} \text{Tr}(G_{\mu\nu} + Q_{\mu\nu} - i[Q_\mu, Q_\nu])^2. \quad (\text{A.9c})$$

Note that $D_\mu = \partial_\mu - iA_{B,\mu}$ and $G_{\mu\nu} = i[D_\mu, D_\nu]$ are the covariant derivative and field strength of the background field alone.

In order to get sensible results out of the path integral, we need to gauge fix. As in the background field method, we employ a gauge fixing condition which is covariant with respect to the background field $A_{B,\mu}$. Namely, the gauge-fixing condition G^a is taken to be $G^a = D^\mu Q_\mu^a$. The re-

²To one-loop order, one only deals with $A_{B,\mu}$ and ∂_μ .

³To keep our discussion short, we are being slightly loose here. In particular, a source term J for the fluctuating fields needs to be introduced. After integrating out the fluctuating field, we obtain an effective action which is a functional of J and the background fields, $W[J, A_B]$. The 1PI effective action, $\Gamma[A_B]$, is obtained by a Legendre transform of W . For more details see, for example, [172].

sultant gauge-fixed Lagrangian—including ghosts to implement the Fadeev-Popov determinant—is, *e.g.* [172, 173],

$$\mathcal{L}_{g.f.} + \mathcal{L}_{gh} = -\frac{1}{2g^2\xi} (D^\mu Q_\mu^a)^2 + D^\mu \bar{c}^a (D_\mu c^a + f^{abc} Q_\mu^b c^c), \quad (\text{A.10})$$

where ξ is the gauge-fixing parameter. The utility of this gauge fixing condition is that the fluctuating Q_μ^a is gauge fixed while the Lagrangian (A.9c) together with $\mathcal{L}_{g.f.} + \mathcal{L}_{gh}$ possesses a manifest gauge symmetry with gauge field $A_{B,\mu}$ that is not gauge fixed. Thus we can perform the path integral over Q_μ^a while leaving the gauge invariance of the effective action of $A_{B,\mu}$ manifest. Under a background gauge symmetry transformation, $A_{B,\mu}$ transforms as a gauge field, $A_{B,\mu} \rightarrow V(A_{B,\mu} + i\partial_\mu)V^\dagger$ while Q_μ (and the ghosts c and \bar{c}) transforms simply as a field in the adjoint representation, $Q_\mu \rightarrow VQ_\mu V^\dagger$. Procedurally, when performing the path integral over Q and c , one can simply think about these fields as regular scalar and fermion⁴ fields in the adjoint of some gauge symmetry and with interactions dictated by the Lagrangians in (A.9c) and (A.10).

The quadratic piece of the combined Yang-Mills, gauge-fixing, and ghost Lagrangian is

$$\mathcal{L} = -\frac{1}{2g^2} Q_\mu^a \left[-g^{\mu\nu} (D^2)^{ac} - \frac{1-\xi}{\xi} (D^\mu D^\nu)^{ac} - 2f^{abc} G^{b\mu\nu} \right] Q_\nu^c + \bar{c}^a [- (D^2)^{ac}] c^c. \quad (\text{A.11})$$

We will work in Feynman gauge with $\xi = 1$ so that we can drop the $D^\mu D^\nu$ term. Note that everything inside the square brackets in the above is in the adjoint representation (recall, $f^{abc} = -i(t^b)_{ac}$). Using the generator for Lorentz transformations on four-vectors, $(\mathcal{J}_{\rho\sigma})^{\mu\nu} = i(\delta_\rho^\mu \delta_\sigma^\nu - \delta_\rho^\nu \delta_\sigma^\mu)$, we can write

$$G^{\mu\nu} = -\frac{i}{2} (G^{\rho\sigma} \mathcal{J}_{\rho\sigma})^{\mu\nu}.$$

The quadratic piece of the Lagrangian is then given by

$$\mathcal{L} = -\frac{1}{2g^2} Q_\mu^a \left[-D^2 \mathbf{1}_4 + G \cdot \mathcal{J} \right]_\nu^{\mu,ac} Q_\nu^c + \bar{c}^a [-D^2]^{ac} c^c, \quad (\text{A.12})$$

where $\mathbf{1}_4$ is the 4×4 identity matrix for the Lorentz indices, *i.e.* $(\mathbf{1}_4)^\mu_\nu = \delta^\mu_\nu$. Performing the path-integral over the gauge and ghost fields we obtain

$$\Gamma_{1\text{-loop}}[A_B] = \frac{i}{2} \text{Tr} \log (D^2 \mathbf{1}_4 - G \cdot \mathcal{J}) - i \text{Tr} \log (D^2), \quad (\text{A.13})$$

where the factor of $1/2$ in the first term is because the Q_μ^a are real bosons, while the factor of -1 in the second term is because the c^a are anti-commuting. Note that the functional traces makes totally transparent the role of the ghosts. The trace of the gauge boson term containing D^2 picks up a factor of 4 from the trace over Lorentz indices, one for each Q_μ $\mu = 0, 1, 2, 3$. Of course, the gauge boson only has two physical degrees of freedom; we see explicitly above that the ghost piece cancels the contribution of two of the degrees of freedom.

⁴Of course ghosts aren't fermions; they are anti-commuting scalars. We are speaking very loosely and by fermion we are referring to their anti-commuting properties.

Each of the traces in the above are of the form $\text{Tr}(-P^2 + U)$, and thus we can immediately apply the transformations leading to the covariant derivative expansion. Switching to our notation $G'_{\mu\nu} = [D_\mu, D_\nu] = -iG'_{\mu\nu}$ and defining

$$U_{\text{gauge}} = -i\mathcal{J}^{\mu\nu}G'_{\mu\nu}, \quad (\text{A.14})$$

we have

$$\begin{aligned} \Gamma_{1\text{-loop}}[A_B] = & \frac{i}{2} \int dx dq \text{tr} \log \left[- \left(q_\mu + \tilde{G}_{\nu\mu} \partial_\nu \right)^2 + \tilde{U}_{\text{gauge}} \right] \\ & - i \int dx dq \text{tr} \log \left[- \left(q_\mu + \tilde{G}_{\nu\mu} \partial_\nu \right)^2 \right], \end{aligned} \quad (\text{A.15})$$

where \tilde{G} and \tilde{U}_{gauge} are defined as in Eq. (2.24) with $U \rightarrow U_{\text{ferm}}$. The first term in the above is from the fluctuating gauge fields, while the second is from the ghosts. Note also that the trace “tr” in the first term includes over the Lorentz indices, just as the trace for fermions in Eq. (A.7) is over the Lorentz (spinor) indices. In fact, it should be clear that U_{gauge} is very similar to the first term in U_{ferm} (Eq. (A.6)): $U_{\text{ferm}} \supset -i(\sigma^{\mu\nu}/2)G'_{\mu\nu}$ where $\sigma^{\mu\nu}/2$ is the generator for Lorentz transformations on spinors.

Note that the effective action (A.15) contains infrared divergences from the massless gauge and ghost fields that we integrated out. These divergences can be regulated by adding a mass term for Q_μ^a and c^a because these mass terms respect the gauge invariance of the background field $A_{B,\mu}$.⁵

Massive gauge bosons

With our understanding of the story for massless gauge bosons, it turns out to be simple to obtain the result for massive gauge bosons. We consider massive vector bosons Q_μ transforming under an unbroken, low-energy gauge group. As is well known, beyond tree-level perturbation theory, the Nambu-Goldstone bosons (NGBs) χ^i “eaten” by the massive vector boson must be included, *i.e.* we cannot work in unitary gauge. By working in a generalized R_ξ gauge, we will be able to maintain manifest covariance of the low-energy gauge group. As we will see, mathematically, the results are essentially the same as the massless case in Eqs. (A.12) and (A.13), modified by the presence of mass terms for the Q_μ and ghosts as well as an additional term for the NGBs.

First, as we mentioned in the main text, the gauge-kinetic piece of the Lagrangian up to quadratic term in Q_μ^i is

$$\mathcal{L}_{\text{g.k.}} \supset \frac{1}{2} Q_\mu^i \left(D^2 g^{\mu\nu} - D^\nu D^\mu + [D^\mu, D^\nu] \right)^{ij} Q_\nu^j, \quad (\text{A.16})$$

where D_μ denotes the covariant derivative that contains only the unbroken gauge fields. *A priori*, one may think that the coefficient of the magnetic dipole term, $Q_\mu^i [D^\mu, D^\nu]^{ij} Q_\nu^j$, could be a free

⁵As stated previously, procedurally one can just think of Q_μ and c as scalars and fermions transforming in the adjoint of some gauge symmetry whose gauge field is $A_{B,\mu}$. Just as scalars and fermions can have mass terms without disturbing gauge-invariance, Q_μ and c can have mass terms without disturbing the background gauge-invariance.

parameter. However, tree-level unitarity forces it be universally unity in the above equation, regardless of the details of symmetry breaking [36, 37]. In appendix B, we provide a new, algebraic derivation of this universality and also explain it via the physical argument of tree-level unitarity.

Second, because we are integrating out the heavy gauge bosons Q_μ^i perturbatively, we need to fix the part of gauge transformation corresponding to Q_μ^i . But we would also like to preserve the unbroken gauge symmetry. To achieve this, we can adopt a generalized R_ξ gauge fixing term as following

$$\mathcal{L}_{\text{g.f.}} = -\frac{1}{2\xi} (\xi m_Q \chi^i + D^\mu Q_\mu^i)^2, \quad (\text{A.17})$$

where $\partial^\mu Q_\mu^i$ from the usual R_ξ gauge fixing is promoted to $D^\mu Q_\mu^i$ to preserve the unbroken gauge symmetry.

Now combining Eq. (A.16) and (A.17) with the appropriate ghost term

$$\mathcal{L}_{\text{ghost}} = \bar{c}^i (-D^2 - \xi m_Q^2)^{ij} c^j, \quad (\text{A.18})$$

the mass term of Q_μ^i due to the symmetry breaking,

$$\mathcal{L}_{\text{mass}} \supset \frac{1}{2} (D_\mu \chi^i - m_Q Q_\mu^i)^2, \quad (\text{A.19})$$

and a generic interaction term quadratic in Q_μ^i ,

$$\mathcal{L}_1 = \frac{1}{2} Q_\mu^i (M^{\mu\nu})^{ij} Q_\nu^j, \quad (\text{A.20})$$

we find the full Lagrangian up to quadratic power in Q_μ^i to be

$$\begin{aligned} \Delta\mathcal{L} &= \frac{1}{2} Q_\mu^i \left(D^2 g^{\mu\nu} - D^\nu D^\mu + m_Q^2 g^{\mu\nu} + [D^\mu, D^\nu] + \frac{1}{\xi} D^\mu D^\nu + M^{\mu\nu} \right)^{ij} Q_\nu^j \\ &\quad + \frac{1}{2} \chi^i (-D^2 - \xi m_Q^2)^{ij} \chi^j + \bar{c}^i (-D^2 - \xi m_Q^2)^{ij} c^j. \end{aligned} \quad (\text{A.21})$$

Taking Feynman gauge $\xi = 1$, we get

$$\begin{aligned} \Delta\mathcal{L} &= \frac{1}{2} Q_\mu^i (D^2 g^{\mu\nu} + m_Q^2 g^{\mu\nu} + 2[D^\mu, D^\nu] + M^{\mu\nu})^{ij} Q_\nu^j \\ &\quad + \frac{1}{2} \chi^i (-D^2 - m_Q^2)^{ij} \chi^j + \bar{c}^i (-D^2 - m_Q^2)^{ij} c^j. \end{aligned} \quad (\text{A.22})$$

This is what we presented in the main text, Eq. (2.35).

A.2 Useful identities

Expansion of $\tilde{G}_{\nu\mu}$

$$\begin{aligned}
\tilde{G}_{\nu\mu} &= \sum_{n=0}^{\infty} \frac{(n+1)}{(n+2)!} (P_{\alpha_1} \dots P_{\alpha_n} G'_{\nu\mu}) \partial_{\alpha_1 \alpha_2 \dots \alpha_n}^n \\
&= \frac{1}{2} G'_{\nu\mu} + \frac{1}{3} (P_{\alpha} G'_{\nu\mu}) \partial_{\alpha} + \frac{1}{8} (P_{\alpha_1} P_{\alpha_2}, G_{\nu\mu}) \partial_{\alpha_1 \alpha_2}^2 + \dots \quad (\text{A.23})
\end{aligned}$$

Commutators/anti-commutators⁶

$$\{q_{\mu}, \partial_{\alpha}\} = 2q_{\mu} \partial_{\alpha} + \delta_{\mu\alpha}, \quad (\text{A.24})$$

$$\{q_{\mu}, \partial_{\alpha_1 \alpha_2}^2\} = 2q_{\mu} \partial_{\alpha_1 \alpha_2}^2 + \delta_{\mu\alpha_1} \partial_{\alpha_2} + \delta_{\mu\alpha_2} \partial_{\alpha_1}, \quad (\text{A.25})$$

$$\{q_{\mu}, \partial_{\alpha_1 \alpha_2 \alpha_3}^3\} = 2q_{\mu} \partial_{\alpha_1 \alpha_2 \alpha_3}^3 + \delta_{\mu\alpha_1} \partial_{\alpha_2 \alpha_3}^2 + \delta_{\mu\alpha_2} \partial_{\alpha_1 \alpha_3}^2 + \delta_{\mu\alpha_3} \partial_{\alpha_1 \alpha_2}^2, \quad (\text{A.26})$$

$$\{q_{\mu}, \partial_{\alpha_1 \dots \alpha_n}^n\} = 2q_{\mu} \partial_{\alpha_1 \dots \alpha_n}^n + \sum_{i=1}^n \delta_{\mu\alpha_i} \prod_{j \neq i} \partial_{\alpha_j}. \quad (\text{A.27})$$

And hence we have

$$\begin{aligned}
\{q_{\mu}, \tilde{G}_{\nu\mu}\} &= G'_{\nu\mu} q_{\mu} + \frac{1}{3} (P_{\alpha} G'_{\nu\mu}) (2q_{\mu} \partial_{\alpha} + \delta_{\mu\alpha}) \\
&\quad + \frac{1}{8} (P_{\alpha_1} P_{\alpha_2} G'_{\nu\mu}) (2q_{\mu} \partial_{\alpha_1 \alpha_2}^2 + \delta_{\mu\alpha_1} \partial_{\alpha_2} + \delta_{\mu\alpha_2} \partial_{\alpha_1}) + \dots \quad (\text{A.28})
\end{aligned}$$

Derivatives and integrals

$$\partial_{\alpha_1} \Delta = (-1) \cdot 2 \cdot q_{\alpha_1} \Delta^2, \quad (\text{A.29})$$

$$\partial_{\alpha_1 \alpha_2}^2 \Delta = (-1) \cdot 2 \cdot \delta_{\alpha_1 \alpha_2} \Delta^2 + (-1)^2 \cdot 2! \cdot 2^2 \cdot q_{\alpha_1} q_{\alpha_2} \Delta^3, \quad (\text{A.30})$$

$$\partial_{\alpha_1 \alpha_2 \alpha_3}^3 \Delta = (-1)^2 \cdot 2! \cdot 2^2 \left(\underbrace{\delta_{\alpha_1 \alpha_2} q_{\alpha_3} + \text{perm}}_{3 \text{ terms}} \right) \Delta^3 + (-1)^3 \cdot 3! \cdot 2^3 \cdot q_{\alpha_1} q_{\alpha_2} q_{\alpha_3} \Delta^4 \quad (\text{A.31})$$

$$\begin{aligned}
\partial_{\alpha_1 \alpha_2 \alpha_3 \alpha_4}^4 \Delta &= (-1)^2 \cdot 2! \cdot 2^2 \left(\underbrace{\delta_{\alpha_1 \alpha_2} \delta_{\alpha_3 \alpha_4} + \text{perm}}_{3 \text{ terms}} \right) \Delta^3 \\
&\quad + (-1)^3 \cdot 3! \cdot 2^3 \left(\underbrace{\delta_{\alpha_1 \alpha_2} q_{\alpha_3} q_{\alpha_4} + \text{perm}}_{6 \text{ terms}} \right) \Delta^4 \\
&\quad + (-1)^4 \cdot 4! \cdot 2^4 \cdot q_{\alpha_1} q_{\alpha_2} q_{\alpha_3} q_{\alpha_4} \Delta^5. \quad (\text{A.32})
\end{aligned}$$

These derivatives, which are part of the integrand, take simplified forms under q -integration:

⁶Note that we are not distinguishing upper and lower indices, so in the following, $\delta_{\mu\nu}$ here should be understood as $g_{\mu\nu}$.

$$\begin{aligned}
\partial_{\alpha_1\alpha_2}^2 \Delta &\rightarrow 2\delta_{\alpha_1\alpha_2}(-\Delta^2 + q^2\Delta^3), \\
q_{\alpha_4} \partial_{\alpha_1\alpha_2\alpha_3}^3 \Delta &\rightarrow 2(\delta_{\alpha_1\alpha_2}\delta_{\alpha_3\alpha_4} + \delta_{\alpha_1\alpha_3}\delta_{\alpha_2\alpha_4} + \delta_{\alpha_1\alpha_4}\delta_{\alpha_2\alpha_3}) [q^2\Delta^3 - (q^2)^2\Delta^4], \\
\partial_{\alpha_1\alpha_2\alpha_3\alpha_4}^4 \Delta &\rightarrow 4(\delta_{\alpha_1\alpha_2}\delta_{\alpha_3\alpha_4} + \delta_{\alpha_1\alpha_3}\delta_{\alpha_2\alpha_4} + \delta_{\alpha_1\alpha_4}\delta_{\alpha_2\alpha_3}) [2\Delta^3 - 6q^2\Delta^4 + 4(q^2)^2\Delta^5], \\
q_{\alpha_5} q_{\alpha_6} \partial_{\alpha_1\alpha_2\alpha_3\alpha_4}^4 \Delta &\rightarrow 2\delta_{\alpha_5\alpha_6}(\delta_{\alpha_1\alpha_2}\delta_{\alpha_3\alpha_4} + \delta_{\alpha_1\alpha_3}\delta_{\alpha_2\alpha_4} + \delta_{\alpha_1\alpha_4}\delta_{\alpha_2\alpha_3}) [q^2\Delta^3 - (q^2)^2\Delta^4] \\
&\quad + 2(\underbrace{\delta_{\alpha_1\alpha_2}\delta_{\alpha_3\alpha_4}\delta_{\alpha_5\alpha_6} + \text{perm}}_{15 \text{ terms}}) [-(q^2)^2\Delta^4 + (q^2)^3\Delta^5].
\end{aligned}$$

The following are useful integrals. They are in Minkowski space, and the powers of the free propagator— n in Δ^n —is assumed large enough to make the integral converge:

$$\begin{aligned}
I_0^{(n)} &\equiv \int \frac{d^4q}{(2\pi)^4} \Delta^n = i \frac{(-1)^n}{(4\pi)^2} \frac{1}{(n-1)(n-2)} \frac{1}{(m^2)^{n-2}}, \\
I_2^{(n)} &\equiv \int \frac{d^4q}{(2\pi)^4} q^2 \Delta^n = -i \frac{(-1)^n}{(4\pi)^2} \frac{2}{(n-1)(n-2)(n-3)} \frac{1}{(m^2)^{n-3}}, \\
I_4^{(n)} &\equiv \int \frac{d^4q}{(2\pi)^4} (q^2)^2 \Delta^n = i \frac{(-1)^n}{(4\pi)^2} \frac{6}{(n-1)(n-2)(n-3)(n-4)} \frac{1}{(m^2)^{n-4}}, \\
I_6^{(n)} &\equiv \int \frac{d^4q}{(2\pi)^4} (q^2)^3 \Delta^n = -i \frac{(-1)^n}{(4\pi)^2} \frac{24}{(n-1)(n-2)(n-3)(n-4)(n-5)} \frac{1}{(m^2)^{n-3}}.
\end{aligned}$$

Operator identities and trace computations

Let us state some basics of covariant derivative calculus. Most of these are obvious, but we list them here because we make use of them over and over in calculations.

- The covariant derivative acting on a matrix is given by the commutator, $D_\mu A = [D_\mu, A]$.
- The basic rules of calculus are the same. In particular, the chain rule holds: $D(AB) = (DA)B + A(DB)$. This implies integration by parts holds, $\int dx \text{tr}[A(DB)] = \int dx \text{tr}[-(DA)B]$.
- The covariant derivative acting on a gauge invariant quantity is just the partial derivative, $D_\mu |H|^2 = \partial_\mu |H|^2$.

$$2 |H^\dagger D_\mu H|^2 = \frac{1}{2} (\partial_\mu |H|^2)^2 - \frac{1}{2} (H^\dagger \overleftrightarrow{D}^\mu H)^2 \Leftrightarrow 2\mathcal{O}_{HD} = \mathcal{O}_H - \mathcal{O}_T. \quad (\text{A.33})$$

A term that often shows up in calculations is

$$(H^\dagger D_\mu H)^2 + ((D_\mu H)^\dagger H)^2 = \mathcal{O}_T + \mathcal{O}_H. \quad (\text{A.34})$$

$$\text{Tr}[D_\mu(HH^\dagger)]^2 = (H^\dagger DH)^2 + ((DH)^\dagger H)^2 + 2 |H|^2 |DH|^2 = \mathcal{O}_T + \mathcal{O}_H + 2\mathcal{O}_r. \quad (\text{A.35})$$

A.3 Evaluating terms in the CDE: results for the \mathcal{I}_n

$$\frac{1}{A^{-1}(1-AB)} = \sum_{n=0}^{\infty} (AB)^n A,$$

$$\mathcal{I}_n \equiv \int dq dm^2 \text{tr} \left[\Delta \left(-\{q\tilde{G}\} - \tilde{G}^2 + \tilde{U} \right) \right]^n \Delta,$$

$$\Delta \mathcal{L}_{\mathcal{I}_n} = -i c_s \mathcal{I}_n.$$

Breaking \mathcal{I}_n into easier to work with pieces, we define integrals involving only \tilde{G} as J_n and integrals involving only \tilde{U} as K_n ,

$$J_n \equiv \int dq dm^2 \text{tr} \left[\Delta \left(-\{q\tilde{G}\} - \tilde{G}^2 \right) \right]^n \Delta,$$

$$K_n \equiv \int dq dm^2 \text{tr} \left[\Delta \tilde{U} \right]^n \Delta.$$

We define L_n for integrals involving mixed \tilde{G} and \tilde{U} terms as L_n ; for example, L_2 is given by

$$L_2 \equiv \int dq dm^2 \text{tr} \left[-\Delta \left(\{q\tilde{G}\} + \tilde{G}^2 \right) \Delta \tilde{U} \Delta - \Delta \tilde{U} \Delta \left(\{q\tilde{G}\} + \tilde{G}^2 \right) \Delta \right].$$

$$\begin{aligned} \Delta \mathcal{L}_{J_1+J_2} = & -\frac{1}{(4\pi)^2} \left[\frac{1}{6} \left(\log \frac{m^2}{\mu^2} - 1 \right) \cdot \left(\frac{1}{2} \text{tr} G'_{\mu\nu} G'_{\mu\nu} \right) + \frac{1}{m^2} \cdot \frac{1}{60} \cdot \text{tr} (P_\mu G'_{\mu\nu})^2 \right. \\ & \left. + \frac{1}{m^2} \cdot \frac{1}{90} \cdot \text{tr} (G'_{\mu\nu} G'_{\nu\sigma} G'_{\sigma\mu}) \right]. \end{aligned}$$

$$\Delta \mathcal{L}_{K_1} = \frac{1}{(4\pi)^2} m^2 \left[-\log \frac{m^2}{\mu^2} + 1 \right] \cdot \text{tr} U,$$

$$\begin{aligned} \Delta \mathcal{L}_{K_2} = & \frac{1}{(4\pi)^2} \left[-\frac{1}{2} \log \frac{m^2}{\mu^2} \cdot \text{tr} U^2 - \frac{1}{m^2} \cdot \frac{1}{12} \cdot \text{tr} ([P_\mu, U]^2) \right. \\ & \left. + \frac{1}{m^4} \cdot \frac{1}{120} \cdot \text{tr} \left([P_\mu [P_\mu, U]] [P_\nu [P_\nu, U]] \right) \right], \end{aligned}$$

$$\Delta \mathcal{L}_{K_3} = \frac{1}{(4\pi)^2} \left[-\frac{1}{m^2} \cdot \frac{1}{6} \cdot \text{tr} (U^3) + \frac{1}{m^4} \cdot \frac{1}{12} \cdot \text{tr} \left(U [P_\mu, U] [P_\mu, U] \right) \right],$$

$$\Delta\mathcal{L}_{K_4} = \frac{1}{(4\pi)^2} \cdot \left[\frac{1}{m^4} \cdot \frac{1}{24} \cdot \text{tr}(U^4) - \frac{1}{m^6} \cdot \frac{1}{20} \cdot \text{tr}(U^2[P_\mu, U][P_\mu, U]) \right. \\ \left. - \frac{1}{m^6} \cdot \frac{1}{30} \cdot \text{tr}(U[P_\mu, U]U[P_\mu, U]) \right],$$

$$\Delta\mathcal{L}_{K_5} = -\frac{1}{(4\pi)^2} \cdot \frac{1}{m^6} \cdot \frac{1}{60} \cdot \text{tr}(U^5),$$

$$\Delta\mathcal{L}_{K_6} = \frac{1}{(4\pi)^2} \cdot \frac{1}{m^8} \cdot \frac{1}{120} \cdot \text{tr}(U^6).$$

$$\Delta\mathcal{L}_{L_2} = -\frac{1}{(4\pi)^2} \cdot \frac{1}{m^2} \cdot \frac{1}{12} \cdot \text{tr}(UG'_{\mu\nu}G'_{\mu\nu}),$$

$$\Delta\mathcal{L}_{L_3} = \frac{1}{(4\pi)^2} \cdot \frac{1}{m^4} \cdot \left[\frac{1}{24} \cdot (U^2G'_{\mu\nu}G'_{\mu\nu}) - \frac{1}{120} \cdot \text{tr}([P_\mu, U], [P_\nu, U])G'_{\mu\nu} \right) \\ - \frac{1}{120} \cdot \text{tr}([U[U, G'_{\mu\nu}])G'_{\mu\nu}) \left. \right].$$

Appendix B

Universality of Magnetic Dipole Term

Assuming that there is a weakly coupled renormalizable UV model,^{1,2,3} we consider a general picture that the full gauge symmetry group G of the UV model is spontaneously broken into a subgroup H . A set of gauge bosons Q_μ^i have “eaten” the Nambu-Goldstone bosons χ^i and obtained mass m_Q . For this setup, it turns out that Q_μ^i form a certain representation of the unbroken gauge group H , and under this representation, the general form of the gauge-kinetic piece of the Lagrangian up to quadratic term in Q_μ^i is given by Eq. (2.34), which we reproduce here for convenience

$$\mathcal{L}_{\text{g.k.}} \supset \frac{1}{2} Q_\mu^i (D^2 g^{\mu\nu} - D^\nu D^\mu + [D^\mu, D^\nu])^{ij} Q_\nu^j, \quad (\text{B.1})$$

with D_μ denoting the covariant derivative that contains only the massless gauge bosons. One remarkable feature of this general gauge-kinetic term is that the coefficient of the “magnetic dipole term” $\frac{1}{2} Q_\mu^i \{[D^\mu, D^\nu]\}^{ij} Q_\nu^j$ is universal, namely that its coefficient is fixed to 1 relative to the “curl” terms $\frac{1}{2} Q_\mu^i \{D^2 g^{\mu\nu} - D^\nu D^\mu\}^{ij} Q_\nu^j$, regardless of the details of the symmetry breaking. We use the word “curl” since the term comes from the quadratic piece in $(D_\mu Q_\nu - D_\nu Q_\mu)^2$.

The universal coefficient of the magnetic dipole term is known to be a consequence of tree-level unitarity [36, 37]. In this appendix, we present an additional, new way of proving Eq. (B.1) that is completely algebraic. We note that these algebraic methods developed may be useful for other purposes since they allow a very compact way of writing the gauge kinetic terms for multiple

¹In general, this need not be the case. For example, the Q_μ could be composite particles in the low-energy effective description of some strongly interacting theory. Another example is when additional massive vector bosons are needed to UV complete the theory. For example, an effective theory with a massive vector transforming as a doublet under a $SU(2)$ gauge symmetry is non-renormalizable—a valid UV completion could be an $SU(3)$ gauge symmetry broken to $SU(2)$, but this requires an additional doublet and singlet vector.

²As in all the other cases considered in this work, although never explicitly stated, we are also assuming the fields we integrate out are weakly coupled amongst themselves and the low-energy fields, so that it makes sense to integrate them out.

³ G itself may be contained in some larger group \mathcal{G} which also contains exact and approximate global symmetries and the same mechanism responsible for breaking $G \rightarrow H$ may also break some of these global symmetries. These generalities do not affect our results below, which concern the transformation of Q_μ and its associated NGBs under H . We therefore stick to our simplified picture for clarity.

gauge groups with different coupling constants, see Eq. (B.10). We also give the physical argument based on tree-level unitarity for the validity of Eq. (B.1), similar to [36, 37].

B.1 Algebraic Proof

Let us first give an algebraic derivation of Eq. (B.1), which we believe is new. Let G have a general structure of product group

$$G = G_1 \times G_2 \times \cdots \times G_n. \quad (\text{B.2})$$

Let T^A be the set of generators of G , with $A = 1, 2, \dots, \dim(G)$. Due to Eq. (B.2), the set of generators T^A are composed by a number of subsets

$$\{T^A\} = \{T_1^{A_1}\} \cup \{T_2^{A_2}\} \cup \cdots \cup \{T_n^{A_n}\}, \quad (\text{B.3})$$

with $A_i = 1, 2, \dots, \dim(G_i)$. Let f_G^{ABC} denote the structure constant of G :

$$[T^A, T^B] = if_G^{ABC} T^C. \quad (\text{B.4})$$

Obviously $f_G^{ABC} = 0$ if any two indices belong to different subsets in Eq. (B.3).

The full covariant derivative \bar{D} of the UV model and its commutator is

$$\bar{D}_\mu = \partial_\mu - ig^A G_\mu^A T^A, \quad (\text{B.5})$$

$$[\bar{D}_\mu, \bar{D}_\nu] = -ig^A G_{\mu\nu}^A T^A, \quad (\text{B.6})$$

where G_μ^A denote the gauge fields, $G_{\mu\nu}^A$ the field strengths, and g^A the gauge couplings that could be arbitrarily different for T^A of different subsets in Eq. (B.3). Here we emphasize that the above expression of the full covariant derivative holds for any representation of G .

Because we have put the arbitrary gauge couplings into the covariant derivative, the gauge boson kinetic term of the UV Lagrangian is simply

$$\mathcal{L}_{\text{g.k.}} = -\frac{1}{4}(G_{\mu\nu}^{A_1})^2 - \frac{1}{4}(G_{\mu\nu}^{A_2})^2 - \cdots - \frac{1}{4}(G_{\mu\nu}^{A_n})^2. \quad (\text{B.7})$$

In order to write this kinetic term in terms of the full covariant derivative \bar{D}_μ , let us define an inner product in the generator space $\{T^A\}$:

$$\langle T^A, T^B \rangle \equiv \frac{1}{2(g^A)^2} \delta^{AB}, \quad (\text{B.8})$$

which just looks like a scaled version of trace. However, we emphasize that, although it should be quite clear from definition, this inner product is essentially very different from the trace. The inner product can only be taken over two vectors in the generator space, while a trace action can be taken over arbitrary powers of generators. Nevertheless, the inner product defined in Eq. (B.8)

has many similar properties as the trace action. For example, if one of the two vectors is given in a form of a commutator of two other generators, a cyclic permutation is allowed

$$\begin{aligned}
 \langle T^A, [T^B, T^C] \rangle &= \langle T^A, i f_G^{BCD} T^D \rangle = i f_G^{BCD} \frac{1}{2(g^A)^2} \delta^{AD} \\
 &= i f_G^{ABC} \frac{1}{2(g^A)^2} = i f_G^{ABC} \frac{1}{2(g^C)^2} \\
 &= i f_G^{CAB} \frac{1}{2(g^C)^2} = \langle T^C, [T^A, T^B] \rangle.
 \end{aligned} \tag{B.9}$$

Note that the second line above is true because for the case $g^A \neq g^C$, $f^{ABC} = 0$. As we shall see shortly, this cyclic permutation property will play a very important role in our derivation. With the inner product defined in Eq. (B.8), the gauge boson kinetic term Eq. (B.7) can be very conveniently written as

$$\mathcal{L}_{\text{g.k.}} = \frac{1}{2} \langle [\bar{D}_\mu, \bar{D}_\nu], [\bar{D}^\mu, \bar{D}^\nu] \rangle. \tag{B.10}$$

Now let us consider the subgroup H of G . Let t^a be the generators of H , which span a subspace of the full group generator space, and have closed algebra

$$[t^a, t^b] = i f_H^{abc} t^c, \tag{B.11}$$

with f_H^{abc} denotes the structure constant of H , and $a = 1, 2, \dots, \dim(H)$. Once the full group G is spontaneously broken into H , it is obviously convenient to divide the full generator space into the unbroken generators t^a and the broken generators X^i , $i = 1, 2, \dots, \dim(G) - \dim(H)$, with the corresponding massless gauge fields A_μ^a and massive gauge bosons Q_μ^i

$$(t^A) = \begin{pmatrix} g_H^a t^a \\ X^i \end{pmatrix}, \quad (W_\mu^A) = \begin{pmatrix} A_\mu^a \\ Q_\mu^i \end{pmatrix}. \tag{B.12}$$

In the above, we write t^A instead of T^A , and W_μ^A instead of G_μ^A , because t^a is generically a linear combination of T^A , and there is a linear transformation between t^A and T^A , as well as between W_μ^A and G_μ^A in accordance. This linear transformation is typically chosen to be orthogonal between gauge field⁴, in order to preserve the universal coefficients structure in Eq. (B.7). Then we have

$$W_\mu^A = O^{AB} G_\mu^B, \quad \text{with } O^T O = 1. \tag{B.13}$$

The full covariant derivative Eq. (B.5) can be rewritten as

$$\bar{D}_\mu = \partial_\mu - i W_\mu^A t^A = \partial_\mu - i g_H^a A_\mu^a t^a - i Q_\mu^i X^i = D_\mu - i Q_\mu^i X^i, \tag{B.14}$$

$$t^A = O^{AB} g^B T^B, \tag{B.15}$$

where the second line serves as the definition of t^A in terms of T^A . Note that a factor g_H^a is needed in Eq. (B.12) to make Eqs. (B.4), (B.11) and (B.15) consistent. This is how one determines the

⁴Other linear transformations will lead to equivalent theories upon field redefinition.

gauge coupling constant g_H^a of the unbroken gauge group. We have also used D_μ to denote the covariant derivative that contains only the massless gauge bosons A_μ^a . The above definition of t^A preserves the orthogonality of them under the inner product defined in Eq. (B.8)

$$\langle t^A, t^B \rangle = \langle O^{AC} g^C T^C, O^{BD} g^D T^D \rangle = \frac{1}{2(g^C)^2} O^{AC} O^{BD} g^C g^D \delta^{CD} = \frac{1}{2} \delta^{AB}, \quad (\text{B.16})$$

which specifically means that

$$\langle t^a, t^b \rangle = \frac{1}{2(g_H^a)^2} \delta^{ab}, \quad \langle X^i, X^j \rangle = \frac{1}{2} \delta^{ij}, \quad \langle t^a, X^i \rangle = 0. \quad (\text{B.17})$$

Let us first prove that Q_μ^i defined through Eq. (B.12) and Eq. (B.13) form a representation under the unbroken gauge group H . This is essentially to prove that the commutator between t^a and X^i is only a linear combination of X^i

$$[t^a, X^i] = -(t_Q^a)^{ij} X^j, \quad (\text{B.18})$$

with a certain set of matrices $(t_Q^a)^{ij}$ that also need to be antisymmetric between i, j . Both points can be easily proven by making use of our inner product defined in Eq. (B.8) and its cyclic permutation property Eq. (B.9). Eq. (B.18) is obvious from

$$\langle t^b, [t^a, X^i] \rangle = \langle X^i, [t^b, t^a] \rangle = 0, \quad (\text{B.19})$$

and the antisymmetry is clear from

$$(t_Q^a)^{ij} = -2 \langle X^j, [t^a, X^i] \rangle = -2 \langle t^a, [X^i, X^j] \rangle. \quad (\text{B.20})$$

Once Eq. (B.18) is proven, it follows that

$$[t^a, Q_\mu^i X^i] = -Q_\mu^i (t_Q^a)^{ij} X^j = (t_Q^a)^{ij} Q_\mu^j X^i, \quad (\text{B.21})$$

where we see that t_Q^a serves as the generator matrix or ‘‘charge’’ of Q_μ^i . And therefore

$$\begin{aligned} [D_\mu, Q_\nu^i X^i] &= (\partial_\mu Q_\nu^i) X^i - i g_H^a A_\mu^a [t^a, Q_\nu^i X^i] = (\partial_\mu Q_\nu^i) X^i - i g_H^a A_\mu^a (t_Q^a)^{ij} Q_\nu^j X^i \\ &= \left[(\partial_\mu Q_\nu^i) - i g_H^a A_\mu^a (t_Q^a)^{ij} Q_\nu^j \right] X^i = (D_\mu Q_\nu^i) X^i. \end{aligned} \quad (\text{B.22})$$

With all the above preparations, we are eventually ready to decompose the full gauge boson kinetic term in Eq. (B.7). First, the commutator of the full covariant derivative is

$$\begin{aligned} [\bar{D}_\mu, \bar{D}_\nu] &= [D_\mu - i Q_\mu^i X^i, D_\nu - i Q_\nu^j X^j] \\ &= [D_\mu, D_\nu] - i \{ [\bar{D}_\mu, Q_\nu^i X^i] - [\bar{D}_\nu, Q_\mu^i X^i] \} - [Q_\mu^i X^i, Q_\nu^j X^j] \\ &= [D_\mu, D_\nu] - i [(D_\mu Q_\nu^i) - (D_\nu Q_\mu^i)] X^i - [Q_\mu^i X^i, Q_\nu^j X^j]. \end{aligned} \quad (\text{B.23})$$

Keeping only terms relevant and up to quadratic power for Q_μ^i , it follows from Eq. (B.10) that

$$\begin{aligned}
\mathcal{L}_{\text{g.k.}} &= \frac{1}{2} \langle [\bar{D}_\mu, \bar{D}_\nu], [\bar{D}^\mu, \bar{D}^\nu] \rangle \\
&\supset -\frac{1}{4} [(D_\mu Q_\nu^i) - (D_\nu Q_\mu^i)]^2 - \langle [D^\mu, D^\nu], [Q_\mu^i X^i, Q_\nu^j X^j] \rangle \\
&= \frac{1}{2} Q_\mu^i (D^2 g^{\mu\nu} - D^\nu D^\mu)^{ij} Q_\nu^j - \langle Q_\mu^i X^i, [Q_\nu^j X^j, [D^\mu, D^\nu]] \rangle \\
&= \frac{1}{2} Q_\mu^i (D^2 g^{\mu\nu} - D^\nu D^\mu)^{ij} Q_\nu^j + \langle Q_\mu^i X^i, [D^\mu, [D^\nu, Q_\nu^j X^j]] \rangle - \langle Q_\mu^i X^i, [D^\nu, [D^\mu, Q_\nu^j X^j]] \rangle \\
&= \frac{1}{2} Q_\mu^i (D^2 g^{\mu\nu} - D^\nu D^\mu)^{ij} Q_\nu^j + Q_\mu^i \langle X^i, (D^\mu D^\nu Q_\nu^j) X^j \rangle - Q_\mu^i \langle X^i, (D^\nu D^\mu Q_\nu^j) X^j \rangle \\
&= \frac{1}{2} Q_\mu^i (D^2 g^{\mu\nu} - D^\nu D^\mu)^{ij} Q_\nu^j + \frac{1}{2} Q_\mu^i (D^\mu D^\nu - D^\nu D^\mu)^{ij} Q_\nu^j \\
&= \frac{1}{2} Q_\mu^i \{ D^2 g^{\mu\nu} - D^\nu D^\mu + [D^\mu, D^\nu] \}^{ij} Q_\nu^j, \tag{B.24}
\end{aligned}$$

where from the second line to the third line, we have used the cyclic permutation property of the inner product, and the fourth line follows from the third line due to Jacobi identity. This finishes our algebraic derivation of Eq. (B.1).

We would like to stress that in spite of the allowance of arbitrary gauge couplings for each simple group G_i , the end gauge-interaction piece of the Lagrangian of the heavy vector boson Q_μ^i has the above universal form, especially that the coefficient of the magnetic dipole term $\frac{1}{2} Q_\mu^i [D^\mu, D^\nu]^{ij} Q_\nu^j$ is fixed at to unity relative to the curl terms $\frac{1}{2} Q_\mu^i \{ D^2 g^{\mu\nu} - D^\nu D^\mu \}^{ij} Q_\nu^j$.

B.2 Physical Proof

Now let us give a physical argument to explain this universality, which is from the tree-level unitarity. This argument is known [36, 37], but we provide it here for completeness. Let us consider one component of the massless background gauge boson and call it a ‘‘photon’’ A_μ with its coupling constant e and generator Q . It is helpful to use a complex linear combination of generators X^i to form X^α and $X^{\alpha\dagger}$ that are ‘‘eigenstates’’ of the generator Q , $[Q, X^\alpha] = q^\alpha X^\alpha$ and $[Q, X^{\alpha\dagger}] = -q^\alpha X^{\alpha\dagger}$. We also define Q_μ^α and $Q_\mu^{\alpha\dagger}$ to keep $Q_\mu^i X^i = Q_\mu^\alpha X^\alpha + Q_\mu^{\alpha\dagger} X^{\alpha\dagger}$. Note that Q_μ^i are real, but Q_μ^α are complex fields. The normalization of Q_μ^α is chosen such that $\frac{1}{2} Q_\mu^i Q^{\mu i} = Q_\mu^{\alpha\dagger} Q^{\mu\alpha}$. It should be clear that in this part of the appendix where we discuss integrating out a heavy gauge boson, indices α, β are used to denote the complex generators $X^\alpha, X^{\alpha\dagger}$, and their accordingly defined complex gauge fields $Q^\alpha, Q^{\alpha\dagger}$. Lorentz indices are denoted by μ, ν, ρ , etc.

First, one can check that the ‘‘curl’’ terms in Eq. (B.1) written in terms of Q_μ^i gives the correct

kinetic term for Q_μ^α coupled to photon according to its charge q^α , because from Eq. (B.22) we have

$$\begin{aligned}
(D_\mu Q_\nu^i) X^i &= [D_\mu, Q_\nu^i X^i] = [D_\mu, Q_\nu^\alpha X^\alpha + Q_\nu^{\alpha\dagger} X^{\alpha\dagger}] \\
&\supset (\partial_\mu Q_\nu^\alpha) X^\alpha + (\partial_\mu Q_\nu^{\alpha\dagger}) X^{\alpha\dagger} - ie A_\mu [Q, Q_\nu^\alpha X^\alpha + Q_\nu^{\alpha\dagger} X^{\alpha\dagger}] \\
&= (\partial_\mu Q_\nu^\alpha) X^\alpha + (\partial_\mu Q_\nu^{\alpha\dagger}) X^{\alpha\dagger} - ie q^\alpha A_\mu (Q_\nu^\alpha X^\alpha - Q_\nu^{\alpha\dagger} X^{\alpha\dagger}) \\
&= (\partial_\mu Q_\nu^\alpha - ie q^\alpha A_\mu Q_\nu^\alpha) X^\alpha + (\partial_\mu Q_\nu^{\alpha\dagger} + ie q^\alpha A_\mu Q_\nu^{\alpha\dagger}) X^{\alpha\dagger}, \tag{B.25}
\end{aligned}$$

and the ‘‘curl’’ form derives from the original Yang-Mills Lagrangian in the UV theory

$$\mathcal{L}_{\text{Yang-Mills}} \supset -\frac{1}{4} (D_\mu Q_\nu^i - D_\nu Q_\mu^i)^2 = \frac{1}{2} Q_\mu^i \{ D^2 g^{\mu\nu} - D^\nu D^\mu \}^{ij} Q_\nu^j. \tag{B.26}$$

What is the least obvious is the universal coefficient for the ‘‘magnetic dipole term’’

$$\frac{1}{2} Q_\mu^i [D^\mu, D^\nu]^{ij} Q_\nu^j = -\frac{1}{2\mu(R)} \text{tr} ([Q_\mu, Q_\nu] [D^\mu, D^\nu]), \tag{B.27}$$

where $Q_\mu \equiv Q_\mu^i X^i = Q_\mu^\alpha X^\alpha + Q_\mu^{\alpha\dagger} X^{\alpha\dagger}$, and $\text{tr}(X^i X^j) = \mu(R) \delta^{ij}$. This term is gauge invariant under the unbroken gauge symmetry and one may wonder whether the coefficient can be arbitrary and model dependent. Focusing on the ‘‘photon’’ coupling piece, this term contains

$$\begin{aligned}
-\frac{1}{2\mu(R)} \text{tr} ([Q_\mu, Q_\nu] [D^\mu, D^\nu]) &\supset \frac{ie \hat{A}^{\mu\nu}}{2\mu(R)} \text{tr} ([Q_\mu, Q_\nu] Q) \\
&= \frac{ie \hat{A}^{\mu\nu}}{2\mu(R)} \text{tr} ([Q, Q_\mu] Q_\nu) \\
&= \frac{ie \hat{A}^{\mu\nu}}{2\mu(R)} \text{tr} \{ (q^\alpha Q_\mu^\alpha X^\alpha - q^\alpha Q_\mu^{\alpha\dagger} X^{\alpha\dagger}) (Q_\nu^\beta X^\beta + Q_\nu^{\beta\dagger} X^{\beta\dagger}) \} \\
&= \frac{-ie \hat{A}^{\mu\nu}}{2} q^\alpha (Q_\mu^{\alpha\dagger} Q_\nu^\alpha - Q_\nu^{\alpha\dagger} Q_\mu^\alpha) \\
&= -ie \hat{A}^{\mu\nu} q^\alpha Q_\mu^{\alpha\dagger} Q_\nu^\alpha, \tag{B.28}
\end{aligned}$$

where $\hat{A}_{\mu\nu} \equiv \partial_\mu A_\nu - \partial_\nu A_\mu$, and we have used the property $\text{tr}(X^\alpha X^{\beta\dagger}) = \mu(R) \delta^{\alpha\beta}$, $\text{tr}(X^\alpha X^\beta) = \text{tr}(X^{\alpha\dagger} X^{\beta\dagger}) = 0$. So it is clear that the coefficient of this ‘‘magnetic dipole term’’ is exactly the ‘‘triple gauge coupling’’ between the heavy gauge boson Q_μ^α and the massless gauge bosons A_μ . One can make it more transparent by taking the SM analog of Eq. (B.28). In the case of SM electroweak symmetry breaking, one recognizes $q^\alpha = -1$, $Q_\nu^\alpha = W_\nu^-$, and $Q_\mu^{\alpha\dagger} = W_\mu^+$, then Eq. (B.28) is nothing but the κ_γ term in Eq. (2.97). It is well known that the amplitude for $\gamma\gamma \rightarrow W^+W^-$ would grow as E_W^2 in the Standard Model if the magnetic dipole moment $\kappa_\gamma \neq 1$. The quadratic part of the Lagrangian (*i.e.* Eq. (B.1)) is sufficient to determine the tree-level amplitude, and the diagrams are exactly the same as those in the Standard Model. Unless $\kappa_\gamma = 1$, it violates perturbative unitarity at high energies. Because the amplitude does not involve the Higgs or other heavy vector bosons, the amplitude is exactly the same as that in the UV theory, which is unitary. Therefore, the perturbative unitarity for this amplitude needs to be satisfied with the quadratic Lagrangian, which requires the dipole moment to have this value.

Appendix C

Supplemental Details for Mapping Wilson Coefficients on to Physical Observables

This appendix shows the calculational details of the mapping step described in Section 2.3. We first list out in Appendix C.1 all the relevant two-point and three-point Feynman rules from the set of dimension-six operators in Table 2.4. Transverse vacuum polarization functions, that can be readily read off from the two-point Feynman rules, are also tabulated. Then in Appendix C.2 and C.3 we present details in calculating the “interference correction” ϵ_I for Higgs decay widths and Higgs production cross sections, respectively. We list out relevant Feynman diagrams, definitions of auxiliary functions, and conventional form factors. Finally, in Appendix C.4 and C.5 we show our calculation steps of the residue modifications and the parameter modifications, which are related to the “residue correction” ϵ_R and the “parametric correction” ϵ_P , respectively.

C.1 Additional Feynman rules from dim-6 effective operators

C.1.1 Feynman rules for vacuum polarization functions

Throughout the calculations in this thesis, the relevant vacuum polarization functions are those of the vector bosons $i\Pi_{VV}^{\mu\nu}(p^2) \in \{i\Pi_{WW}^{\mu\nu}(p^2), i\Pi_{ZZ}^{\mu\nu}(p^2), i\Pi_{\gamma\gamma}^{\mu\nu}(p^2), i\Pi_{\gamma Z}^{\mu\nu}(p^2)\}$ and that of the Higgs boson $-i\Sigma(p^2)$. It is straightforward to expand out the dim-6 effective operators listed in Table 2.4, identify the relevant Lagrangian pieces, and obtain the Feynman rules. The relevant Lagrangian pieces are shown in Eq. (C.5)-Eq. (C.9). The resulting Feynman rules of the vacuum polarization functions are drawn in Fig. C.1, with the detailed values listed in Eq. (C.10)-Eq. (C.14). In the diagrams, we use a big solid dot to denote the interactions due to the dim-6 effective operators (*i.e.* due to Wilson coefficients c_i), while a simple direct connecting would represent the SM interaction.

For vector bosons, one can easily identify the transverse part of the vacuum polarization func-

$$\begin{aligned}
 \Pi_{WW}(p^2) &= p^4 \left(-\frac{1}{\Lambda^2} c_{2W} \right) + p^2 \frac{2m_W^2}{\Lambda^2} (4c_{WW} + c_W) + m_W^2 \frac{v^2}{\Lambda^2} c_R \\
 \Pi_{ZZ}(p^2) &= p^4 \left[-\frac{1}{\Lambda^2} (c_Z^2 c_{2W} + s_Z^2 c_{2B}) \right] + p^2 \frac{2m_Z^2}{\Lambda^2} \left[4(c_Z^4 c_{WW} + s_Z^4 c_{BB} + c_Z^2 s_Z^2 c_{WB}) \right. \\
 &\quad \left. + (c_Z^2 c_W + s_Z^2 c_B) \right] + m_Z^2 \frac{v^2}{\Lambda^2} (-2c_T + c_R) \\
 \Pi_{\gamma\gamma}(p^2) &= p^4 \left[-\frac{1}{\Lambda^2} (s_Z^2 c_{2W} + c_Z^2 c_{2B}) \right] + p^2 \frac{8m_Z^2}{\Lambda^2} c_Z^2 s_Z^2 (c_{WW} + c_{BB} - c_{WB}) \\
 \Pi_{\gamma Z}(p^2) &= p^4 \left[-\frac{1}{\Lambda^2} c_Z s_Z (c_{2W} - c_{2B}) \right] + p^2 \frac{m_Z^2}{\Lambda^2} c_Z s_Z \left[8(c_Z^2 c_{WW} - s_Z^2 c_{BB}) \right. \\
 &\quad \left. - 4(c_Z^2 - s_Z^2) c_{WB} + (c_W - c_B) \right] \\
 \Sigma(p^2) &= p^4 \left(-\frac{1}{\Lambda^2} c_D \right) + p^2 \left[-\frac{v^2}{\Lambda^2} (2c_H + c_R) \right]
 \end{aligned}$$

Table C.1: Transverse Vacuum polarization functions in terms of Wilson coefficients.

$$\begin{aligned}
 \Pi_{WW}(p^2) - \Pi_{33}(p^2) &= m_W^2 \frac{2v^2}{\Lambda^2} c_T \\
 \Pi_{33}(p^2) &= p^4 \left(-\frac{1}{\Lambda^2} c_{2W} \right) + p^2 \frac{2m_W^2}{\Lambda^2} (4c_{WW} + c_W) + m_W^2 \frac{v^2}{\Lambda^2} (-2c_T + c_R) \\
 \Pi_{BB}(p^2) &= p^4 \left(-\frac{1}{\Lambda^2} c_{2B} \right) + p^2 \frac{2m_Z^2 s_Z^2}{\Lambda^2} (4c_{BB} + c_B) + m_Z^2 s_Z^2 \frac{v^2}{\Lambda^2} (-2c_T + c_R) \\
 \Pi_{3B}(p^2) &= p^2 \left(-\frac{m_Z^2}{\Lambda^2} c_Z s_Z \right) (4c_{WB} + c_W + c_B) + m_Z^2 \frac{v^2}{\Lambda^2} c_Z s_Z (2c_T - c_R)
 \end{aligned}$$

Table C.2: Alternative set of transverse vacuum polarization functions that are used in our definitions of EWPO parameters Table 2.5.

tions $\Pi_{VV}(p^2)$ from

$$i\Pi_{VV}^{\mu\nu}(p^2) = i \left(g^{\mu\nu} - \frac{p^\mu p^\nu}{p^2} \right) \Pi_{VV}(p^2) + \left(i \frac{p^\mu p^\nu}{p^2} \text{ term} \right). \quad (\text{C.1})$$

These transverse vacuum polarization functions $\{\Pi_{WW}(p^2), \Pi_{ZZ}(p^2), \Pi_{\gamma\gamma}(p^2), \Pi_{\gamma Z}(p^2)\}$ together with $-i\Sigma(p^2)$ are summarized in Table C.1. In some occasions, such as defining the EWPO parameters, it is more concise to use the alternative set $\{\Pi_{33}, \Pi_{BB}, \Pi_{3B}\}$ instead of $\{\Pi_{ZZ}, \Pi_{\gamma\gamma}, \Pi_{\gamma Z}\}$. Due to the relation $W^3 = c_Z Z + s_Z A$ and $B = -s_Z Z + c_Z A$, there is a simple transformation between these two sets

$$\Pi_{33} = c_Z^2 \Pi_{ZZ} + s_Z^2 \Pi_{\gamma\gamma} + 2c_Z s_Z \Pi_{\gamma Z}, \quad (\text{C.2})$$

$$\Pi_{BB} = s_Z^2 \Pi_{ZZ} + c_Z^2 \Pi_{\gamma\gamma} - 2c_Z s_Z \Pi_{\gamma Z}, \quad (\text{C.3})$$

$$\Pi_{3B} = -c_Z s_Z \Pi_{ZZ} + c_Z s_Z \Pi_{\gamma\gamma} + (c_Z^2 - s_Z^2) \Pi_{\gamma Z}, \quad (\text{C.4})$$

where we have adopted the notation $c_Z \equiv \cos \theta_Z$ etc., with θ_Z denoting the weak mixing angle. This alternative set of vector boson transverse vacuum polarization functions are summarized in Table C.2.

$$\begin{aligned}
 \mathcal{L}_{WW} &= W_\mu^+ (\partial^4 g^{\mu\nu} - \partial^2 \partial^\mu \partial^\nu) W_\nu^- \cdot \left(-\frac{1}{\Lambda^2} c_{2W} \right) \\
 &+ W_\mu^+ (-\partial^2 g^{\mu\nu} + \partial^\mu \partial^\nu) W_\nu^- \cdot \frac{2m_W^2}{\Lambda^2} (4c_{WW} + c_W) \\
 &+ m_W^2 W_\mu^+ W^{-\mu} \cdot \frac{v^2}{\Lambda^2} c_R - W^{-\mu} (\partial_\mu \partial_\nu) W^{+\nu} \cdot \frac{m_W^2}{\Lambda^2} c_D,
 \end{aligned} \tag{C.5}$$

$$\begin{aligned}
 \mathcal{L}_{ZZ} &= \frac{1}{2} Z_\mu (\partial^4 g^{\mu\nu} - \partial^2 \partial^\mu \partial^\nu) Z_\nu \cdot \left[-\frac{1}{\Lambda^2} (c_Z^2 c_{2W} + s_Z^2 c_{2B}) \right] \\
 &+ \frac{1}{2} Z_\mu (-\partial^2 g^{\mu\nu} + \partial^\mu \partial^\nu) Z_\nu \cdot \frac{2m_Z^2}{\Lambda^2} \left[4(c_Z^4 c_{WW} + s_Z^4 c_{BB} + c_Z^2 s_Z^2 c_{WB}) \right. \\
 &\quad \left. + (c_Z^2 c_W + s_Z^2 c_B) \right] \\
 &+ \frac{1}{2} m_Z^2 Z_\mu Z^\mu \cdot \frac{v^2}{\Lambda^2} (-2c_T + c_R),
 \end{aligned} \tag{C.6}$$

$$\begin{aligned}
 \mathcal{L}_{\gamma\gamma} &= \frac{1}{2} A_\mu (\partial^4 g^{\mu\nu} - \partial^2 \partial^\mu \partial^\nu) A_\nu \cdot \left[-\frac{1}{\Lambda^2} (s_Z^2 c_{2W} + c_Z^2 c_{2B}) \right] \\
 &+ \frac{1}{2} A_\mu (-\partial^2 g^{\mu\nu} + \partial^\mu \partial^\nu) A_\nu \cdot \frac{8m_Z^2}{\Lambda^2} c_Z^2 s_Z^2 (c_{WW} + c_{BB} - c_{WB}),
 \end{aligned} \tag{C.7}$$

$$\begin{aligned}
 \mathcal{L}_{\gamma Z} &= A_\mu (\partial^4 g^{\mu\nu} - \partial^2 \partial^\mu \partial^\nu) Z_\nu \cdot \left[-\frac{1}{\Lambda^2} c_Z s_Z (c_{2W} - c_{2B}) \right] \\
 &+ A_\mu (-\partial^2 g^{\mu\nu} + \partial^\mu \partial^\nu) Z_\nu \cdot \frac{m_Z^2}{\Lambda^2} c_Z s_Z \left[\frac{8(c_Z^2 c_{WW} - s_Z^2 c_{BB})}{-4(c_Z^2 - s_Z^2) c_{WB} + (c_W - c_B)} \right],
 \end{aligned} \tag{C.8}$$

$$\mathcal{L}_{hh} = \frac{1}{2} h (\partial^4) h \cdot \frac{1}{\Lambda^2} c_D + \frac{1}{2} h (-\partial^2) h \cdot \frac{v^2}{\Lambda^2} (2c_H + c_R). \tag{C.9}$$

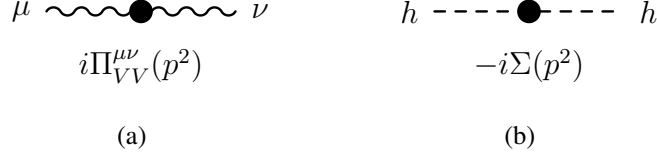


Figure C.1: Feynman rules for vacuum polarization functions.

$$\begin{aligned}
 i\Pi_{WW}^{\mu\nu}(p^2) &= i \left(g^{\mu\nu} - \frac{p^\mu p^\nu}{p^2} \right) \cdot \left[p^4 \left(-\frac{1}{\Lambda^2} c_{2W} \right) + p^2 \frac{2m_W^2}{\Lambda^2} (4c_{WW} + c_W) \right. \\
 &\quad \left. + m_W^2 \frac{v^2}{\Lambda^2} c_R \right] + i \frac{p^\mu p^\nu}{p^2} \cdot \left(p^2 \frac{m_W^2}{\Lambda^2} c_D + m_W^2 \frac{v^2}{\Lambda^2} c_R \right), \tag{C.10}
 \end{aligned}$$

$$\begin{aligned}
 i\Pi_{ZZ}^{\mu\nu}(p^2) &= i \left(g^{\mu\nu} - \frac{p^\mu p^\nu}{p^2} \right) \cdot \left\{ p^4 \left[-\frac{1}{\Lambda^2} (c_Z^2 c_{2W} + c_{2B} s_Z^2) \right] \right. \\
 &\quad \left. + p^2 \frac{2m_Z^2}{\Lambda^2} [4 (c_Z^4 c_{WW} + s_Z^4 c_{BB} + c_Z^2 s_Z^2 c_{WB}) + (c_Z^2 c_W + s_Z^2 c_B)] \right. \\
 &\quad \left. + m_Z^2 \frac{v^2}{\Lambda^2} (-2c_T + c_R) \right\} + i \frac{p^\mu p^\nu}{p^2} \cdot m_Z^2 \frac{v^2}{\Lambda^2} (-2c_T + c_R), \tag{C.11}
 \end{aligned}$$

$$\begin{aligned}
 i\Pi_{\gamma\gamma}^{\mu\nu}(p^2) &= i \left(g^{\mu\nu} - \frac{p^\mu p^\nu}{p^2} \right) \cdot \left\{ p^4 \left[-\frac{1}{\Lambda^2} (s_Z^2 c_{2W} + c_Z^2 c_{2B}) \right] \right. \\
 &\quad \left. + p^2 \frac{8m_Z^2}{\Lambda^2} c_Z^2 s_Z^2 (c_{WW} + c_{BB} - c_{WB}) \right\}, \tag{C.12}
 \end{aligned}$$

$$\begin{aligned}
 i\Pi_{\gamma Z}^{\mu\nu}(p^2) &= i \left(g^{\mu\nu} - \frac{p^\mu p^\nu}{p^2} \right) \cdot \left\{ p^4 \left[-\frac{1}{\Lambda^2} c_Z s_Z (c_{2W} - c_{2B}) \right] \right. \\
 &\quad \left. + p^2 \frac{m_Z^2}{\Lambda^2} c_Z s_Z [8 (c_Z^2 c_{WW} - s_Z^2 c_{BB}) - 4 (c_Z^2 - s_Z^2) c_{WB} + c_W - c_B] \right\}, \tag{C.13}
 \end{aligned}$$

$$-i\Sigma(p^2) = ip^4 \frac{1}{\Lambda^2} c_D + ip^2 \frac{v^2}{\Lambda^2} (2c_H + c_R). \tag{C.14}$$

C.1.2 Feynman rules for three-point vertices

In this work, the relevant three-point vertices are hWW , hZZ , $h\gamma Z$, $h\gamma\gamma$, and hgg vertices. As with the vacuum polarization functions case, we expand out the dim-6 effective operators in

Table 2.4 and identify the relevant Lagrangian pieces (Eq. (C.15)-Eq. (C.19)). These Lagrangian pieces generate the Feynman rules shown in Fig. C.2, with detailed values listed in Eq. (C.20)-Eq. (C.24).

$$\begin{aligned} \mathcal{L}_{hWW} = & \frac{\sqrt{2}m_W^2}{v} \left\{ \frac{1}{2} h \hat{W}_{\mu\nu}^+ \hat{W}^{-\mu\nu} \cdot \frac{1}{\Lambda^2} 8c_{WW} + h \left[\begin{array}{l} W_{\mu}^+ (-\partial^2 g^{\mu\nu} + \partial^\mu \partial^\nu) W_{\nu}^- \\ + W_{\mu}^- (-\partial^2 g^{\mu\nu} + \partial^\mu \partial^\nu) W_{\nu}^+ \end{array} \right] \cdot \frac{1}{\Lambda^2} c_W \right. \\ & \left. - \left[\begin{array}{l} (\partial^2 h) W_{\mu}^- W^{+\mu} + h (\partial_{\mu} W^{-\mu}) (\partial_{\nu} W^{+\nu}) \\ h W^{+\mu} (\partial_{\mu} \partial_{\nu}) W^{-\nu} + h W^{-\mu} (\partial_{\mu} \partial_{\nu}) W^{+\nu} \end{array} \right] \cdot \frac{1}{\Lambda^2} c_D + h W_{\mu}^+ W^{-\mu} \cdot \frac{2v^2}{\Lambda^2} c_R \right\}, \quad (\text{C.15}) \end{aligned}$$

$$\begin{aligned} \mathcal{L}_{hZZ} = & \frac{\sqrt{2}m_Z^2}{v} \left\{ \frac{1}{4} h \hat{Z}_{\mu\nu} \hat{Z}^{\mu\nu} \cdot \frac{1}{\Lambda^2} 8 (c_Z^4 c_{WW} + s_Z^4 c_{BB} + c_Z^2 s_Z^2 c_{WB}) \right. \\ & + \frac{1}{2} h Z_{\mu} (-\partial^2 g^{\mu\nu} + \partial^\mu \partial^\nu) Z_{\nu} \cdot \frac{1}{\Lambda^2} 2 (c_Z^2 c_W + s_Z^2 c_B) \\ & + \left[-\frac{1}{2} (\partial^2 h) (Z_{\mu} Z^{\mu}) - \frac{1}{2} h (\partial_{\mu} Z^{\mu}) (\partial_{\nu} Z^{\nu}) - h Z^{\mu} (\partial_{\mu} \partial_{\nu}) Z^{\nu} \right] \cdot \frac{1}{\Lambda^2} c_D \\ & \left. + \frac{1}{2} h Z_{\mu} Z^{\mu} \cdot \frac{2v^2}{\Lambda^2} (-2c_T + c_R) \right\}, \quad (\text{C.16}) \end{aligned}$$

$$\begin{aligned} \mathcal{L}_{h\gamma Z} = & \frac{\sqrt{2}m_Z^2}{v} \left\{ \frac{1}{2} h \hat{Z}_{\mu\nu} A^{\mu\nu} \cdot \frac{1}{\Lambda^2} 4c_Z s_Z \left[2 (c_Z^2 c_{WW} - s_Z^2 c_{BB}) - (c_Z^2 - s_Z^2) c_{WB} \right] \right. \\ & \left. + h Z_{\mu} (-\partial^2 g^{\mu\nu} + \partial^\mu \partial^\nu) A_{\nu} \cdot \frac{1}{\Lambda^2} c_Z s_Z (c_W - c_B) \right\}, \quad (\text{C.17}) \end{aligned}$$

$$\mathcal{L}_{h\gamma\gamma} = \frac{\sqrt{2}m_Z^2}{v} \frac{1}{4} h A_{\mu\nu} A^{\mu\nu} \cdot \frac{1}{\Lambda^2} 8c_Z^2 s_Z^2 (c_{WW} + c_{BB} - c_{WB}), \quad (\text{C.18})$$

$$\mathcal{L}_{hgg} = \frac{\sqrt{2}g_s^2 v^2}{2v} \frac{1}{4} h G_{\mu\nu}^a G^{a,\mu\nu} \cdot \frac{1}{\Lambda^2} 8c_{GG}. \quad (\text{C.19})$$

$$\begin{aligned}
 iM_{hWW}^{\mu\nu}(p_1, p_2) = & i \frac{\sqrt{2}m_W^2}{v} \left\{ - (p_1 p_2 g^{\mu\nu} - p_1^\nu p_2^\mu) \frac{1}{\Lambda^2} 8c_{WW} \right. \\
 & + \left[(p_1^2 g^{\mu\nu} - p_1^\mu p_1^\nu) + (p_2^2 g^{\mu\nu} - p_2^\mu p_2^\nu) \right] \frac{1}{\Lambda^2} c_W \\
 & \left. + \left[(p_1 + p_2)^2 g^{\mu\nu} + p_1^\mu p_2^\nu + p_1^\nu p_2^\mu + p_2^\mu p_2^\nu \right] \frac{1}{\Lambda^2} c_D + g^{\mu\nu} \frac{2v^2}{\Lambda^2} c_R \right\}, \quad (C.20)
 \end{aligned}$$

$$\begin{aligned}
 iM_{hZZ}^{\mu\nu}(p_1, p_2) = & i \frac{\sqrt{2}m_Z^2}{v} \left\{ - (p_1 p_2 g^{\mu\nu} - p_1^\nu p_2^\mu) \frac{1}{\Lambda^2} 8(c_Z^4 c_{WW} + s_Z^4 c_{BB} + c_Z^2 s_Z^2 c_{WB}) \right. \\
 & + \left[(p_1^2 g^{\mu\nu} - p_1^\mu p_1^\nu) + (p_2^2 g^{\mu\nu} - p_2^\mu p_2^\nu) \right] \frac{1}{\Lambda^2} (c_Z^2 c_W + s_Z^2 c_B) \\
 & + \left[(p_1 + p_2)^2 g^{\mu\nu} + p_1^\mu p_2^\nu + p_1^\nu p_2^\mu + p_2^\mu p_2^\nu \right] \frac{1}{\Lambda^2} c_D \\
 & \left. + g^{\mu\nu} \frac{2v^2}{\Lambda^2} (-2c_T + c_R) \right\}, \quad (C.21)
 \end{aligned}$$

$$\begin{aligned}
 iM_{h\gamma Z}^{\mu\nu}(p_1, p_2) = & i \frac{\sqrt{2}m_Z^2}{v} \left\{ - (p_1 p_2 g^{\mu\nu} - p_1^\nu p_2^\mu) \frac{4c_Z s_Z}{\Lambda^2} \left[2(c_Z^2 c_{WW} - s_Z^2 c_{BB}) - (c_Z^2 - s_Z^2) c_{WB} \right] \right. \\
 & \left. + (p_1^2 g^{\mu\nu} - p_1^\mu p_1^\nu) \frac{1}{\Lambda^2} c_Z s_Z (c_W - c_B) \right\}, \quad (C.22)
 \end{aligned}$$

$$iM_{h\gamma\gamma}^{\mu\nu}(p_1, p_2) = -i \frac{\sqrt{2}m_Z^2}{v} (p_1 p_2 g^{\mu\nu} - p_1^\nu p_2^\mu) \frac{1}{\Lambda^2} 8c_Z^2 s_Z^2 (c_{WW} + c_{BB} - c_{WB}), \quad (C.23)$$

$$iM_{hgg}^{\mu\nu}(p_1, p_2) = -i \frac{\sqrt{2}g_s^2 v^2}{2v} (p_1 p_2 g^{\mu\nu} - p_1^\nu p_2^\mu) \frac{1}{\Lambda^2} 8c_{GG}. \quad (C.24)$$

C.2 Details on interference corrections to the Higgs decay widths

There is no new amputated diagrams for $h \rightarrow f\bar{f}$ decay modes up to leading order (linear power and tree level) in Wilson coefficients, because we are considering only the bosonic dim-6 effective operators (Table 2.4). The $h \rightarrow gg$, $h \rightarrow \gamma\gamma$, and $h \rightarrow \gamma Z$ decay widths are already at one-loop order in the SM, so the only new amputated diagram up to leading order in Wilson coefficients is given by the new three-point vertices $iM_{hgg}^{\mu\nu}(p_1, p_2)$, $iM_{h\gamma\gamma}^{\mu\nu}(p_1, p_2)$, and $iM_{h\gamma Z}^{\mu\nu}(p_1, p_2)$ (Fig. C.2(d)),

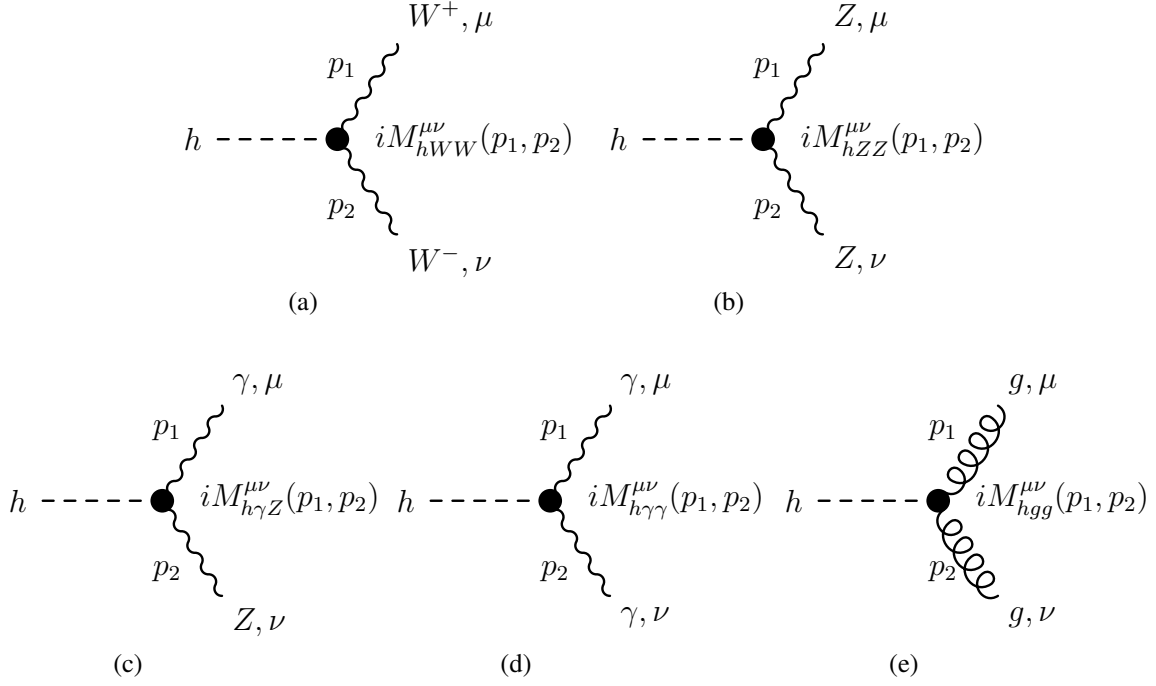


Figure C.2: Feynman rules for three-point vertices.

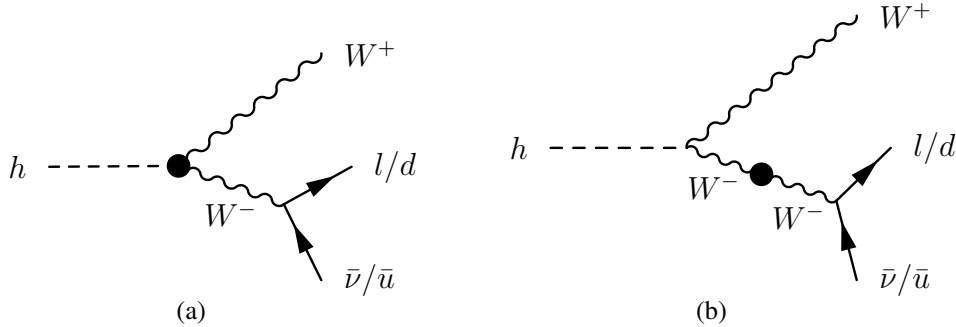


Figure C.3: New amputated Feynman diagrams for Γ_{hWW^*} .

Fig. C.2(e), and Fig. C.2(c)) multiplied by appropriate polarization vectors

$$iM_{hgg, \text{AD,new}} = iM_{hgg}^{\mu\nu}(p_1, p_2)\epsilon_\mu^*(p_1)\epsilon_\nu^*(p_2), \quad (\text{C.25})$$

$$iM_{h\gamma\gamma, \text{AD,new}} = iM_{h\gamma\gamma}^{\mu\nu}(p_1, p_2)\epsilon_\mu^*(p_1)\epsilon_\nu^*(p_2), \quad (\text{C.26})$$

$$iM_{h\gamma Z, \text{AD,new}} = iM_{h\gamma Z}^{\mu\nu}(p_1, p_2)\epsilon_\mu^*(p_1)\epsilon_\nu^*(p_2). \quad (\text{C.27})$$

The $h \rightarrow WW^*$ and $h \rightarrow ZZ^*$ modes are a little more complicated, because they are at tree level in the SM. It turns out that there are two new amputated diagrams for $h \rightarrow WW^*$ mode as shown in Fig. C.3, and four new amputated diagrams for $h \rightarrow ZZ^*$ mode as shown in Fig. C.4.

It is straightforward to evaluate these relevant new diagrams using the new Feynman rules listed in Section C.1 (together with the SM Feynman rules). One can then compute the interference

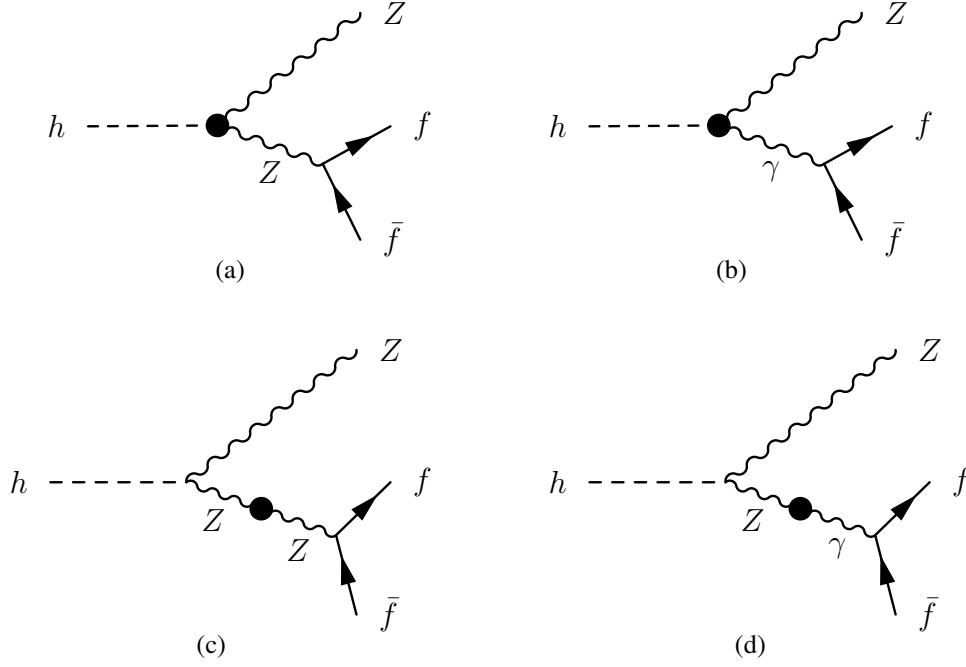


Figure C.4: New amputated Feynman diagrams for Γ_{hZZ^*} .

correction ϵ_I for each decay mode from its definition (Eq. (2.103)). The three-body phase space integrals are analytically manageable, albeit a little bit tedious. We summarize the final results of ϵ_I in Table 2.8, where the auxiliary integrals $I_a(\beta)$, $I_b(\beta)$, $I_c(\beta)$, and $I_d(\beta)$ are defined as

$$I_{\text{SM}}(\beta) \equiv \frac{1}{8\beta^2} [I_2(\beta) + 2(1 - 6\beta^2)I_1(\beta) + (1 - 4\beta^2 + 12\beta^4)I_0(\beta)], \quad (\text{C.28})$$

$$I_a(\beta) \equiv \frac{1}{8\beta^4 I_{\text{SM}}(\beta)} \left[\begin{array}{l} I_3(\beta) + (1 - 16\beta^2)I_2(\beta) + (1 - 12\beta^2 + 62\beta^4)I_1(\beta) \\ -4(\beta^2 - 5\beta^4 + 18\beta^6)I_0(\beta) + 2(\beta^4 - 4\beta^6 + 12\beta^8)I_{-1}(\beta) \end{array} \right] \quad (\text{C.29})$$

$$I_b(\beta) \equiv \frac{1}{4\beta^2 I_{\text{SM}}(\beta)} \left[\begin{array}{l} -2I_2(\beta) - (4 - 25\beta^2)I_1(\beta) - 2(1 - 5\beta^2 + 18\beta^4)I_0(\beta) \\ +\beta^2(1 - 4\beta^2 + 12\beta^4)I_{-1}(\beta) \end{array} \right], \quad (\text{C.30})$$

$$I_c(\beta) \equiv \frac{5I_2(\beta) + 2(2 - 3\beta^2)I_1(\beta) - (1 + 2\beta^2)I_0(\beta)}{2\beta^2 I_{\text{SM}}(\beta)}, \quad (\text{C.31})$$

$$I_d(\beta) \equiv \frac{7I_2(\beta) + 8(1 - 3\beta^2)I_1(\beta) + (1 - 4\beta^2 + 12\beta^4)I_0(\beta)}{2\beta^2 I_{\text{SM}}(\beta)}, \quad (\text{C.32})$$

where another set of auxiliary integrals $I_0(\beta)$, $I_1(\beta)$, $I_2(\beta)$, $I_3(\beta)$, $I_{-1}(\beta)$ are defined as follows,

with $\beta \in (\frac{1}{2}, 1)$

$$I_0(\beta) \equiv \int_{2\beta-1}^{\beta^2} \frac{dy \sqrt{(y+1)^2 - 4\beta^2}}{y^2} = 1 - \frac{1}{\beta^2} - \ln \beta + \frac{\frac{\pi}{2} - \arcsin \frac{3\beta^2-1}{2\beta^3}}{\sqrt{4\beta^2-1}},$$

$$I_1(\beta) \equiv \int_{2\beta-1}^{\beta^2} \frac{dy \sqrt{(y+1)^2 - 4\beta^2}}{y^2} y = 1 - \beta^2 - \ln \beta - \frac{\frac{\pi}{2} - \arcsin \frac{3\beta^2-1}{2\beta^3}}{\sqrt{4\beta^2-1}} (4\beta^2 - 1),$$

$$I_2(\beta) \equiv \int_{2\beta-1}^{\beta^2} \frac{dy \sqrt{(y+1)^2 - 4\beta^2}}{y^2} y^2 = \frac{1}{2} (1 - \beta^4) + 2\beta^2 \ln \beta,$$

$$I_3(\beta) \equiv \int_{2\beta-1}^{\beta^2} \frac{dy \sqrt{(y+1)^2 - 4\beta^2}}{y^2} (y^3 + y^2) = \frac{1}{3} (1 - \beta^2)^3,$$

$$I_{-1}(\beta) \equiv \int_{2\beta-1}^{\beta^2} \frac{dy \sqrt{(y+1)^2 - 4\beta^2}}{y^3} = \frac{2\beta^2 \left(\frac{\pi}{2} - \arcsin \frac{3\beta^2-1}{2\beta^3} \right)}{(4\beta^2 - 1)^{\frac{3}{2}}} - \frac{(1 - \beta^2)(3\beta^2 - 1)}{2\beta^4(4\beta^2 - 1)}.$$

The A_{hgg}^{SM} , $A_{h\gamma\gamma}^{\text{SM}}$, and $A_{h\gamma Z}^{\text{SM}}$ in Table 2.8 are the standard form factors

$$A_{hgg}^{\text{SM}} = \sum_Q A_{1/2}(\tau_Q), \quad (\text{C.33})$$

$$A_{h\gamma\gamma}^{\text{SM}} = A_1(\tau_W) + \sum_f N_C Q_f^2 A_{1/2}(\tau_f), \quad (\text{C.34})$$

$$A_{h\gamma Z}^{\text{SM}} = A_1(\tau_W, \lambda_W) + \sum_f N_C \frac{2Q_f}{c_Z} (T_f^3 - 2s_Z^2 Q_f) A_{1/2}(\tau_f, \lambda_f), \quad (\text{C.35})$$

with $\tau_i \equiv \frac{4m_i^2}{m_h^2}$, $\lambda_i \equiv \frac{4m_i^2}{m_Z^2}$, and $A_{1/2}(\tau)$, $A_1(\tau)$, $A_{1/2}(\tau, \lambda)$, $A_1(\tau, \lambda)$ being the conventional form factors (for example see [105])

$$A_{1/2}(\tau) = 2\tau^{-2} \left[\tau + (\tau - 1) f(\tau) \right], \quad (\text{C.36})$$

$$A_1(\tau) = -\tau^{-2} \left[2\tau^2 + 3\tau + 3(2\tau - 1) f(\tau) \right], \quad (\text{C.37})$$

$$A_{1/2}(\tau, \lambda) = B_1(\tau, \lambda) - B_2(\tau, \lambda), \quad (\text{C.38})$$

$$A_1(\tau, \lambda) = c_Z \left\{ 4 \left(3 - \frac{s_Z^2}{c_Z^2} \right) B_2(\tau, \lambda) + \left[\left(1 + \frac{2}{\tau} \right) \frac{s_Z^2}{c_Z^2} - \left(5 + \frac{2}{\tau} \right) \right] B_1(\tau, \lambda) \right\} \quad (\text{C.39})$$

with

$$B_1(\tau, \lambda) \equiv \frac{\tau\lambda}{2(\tau - \lambda)} + \frac{\tau^2\lambda^2}{2(\tau - \lambda)^2} \left[f\left(\frac{1}{\tau}\right) - f\left(\frac{1}{\lambda}\right) \right] + \frac{\tau^2\lambda}{(\tau - \lambda)^2} \left[g\left(\frac{1}{\tau}\right) - g\left(\frac{1}{\lambda}\right) \right],$$

$$B_2(\tau, \lambda) \equiv -\frac{\tau\lambda}{2(\tau - \lambda)} \left[f\left(\frac{1}{\tau}\right) - f\left(\frac{1}{\lambda}\right) \right],$$

and

$$f(\tau) = \begin{cases} \arcsin^2 \sqrt{\tau} & \tau \leq 1 \\ -\frac{1}{4} \left[\log \frac{1 + \sqrt{1 - \tau^{-1}}}{1 - \sqrt{1 - \tau^{-1}}} - i\pi \right]^2 & \tau > 1 \end{cases}, \quad (\text{C.40})$$

$$g(\tau) = \begin{cases} \sqrt{\tau^{-1} - 1} \arcsin \sqrt{\tau} & \tau \leq 1 \\ \frac{\sqrt{1 - \tau^{-1}}}{2} \left[\log \frac{1 + \sqrt{1 - \tau^{-1}}}{1 - \sqrt{1 - \tau^{-1}}} - i\pi \right] & \tau > 1 \end{cases}. \quad (\text{C.41})$$

C.3 Details on interference corrections to Higgs production cross section

The ggF Higgs production mode is just the time reversal of the $h \rightarrow gg$ decay. Again as it is already at one-loop order in the SM, the only new amputated diagram up to leading order in Wilson coefficients is given by the new three-point vertex $iM_{hgg}^{\mu\nu}(p_1, p_2)$ (Fig. C.2(e)) multiplied by the polarization vectors

$$iM_{ggF, \text{AD,new}} = iM_{hgg}^{\mu\nu}(p_1, p_2)\epsilon_\mu(p_1)\epsilon_\nu(p_2). \quad (\text{C.42})$$

Obviously, the interference correction to ggF production cross section is the same as that to $h \rightarrow gg$ decay width

$$\epsilon_{ggF, I} = \epsilon_{hgg, I} = \frac{(4\pi)^2}{\text{Re}(A_{hgg}^{\text{SM}})} \frac{16v^2}{\Lambda^2} c_{GG}. \quad (\text{C.43})$$

The vector boson fusion production mode σ_{WW_h} has three new amputated diagrams as shown in Fig. C.7 (in which one of the fermion lines can be inverted to take account of production mode in lepton colliders such as the ILC). For the vector boson associate production modes, there are two new diagrams for σ_{Wh} (Fig. C.5) and four for σ_{Zh} (Fig. C.6).

Again from the definition (Eq. (2.103)), we compute the interference correction ϵ_I for each Higgs production mode. The final results are summarized in Table 2.10. For σ_{Wh} and σ_{Zh} , the final states phase space integral is only two-body and quite simple. On the other hand, σ_{WW_h} requires to integrate over a three-body phase space, which turns out to be quite involved. The analytical result $\epsilon_{WW_h, I}(s)$ is several pages long and hence would not be that useful. Instead, we provide numerical results of it in Table 2.10, where three auxiliary functions $f_a(s)$, $f_b(s)$, and $f_c(s)$ are defined. We provide the numerical results of these auxiliary functions (Fig. 2.4) as well as mathematica code of their calculations.

To show the definition of $f_a(s)$, $f_b(s)$, and $f_c(s)$, we need to describe the three-body phase space integral of σ_{WW_h} . We take the center of mass frame of the colliding fermions and setup the spherical coordinates with the positive z -axis being the direction of \vec{p}_a . Then the various momenta

labeled in Fig. C.7 can be expressed as

$$p_a = \frac{\sqrt{s}}{2}(1, 0, 0, 1), \quad (\text{C.44})$$

$$p_b = \frac{\sqrt{s}}{2}(1, 0, 0, -1), \quad (\text{C.45})$$

$$p_3 = \frac{\sqrt{s}}{2}x_3(1, s_3, 0, c_3), \quad (\text{C.46})$$

$$p_4 = \frac{\sqrt{s}}{2}x_4(1, s_4 \cos \phi, s_4 \sin \phi, c_4). \quad (\text{C.47})$$

where we have defined $x_3 \equiv \frac{2E_3}{\sqrt{s}}$, $x_4 \equiv \frac{2E_4}{\sqrt{s}}$, and adopted the notation $c_3 \equiv \cos \theta_3$ etc. Due to the axial symmetry around the z -axis, we have also taken the parametrization $\phi_3 = 0$ and $\phi_4 = \phi$ without loss of generality. For further convenience, let us also define $\eta_h \equiv \frac{m_h}{\sqrt{s}}$, $\eta_W \equiv \frac{m_W}{\sqrt{s}}$, and $\alpha_\phi \equiv \frac{1}{2}(1 - c_3 c_4 - s_3 s_4 \cos \phi)$. The three-body phase space has nine variables to integrate over. But the axial symmetry and the δ -function of 4-momentum make five of them trivial, leaving us with four nontrivial ones, which we choose to be x_3 , c_3 , c_4 , and ϕ . Sometimes, we will still use the quantity x_4 to make the expression short, but it has been fixed by the energy δ -function and should be understood as a function of the other four

$$x_4(x_3, c_3, c_4, \phi) = \frac{1 - \eta_h^2 - x_3}{1 - \alpha_\phi x_3}. \quad (\text{C.48})$$

Now the phase space integral can be written as

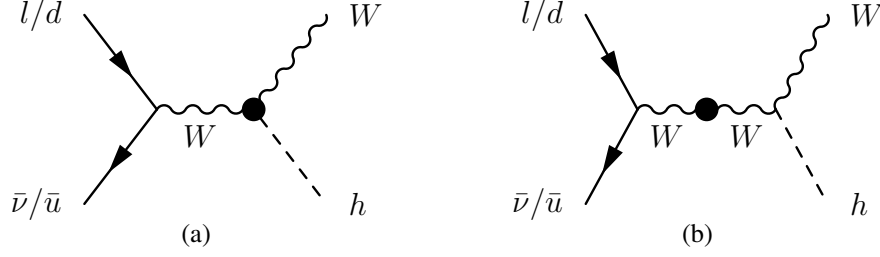
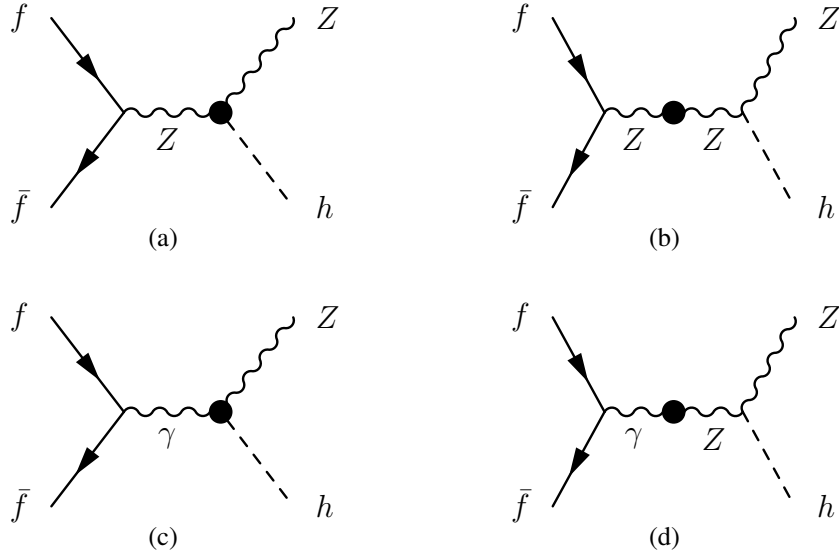
$$\begin{aligned} \frac{1}{2s} \int d\Pi_3(1, 3, 4) &= \frac{1}{2s} \int \frac{d^3\vec{p}_3}{(2\pi)^3} \frac{1}{2E_3} \frac{d^3\vec{p}_4}{(2\pi)^3} \frac{1}{2E_4} \frac{d^3\vec{p}_1}{(2\pi)^3} \frac{1}{2E_1} (2\pi)^4 \delta^4(p_1 + p_3 + p_4 - p) \\ &= \frac{1}{2048\pi^4} \int_0^{1-\eta_h^2} dx_3 \int_{-1}^1 dc_3 dc_4 \int_0^{2\pi} d\phi \frac{(1 - \eta_h^2 - x_3)x_3}{(1 - \alpha_\phi x_3)^2}. \end{aligned} \quad (\text{C.49})$$

The modulus square of the SM invariant amplitude is

$$\begin{aligned} \overline{|M_{WW h, SM}|^2} &= \left(\frac{g}{\sqrt{2}}\right)^4 \frac{2m_W^4}{v^2} \frac{g^{\mu\nu} g^{\alpha\beta} \frac{1}{4} \text{tr}(\not{p}_a \gamma_\alpha \not{p}_3 \gamma_\mu P_L) \text{tr}(\not{p}_b \gamma_\nu \not{p}_4 \gamma_\beta P_L)}{(k_1^2 - m_W^2)^2 (k_2^2 - m_W^2)^2} \\ &= \frac{m_W^4}{v^6} 2\eta_W^4 \frac{4x_3 x_4 (1 + c_3)(1 - c_4)}{[x_3(1 - c_3) + 2\eta_W^2]^2 [x_4(1 + c_4) + 2\eta_W^2]^2}. \end{aligned} \quad (\text{C.50})$$

Now we are about ready to show the definition of $f_a(s)$, $f_b(s)$, and $f_c(s)$. Let us introduce an ‘‘average’’ definition of A as

$$\langle A \rangle \equiv \frac{\frac{1}{2s} \int d\Pi_3(1, 3, 4) \overline{|M_{WW h, SM}|^2} A}{\frac{1}{2s} \int d\Pi_3(1, 3, 4) \overline{|M_{WW h, SM}|^2}}. \quad (\text{C.51})$$


 Figure C.5: New amputated Feynman diagrams for σ_{Wh} .

 Figure C.6: New amputated Feynman diagrams for σ_{Zh} .

Then $f_a(s)$, $f_b(s)$, and $f_c(s)$ are defined as

$$\begin{aligned}
 f_a(s) &\equiv \left\langle \frac{(k_1 k_2 g^{\mu\nu} - k_1^\nu k_2^\mu) g^{\alpha\beta} \frac{1}{4} \text{tr}(\not{p}_a \gamma_\alpha \not{p}_3 \gamma_\mu P_L) \text{tr}(\not{p}_b \gamma_\nu \not{p}_4 \gamma_\beta P_L) + c.c.}{m_W^2 g^{\mu\nu} g^{\alpha\beta} \frac{1}{4} \text{tr}(\not{p}_a \gamma_\alpha \not{p}_3 \gamma_\mu P_L) \text{tr}(\not{p}_b \gamma_\nu \not{p}_4 \gamma_\beta P_L)} \right\rangle \\
 &= \left\langle -\frac{1}{2\eta_W^2} \left(\frac{x_4}{1+c_3} + \frac{x_3}{1-c_4} \right) s_3 s_4 \cos \phi \right\rangle, \tag{C.52}
 \end{aligned}$$

$$f_b(s) \equiv \left\langle \frac{k_1^2 + k_2^2}{m_W^2} \right\rangle = \left\langle -\frac{1}{2\eta_W^2} [x_3(1-c_3) + x_4(1+c_4)] \right\rangle, \tag{C.53}$$

$$f_c(s) \equiv \left\langle \frac{k_1^2}{k_1^2 - m_W^2} + \frac{k_2^2}{k_2^2 - m_W^2} \right\rangle = \left\langle \frac{x_3(1-c_3)}{x_3(1-c_3) + 2\eta_W^2} + \frac{x_4(1+c_4)}{x_4(1+c_4) + 2\eta_W^2} \right\rangle \tag{C.54}$$

where various momenta are as labeled in Fig. C.7, and $P_L = \frac{1-\gamma^5}{2}$, with the γ matrices defined as usual.

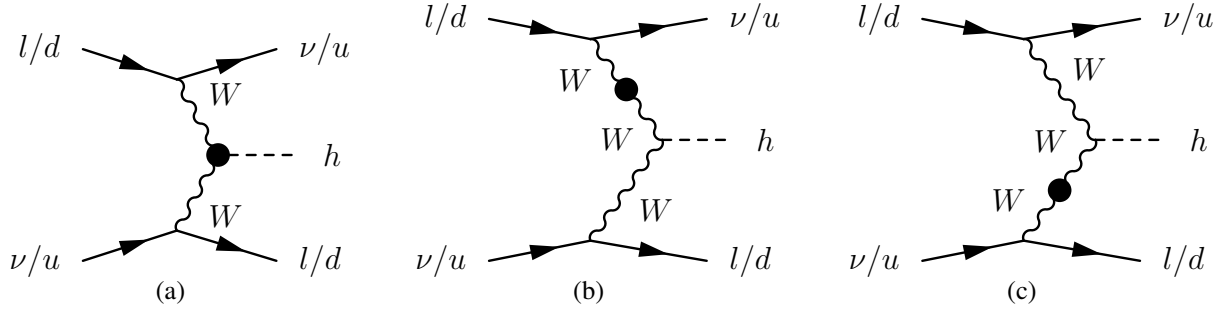


Figure C.7: New amputated Feynman diagrams for $\sigma_{WW h}$.

$\Delta r_h = -\frac{v^2}{\Lambda^2} (2c_H + c_R) - \frac{2m_h^2}{\Lambda^2} c_D$ $\Delta r_Z = \frac{2m_Z^2}{\Lambda^2} \left[-c_Z^2 c_{2W} - s_Z^2 c_{2B} + 4(c_Z^4 c_{WW} + s_Z^4 c_{BB} + c_Z^2 s_Z^2 c_{WB}) + c_Z^2 c_W + s_Z^2 c_B \right]$ $\Delta r_W = \frac{2m_W^2}{\Lambda^2} (-c_{2W} + 4c_{WW} + c_W)$

Table C.3: Residue modifications Δr in terms of Wilson coefficients.

C.4 Calculation of residue modifications

The mass pole residue modification Δr_k of each external leg k can be computed using the corresponding vacuum polarization function. In this work, the relevant mass pole residue modifications are

$$\Delta r_h = \left. \frac{d\Sigma(p^2)}{dp^2} \right|_{p^2=m_h^2}, \quad (\text{C.55})$$

$$\Delta r_W = \left. \frac{d\Pi_{WW}(p^2)}{dp^2} \right|_{p^2=m_W^2}, \quad (\text{C.56})$$

$$\Delta r_Z = \left. \frac{d\Pi_{ZZ}(p^2)}{dp^2} \right|_{p^2=m_Z^2}, \quad (\text{C.57})$$

where $-i\Sigma(p^2)$ denotes the vacuum polarization function of the physical Higgs field h . With all the vacuum polarization functions listed in Table C.1, it is straightforward to calculate Δr . The results are summarized in Table C.3.

C.5 Calculation of Lagrangian parameter modifications

The set of Lagrangian parameters relevant for us are $\{\rho\} = \{g^2, v^2, s_Z^2, y_f^2\}$. We would like to compute them in terms of the physical observables and the Wilson coefficients $\rho = \rho(obs, c_i)$, where the set of observables relevant to us can be taken as $\{obs\} = \{\hat{\alpha}, \hat{G}_F, \hat{m}_Z^2, \hat{m}_f^2\}$. We put

a hat on the quantities to denote that it is a physical observable measured from the experiments. On the other hand, for notation convenience, we also define the following auxiliary Lagrangian parameters that are related to the basic ones $\{\rho\} = \{g^2, v^2, s_Z^2, y_f^2\}$:

$$m_W^2 \equiv \frac{1}{2}g^2v^2, \quad (\text{C.58})$$

$$m_Z^2 \equiv \frac{1}{2}g^2v^2 \frac{1}{1 - s_Z^2}. \quad (\text{C.59})$$

These auxiliary Lagrangian parameters are not hatted.

As explained in Section 2.3, in order to obtain $\rho = \rho(obs, c_i)$, we first need to compute the function $obs = obs(\rho, c_i)$, which up to linear order in c_i are

$$\hat{\alpha} = \frac{g^2 s_Z^2}{4\pi} \frac{p^2}{p^2 - \Pi_{\gamma\gamma}(p^2)} \Big|_{p^2 \rightarrow 0} = \frac{g^2 s_Z^2}{4\pi} [1 + \Pi'_{\gamma\gamma}(0)], \quad (\text{C.60})$$

$$\hat{G}_F = \frac{\sqrt{2}g^2}{8} \frac{-1}{p^2 - m_W^2 - \Pi_{WW}(p^2)} \Big|_{p^2=0} = \frac{1}{2\sqrt{2}v^2} \left[1 - \frac{1}{m_W^2} \Pi_{WW}(0) \right], \quad (\text{C.61})$$

$$\hat{m}_Z^2 = m_Z^2 + \Pi_{ZZ}(m_Z^2) = \frac{1}{2}g^2v^2 \frac{1}{1 - s_Z^2} \left[1 + \frac{1}{m_Z^2} \Pi_{ZZ}(m_Z^2) \right], \quad (\text{C.62})$$

$$\hat{m}_f^2 = y_f^2 v^2. \quad (\text{C.63})$$

Note that the vacuum polarization functions are linear in c_i and hence only kept up to first order. Next we need to take the inverse of these to get the function $\rho = \rho(obs, c_i)$. Again, because the vacuum polarization functions are already linear in c_i , one can neglect the modification of the Lagrangian parameters multiplying them when taking the inverse at the leading order. This gives

$$g^2 s_Z^2 = 4\pi \hat{\alpha} [1 - \Pi'_{\gamma\gamma}(0)], \quad (\text{C.64})$$

$$v^2 = \frac{1}{2\sqrt{2}\hat{G}_F} \left[1 - \frac{1}{m_W^2} \Pi_{WW}(0) \right], \quad (\text{C.65})$$

$$s_Z^2(1 - s_Z^2) = \frac{\pi \hat{\alpha}}{\sqrt{2}\hat{G}_F \hat{m}_Z^2} [1 - \Pi'_{\gamma\gamma}(0)] \left[1 - \frac{1}{m_W^2} \Pi_{WW}(0) \right] \left[1 + \frac{1}{m_Z^2} \Pi_{ZZ}(m_Z^2) \right], \quad (\text{C.66})$$

$$y_f^2 = 2\sqrt{2}\hat{G}_F \hat{m}_f^2 \left[1 + \frac{1}{m_W^2} \Pi_{WW}(0) \right]. \quad (\text{C.67})$$

Then taking log and derivative on both sides, we obtain

$$\Delta w_{g^2} + \Delta w_{s_Z^2} = -\Pi'_{\gamma\gamma}(0), \quad (\text{C.68})$$

$$\Delta w_{v^2} = -\frac{1}{m_W^2} \Pi_{WW}(0), \quad (\text{C.69})$$

$$\frac{c_Z^2 - s_Z^2}{c_Z^2} \Delta w_{s_Z^2} = -\Pi'_{\gamma\gamma}(0) - \frac{1}{m_W^2} \Pi_{WW}(0) + \frac{1}{m_Z^2} \Pi_{ZZ}(m_Z^2), \quad (\text{C.70})$$

$$\Delta w_{y_f^2} = \frac{1}{m_W^2} \Pi_{WW}(0), \quad (\text{C.71})$$

$$\begin{aligned}
 \Delta w_{g^2} &= \frac{m_W^2}{\Lambda^2} \frac{1}{c_Z^2 - s_Z^2} \left\{ (c_Z^2 c_{2W} + s_Z^2 c_{2B}) - 8 \left[(c_Z^2 - s_Z^2) c_{WW} + s_Z^2 c_{WB} \right] \right. \\
 &\quad \left. - 2(c_Z^2 c_W + s_Z^2 c_B) \right\} + \frac{c_Z^2}{c_Z^2 - s_Z^2} \frac{2v^2}{\Lambda^2} c_T \\
 \Delta w_{v^2} &= -\frac{v^2}{\Lambda^2} c_R \\
 \Delta w_{s_Z^2} &= \frac{m_W^2}{\Lambda^2} \frac{1}{c_Z^2 - s_Z^2} \left\{ - (c_Z^2 c_{2W} + s_Z^2 c_{2B}) + 8 \left[(c_Z^2 - s_Z^2) (c_Z^2 c_{WW} - s_Z^2 c_{BB}) + 2c_Z^2 s_Z^2 c_{WB} \right] \right. \\
 &\quad \left. + 2(c_Z^2 c_W + s_Z^2 c_B) \right\} - \frac{c_Z^2}{c_Z^2 - s_Z^2} \frac{2v^2}{\Lambda^2} c_T \\
 \Delta w_{y_f^2} &= \frac{v^2}{\Lambda^2} c_R
 \end{aligned}$$

Table C.4: Parameter modifications Δw_ρ in terms of Wilson coefficients.

which leads us to the final results

$$\Delta w_{g^2} = -\Pi'_{\gamma\gamma}(0) - \frac{c_Z^2}{c_Z^2 - s_Z^2} \left[-\Pi'_{\gamma\gamma}(0) - \frac{1}{m_W^2} \Pi_{WW}(0) + \frac{1}{m_Z^2} \Pi_{ZZ}(m_Z^2) \right], \quad (\text{C.72})$$

$$\Delta w_{v^2} = -\frac{1}{m_W^2} \Pi_{WW}(0), \quad (\text{C.73})$$

$$\Delta w_{s_Z^2} = \frac{c_Z^2}{c_Z^2 - s_Z^2} \left[-\Pi'_{\gamma\gamma}(0) - \frac{1}{m_W^2} \Pi_{WW}(0) + \frac{1}{m_Z^2} \Pi_{ZZ}(m_Z^2) \right], \quad (\text{C.74})$$

$$\Delta w_{y_f^2} = \frac{1}{m_W^2} \Pi_{WW}(0). \quad (\text{C.75})$$

Plugging in the vacuum polarization functions listed in Table C.1, one can get the Lagrangian parameter modifications Δw_ρ summarized in Table C.4.

Appendix D

Observational Abundances of Light Elements

In studying the constraints on dark matter from big bang nucleosynthesis in chapter 3, we used the results of reference [119] as a starting point for our analysis. In this appendix, we review the primordial abundances that [119] used in their analysis.

The primordial D/H abundance is inferred from the QSO absorption line in metal poor systems,

$$(n_{\text{D}}/n_{\text{H}})_{\text{p}} = (2.82 \pm 0.26) \times 10^{-5}. \quad (\text{D.1})$$

This value, used in Ref [119], is the weighted average of six observed QSO absorption systems. A more recent work by the same group includes a seventh measurement that doesn't change the central value, but lowers the dispersion to $\pm 0.20 \times 10^{-5}$ [122].

An upper bound on the primordial ${}^3\text{He}$ abundance is obtained from ${}^3\text{He}/\text{D}$ measurements in protosolar clouds,

$$(n_{3\text{He}}/n_{\text{D}})_{\text{p}} < 0.83 + 0.27. \quad (\text{D.2})$$

While we do not use Li to place bounds in this work, we comment here on its measurement and the so-called lithium problem. ${}^7\text{Li}$ is observed in the atmospheres of metal-poor Population II stars in our galactic halo. ${}^6\text{Li}$ has been observed in these systems as well [174], although the total number of systems with observable ${}^6\text{Li}$ is somewhat controversial due to observational difficulties in distinguishing ${}^6\text{Li}$ and ${}^7\text{Li}$ spectra [175].

Both the ${}^7\text{Li}$ and ${}^6\text{Li}$ measurements conflict with the theoretical values predicted by standard BBN and are collectively referred to as the lithium problem (for a review, see [176]). For ${}^7\text{Li}$, the observed abundance is lower by a factor of about three than the theoretical value predicted by standard BBN, with a $4 - 5\sigma$ significance. In the case of ${}^6\text{Li}$, the observed abundance is more than a factor of 10^2 larger than the standard BBN prediction. While the solution to the lithium problems may be unknown, a conservative approach, as used in [119], is to take the observed ${}^6\text{Li}$ and ${}^7\text{Li}$ abundances as upper limits for their primordial abundances. There is also an extra uncertainty in the primordial abundances that comes from the possibility that stellar burning may deplete primordial ${}^6\text{Li}$ and ${}^7\text{Li}$ [177]. In this case, the conservative approach is to include this depletion as an uncertainty that raises the primordial abundance [119].

Appendix E

Axion Potential and Dilaton Stabilization

This appendix pertains to details and issues brought up in our discussion on the keV string axion of Chapter 4. In particular, we explicitly derive the axion potential that is central to determining the mass of the light axion in section E.1 and also discuss a mechanism of dilaton stabilization in section E.2.

E.1 Axion potential

Here we derive the low-energy effective axion potential for the IYIT model discussed in section 4.1. In order to properly capture the axion dynamics—in particular, the mixing of the hidden sector axion and string axion—the Lagrange multiplier \mathcal{A} that enforces the $SU(2)$ quantum constraint, see Eq. 4.2, must be kept in the spectrum. This is because, in the absence of the string axion, the hidden sector axion and Lagrange multiplier pair up to become heavy together. Therefore, this analysis differs from the usual situation where the Lagrange multiplier is immediately integrated out of the spectrum, and we feel it is worthwhile, especially for non-experts of supersymmetric dynamics, to carefully lay out the steps of the calculation. In order to elucidate the physics, we first describe the simpler case of the model with no tree-level superpotential and no string axion and then add these terms to find the axion spectrum quoted in chapter 4.

E.1.1 $W_{\text{tree}} = 0$

We begin by considering $SU(2)$ supersymmetric gauge theory with four quark superfields and no tree-level superpotential. Mesons $M^{ij} = \epsilon^{\alpha\beta} Q_\alpha^i Q_\beta^j$ —in the $\mathbf{6}$ of the $SU(4)$ flavor symmetry—parameterize the moduli space of the low-energy supersymmetric vacua. In the quantum theory, instantons deform the moduli space and the mesons are subject to the constraint $\text{Pf } M = \Lambda^4$ [178], where Λ is the $SU(2)$ dynamical scale and can always be made real by an anomalous $U(1)_h$ rotation under which Q has unit charge. This constraint may be enforced in the low energy theory through a Lagrange multiplier, $W = \mathcal{A}(\text{Pf } M - \Lambda^4)$. In the following, we make use of the local

Lie group isomorphism $SU(4) \simeq SO(6)$ to describe the flavor symmetry; in this language, the mesons are in the vector representation of $SO(6)$ and the quantum constraint is $M_i^2 = \Lambda^4$.

Let us describe the qualitative features of the low-energy vacua. The quantum constraint spontaneously breaks the $SO(6)$ flavor symmetry. At points of enhanced symmetry, the flavor symmetry is broken from $SO(6) \rightarrow SO(5)$ by the vacuum expectation value

$$\langle M_6 \rangle = \Lambda^2, \quad (\text{E.1})$$

giving rise to five massless Nambu-Goldstone bosons. The quantum constraint also spontaneously breaks the anomalous $U(1)_h$ symmetry under which Q has unit charge. The would-be NGB associated with the spontaneous breaking of $U(1)_h$ gets a mass of order Λ through the anomaly and should be integrated out of the low energy theory. This would-be NGB, analogous to the η' meson of QCD, is what we refer to as the axion a_h .

In summary, the quantum constraint, when satisfied as in Eq. (E.1), breaks the flavor symmetry as $SO(6) \times U(1)_h \rightarrow SO(5)$ and five of the mesons are massless while the sixth one, the axion, gains a mass of order the dynamical scale. In the rest of this subsection, we show how this qualitative picture works out quantitatively in the effective theory. We then demonstrate how introducing a string-like axion leaves a massless axion in the low-energy theory.

In terms of the canonically normalized mesons $\hat{M} \equiv M/\Lambda$, the effective superpotential and Kähler potential are given by

$$W_{\text{eff}} = \frac{1}{16\pi^2} \mathcal{A}(\hat{M}_i^2 - \Lambda^2) \quad (\text{E.2a})$$

$$K_{\text{eff}} = \frac{1}{16\pi^2} K_{\text{dyn}}(\hat{M}, \mathcal{A}), \quad (\text{E.2b})$$

where \mathcal{A} is a Lagrange multiplier enforcing the quantum constraint. The factors of 4π are included to ensure that the effective theory becomes strongly coupled at the scale Λ and are counted using naïve dimensional analysis [161, 162]. We note that estimates using naïve dimensional analysis have an uncertainty factor of a few; we take this uncertainty to be implicit in our results and do not explicitly keep track of it. Since the quantum moduli space is smoothly described by the meson fields [178], we can take a canonical kinetic term for the meson fields as an approximation. Our results are not sensitive to this approximation. Further, a kinetic term for \mathcal{A} is generated at one-loop via the interaction $\mathcal{A}\hat{M}^2$ in the effective superpotential. Therefore, at leading order the dynamical Kähler potential is given by

$$K_{\text{dyn}}(\hat{M}, \mathcal{A}) \approx \hat{M}^\dagger \hat{M} + \kappa \mathcal{A}^\dagger \mathcal{A}$$

where $\kappa \approx 5$ since there are five light mesons—the Nambu-Goldstone bosons—running in the loop that generates the kinetic term for \mathcal{A} .

To study the $SO(6) \times U(1)_h/SO(5)$ vacuum we parameterize the mesons as

$$\hat{M} = e^{2A_h/f_h} \left(\hat{M}_a, \sqrt{\Lambda^2 - \hat{M}_a^2} \right), \quad a = 1, \dots, 5. \quad (\text{E.3})$$

The \hat{M}_a are the five NGB supermultiplets associated with the breaking $SO(6) \rightarrow SO(5)$, while the axion supermultiplet A_h , with scalar component $s_h + ia_h$, is associated with the breaking of $U(1)_h$.

Inserting this parameterization into Eq. (E.2b), expanding around small field values, and requiring a canonical kinetic term for the axion, we find the axion decay constant is given by $f_h = \Lambda/(\sqrt{2}\pi)$. The superpotential is

$$W = \frac{\Lambda^2}{(4\pi)^2} \mathcal{A}(e^{4A_h/f_h} - 1), \quad (\text{E.4})$$

and the F -term for \mathcal{A} gives the axion potential. In components, the vacuum lies at $\langle s_h \rangle = 0$ and the axion potential is

$$V(a_h) = \frac{\Lambda^4}{8\pi^2\kappa} \left(1 - \cos \frac{4a_h}{f_h} \right). \quad (\text{E.5})$$

The axion mass is easily seen to be

$$m_{a_h}^2 = \frac{2\Lambda^4}{\kappa\pi^2 f_h^2} = \frac{4}{\kappa} \Lambda^2.$$

Now we consider an additional string axion coupled to the $SU(2)$ gauge dynamics,

$$\mathcal{L} \supset - \int d^2\theta \frac{1}{16\pi^2} \frac{A_s}{f_s} \text{Tr}(W_\alpha^2) + \text{h.c.}, \quad A_s = s_s + ia_s + \sqrt{2}\theta\psi_s + \dots \quad (\text{E.6})$$

This coupling means that the $SU(2)$ dynamical scale now depends on A_s ,

$$\Lambda^4 \rightarrow \Lambda^4 e^{A_s/f_s}.$$

It is a simple matter to find the effective potential including the string axion; we proceed exactly as above and find that the superpotential is

$$W = \frac{\Lambda^2}{(4\pi)^2} \mathcal{A}\left(e^{4A_h/f_h} - e^{A_s/f_s}\right) \quad (\text{E.7})$$

Here we will assume the dilaton in A_s to be heavy and decoupled by some unspecified dynamics, while in the next section, Appendix E.2, we present a new method to fix the dilaton. Then, the low energy axion potential is given by

$$V(a_s, a_h) = \frac{\Lambda^4}{8\pi^2\kappa} \left[1 - \cos \left(\frac{4a_h}{f_h} - \frac{a_s}{f_s} \right) \right]. \quad (\text{E.8})$$

The above potential makes it clear that one linear combination of axions gets a mass of order Λ while the orthogonal direction is massless. It is a simple procedure to find the mass eigenstates; in the limit of $f_s \gg f_h$ the heavy and light modes are given by:

$$\begin{aligned} \text{Light } a : \quad & m_a^2 = 0, \quad a \approx a_s + \frac{f_h}{4f_s} a_h + \mathcal{O}\left(\frac{f_h^2}{f_s^2}\right), \quad f_a = \sqrt{16f_s^2 + f_h^2} \approx 4f_s \\ \text{Heavy } a' : \quad & m_{a'}^2 = \frac{1}{8\pi^2\kappa} \frac{\Lambda^4}{f_{a'}^2} \approx \frac{2\Lambda^4}{\kappa\pi^2 f_h^2}, \quad a' \approx -a_h + \frac{f_h}{4f_s} a_s + \mathcal{O}\left(\frac{f_h^2}{f_s^2}\right), \quad f_{a'} = \frac{f_s f_h}{\sqrt{16f_s^2 + f_h^2}} \approx \frac{f_h}{4} \end{aligned} \quad (\text{E.9})$$

Note that the light axion picks up the larger decay constant, $f_a \approx b_0 f_s$.

E.1.2 $W_{\text{tree}} \neq 0$

Now we consider the theory with the tree level superpotential considered in chapter 4,

$$W_{\text{tree}} = W_{\text{IYIT}} + W_{\mathcal{U}(1)}, \quad (\text{E.10})$$

where $W_{\text{IYIT}} = \lambda Z Q Q$ spontaneously breaks supersymmetry and $W_{\mathcal{U}(1)}$ is a term which explicitly breaks the $U(1)_h$ symmetry.

We first consider $W_{\mathcal{U}(1)} = 0$ and briefly review how the IYIT superpotential spontaneously breaks SUSY [159] and the location of the vacuum [163]. For small Z the low-energy theory is still described by mesons and the effective superpotential is

$$W_{\text{eff}} = \frac{1}{(4\pi)^2} \left[\lambda \Lambda Z_i \hat{M}_i + \mathcal{A} (\hat{M}_i^2 - \Lambda^2) \right] \quad (\text{E.11})$$

where the singlets Z_i are in the **6** of the $SO(6)$ flavor symmetry. SUSY is broken through the F -term for Z , which is incompatible with the quantum constraint $\hat{M}_i^2 = \Lambda^2$. The vacuum lies in the direction where the $SO(6)$ symmetry is broken to $SO(5)$; this gives rise to five massless NGBs while their supersymmetric scalar partners gain a SUSY breaking mass of order $\lambda\Lambda$. Note that the singlets have canonical kinetic terms, $K_{\text{eff}} \supset Z^\dagger Z$ (with no factors of 4π). Therefore the SUSY breaking scale is suppressed from the dynamical scale Λ by extra factors of 4π [161]

$$F = \frac{\lambda}{(4\pi)^2} \Lambda^2. \quad (\text{E.12})$$

The superpotential in Eq. (E.11) is an O’Raifeartaigh model of SUSY breaking and therefore comes with a classically flat direction; namely, in the vacuum $\langle \hat{M}_6 \rangle = \Lambda$ the singlet Z_6 is massless at tree-level and its value is undetermined. For perturbative values of the coupling λ , the theory is calculable near the origin and one finds that there is a stable, local minimum located at $\langle Z_6 \rangle = 0$ [163].¹

Turning on the explicit $U(1)_h$ breaking term, $W_{\mathcal{U}(1)}$, the light axion in Eq. (E.9) will gain a small, non-zero mass. It is simple to estimate the size of this mass; the explicit breaking term is of the form

$$W_{\mathcal{U}(1)} = \frac{\lambda'}{M_{\text{pl}}^n} \mathcal{O}_{\mathcal{U}(1)}$$

with $\mathcal{O}_{\mathcal{U}(1)}$ a dimension $n + 3$ operator that explicitly breaks $U(1)_h$. The light axion carries the string decay constant f_s (see Eq. (E.9)) and the only other dimensionful scales in the problem are M_{pl} and Λ (since we are in the vacuum where $\langle Z_6 \rangle = 0$). Therefore, up to numerical factors, the light axion mass is

$$m_a^2 \sim \lambda' \frac{\Lambda^{n+4}}{M_{\text{pl}}^n f_s^2}.$$

¹If we explicitly keep the heavy axion and Lagrange multiplier \mathcal{A} in the effective theory, as in the meson parameterization in Eq. (E.3), then the classically flat direction is not Z_6 but instead it is a linear combination of Z_6 and \mathcal{A} . The results of the preceding paragraph and reference [163] remain the same for this classically flat direction.

In the chapter 4 we consider the leading operator that breaks $U(1)_h$ while preserving $U(1)_R$, $\mathcal{O}_{U(1)} \sim \lambda' Z (QQ)^3 \sim \Lambda^3 \lambda^{ijkl} Z_i \hat{M}_j \hat{M}_k \hat{M}_l$. For simplicity, we may take the $SO(6)$ preserving interaction with $\lambda^{ijkl} = \lambda' \delta^{ij} \delta^{kl}$ —flavor violating effects can be considered as perturbations around this and do not significantly change the results. Thus, we examine the effective superpotential

$$W_{\text{eff}} = \frac{1}{(4\pi)^2} \left[\lambda \Lambda Z_i \hat{M}_i + \lambda' \frac{\Lambda^3}{M_{\text{pl}}^4} Z_i \hat{M}_i \hat{M}_j^2 + \mathcal{A}(\hat{M}_i^2 - \Lambda^2 e^{A_s/f_s}) \right]. \quad (\text{E.13})$$

It is straightforward to compute the axion potential; there is a contribution from \mathcal{A} 's F -term (Eq. (E.8)) while the explicit breaking manifests itself in the F -term for Z giving

$$\delta V(a_h, a_s) = \frac{\Lambda^4}{(4\pi)^4} \left[\lambda^2 + \lambda'^2 \frac{\Lambda^8}{M_{\text{pl}}^8} + 2\lambda\lambda' \frac{\Lambda^4}{M_{\text{pl}}^4} \cos\left(\frac{4a_h}{f_h}\right) \right] \quad (\text{E.14})$$

The full axion potential is given by Eq. (E.8) plus the above contribution. To leading order in f_h/f_s the mass of the heavy axion is unchanged from Eq. (E.9) while the light axion gains a mass of

$$m_a^2 \approx \frac{2\lambda\lambda'}{(4\pi)^4} \frac{\Lambda^8}{M_{\text{pl}}^4 f_s^2} = \frac{2\lambda\lambda'}{(\lambda/4\pi)^4} \frac{F^4}{M_{\text{pl}}^4 f_s^2}, \quad (\text{E.15})$$

where in the last equality we expressed the mass in terms of the SUSY breaking scale in Eq. (E.12).

Finally, we comment on the value of the yukawa coupling λ . In the strongly coupled vacuum, λ quickly becomes non-perturbative as the wave-function for the quarks shrinks to zero. For $\lambda = 4\pi$ we cannot prove that $\langle Z \rangle = 0$ is a stable minimum [163]. Thus we must assume it is the case.

E.2 Dilaton Stabilization

Dilaton stabilization, or more generally, moduli stabilization, is a notorious problem in string theory. When the string axion couples to the sector responsible for dynamical SUSY breaking there are several typical issues. First, there is a runaway direction in which SUSY is preserved. More concretely, the vacuum energy is order $V \sim \Lambda^4$, where Λ is the dynamical scale of the hidden sector. With the string axion, this is modified to $V \sim \Lambda^4 e^{(\phi+\phi^*)/f_s}$, where ϕ is the scalar modulus of the string axion supermultiplet so that $s \equiv \phi + \phi^*$ is the dilaton. Clearly, the potential is minimized for $s \rightarrow -\infty$ with $V \rightarrow 0$ and SUSY is restored.

There are ways to stabilize moduli, such as KKLT [179] or racetrack scenarios [180]. However, these are supersymmetric preserving mechanisms, so both the dilaton and the string axion are fixed. One may want, as in this work, a mechanism which stabilizes the dilaton but leaves the string axion free. This is clearly a non-supersymmetric request, and therefore any such mechanism that achieves this must make use of the dynamical supersymmetry breaking sector or some other source of supersymmetry breaking. In these setups, the dilaton typically has a gravitino sized mass, $m_{3/2}$. Such scenarios are not easily constructed, and they typically have other issues, such as so-called dilaton domination of SUSY breaking [181]. Here, due to the dilaton's coupling to the Standard

Model gauge sector, gauginos get very large masses, $m_{1/2} \gtrsim m_{3/2}$. In anomaly mediated SUSY breaking $m_{3/2} \sim \mathcal{O}(100)$ TeV, making the phenomenology uninteresting.

In this appendix, we suggest a novel mechanism that both stabilizes the dilaton and does not introduce a large gaugino mass despite a large F term for the dilaton. As we will see, the gaugino mass coming from the dilaton is comparable to its mass from anomaly mediation. This means that the anomaly mediated mass may be $\mathcal{O}(1)$ changed, which is exciting in its own right. The key observation in this setup is to take both the modulus and the IYIT singlet fields Z to live in a strongly coupled sector [182]. By analogy with composite models, we make the crucial assumption that a form of naïve dimensional analysis (NDA) also holds for these fields. Properly counting the factors of 4π coming from NDA then gives the results outlined above.

A comment on notation: in this appendix ϕ refers to a modulus field like the string axion supermultiplet. In relation to string axion multiplet A_s and the hidden sector multiplet A_h considered in chapter 4, ϕ is the linear combination of them that is light.² For clarity, we ignore $\mathcal{O}(1)$ constants such as the one-loop beta function coefficient b_0 ; these are easily restored and do not alter our results.

We assume that there is a Kähler coupling between the string axion multiplet and the singlet fields,

$$K \supset g(\phi + \phi^*) + h(\phi + \phi^*)Z^\dagger Z \quad (\text{E.16a})$$

$$\approx M(\phi + \phi^*) + \frac{1}{2}(\phi + \phi^*)^2 + \dots + Z^\dagger Z \left(1 + \frac{\phi + \phi^*}{M} + \dots \right), \quad (\text{E.16b})$$

where the scale M corresponds to the Plank scale, $M \simeq 2.4 \times 10^{18}$ GeV. In this case, the vacuum energy is given by

$$V = K^{ZZ^\dagger} \left| \frac{\partial W}{\partial Z} \right|^2 \sim \frac{\lambda^2 \Lambda^4 e^{s/f_s}}{1 + \frac{s}{M} + \dots}. \quad (\text{E.17})$$

The potential is minimized for $s = -M + f_s \sim -M$ with vacuum energy $V \sim \lambda^2 \Lambda^4 e^{-M/f_s} / (f_s/M)$. While the dilaton is technically stabilized and SUSY is still broken, the vacuum energy is tiny for the typical string axion parameters we are considering as it is suppressed by $e^{-M/f_s} \sim e^{-10^3}$.

Moreover, the dilaton acquires a large F -term, $F_\phi \sim M m_{3/2}$:

$$F_\phi \approx K^{\phi\phi^*} \left(W_\phi + K_\phi W / M_{\text{pl}}^2 \right) \approx \frac{K_\phi W}{M_{\text{pl}}^2} \approx M m_{3/2}, \quad (\text{E.18})$$

where we have taken the superpotential to contain a constant so as to cancel the cosmological constant, $W \sim Z \Lambda^2 e^{\phi/f_s} + m_{3/2} M_{\text{pl}}^2$, and evaluated F_ϕ in the vacuum $\langle Z \rangle = 0$. As the string axion couples to the Standard Model sector, this F -term leads to a large gaugino mass,

$$\int d^2\theta \frac{\phi}{32\pi^2 f_s} W_{\text{SM},\alpha} W_{\text{SM}}^\alpha \Rightarrow m_{1/2} \sim \frac{M}{32\pi^2 f_s} m_{3/2} \gg m_{3/2}, \quad (\text{E.19})$$

²In Eq. (E.7) and the following discussion it is easy to see that an entire chiral superfield is left massless if the dilaton is not fixed. Note that this linear combination generically picks up the larger decay constant (e.g. section VI.F.4 of [183]), i.e. the string decay constant (see also Eq. (E.9)). Therefore this ϕ really does behave like a string modulus and the results of this section apply more generally.

with $32\pi^2 f_s \sim 10^{17}$ GeV for $f_s \sim 10^{15}$ GeV.

These results change if dilaton sector is strongly coupled. We then imagine that the proper low-energy effective theory becomes strongly coupled at the compactification scale. We are led to consider the string scale as a composite scale, which we label M_c , and apply the rules of naïve dimensional analysis.

Let us briefly review the rules of NDA [161, 162, 184]: multiply the effective action by an overall factor of $1/16\pi^2$, replace the composite fields as $\Phi \rightarrow 4\pi\Phi$, and relabel the cutoff $M \rightarrow M_c$. For example, the coupling of the dilaton to SM gauge fields in Eq. (E.19) becomes

$$\frac{\phi}{M} W_{\text{SM},\alpha} W_{\text{SM}}^\alpha \rightarrow \frac{4\pi\phi}{16\pi^2 M_c} W_{\text{SM},\alpha} W_{\text{SM}}^\alpha. \quad (\text{E.20})$$

As the above operator is responsible for the string axion decay to photons considered in chapter 4, it sets the scale M_c :

$$\int d^2\theta \frac{\phi}{4\pi M_c} W_{\text{EM},\alpha} W_{\text{EM}}^\alpha \supset \frac{a}{32\pi^2 f_s} F_{\text{EM}} \tilde{F}_{\text{EM}}, \quad (\text{E.21})$$

so that for the observed value $f_s \sim 10^{15}$ GeV we have $M_c \sim 10^{16}$ GeV.

Let us assume that the singlet fields Z also live in the strongly coupled sector; then we can view them as “composite” particles just like the string axion. Using NDA, the relevant terms in the effective Kähler potential are

$$K \sim \frac{1}{16\pi^2} \left[4\pi M_c (\phi + \phi^*) + \frac{(4\pi)^3}{M_c} Z^\dagger Z (\phi + \phi^*) \right]. \quad (\text{E.22})$$

The vacuum energy as a function of the dilaton is then of the same form as Eq. (E.17) with $M = M_c/4\pi$ and $f_s = M_c/8\pi$. Since $M \sim f_s \sim 0.1M_c$, we immediately see that the vacuum energy is no longer tiny: at the minimum $V'(s) = 0$ we have $s = -M + f_s \sim -f_s \sim -M_c/8\pi$ so that the vacuum energy is $V \sim \lambda^2 \Lambda^4 e^{-1}/\mathcal{O}(1)$. The dilaton F-term is $F_\phi = M_c m_{3/2}/4\pi \approx f_s m_{3/2}$; this gives the gauginos a mass of order

$$m_{1/2} \approx \frac{F_\phi}{32\pi^2 f_s} m_{3/2} \approx \frac{1}{32\pi^2} m_{3/2}. \quad (\text{E.23})$$

This contribution to the gaugino mass from the dilaton is comparable in size to the gaugino mass coming from anomaly mediation.

In summary, we have outlined a mechanism to stabilize the dilaton—while leaving the string axion free—that is phenomenologically viable with supersymmetry breaking and a string axion decay constant that could explain the 3.5 keV line, as described in chapter 4. Moreover, the stabilization mechanism may allow for the anomaly mediation relations for gaugino masses to be changed by an $\mathcal{O}(1)$ amount, which could prove useful for model building. The crucial assumption in achieving these results is that the effective action of the dilaton should become strongly coupled at the compactification scale. This led us to applying naïve dimensional analysis to ensure this behavior of the effective action. By also considering the singlets involved in SUSY breaking to live in the strongly coupled sector we obtain the stated results.

Bibliography

- [1] B. Henning, X. Lu, and H. Murayama, “What do precision Higgs measurements buy us?” (2014), [1404.1058](#).
- [2] B. Henning, X. Lu, and H. Murayama, “How to use the Standard Model effective field theory” (2014), [1412.1837](#).
- [3] B. Henning and H. Murayama, “Constraints on Light Dark Matter from Big Bang Nucleosynthesis” (2012), [1205.6479](#).
- [4] B. Henning, J. Kehayias, H. Murayama, D. Pinner, and T. T. Yanagida, “A keV String Axion from High Scale Supersymmetry”. *Phys.Rev.* **D91(4)**:045036 (2015), [1408.0286](#).
- [5] G. Aad et al., “Observation of a new particle in the search for the Standard Model Higgs boson with the ATLAS detector at the LHC”. *Phys.Lett.* **B716**:1–29 (2012), [1207.7214](#).
- [6] S. Chatrchyan et al., “Observation of a new boson at a mass of 125 GeV with the CMS experiment at the LHC”. *Phys.Lett.* **B716**:30–61 (2012), [1207.7235](#).
- [7] ATLAS, “Measurements of the Higgs boson production and decay rates and coupling strengths using pp collision data at $\sqrt{s} = 7$ and 8 TeV in the ATLAS experiment” (2015).
- [8] T. Behnke, J. E. Brau, B. Foster, J. Fuster, M. Harrison, et al., “The International Linear Collider Technical Design Report - Volume 1: Executive Summary” (2013), [1306.6327](#); H. Baer, T. Barklow, K. Fujii, Y. Gao, A. Hoang, et al., “The International Linear Collider Technical Design Report - Volume 2: Physics” (2013), [1306.6352](#); C. Adolphsen, M. Barone, B. Barish, K. Buesser, P. Burrows, et al., “The International Linear Collider Technical Design Report - Volume 3.I: Accelerator & in the Technical Design Phase” (2013), [1306.6353](#); C. Adolphsen, M. Barone, B. Barish, K. Buesser, P. Burrows, et al., “The International Linear Collider Technical Design Report - Volume 3.II: Accelerator Baseline Design” (2013), [1306.6328](#); T. Behnke, J. E. Brau, P. N. Burrows, J. Fuster, M. Peskin, et al., “The International Linear Collider Technical Design Report - Volume 4: Detectors” (2013), [1306.6329](#).
- [9] M. Bicer et al., “First Look at the Physics Case of TLEP”. *JHEP* **1401**:164 (2014), [1308.6176](#).

- [10] C. Prescott, W. Atwood, R. L. Cottrell, H. DeStaebler, E. L. Garwin, et al., “Further Measurements of Parity Nonconservation in Inelastic electron Scattering”. *Phys.Lett.* **B84**:524 (1979).
- [11] G. Alexander et al., “Electroweak parameters of the Z^0 resonance and the Standard Model: the LEP Collaborations”. *Phys.Lett.* **B276**:247–253 (1992).
- [12] S. Schael et al., “Precision electroweak measurements on the Z resonance”. *Phys.Rept.* **427**:257–454 (2006), [hep-ex/0509008](#).
- [13] F. Abe et al., “Observation of top quark production in $\bar{p}p$ collisions”. *Phys.Rev.Lett.* **74**:2626–2631 (1995), [hep-ex/9503002](#).
- [14] S. Abachi et al., “Observation of the top quark”. *Phys.Rev.Lett.* **74**:2632–2637 (1995), [hep-ex/9503003](#).
- [15] M. Gaillard, “The Effective One Loop Lagrangian With Derivative Couplings”. *Nucl.Phys.* **B268**:669 (1986).
- [16] K. G. Begeman, A. H. Broeils, and R. H. Sanders, “Extended rotation curves of spiral galaxies: Dark haloes and modified dynamics”. *Mon. Not. Roy. Astron. Soc.* **249**:523 (1991).
- [17] R. Adam et al., “Planck 2015 results. I. Overview of products and scientific results” (2015), [1502.01582](#).
- [18] D. Clowe, M. Bradac, A. H. Gonzalez, M. Markevitch, S. W. Randall, C. Jones, and D. Zaritsky, “A direct empirical proof of the existence of dark matter”. *Astrophys. J.* **648**:L109–L113 (2006), [astro-ph/0608407](#).
- [19] W. Hu, R. Barkana, and A. Gruzinov, “Cold and fuzzy dark matter”. *Phys.Rev.Lett.* **85**:1158–1161 (2000), [astro-ph/0003365](#).
- [20] P. Tisserand et al., “Limits on the Macho Content of the Galactic Halo from the EROS-2 Survey of the Magellanic Clouds”. *Astron.Astrophys.* **469**:387–404 (2007), [astro-ph/0607207](#).
- [21] V. F. Mukhanov, “Nucleosynthesis without a computer”. *Int. J. Theor. Phys.* **43**:669–693 (2004), [astro-ph/0303073](#).
- [22] A. Boyarsky, J. Lesgourgues, O. Ruchayskiy, and M. Viel, “Lyman-alpha constraints on warm and on warm-plus-cold dark matter models”. *JCAP* **0905**:012 (2009), [0812.0010](#).
- [23] K. Griest and M. Kamionkowski, “Unitarity Limits on the Mass and Radius of Dark Matter Particles”. *Phys.Rev.Lett.* **64**:615 (1990).

- [24] E. Bulbul, M. Markevitch, A. Foster, R. K. Smith, M. Loewenstein, et al., “Detection of An Unidentified Emission Line in the Stacked X-ray spectrum of Galaxy Clusters”. *Astrophys.J.* **789**:13 (2014), [1402.2301](#).
- [25] A. Boyarsky, O. Ruchayskiy, D. Iakubovskiy, and J. Franse, “An unidentified line in X-ray spectra of the Andromeda galaxy and Perseus galaxy cluster” (2014), [1402.4119](#).
- [26] D. Malyshev, A. Neronov, and D. Eckert, “Constraints on 3.55 keV line emission from stacked observations of dwarf spheroidal galaxies”. *Phys.Rev.* **D90(10)**:103506 (2014), [1408.3531](#); M. E. Anderson, E. Churazov, and J. N. Bregman, “Non-Detection of X-Ray Emission From Sterile Neutrinos in Stacked Galaxy Spectra” (2014), [1408.4115](#); T. Tamura, R. Iizuka, Y. Maeda, K. Mitsuda, and N. Y. Yamasaki, “An X-ray Spectroscopic Search for Dark Matter in the Perseus Cluster with Suzaku” (2014), [1412.1869](#).
- [27] H. Murayama, “Future Experimental Programs”. *Phys.Scripta* **T158**:014025 (2013), [1401.0966](#).
- [28] S. Dawson, A. Gritsan, H. Logan, J. Qian, C. Tully, et al., “Higgs Working Group Report of the Snowmass 2013 Community Planning Study” (2013), [1310.8361](#).
- [29] M. Baak, M. Goebel, J. Haller, A. Hoecker, D. Kennedy, et al., “The Electroweak Fit of the Standard Model after the Discovery of a New Boson at the LHC”. *Eur.Phys.J.* **C72**:2205 (2012), [1209.2716](#).
- [30] M. Baak, A. Blondel, A. Bodek, R. Caputo, T. Corbett, et al., “Study of Electroweak Interactions at the Energy Frontier” (2013), [1310.6708](#).
- [31] J. Fan, M. Reece, and L.-T. Wang, “Possible Futures of Electroweak Precision: ILC, FCC-ee, and CEPC” (2014), [1411.1054](#).
- [32] A. David et al., “LHC HXSWG interim recommendations to explore the coupling structure of a Higgs-like particle” (2012), [1209.0040](#).
- [33] A. V. Manohar, “Effective field theories”. *Lect.Notes Phys.* **479**:311–362 (1997), [hep-ph/9606222](#); C. Burgess, “Introduction to Effective Field Theory”. *Ann.Rev.Nucl.Part.Sci.* **57**:329–362 (2007), [hep-th/0701053](#); H. Georgi, “Weak Interactions and Modern Particle Theory” (1984).
- [34] N. Craig, M. Farina, M. McCullough, and M. Perelstein, “Precision Higgsstrahlung as a Probe of New Physics” (2014), [1411.0676](#).
- [35] O. Cheyette, “Effective Action for the Standard Model With Large Higgs Mass”. *Nucl.Phys.* **B297**:183 (1988).
- [36] S. Weinberg, S. Deser, M. Grisaru, and H. Pendleton, “Lectures on elementary particles and quantum field theory”. *Proceedings of the Summer Institute, Brandeis University* **1** (1970).

- [37] S. Ferrara, M. Porrati, and V. L. Telegdi, “ $g = 2$ as the natural value of the tree level gyromagnetic ratio of elementary particles”. *Phys.Rev.* **D46**:3529–3537 (1992).
- [38] C. Grojean, E. E. Jenkins, A. V. Manohar, and M. Trott, “Renormalization Group Scaling of Higgs Operators and $\Gamma(h \rightarrow \gamma\gamma)$ ”. *JHEP* **1304**:016 (2013), [1301.2588](#).
- [39] J. Elias-Miró, J. Espinosa, E. Masso, and A. Pomarol, “Renormalization of dimension-six operators relevant for the Higgs decays $h \rightarrow \gamma\gamma, \gamma Z$ ”. *JHEP* **1308**:033 (2013), [1302.5661](#).
- [40] E. E. Jenkins, A. V. Manohar, and M. Trott, “Renormalization Group Evolution of the Standard Model Dimension Six Operators I: Formalism and lambda Dependence”. *JHEP* **1310**:087 (2013), [1308.2627](#).
- [41] E. E. Jenkins, A. V. Manohar, and M. Trott, “Renormalization Group Evolution of the Standard Model Dimension Six Operators II: Yukawa Dependence”. *JHEP* **1401**:035 (2014), [1310.4838](#).
- [42] R. Alonso, E. E. Jenkins, A. V. Manohar, and M. Trott, “Renormalization Group Evolution of the Standard Model Dimension Six Operators III: Gauge Coupling Dependence and Phenomenology”. *JHEP* **1404**:159 (2014), [1312.2014](#).
- [43] R. Alonso, H.-M. Chang, E. E. Jenkins, A. V. Manohar, and B. Shotwell, “Renormalization group evolution of dimension-six baryon number violating operators”. *Phys.Lett.* **B734**:302 (2014), [1405.0486](#).
- [44] J. Elias-Miró, J. Espinosa, E. Masso, and A. Pomarol, “Higgs windows to new physics through $d=6$ operators: constraints and one-loop anomalous dimensions”. *JHEP* **1311**:066 (2013), [1308.1879](#).
- [45] J. Elias-Miró, C. Grojean, R. S. Gupta, and D. Marzocca, “Scaling and tuning of EW and Higgs observables”. *JHEP* **1405**:019 (2014), [1312.2928](#).
- [46] E. E. Jenkins, A. V. Manohar, and M. Trott, “On Gauge Invariance and Minimal Coupling”. *JHEP* **1309**:063 (2013), [1305.0017](#).
- [47] A. V. Manohar, “An Exactly Solvable Model for Dimension Six Higgs Operators and $h \rightarrow \gamma\gamma$ ”. *Phys.Lett.* **B726**:347–351 (2013), [1305.3927](#).
- [48] E. E. Jenkins, A. V. Manohar, and M. Trott, “Naive Dimensional Analysis Counting of Gauge Theory Amplitudes and Anomalous Dimensions”. *Phys.Lett.* **B726**:697–702 (2013), [1309.0819](#).
- [49] R. Alonso, E. E. Jenkins, and A. V. Manohar, “Holomorphy in the Standard Model Effective Field Theory” (2014), [1409.0868](#).

- [50] Z. Han and W. Skiba, “Effective theory analysis of precision electroweak data”. *Phys.Rev.* **D71**:075009 (2005), [hep-ph/0412166](#).
- [51] G. Cacciapaglia, C. Csaki, G. Marandella, and A. Strumia, “The Minimal Set of Electroweak Precision Parameters”. *Phys.Rev.* **D74**:033011 (2006), [hep-ph/0604111](#).
- [52] F. Bonnet, M. Gavela, T. Ota, and W. Winter, “Anomalous Higgs couplings at the LHC, and their theoretical interpretation”. *Phys.Rev.* **D85**:035016 (2012), [1105.5140](#); F. Bonnet, T. Ota, M. Rauch, and W. Winter, “Interpretation of precision tests in the Higgs sector in terms of physics beyond the Standard Model”. *Phys.Rev.* **D86**:093014 (2012), [1207.4599](#).
- [53] F. del Aguila and J. de Blas, “Electroweak constraints on new physics”. *Fortsch.Phys.* **59**:1036–1040 (2011), [1105.6103](#); J. de Blas, M. Chala, and J. Santiago, “Global Constraints on Lepton-Quark Contact Interactions”. *Phys.Rev.* **D88**:095011 (2013), [1307.5068](#); J. de Blas, “Electroweak limits on physics beyond the Standard Model”. *EPJ Web Conf.* **60**:19008 (2013), [1307.6173](#).
- [54] B. Dumont, S. Fichet, and G. von Gersdorff, “A Bayesian view of the Higgs sector with higher dimensional operators”. *JHEP* **1307**:065 (2013), [1304.3369](#).
- [55] A. Pomarol and F. Riva, “Towards the Ultimate SM Fit to Close in on Higgs Physics”. *JHEP* **1401**:151 (2014), [1308.2803](#).
- [56] C.-Y. Chen, S. Dawson, and C. Zhang, “Electroweak Effective Operators and Higgs Physics”. *Phys.Rev.* **D89**:015016 (2014), [1311.3107](#).
- [57] S. Willenbrock and C. Zhang, “Effective Field Theory Beyond the Standard Model” (2014), [1401.0470](#).
- [58] R. S. Gupta, A. Pomarol, and F. Riva, “BSM Primary Effects” (2014), [1405.0181](#); R. S. Gupta, “BSM Primary Effects: The complete set of predictions from the dimension-6 BSM Lagrangian”. *PoS DIS2014*:133 (2014), [1407.8448](#).
- [59] E. Masso, “An Effective Guide to Beyond the Standard Model Physics”. *JHEP* **1410**:128 (2014), [1406.6376](#).
- [60] C. Englert and M. Spannowsky, “Effective Theories and Measurements at Colliders”. *Phys.Lett.* **B740**:8–15 (2014), [1408.5147](#).
- [61] M. Ciuchini, E. Franco, S. Mishima, M. Pierini, L. Reina, et al., “Update of the electroweak precision fit, interplay with Higgs-boson signal strengths and model-independent constraints on new physics” (2014), [1410.6940](#).
- [62] J. Ellis, V. Sanz, and T. You, “The Effective Standard Model after LHC Run I” (2014), [1410.7703](#).

- [63] A. Falkowski and F. Riva, “Model-independent precision constraints on dimension-6 operators” (2014), [1411.0669](#).
- [64] M. K. Gaillard, “Effective One Loop Scalar Actions in (Mostly) Four-Dimensions” (1986).
- [65] L. Chan, “Effective Action Expansion in Perturbation Theory”. *Phys.Rev.Lett.* **54**:1222–1225 (1985).
- [66] O. Cheyette, “Derivative Expansion of the Effective Action”. *Phys.Rev.Lett.* **55**:2394 (1985).
- [67] V. Novikov, M. A. Shifman, A. Vainshtein, and V. I. Zakharov, “Calculations in External Fields in Quantum Chromodynamics. Technical Review”. *Fortsch.Phys.* **32**:585 (1984).
- [68] R. Ball, “Chiral Gauge Theory”. *Phys.Rept.* **182**:1 (1989).
- [69] H. Georgi and M. Machacek, “Doubly Charged Higgs Bosons”. *Nucl.Phys.* **B262**:463 (1985); M. S. Chanowitz and M. Golden, “Higgs Boson Triplets With $M(W) = M(Z) \cos \theta_w$ ”. *Phys.Lett.* **B165**:105 (1985).
- [70] C. Englert, E. Re, and M. Spannowsky, “Pinning down Higgs triplets at the LHC”. *Phys.Rev.* **D88**:035024 (2013), [1306.6228](#).
- [71] Z. U. Khandker, D. Li, and W. Skiba, “Electroweak Corrections from Triplet Scalars”. *Phys.Rev.* **D86**:015006 (2012), [1201.4383](#); W. Skiba, “TASI Lectures on Effective Field Theory and Precision Electroweak Measurements” (2010), [1006.2142](#).
- [72] R. Barbieri, L. J. Hall, and V. S. Rychkov, “Improved naturalness with a heavy Higgs: An Alternative road to LHC physics”. *Phys.Rev.* **D74**:015007 (2006), [hep-ph/0603188](#).
- [73] N. Manton, “A New Six-Dimensional Approach to the Weinberg-Salam Model”. *Nucl.Phys.* **B158**:141 (1979).
- [74] N. Arkani-Hamed, A. Cohen, E. Katz, A. Nelson, T. Gregoire, et al., “The Minimal moose for a little Higgs”. *JHEP* **0208**:021 (2002), [hep-ph/0206020](#); N. Arkani-Hamed, A. Cohen, E. Katz, and A. Nelson, “The Littlest Higgs”. *JHEP* **0207**:034 (2002), [hep-ph/0206021](#).
- [75] H.-C. Cheng, K. T. Matchev, and M. Schmaltz, “Radiative corrections to Kaluza-Klein masses”. *Phys.Rev.* **D66**:036005 (2002), [hep-ph/0204342](#).
- [76] H.-C. Cheng and I. Low, “TeV symmetry and the little hierarchy problem”. *JHEP* **0309**:051 (2003), [hep-ph/0308199](#); H.-C. Cheng and I. Low, “Little hierarchy, little Higgses, and a little symmetry”. *JHEP* **0408**:061 (2004), [hep-ph/0405243](#).
- [77] N. Arkani-Hamed, A. G. Cohen, and H. Georgi, “Electroweak symmetry breaking from dimensional deconstruction”. *Phys.Lett.* **B513**:232–240 (2001), [hep-ph/0105239](#).

- [78] L. Randall and R. Sundrum, “A Large mass hierarchy from a small extra dimension”. *Phys.Rev.Lett.* **83**:3370–3373 (1999), [hep-ph/9905221](#).
- [79] W. Buchmuller and D. Wyler, “Effective Lagrangian Analysis of New Interactions and Flavor Conservation”. *Nucl.Phys.* **B268**:621–653 (1986).
- [80] B. Grzadkowski, M. Iskrzynski, M. Misiak, and J. Rosiek, “Dimension-Six Terms in the Standard Model Lagrangian”. *JHEP* **1010**:085 (2010), [1008.4884](#).
- [81] K. Hagiwara, S. Ishihara, R. Szalapski, and D. Zeppenfeld, “Low-energy effects of new interactions in the electroweak boson sector”. *Phys.Rev.* **D48**:2182–2203 (1993).
- [82] G. Giudice, C. Grojean, A. Pomarol, and R. Rattazzi, “The Strongly-Interacting Light Higgs”. *JHEP* **0706**:045 (2007), [hep-ph/0703164](#).
- [83] J. Beringer et al., “Review of Particle Physics (RPP)”. *Phys.Rev.* **D86**:010001 (2012).
- [84] I. Maksymyk, C. Burgess, and D. London, “Beyond S, T and U”. *Phys.Rev.* **D50**:529–535 (1994), [hep-ph/9306267](#); C. Burgess, S. Godfrey, H. Konig, D. London, and I. Maksymyk, “A Global fit to extended oblique parameters”. *Phys.Lett.* **B326**:276–281 (1994), [hep-ph/9307337](#).
- [85] M. E. Peskin and T. Takeuchi, “Estimation of oblique electroweak corrections”. *Phys.Rev.* **D46**:381–409 (1992).
- [86] A. Kundu and P. Roy, “A General treatment of oblique parameters”. *Int.J.Mod.Phys.* **A12**:1511–1530 (1997), [hep-ph/9603323](#).
- [87] R. Barbieri, A. Pomarol, R. Rattazzi, and A. Strumia, “Electroweak symmetry breaking after LEP-1 and LEP-2”. *Nucl.Phys.* **B703**:127–146 (2004), [hep-ph/0405040](#).
- [88] G. Degrassi, B. A. Kniehl, and A. Sirlin, “Gauge invariant formulation of the S, T, and U parameters”. *Phys.Rev.* **D48**:3963–3966 (1993).
- [89] D. Binosi and J. Papavassiliou, “Pinch Technique: Theory and Applications”. *Phys.Rept.* **479**:1–152 (2009), [0909.2536](#).
- [90] K. Gaemers and G. Gounaris, “Polarization Amplitudes for $e^+e^- \rightarrow W^+W^-$ and $e^+e^- \rightarrow ZZ$ ”. *Z.Phys.* **C1**:259 (1979).
- [91] K. Hagiwara, R. Peccei, D. Zeppenfeld, and K. Hikasa, “Probing the Weak Boson Sector in $e^+e^- \rightarrow W^+W^-$ ”. *Nucl.Phys.* **B282**:253 (1987); K. Hagiwara, S. Ishihara, R. Szalapski, and D. Zeppenfeld, “Low-energy constraints on electroweak three gauge boson couplings”. *Phys.Lett.* **B283**:353–359 (1992).
- [92] G. Gounaris, J. Kneur, D. Zeppenfeld, Z. Ajaltouni, A. Arhrib, et al., “Triple gauge boson couplings” (1996), [hep-ph/9601233](#).

- [93] S. Schael et al., “Electroweak Measurements in Electron-Positron Collisions at W-Boson-Pair Energies at LEP”. Phys.Rept. **532**:119–244 (2013), [1302.3415](#).
- [94] C. Grojean, G. Servant, and J. D. Wells, “First-order electroweak phase transition in the standard model with a low cutoff”. Phys.Rev. **D71**:036001 (2005), [hep-ph/0407019](#).
- [95] J. R. Ellis, J. Gunion, H. E. Haber, L. Roszkowski, and F. Zwirner, “Higgs Bosons in a Nonminimal Supersymmetric Model”. Phys.Rev. **D39**:844 (1989).
- [96] X. Lu, H. Murayama, J. T. Ruderman, and K. Tobioka, “A Natural Higgs Mass in Supersymmetry from Non-Decoupling Effects” (2013), [1308.0792](#).
- [97] R. Barbieri, L. J. Hall, Y. Nomura, and V. S. Rychkov, “Supersymmetry without a Light Higgs Boson”. Phys.Rev. **D75**:035007 (2007), [hep-ph/0607332](#).
- [98] S. Mishima, “Talk given at the Sixth TLEP Workshop”. URL <http://indico.cern.ch/event/257713/session/1/contribution/30> (2013).
- [99] N. Craig, C. Englert, and M. McCullough, “A New Probe of Naturalness”. Phys.Rev.Lett. **111**:121803 (2013), [1305.5251](#).
- [100] C. Englert and M. McCullough, “Modified Higgs Sectors and NLO Associated Production”. JHEP **1307**:168 (2013), [1303.1526](#).
- [101] S. Gori and I. Low, “Precision Higgs Measurements: Constraints from New Oblique Corrections”. JHEP **1309**:151 (2013), [1307.0496](#).
- [102] M. E. Peskin, “Estimation of LHC and ILC Capabilities for Precision Higgs Boson Coupling Measurements” (2013), [1312.4974](#).
- [103] C. Delaunay, C. Grojean, and J. D. Wells, “Dynamics of Non-renormalizable Electroweak Symmetry Breaking”. JHEP **0804**:029 (2008), [0711.2511](#).
- [104] M. Papucci, J. T. Ruderman, and A. Weiler, “Natural SUSY Endures”. JHEP **1209**:035 (2012), [1110.6926](#).
- [105] A. Djouadi, “The Anatomy of electro-weak symmetry breaking. I: The Higgs boson in the standard model”. Phys.Rept. **457**:1–216 (2008), [hep-ph/0503172](#).
- [106] S. Heinemeyer, W. Hollik, and G. Weiglein, “FeynHiggs: A Program for the calculation of the masses of the neutral CP even Higgs bosons in the MSSM”. Comput.Phys.Commun. **124**:76–89 (2000), [hep-ph/9812320](#); S. Heinemeyer, W. Hollik, and G. Weiglein, “The Masses of the neutral CP - even Higgs bosons in the MSSM: Accurate analysis at the two loop level”. Eur.Phys.J. **C9**:343–366 (1999), [hep-ph/9812472](#); G. Degrandi, S. Heinemeyer, W. Hollik, P. Slavich, and G. Weiglein, “Towards high precision predictions for the

- MSSM Higgs sector”. *Eur.Phys.J.* **C28**:133–143 (2003), [hep-ph/0212020](#); M. Frank, T. Hahn, S. Heinemeyer, W. Hollik, H. Rzehak, et al., “The Higgs Boson Masses and Mixings of the Complex MSSM in the Feynman-Diagrammatic Approach”. *JHEP* **0702**:047 (2007), [hep-ph/0611326](#).
- [107] L. J. Hall, D. Pinner, and J. T. Ruderman, “A Natural SUSY Higgs Near 126 GeV”. *JHEP* **1204**:131 (2012), [1112.2703](#).
- [108] M. Cirelli, “Indirect Searches for Dark Matter: a Status Review” (2012), [1202.1454](#).
- [109] M. Reno and D. Seckel, “Primordial Nucleosynthesis: The Effects of Injecting Hadrons”. *Phys.Rev.* **D37**:3441 (1988).
- [110] S. Dimopoulos, R. Esmailzadeh, L. J. Hall, and G. Starkman, “Is the Universe Closed by Baryons? Nucleosynthesis with a Late Decaying Massive Particle”. *Astrophys.J.* **330**:545 (1988).
- [111] R. H. Cyburt, J. R. Ellis, B. D. Fields, and K. A. Olive, “Updated nucleosynthesis constraints on unstable relic particles”. *Phys.Rev.* **D67**:103521 (2003), [astro-ph/0211258](#).
- [112] M. Kawasaki, K. Kohri, and T. Moroi, “Big-Bang nucleosynthesis and hadronic decay of long-lived massive particles”. *Phys.Rev.* **D71**:083502 (2005), [astro-ph/0408426](#).
- [113] K. Jedamzik, “Did something decay, evaporate, or annihilate during Big Bang nucleosynthesis?” *Phys.Rev.* **D70**:063524 (2004), [astro-ph/0402344](#).
- [114] K. Jedamzik, “Big bang nucleosynthesis constraints on hadronically and electromagnetically decaying relic neutral particles”. *Phys.Rev.* **D74**:103509 (2006), [hep-ph/0604251](#).
- [115] X.-L. Chen and M. Kamionkowski, “Particle decays during the cosmic dark ages”. *Phys.Rev.* **D70**:043502 (2004), [astro-ph/0310473](#).
- [116] S. Kasuya, M. Kawasaki, and N. Sugiyama, “Partially ionizing the universe by decaying particles”. *Phys.Rev.* **D69**:023512 (2004), [astro-ph/0309434](#).
- [117] L. Zhang, X. Chen, M. Kamionkowski, Z.-g. Si, and Z. Zheng, “Constraints on radiative dark-matter decay from the cosmic microwave background”. *Phys.Rev.* **D76**:061301 (2007), [0704.2444](#).
- [118] J. A. Frieman, E. W. Kolb, and M. S. Turner, “Eternal Annihilations: New Constraints on Longlived Particles from Big Bang Nucleosynthesis”. *Phys.Rev.* **D41**:3080 (1990).
- [119] J. Hisano, M. Kawasaki, K. Kohri, T. Moroi, and K. Nakayama, “Cosmic Rays from Dark Matter Annihilation and Big-Bang Nucleosynthesis”. *Phys.Rev.* **D79**:083522 (2009), [0901.3582](#).

- [120] J. Hisano, M. Kawasaki, K. Kohri, and K. Nakayama, “Positron/Gamma-Ray Signatures of Dark Matter Annihilation and Big-Bang Nucleosynthesis”. *Phys.Rev.* **D79**:063514 (2009), [0810.1892](#).
- [121] K. Jedamzik and M. Pospelov, “Big Bang Nucleosynthesis and Particle Dark Matter”. *New J.Phys.* **11**:105028 (2009), [0906.2087](#).
- [122] J. Hisano, M. Kawasaki, K. Kohri, T. Moroi, K. Nakayama, et al., “Cosmological constraints on dark matter models with velocity-dependent annihilation cross section”. *Phys.Rev.* **D83**:123511 (2011), [1102.4658](#).
- [123] N. Padmanabhan and D. P. Finkbeiner, “Detecting dark matter annihilation with CMB polarization: Signatures and experimental prospects”. *Phys.Rev.* **D72**:023508 (2005), [astro-ph/0503486](#).
- [124] T. Kanzaki, M. Kawasaki, and K. Nakayama, “Effects of Dark Matter Annihilation on the Cosmic Microwave Background”. *Prog.Theor.Phys.* **123**:853–865 (2010), [0907.3985](#).
- [125] S. Galli, F. Iocco, G. Bertone, and A. Melchiorri, “CMB constraints on Dark Matter models with large annihilation cross-section”. *Phys.Rev.* **D80**:023505 (2009), [0905.0003](#).
- [126] T. R. Slatyer, N. Padmanabhan, and D. P. Finkbeiner, “CMB Constraints on WIMP Annihilation: Energy Absorption During the Recombination Epoch”. *Phys.Rev.* **D80**:043526 (2009), [0906.1197](#).
- [127] D. P. Finkbeiner, S. Galli, T. Lin, and T. R. Slatyer, “Searching for Dark Matter in the CMB: A Compact Parameterization of Energy Injection from New Physics”. *Phys.Rev.* **D85**:043522, (2012), [1109.6322](#).
- [128] A. Natarajan, “A closer look at CMB constraints on WIMP dark matter” [1201.3939](#).
- [129] E. W. Kolb and M. S. Turner, “The Early universe”. *Front.Phys.* **69**:1–547 (1990).
- [130] Y. L. Dokshitzer, V. S. Fadin, and V. A. Khoze, “Double Logs of Perturbative QCD for Parton Jets and Soft Hadron Spectra”. *Z.Phys.* **C15**:325 (1982).
- [131] O. Biebel, P. Nason, and B. Webber, “Jet fragmentation in e+e- annihilation” (2001), [hep-ph/0109282](#).
- [132] B. Webber, “Average Multiplicities in Jets”. *Phys.Lett.* **B143**:501 (1984).
- [133] M. Kawasaki and T. Moroi, “Electromagnetic cascade in the early universe and its application to the big bang nucleosynthesis”. *Astrophys.J.* **452**:506 (1995), [astro-ph/9412055](#).
- [134] K. Jedamzik, “Lithium 6: A Probe of the early universe”. *Phys.Rev.Lett.* **84**:3248 (2000), [astro-ph/9909445](#).

- [135] M. Kawasaki, K. Kohri, and T. Moroi, “Radiative decay of a massive particle and the nonthermal process in primordial nucleosynthesis”. *Phys.Rev.* **D63**:103502 (2001), [hep-ph/0012279](#).
- [136] J. Calarco, B. Berman, and T. W. Donnelly, “Implications of the experimental results on the photodisintegration of He-4”. *Phys.Rev.* **C27**:1866–1875 (1983).
- [137] J. Gratsias, R. J. Scherrer, and D. N. Spergel, “Indirect photofission of light elements from high-energy neutrinos in the early universe”. *Phys.Lett.* **B262**:298–302 (1991).
- [138] M. Kawasaki and T. Moroi, “Gravitino decay into a neutrino and a sneutrino in the inflationary universe”. *Phys.Lett.* **B346**:27–34 (1995), [hep-ph/9408321](#).
- [139] T. Kanzaki, M. Kawasaki, K. Kohri, and T. Moroi, “Cosmological Constraints on Neutrino Injection”. *Phys.Rev.* **D76**:105017 (2007), [0705.1200](#).
- [140] J. Hisano, S. Matsumoto, and M. M. Nojiri, “Explosive dark matter annihilation”. *Phys.Rev.Lett.* **92**:031303 (2004), [hep-ph/0307216](#).
- [141] M. Ibe, H. Murayama, and T. Yanagida, “Breit-Wigner Enhancement of Dark Matter Annihilation”. *Phys.Rev.* **D79**:095009 (2009), [0812.0072](#).
- [142] G. Aad et al., “Search for squarks and gluinos with the ATLAS detector in final states with jets and missing transverse momentum using $\sqrt{s} = 8$ TeV proton–proton collision data” (2014), [1405.7875](#); C. Collaboration, “Search for supersymmetry in hadronic final states using M_{T2} with the CMS detector at $\sqrt{s} = 8$ TeV” (2014).
- [143] G. Aad et al., “Observation of a new particle in the search for the Standard Model Higgs boson with the ATLAS detector at the LHC”. *Phys.Lett.* **B716**:1–29 (2012), [1207.7214](#); S. Chatrchyan et al., “Observation of a new boson at a mass of 125 GeV with the CMS experiment at the LHC”. *Phys.Lett.* **B716**:30–61 (2012), [1207.7235](#).
- [144] Y. Okada, M. Yamaguchi, and T. Yanagida, “Upper bound of the lightest Higgs boson mass in the minimal supersymmetric standard model”. *Prog.Theor.Phys.* **85**:1–6 (1991); Y. Okada, M. Yamaguchi, and T. Yanagida, “Renormalization group analysis on the Higgs mass in the softly broken supersymmetric standard model”. *Phys.Lett.* **B262**:54–58 (1991); J. R. Ellis, G. Ridolfi, and F. Zwirner, “On radiative corrections to supersymmetric Higgs boson masses and their implications for LEP searches”. *Phys.Lett.* **B262**:477–484 (1991); H. E. Haber and R. Hempfling, “Can the mass of the lightest Higgs boson of the minimal supersymmetric model be larger than $m(Z)$?” *Phys.Rev.Lett.* **66**:1815–1818 (1991).
- [145] A. Kusenko, “Sterile neutrinos: The Dark side of the light fermions”. *Phys.Rept.* **481**:1–28 (2009), [0906.2968](#).
- [146] K. Hamaguchi, M. Ibe, T. T. Yanagida, and N. Yokozaki, “Testing the Minimal Direct Gauge Mediation at the LHC” (2014), [1403.1398](#).

- [147] T. Moroi, H. Murayama, and M. Yamaguchi, “Cosmological constraints on the light stable gravitino”. *Phys.Lett.* **B303**:289–294 (1993).
- [148] A. de Gouvea, T. Moroi, and H. Murayama, “Cosmology of supersymmetric models with low-energy gauge mediation”. *Phys.Rev.* **D56**:1281–1299 (1997), [hep-ph/9701244](#).
- [149] J. Hashiba, M. Kawasaki, and T. Yanagida, “Cosmological constraint on the string dilaton in gauge mediated supersymmetry breaking theories”. *Phys.Rev.Lett.* **79**:4525–4528 (1997), [hep-ph/9708226](#).
- [150] T. Asaka, J. Hashiba, M. Kawasaki, and T. Yanagida, “Cosmological moduli problem in gauge mediated supersymmetry breaking theories”. *Phys.Rev.* **D58**:083509 (1998), [hep-ph/9711501](#).
- [151] M. Kawasaki and T. Yanagida, “Constraint on cosmic density of the string moduli field in gauge mediated supersymmetry breaking theories”. *Phys.Lett.* **B399**:45–48 (1997), [hep-ph/9701346](#).
- [152] A. Kusenko, M. Loewenstein, and T. T. Yanagida, “Moduli dark matter and the search for its decay line using Suzaku X-ray telescope”. *Phys.Rev.* **D87(4)**:043508 (2013), [1209.6403](#).
- [153] G. F. Giudice, M. A. Luty, H. Murayama, and R. Rattazzi, “Gaugino mass without singlets”. *JHEP* **9812**:027 (1998), [hep-ph/9810442](#); J. D. Wells, “Implications of supersymmetry breaking with a little hierarchy between gauginos and scalars” (2003), [hep-ph/0306127](#); J. D. Wells, “PeV-scale supersymmetry”. *Phys.Rev.* **D71**:015013 (2005), [hep-ph/0411041](#).
- [154] M. Ibe, T. Moroi, and T. Yanagida, “Possible Signals of Wino LSP at the Large Hadron Collider”. *Phys.Lett.* **B644**:355–360 (2007), [hep-ph/0610277](#); M. Ibe and T. T. Yanagida, “The Lightest Higgs Boson Mass in Pure Gravity Mediation Model”. *Phys.Lett.* **B709**:374–380 (2012), [1112.2462](#); M. Ibe, S. Matsumoto, and T. T. Yanagida, “Pure Gravity Mediation with $m_{3/2} = 10\text{-}100$ TeV”. *Phys.Rev.* **D85**:095011 (2012), [1202.2253](#).
- [155] N. Arkani-Hamed, A. Gupta, D. E. Kaplan, N. Weiner, and T. Zorawski, “Simply Unnatural Supersymmetry” (2012), [1212.6971](#).
- [156] T. Higaki, K. S. Jeong, and F. Takahashi, “The 7 keV axion dark matter and the X-ray line signal” (2014), [1402.6965](#); J. Jaeckel, J. Redondo, and A. Ringwald, “A 3.55 keV hint for decaying axion-like particle dark matter” (2014), [1402.7335](#); H. M. Lee, S. C. Park, and W.-I. Park, “Cluster X-ray line at 3.5 keV from axion-like dark matter” (2014), [1403.0865](#); F. S. Queiroz and K. Sinha, “The Poker Face of the Majoron Dark Matter Model: LUX to keV Line”. *Phys.Lett.* **B735**:69–74 (2014), [1404.1400](#).
- [157] P. Svrcek and E. Witten, “Axions In String Theory”. *JHEP* **0606**:051 (2006), [hep-th/0605206](#).

- [158] T. Banks and N. Seiberg, “Symmetries and Strings in Field Theory and Gravity”. *Phys.Rev.* **D83**:084019 (2011), [1011.5120](#).
- [159] K.-I. Izawa and T. Yanagida, “Dynamical supersymmetry breaking in vector - like gauge theories”. *Prog.Theor.Phys.* **95**:829–830 (1996), [hep-th/9602180](#); K. A. Intriligator and S. D. Thomas, “Dynamical supersymmetry breaking on quantum moduli spaces”. *Nucl.Phys.* **B473**:121–142 (1996), [hep-th/9603158](#).
- [160] M. Dine, A. E. Nelson, Y. Nir, and Y. Shirman, “New tools for low-energy dynamical supersymmetry breaking”. *Phys.Rev.* **D53**:2658–2669 (1996), [hep-ph/9507378](#).
- [161] M. A. Luty, “Naive dimensional analysis and supersymmetry”. *Phys.Rev.* **D57**:1531–1538 (1998), [hep-ph/9706235](#).
- [162] A. G. Cohen, D. B. Kaplan, and A. E. Nelson, “Counting 4 pis in strongly coupled supersymmetry”. *Phys.Lett.* **B412**:301–308 (1997), [hep-ph/9706275](#).
- [163] Z. Chacko, M. A. Luty, and E. Ponton, “Calculable dynamical supersymmetry breaking on deformed moduli spaces”. *JHEP* **9812**:016 (1998), [hep-th/9810253](#).
- [164] P. Ade et al., “Detection of B-Mode Polarization at Degree Angular Scales by BICEP2”. *Phys.Rev.Lett.* **112**:241101 (2014), [1403.3985](#).
- [165] R. Flauger, J. C. Hill, and D. N. Spergel, “Toward an Understanding of Foreground Emission in the BICEP2 Region”. *JCAP* **1408**:039 (2014), [1405.7351](#).
- [166] R. Adam et al., “Planck intermediate results. XXX. The angular power spectrum of polarized dust emission at intermediate and high Galactic latitudes” (2014), [1409.5738](#).
- [167] P. Ade et al., “Planck 2013 results. XXII. Constraints on inflation”. *Astron.Astrophys.* **571**:A22 (2014), [1303.5082](#).
- [168] M. Kawasaki, M. Yamaguchi, and T. Yanagida, “Natural chaotic inflation in supergravity”. *Phys.Rev.Lett.* **85**:3572–3575 (2000), [hep-ph/0004243](#).
- [169] A. D. Linde, “Relaxing the cosmological moduli problem”. *Phys.Rev.* **D53**:4129–4132 (1996), [hep-th/9601083](#); K. Nakayama, F. Takahashi, and T. T. Yanagida, “Gravity mediation without a Polonyi problem”. *Phys.Lett.* **B714**:256–261 (2012), [1203.2085](#).
- [170] B. Bhattacharjee, M. Ibe, K. Ichikawa, S. Matsumoto, and K. Nishiyama, “Wino Dark Matter and Future dSph Observations” (2014), [1405.4914](#); T. Cohen, M. Lisanti, A. Pierce, and T. R. Slatyer, “Wino Dark Matter Under Siege”. *JCAP* **1310**:061 (2013), [1307.4082](#); J. Fan and M. Reece, “In Wino Veritas? Indirect Searches Shed Light on Neutralino Dark Matter”. *JHEP* **1310**:124 (2013), [1307.4400](#).

- [171] G. Aad et al., “Search for charginos nearly mass degenerate with the lightest neutralino based on a disappearing-track signature in pp collisions at $\sqrt{s}=8\text{TeV}$ with the ATLAS detector”. *Phys.Rev.* **D88(11)**:112006 (2013), [1310.3675](#).
- [172] L. Abbott, “Introduction to the Background Field Method”. *Acta Phys.Polon.* **B13**:33 (1982).
- [173] M. E. Peskin and D. V. Schroeder, “An Introduction to quantum field theory” (1995).
- [174] M. Asplund, D. L. Lambert, P. E. Nissen, F. Primas, and V. V. Smith, “Lithium isotopic abundances in metal-poor halo stars”. *Astrophys.J.* **644**:229–259 (2006), [astro-ph/0510636](#).
- [175] R. Cayrel, M. Steffen, P. Bonifacio, H.-G. Ludwig, and E. Caffau, “Overview of the lithium problem in metal-poor stars and new results on 6Li ” (2008), [0810.4290](#).
- [176] B. D. Fields, “The Primordial Lithium Problem”. *Ann.Rev.Nucl.Part.Sci.* **61**:47–68 (2011), [1203.3551](#).
- [177] M. Pinsonneault, T. Walker, G. Steigman, and V. Narayanan, “Halo star lithium depletion”. *Astrophys.J.* **527**:180–198 (2002), [astro-ph/9803073](#).
- [178] N. Seiberg, “Exact results on the space of vacua of four-dimensional SUSY gauge theories”. *Phys.Rev.* **D49**:6857–6863 (1994), [hep-th/9402044](#).
- [179] S. Kachru, R. Kallosh, A. D. Linde, and S. P. Trivedi, “De Sitter vacua in string theory”. *Phys.Rev.* **D68**:046005 (2003), [hep-th/0301240](#).
- [180] N. Krasnikov, “On Supersymmetry Breaking in Superstring Theories”. *Phys.Lett.* **B193**:37–40 (1987); L. J. Dixon, “Supersymmetry Breaking in String Theory” (1990); J. Casas, Z. Lalak, C. Munoz, and G. G. Ross, “Hierarchical Supersymmetry Breaking and Dynamical Determination of Compactification Parameters by Nonperturbative Effects”. *Nucl.Phys.* **B347**:243–269 (1990).
- [181] M. Baryakhtar, E. Hardy, and J. March-Russell, “Axion Mediation”. *JHEP* **1307**:096 (2013), [1301.0829](#).
- [182] E. Dudas, A. Linde, Y. Mambrini, A. Mustafayev, and K. A. Olive, “Strong moduli stabilization and phenomenology”. *Eur.Phys.J.* **C73**:2268 (2013), [1209.0499](#).
- [183] J. E. Kim and G. Carosi, “Axions and the Strong CP Problem”. *Rev.Mod.Phys.* **82**:557–602 (2010), [0807.3125](#).
- [184] A. Manohar and H. Georgi, “Chiral Quarks and the Nonrelativistic Quark Model”. *Nucl.Phys.* **B234**:189 (1984); H. Georgi and L. Randall, “Flavor Conserving CP Violation in Invisible Axion Models”. *Nucl.Phys.* **B276**:241 (1986).